Università degli Studi di Napoli Federico II

Dottorato di Ricerca in Ingegneria Strutturale, Geotecnica e Rischio Sismico – XXXV ciclo

THESIS FOR THE DEGREE OF DOCTOR OF PHILOSOPHY (Ph.D)

Seismic assessment of nonstructural elements: shake table tests and qualification protocols

by
Martino Zito

Advisor: **Prof. Gennaro Magliulo**

Co-advisor: **Dr. Danilo D'Angela**

SCUOLA POLITECNICA E DELLE SCIENZE DI BASE
DIPARTIMENTO D STRUTTURE PER L'INGEGNERIA E L'ARCHITETTURA – via Claudio, 21 (Napoli, Italia)

To Letizia

L'unica vera saggezza è sapere di non sapere nulla
(Socrate)

Seismic assessment of nonstructural elements: shake table tests and qualification protocols

Ph.D. Thesis presented for the fulfillment of the Degree of Doctor of Philosophy in Ingegneria Strutturale, Geotecnica e Rischio Sismico

by

Martino Zito

February 2023

Approved as to style and content by

____

Prof. Gennaro Magliulo, Advisor

____

Dr. Danilo D’Angela, Co-advisor

Università degli Studi di Napoli Federico II

Ph.D. Program in Ingegneria Strutturale, Geotecnica e Rischio Sismico

XXXV cycle - Coordinator: Prof. Iunio Iervolino

www.dist.unina.it/dottorati-di-ricerca/dottorati

Candidate’s declaration

Martino Zito hereby declare that this thesis submitted to obtain the academic degree of Philosophiæ Doctor (Ph.D.) in Ingegneria Strutturale, Geotecnica e Rischio Sismico is my own unaided work, that have not used other than the sources indicated, and that all direct and indirect sources are acknowledged as references.

Parts of this dissertation have been published in international journals and/or conference proceedings.

Napoli, February 16, 2023

____

Martino Zito

Abstract

Nonstructural elements (NEs) are generally defined as elements typically part of or housed within buildings/facilities that are not included in the structural system. NEs are often classified as architectural elements, mechanical/electrical/hydraulic systems, and building contents. NEs are often associated with critical seismic risk due to high vulnerability and exposure to seismic actions, especially for critical facilities such as hospitals, museums, and nuclear plant facilities.

NE seismic behavior typically affects facility functioning and can be associated with significant economic losses; moreover, damage to NEs might even cause human losses. The seismic capacity and performance of NEs can be generally assessed by means of analytical, numerical, experimental, observational, and mixed methods. Experimental testing is the most common method used to assess NEs as this is typically considered to be the most reliable and robust option.

The dissertation reviews and evaluates the main international testing approaches and protocols for seismic assessment of NEs by means of experimental methods, which are also referred to for seismic qualification. Moreover, novel perspectives and a unified approach for seismic assessment and qualification of NEs are proposed. Then, shake table tests carried out to evaluate the seismic behavior of two critical NEs are reported, considering i) an innovative cleanroom used in the pharmaceutical and healthcare industries and ii) a typical museum display case containing a representative art object of the exhibition equipment of the National Archaeological Museum of Naples (MANN), Italy. The shake table tests were carried out according to the ICC-ES AC156 protocol, which represents the international reference for seismic qualification and certification of acceleration-sensitive nonstructural elements.

After highlighting existing protocols criticalities, the dissertation points out the need for the development of novel assessment and qualification approaches and protocols. A novel testing protocol is developed in light of these criticalities. The most significant and scientific contribution parts of the developed protocol consist in the definition of novel required response spectra and the generation of signals for seismic performance evaluation tests. The seismic scenario representativity and reliability of existing reference shake table protocols are evaluated, also including the shake table protocol developed in this study. In particular, these protocols are assessed in terms of seismic damage potential/severity considering the inelastic single degree of freedom (SDOF) systems and assuming the reliability index as an evaluation parameter. Safety factors towards a reliability-targeted assessment of NEs are finally proposed.

Keywords: earthquake engineering, nonstructural elements, shake table, testing protocol, seismic fragility, seismic reliability.

Sintesi in lingua italiana

Gli elementi non strutturali (ENS) sono generalmente definiti come elementi installati all'interno di edifici/strutture che non fanno parte del sistema strutturale. Gli ENS sono spesso classificati come elementi architettonici, sistemi e apparecchiature meccanici/elettrici/idraulici e contenuti dell'edificio. Essi sono spesso associati ad un notevole rischio sismico a causa dell'elevata vulnerabilità ed esposizione alle azioni sismiche, soprattutto per le strutture critiche come ospedali, musei e impianti nucleari.

Il comportamento sismico degli ENS influisce tipicamente sul funzionamento degli edifici e può essere associato a significative perdite economiche; inoltre, i danni agli ENS possono persino causare perdite in termini di vite umane. La capacità e le prestazioni sismiche degli ENS possono essere generalmente valutate con metodi analitici, numerici, sperimentali, osservazionali e misti. Le prove sperimentali sono il metodo più comunemente utilizzato per valutare il comportamento dinamico degli ENS, in quanto sono considerate come l'opzione più affidabile e robusta.

La tesi passa in rassegna e valuta i principali approcci e protocolli di prova internazionali per la valutazione sismica degli ENS mediante metodi sperimentali, a cui si fa anche riferimento per la qualificazione sismica. Inoltre, vengono proposte nuove prospettive e un approccio unificato per la valutazione e la qualificazione sismica degli ENS. Vengono poi descritte le prove su tavola vibrante per valutare il comportamento sismico di due ENS critici/complessi: i) una camera bianca innovativa utilizzata nell'industria farmaceutica e sanitaria e ii) una tipica vetrina museale contenente un oggetto d'arte, parte dell'allestimento del Museo Archeologico Nazionale di Napoli (MANN), Italia. Le prove su tavola vibrante sono state condotte in accordo al protocollo ICC-ES AC156, che rappresenta il riferimento internazionale per la qualificazione e la certificazione sismica di ENS sensibili all'accelerazione.

Dopo aver evidenziato le criticità dei protocolli esistenti, la tesi sottolinea la necessità di sviluppare nuovi approcci e protocolli di valutazione e qualificazione. Alla luce di queste criticità, viene sviluppato un nuovo protocollo di prova. Le parti più significative del protocollo e il contributo scientifico consistono nella definizione di nuovi spettri di risposta richiesti e nella generazione di segnali per le prove di valutazione delle prestazioni sismiche. È stata valutata la rappresentatività dello scenario sismico e l'affidabilità degli attuali protocolli di riferimento. I protocolli di riferimento sono stati valutati in termini di potenziale di danno sismico/severità considerando i sistemi anelastici a singolo grado di libertà (SDOF) e assumendo l'indice di affidabilità come parametro di valutazione. Infine, lo studio propone coefficienti di sicurezza finalizzati ad una valutazione degli elementi non strutturali basata su definiti livelli di affidabilità.

Parole chiave: ingegneria sismica, elementi non strutturali, prova su tavola vibrante, protocollo di prova, fragilità sismica, affidabilità sismica.

Contents

Acknowledgements

The dissertation acknowledgements section is available only in the printed version.

List of Figures

List of Tables

Chapter 1

1 Introduction

Non-structural elements (NEs) of a building consist of building elements/components and contents that are not part of the structural resisting system (Figure 1.1). NEs can be either single elements or distributed systems (e.g., networks). They are typically not intended to be load-bearing elements and are often attached/connected to structural/building elements. NEs can also be not connected to the structure/building and can be moved or relocated during their lifetime, i.e., freestanding elements (e.g., furniture).

NEs can be divided into three broad categories based on their service and function, namely: 1) architectural elements, such as infill and partition walls, curtain walls, ceiling systems, and architectural ornamentations; 2) mechanical, electrical, and plumbing elements for example pumps, chillers, fans, air handling units, motor control centers, electrical cabinets, distribution panels, transformers, and piping; 3) furniture, fixtures and equipment, and contents such as shelving and bookcases, industrial storage racks, medical records, computers and desktop equipment, wall and ceiling-mounted TVs and monitors, industrial chemicals or hazardous materials, museum artifacts [1].

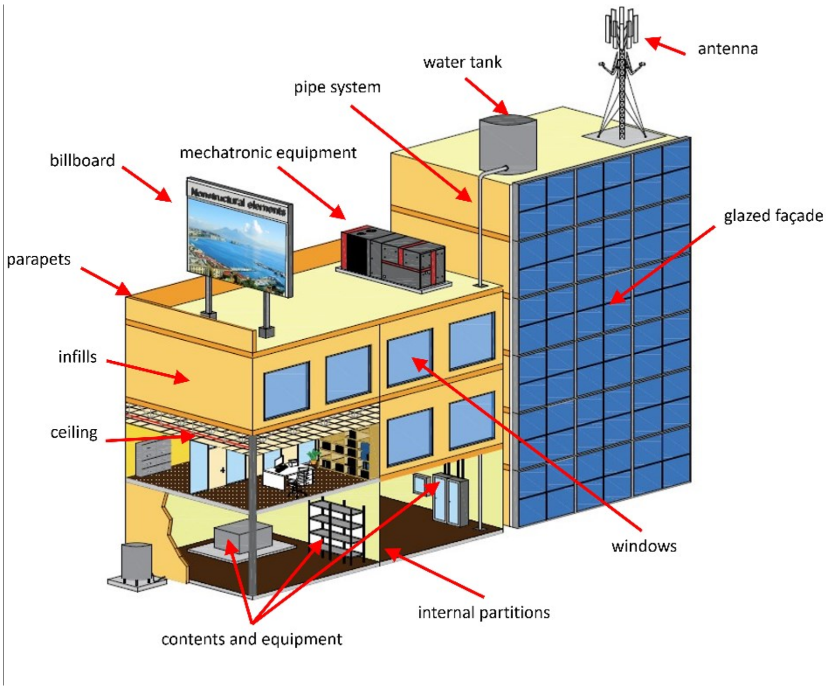

Figure 1.1: A three-dimensional view of a portion of a building. This figure shows both structural and nonstructural elements.

1.1 Motivations

The dynamic behavior of NEs is typically associated with high seismic risk since NEs are often highly vulnerable and exposed to damage caused by seismic actions (Figure 1.2). The critical seismic response of NEs was highlighted by several recent earthquake events, e.g., the 2010 Darfield, 2011 Christchurch, and 2016 Kaikōura earthquakes in New Zealand [2-4], the 2010 offshore Maule earthquake in Chile [5], the 2009 L'Aquila (Italy) earthquake [6], the 2012 Emilia (Italy) earthquake [7], the 2016 Central Italy earthquake [8] and the 2020 Petrinja (Croatia) earthquake [9]. In particular, these and other seismic events proved that damage to NEs can be significant even within buildings that exhibited minor or negligible structural damage, potentially resulting in major economic losses and casualties.

(a)

(b)

Figure 1.2: Typical damage to: a) ceiling system in commercial building during the 2010 Darfield earthquakes in New Zealand [2], and b) display case at the Archaeological Museum of Zagreb during the 2020 Zagreb earthquake, Croatia [12].

Earthquake ground shaking generally has four primary effects on NEs in buildings: (1) inertial or shaking effects, (2) distortions imposed on NEs when the building structure sways back and forth, (3) separation or pounding at the interface between adjacent structures, and (4) interaction between adjacent NEs [1]. There are many factors affecting the performance of NEs during an earthquake and the extent to which they will sustain damage. The degree of damage caused by the four principal effects previously mentioned depends upon considerations such as the components' dynamic characteristics, their location in the building, and their proximity to other structural or NEs. Other factors include the type of ground motion, the structural system of the building, the location and placement of the loads, the type of anchorage or bracing, if any, the strength of the structural supports used for anchorage, potential interaction with other NEs.

Damage of NEs may result in injuries or fatalities, costly property damage to buildings and their contents, and functioning disruptions. In particular, the potential consequences of earthquake damage to NEs are typically divided into three types of risk referred to as the 3Ds: Deaths, Dollars, and Downtime [1]. The first type of risk is that people could be injured or killed by damage (or response of) NEs. Furthermore, life safety can also be compromised if the damaged NEs block emergency paths and exits in a building [13]. Damage to life safety systems such as fire protection components or devices can also pose a safety concern in case of fire after an earthquake or prior to fully restore the system. Examples of potentially hazardous nonstructural damage that have occurred during past earthquakes include but is not limited to glass breaking, cabinets overturning, falling of ceilings and overhead light fixtures, rupture of gas lines and other piping containing hazardous materials, damage of friable asbestos materials, collapse of decorative molding parts, failure of masonry infill walls, parapets, and chimneys (e.g., [10,14]).

The property losses (Dollars) may be the result of direct damage to NEs or the consequences produced by its damage/response [1]. In most buildings, the biggest contributor to economic losses resulting from earthquakes is damage to NEs. In particular, NEs represent a large percentage of the total construction cost [10]. Figure 1.3 presents the cost distribution of four sample buildings including reinforced concrete (RC) residential buildings, hotels, office buildings, and hospitals, in the United States [10,15]. The cost of NEs is the highest in hospitals, where approximately 92% of total construction costs are due to NEs; this number reduces to 87% for hotels, 82% for office buildings, and 60% for RC residential buildings. Furthermore, NEs are likely to exhibit moderate to severe damage even under relatively frequent earthquakes. Accordingly, the combination of major exposure and vulnerability makes NEs extremely critical in terms of seismic risk even over low to moderate seismicity areas (e.g., over the whole Italian territory).

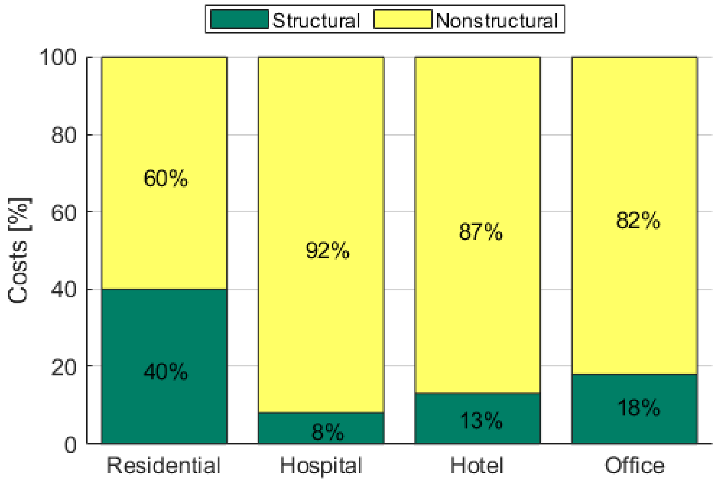

Figure 1.3: Cost breakdown of RC residential buildings, office buildings, hotels, and hospitals [10,15].

The loss can be associated with private or public properties and might be particularly critical (even priceless) in case of damage to museum/historical/monumental facilities/objects or archives/storages. For example, the 2016 Central Italy earthquake caused major damage to stuccoes and decorations of monumental churches and historical palaces [8], the 2009 L'Aquila earthquake partial or total collapse of precious sculptures located in the Spanish Fortress (L'Aquila) [16], and the 2010 Darfield earthquake caused damage to valuable furniture and artifacts in a church of Christchurch [2].

Several earthquake events highlighted that functioning of buildings can be typically disrupted by damage to NE even though structural damage is not exhibited or negligible (e.g., they were designed according to modern codes). For example, severe damage to masonry infills and partitions was observed after the 2009 L'Aquila earthquake, involving a large number of buildings that were designed and constructed not much time earlier than the earthquake; this caused significant losses in terms of Downtime [6]. Post-earthquake downtime is highly critical when the building/facility functioning is considered vital, especially in the aftermath of the event, e.g., for hospitals, fire stations, manufacturing facilities, and government offices. Furthermore, downtime has a huge impact in situations where seismic and other emergencies/crises (e.g., sanitary emergencies) are combined. For instance, in 2020, in Croatia, the combination of the COVID-19 pandemic and two destructive earthquakes had an extremely critical impact on the population in terms of physical, economical, and social/psychological burden [9].

1.2 Aim and objectives

The current European and international codes and standards (e.g., [17–22]) establish rules and criteria for seismic design and verification of NEs considering the effects of earthquakes in terms of inertial forces (e.g., accelerations) and deformations (e.g., displacements). The dynamic proprieties of NEs should be typically known in order to apply methods and criteria established by the codes and standards for the determination of seismic demand measures, whereas the seismic capacities of NEs should be estimated in order to carry out the design and assessment safety verifications.

In this regard, the main aim of the dissertation is the evaluation of the seismic behavior of critical NEs. The evaluation of the dynamic proprieties and seismic capacities of NEs can be carried out via different methods. Experimental testing is generally favored and considered to be most reliable and robust option, especially for critical and complex NEs [19]. For this reason, the seismic evaluation of the NEs considered are performed via experimental testing methods.

The experimental tests are conducted through the earthquake simulator available at the Department of Structures for Engineering Architecture of University of Naples “Federico II”, i.e., a two degree of freedom shake table. The main objectives of the experimental tests consist in the evaluation of a relationship between Engineering Demand Parameters (EDPs), e.g., the interstory drift ratio (IDR) or the peak floor acceleration (PFA), and a predefined Damage States (DSs), according to the Performance-Based earthquake Engineering (PBEE) approach [23]. Another objective was the evaluation of the vibration modes, natural frequency, damping ratio and component amplification factor of the NEs.

The dissertation firstly critically reviews existing methods and testing protocols, highlighting their strengths and criticalities and pointing out the need for the development of novel assessment and qualification approaches and protocols. For this reason, a novel protocol is developed in the light of the identified criticalities, considering the most recent advances in the field and the specific expertise of the research team involved in the reserach. The most significant and contributing parts of the developed protocol consist in the definition of novel required response spectra (RRS) and generation of signals for seismic performance evaluation tests. This study is mainly focused on acceleration-sensitive nonstructural elements.

Existing reference shake table protocols defined by regulations/codes [24-26] and the novel protocol defined by Zito et al. [27] are assessed in terms of seismic damage potential/severity, considering inelastic single degree of freedom (SDOF) systems and assuming the reliability index as an evaluation parameter. The operative outcome is associated with the accurate estimation of the reliability index of the reference protocols and with the estimation of applicative safety coefficients, towards the reliability-targeted assessment of nonstructural elements.

1.3 Outline

The dissertation is organized as follows:

in the second chapter, the main international testing approaches, methods, and protocols for experimental seismic assessment of NEs are reviewed and technically evaluated, also referring to seismic qualification;

in the third chapter, methodology and results regarding shake table performance evaluation of an innovative cleanroom with walkable ceiling system under operation conditions are described;

in the fourth chapter, methodology and results regarding shake table tests of a typical museum display case containing an art object are reported;

in the fifth chapter, a shake table protocol for seismic assessment and qualification of acceleration-sensitive nonstructural elements is developed;

in the sixth chapter, the seismic scenario representativity and reliability of existing reference shake table protocols defined by regulations/codes is assessed;

in the seventh chapter, conclusions and novel perspectives are drawn in the light of the whole study.

1.4 References

[1] FEMA E-74 Reducing the Risks of Nonstructural Earthquake Damage-A Practical Guide; 2012.

[2] Dhakal, R.P. Damage to Non-Structural Components and Contents in 2010 Darfield Earthquake. Bulletin of the New Zealand Society for Earthquake Engineering (BNZSEE) 2010, 43.

[3] Baird, A.; Ferner, H. Damage to Non-Structural Elements in the 2016 Kaikōura Earthquake. Bulletin of the New Zealand Society for Earthquake Engineering (BNZSEE) 2017, 50.

[4] Baird, A.; Tasligedik, A.S.; Palermo, A.; Pampanin, S. Seismic Performance of Vertical Nonstructural Components in the 22 February 2011 Christchurch Earthquake. Earthquake Spectra 2014, 30, 401–425.

[5] Miranda, E.; Mosqueda, G.; Retamales, R.; Pekcan, G. Performance of Nonstructural Components during the 27 February 2010 Chile Earthquake. Earthquake Spectra 2012, 28, doi:10.1193/1.4000032.

[6] Braga, F.; Manfredi, V.; Masi, A.; Salvatori, A.; Vona, M. Performance of Non-Structural Elements in RC Buildings during the L'Aquila, 2009 Earthquake. Bulletin of Earthquake Engineering 2011, 9, 307–324, doi:10.1007/s10518-010-9205-7.

[7] Magliulo, G.; Ercolino, M.; Petrone, C.; Coppola, O.; Manfredi, G. The Emilia Earthquake: Seismic Performance of Precast Reinforced Concrete Buildings. Earthquake Spectra 2014, 30, 891–912, doi:10.1193/091012EQS285M.

[8] Perrone, D.; Calvi, P.M.; Nascimbene, R.; Fischer, E.C.; Magliulo, G. Seismic Performance of Non-Structural Elements during the 2016 Central Italy Earthquake. Bulletin of Earthquake Engineering 2019, 17, doi:10.1007/s10518-018-0361-5.

[9] Miranda, E.; Brzev, S.; Bijelić, N. STEER-EERI: Petrinja, Croatia December 29, 2020, Mw 6.4 Earthquake Joint Reconnaissance Report (JRR); 2021.

[10] Taghavi, S.; Miranda, E. Response Assessment of Nonstructural Building Elements - PEER 2003/05; 2003.

[11] Takahashi, N.; Shiohara, H. Life Cycle Economic Loss Due to Seismic Damage of nonstructural Elements. In Proceedings of the 13th World Conference on Earthquake Engineering Vancouver, B.C., Canada; August 1 2004.

[12] https://culturetourist.com/museums/museum-reviews/zagreb-museums-are-severely-damaged-in-the-recent-earthquake/

[13] Ikuta, E.; Miyano, M. Study of Damage to the Human Body Caused by Earthquakes: Development of a Mannequin for Thoracic Compression Experiments and Cyber Mannequin Using the Finite Element Method. In Human Casualties in Earthquakes: Progress in Modelling and Mitigation; Spence Robin and So, E.

and S.C., Ed.; Springer Netherlands: Dordrecht, 2011; pp. 275–289 ISBN 978-90-481-9455-1.
[14] Filiatrault, A.; Uang, C.-M.; Folz, B.; Chrstopoulos, C.; Gatto, K. Structural Systems Research Project Reconnaissance Report of the February 28, 2001 Nisqually (Seattle-Olympia) Earthquake.; 2001.
[15] Takahashi, N.; Shiohara, H. Life Cycle Economic Loss Due to Seismic Damage of nonstructural Elements. In Proceedings of the 13th World Conference on Earthquake Engineering Vancouver, B.C., Canada; August 1 2004.
[16] Parisi, F.; Augenti, N. Earthquake Damages to Cultural Heritage Constructions and Simplified Assessment of Artworks. Eng Fail Anal 2013, 34, 735–760, doi:10.1016/j.engfailanal.2013.01.005.
[17] Comité Européen de Normalisation (CEN) Eurocode 8: Design of Structures for Earthquake Resistance; 2005.
[18] Ministero delle infrastrutture e dei trasporti Aggiornamento Delle “Norme Tecniche per Le Costruzioni” Decreto 17 Gennaio 2018.; (in italian), 2018; Vol. 20, pp. 23–35.
[19] ASCE 7-16 Minimum Design Loads and Associated Criteria for Buildings and Other Structures; American Society of Civil Engineers (ASCE), 2016; pp. 1–889.
[20] New Zealand Standards New Zealand Standard (NZS): Seismic Performance of Engineering Systems in Buildings. NZS 4219:2009 2009, 1–114.
[21] Instituto Nacional de Normalización NCh3357: Seismic Design of Non-Structural Components and Systems; 2015.
[22] Canadian Commission on Building and Fire Codes National Building Code of Canada 2015; 2015.
[23] Porter, K. (2020). A Beginner’s Guide to Fragility, Vulnerability, and Risk. Denver CO USA.
[24] Federal Emergency Management Agency (FEMA). Interim protocols for determining seismic performance characteristics of structural and nonstructural components through laboratory testing. Report No. FEMA 461, 2007. Washington D.C., USA.
[25] International Code Council Evaluation Service (ICC-ES). AC156 Acceptance Criteria for the Seismic Qualification of Nonstructural Components. Brea, California, USA: 2012.
[26] Institute of Electrical and Electronics Engineers. 693-2006 IEEE Recommended practice for seismic design for substations. New York: Institute of Electrical and Electronics Engineers; 2006.
[27] Zito, M., D’Angela, D., Maddaloni, G., & Magliulo, G. (2022). A shake table protocol for seismic assessment and qualification of acceleration-sensitive nonstructural elements. Computer-Aided Civil and Infrastructure Engineering, 1–28.https://doi.org/10.1111/mice.12951

Chapter 2

2 Experimental assessment of nonstructural elements: testing protocols and novel perspectives

Nonstructural elements (NEs) are generally defined as elements typically housed within buildings/facilities that are not part of the structural system. NEs are often classified as architectural elements, mechanical/electrical/hydraulic systems, and building contents. NEs are often associated with critical seismic risk due to high vulnerability and exposure to seismic actions, especially for critical facilities such as hospitals and nuclear plant facilities. Accordingly, the combination of major exposure and vulnerability makes NEs extremely critical in terms of seismic risk even over for low to moderate seismicity. The chapter reviews and evaluates the main international testing approaches and protocols for seismic assessment of NEs by means of experimental methods, which are referred to for seismic qualification. Existing test protocols are technically analyzed considering quasi-static, single-floor dynamic and multi-floor dynamic procedures, supplying technical and operative guidance for their implementation, according to the latest advances in the field. The chapter proposes novel perspectives and a unified approach for seismic assessment and qualification of NEs. The technical recommendations lay the groundwork for a more robust and standardized testing and qualification framework. In particular, the provided data might represent the first step for developing code and regulation criteria for experimental seismic assessment and qualification of NEs.

2.1 Introduction

Over the last twenty years, the research community has been investigating seismic assessment of NEs, and copious literature was developed accordingly.. As a result, the current European and international codes and standards (e.g., [1–6]) refer to Performance-Based Earthquake Engineering (PBEE) approach and methods for design and assessment of NEs. Significant attention has been recently focused on the estimation of (building) floor accelerations for the assessment of seismic demands on NEs in buildings [7–13]. Existing codes establish rules and criteria for seismic design and verification of NEs considering the effects of the earthquake in terms of forces (i.e., accelerations) and displacements (i.e., deformations). The dynamic proprieties of NEs should be typically known in order to apply criteria and methods established by the codes and standards for the determination of seismic demand measures, whereas the seismic capacities of NEs should be estimated in order to carry out the design and assessment safety verifications. The evaluation of the seismic capacities shall be carried out via one of the following methods: (a) analysis, (b) (experimental) testing, (c) experience data, (d) a combination of methods (a), (b) and (c) [3,14,15]. Seismic assessment of NEs aiming at producing robust standard capacity estimations and safety evaluations is often referred to seismic qualification and, in some cases, seismic certification [3,14,16].

Several analytical/numerical models were developed in the literature for the seismic evaluation of NEs. However, each study is typically associated with a specific NE and is not generally extendable to different NE properties and characteristics [17–23]. Experimental testing is the most common method used to assess NEs as this is typically considered to be the most reliable and robust option. Many research activities focused on the seismic assessment/qualification of NEs by experimental tests, such as plaster-board partition walls [24–34], masonry infill walls [35–39], innovative partition walls [40–43], ceiling systems [44–50], curtain walls [51–54], technical equipment and systems [55–60], hospital components [61–63], museum artifacts and art objects [64–66], among many others. Seismic assessment and qualification through experience data might be theoretically more representative than other methods since the NE response is estimated according to actual seismic events, but this is limited to specific characteristics of NEs, buildings, and seismic events. Regarding experimental test methods, testing protocols available in the literature generally vary depending on the type of NEs involved and the reference code. Finally, it is possible to develop hybrid methods to optimize the best characteristics of the single methods. Therefore, experimental testing is generally favored and considered to be more generally applicable and efficient, especially for critical and complex NEs.

The present chapter discusses and evaluates the main international testing approaches and protocols, also considering available codes and guidelines for seismic qualification. Existing test protocols are subdivided into three categories: 1) quasi-static, 2) single-floor dynamic and 3) multi-floor dynamic. In light of the above-mentioned evaluation, the chapter proposes a unified approach for the seismic assessment and qualification of NEs, to be possibly implemented in current regulations and technical guidelines. The technical and scientific novelty developed in the study fills a critical gap identified in the literature, and the technical recommendations and innovative perspectives potentially contribute towards a more reliable and robust seismic assessment of NEs.

2.2 Nonstructural elements (NEs) classifications

NEs can be divided into three broad categories based on their service and function, namely: 1) architectural elements, such as infill and partition walls, curtain walls, ceiling systems, and architectural ornamentations; 2) mechanical, electrical, and plumbing elements for example pumps, chillers, fans, air handling units, motor control centers, electrical cabinets, distribution panels, transformers, and piping; 3) furniture, fixtures and equipment, and contents such as shelving and bookcases, industrial storage racks, medical records, computers and desktop equipment, wall and ceiling-mounted TVs and monitors, industrial chemicals or hazardous materials, museum artifacts [67].

NEs are also generally classified in relation to one or more response parameters of the structure, namely engineering demand parameters (EDPs), and related damage sensitivity of NEs [68]. Seismic actions potentially cause damage to (building) NEs according to four main modalities, as it is depicted in Figure 2.1: a) inertial or shaking effects, causing component motion/oscillation, sliding, rocking or overturning; b) building deformations, damaging interconnected NEs; c) building separations damaging NEs at the seismic building joints due to differential displacements or at the boundaries of the facility; d) interaction between adjacent NEs having relative displacement/response [67]. According to the abovementioned classification, NEs can be grouped into three classes: a) force-sensitive or acceleration-sensitive NEs, where inertial forces or accelerations can be considered as main EDPs, b) displacement-sensitive or interstory-drift-sensitive NEs, where relative displacements/deformations can be assumed as main EDPs, c) combined force/displacement-sensitive NEs, where, both inertial forces/acceleration and relative displacements/deformations can be considered as main EDPs. There might be cases in which NEs are particularly sensitive to alternative or additional EDPs, such as velocities, as it can be observed with regard to rocking-dominated NEs [69]; therefore, these classifications represent the basic reference and might not be exhaustive over the wide range of NE scenarios, especially for components that exhibit complex seismic response, with regard to multiple response and damage mechanisms.

NEs can also be classified as a function of their dynamic parameters. In particular, ASCE 7-16 establishes in relation the fundamental period of the NEs two types: flexible NEs, with a fundamental period larger than 0.06 s; and rigid NEs, with a fundamental period lower than or equal to 0.06 s. Finally, NEs can be defined according to the way they are built/assembled, e.g., the Italian code [2] defines two categories: built on-site NEs and assembled/mounted on-site NEs.

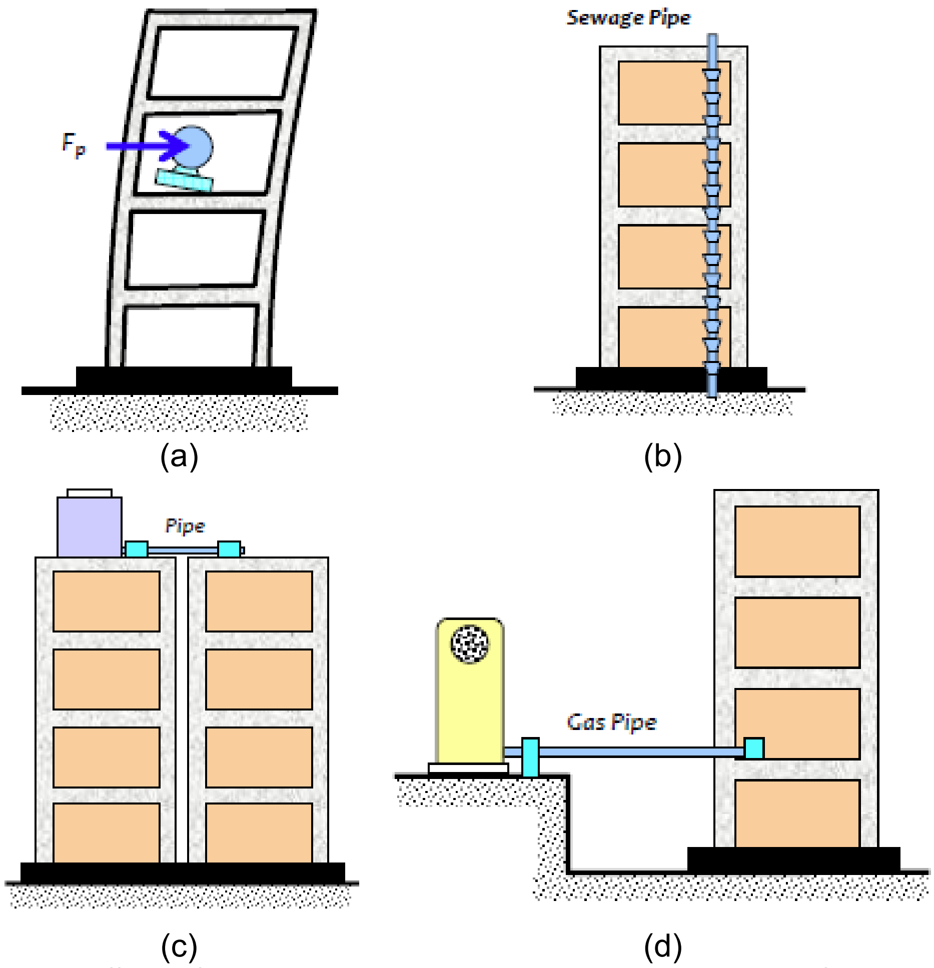

Figure 2.1: Effects of seismic motion on NEs: (a) inertial, (b) imposed deformations by building, (c) building separations, and (d) elements outside connected to inside the building [70].

2.3 Testing protocols

2.3.1 Outline

Seismic tests are typically classified into quasi-static and dynamic according to the testing procedure and protocol. Single-floor dynamic tests define the traditional and most common dynamic tests, which are often carried out by means of shake tables. More recently, multi-floor dynamic testing has been developed to replicate the actual seismic demands on NEs in a more accurate manner; in particular, this novel testing approach allows to account for the response of the hosting buildings/facilities (in terms of both acceleration and deformation inputs) towards more representative and consistent seismic tests on NEs.

2.3.2 Quasi-static testing protocols

Quasi-static tests are often performed to test displacement-sensitive NEs, or more in general, to NEs that are sensitive to deformations. Examples of NEs that may be tested in accordance with this protocol include infill/cladding/partition panels (along their in-plane directions), piping and electrical network systems, fixed ladder systems, technical equipment fixed to multiple stories, and other systems that are connected to multiple building parts that might exhibit relative displacement under earthquake actions.

Quasi-static tests are typically carried out by implementing cyclic loading procedures, i.e., slow load/deformation cycles, which can be conducted in force or deformation control (or a combination of the two when accurate force and deformation da-ta are needed). Overall, it is preferred to adopt a deformation-controlled testing protocol, except when forces govern the response of the NEs or the deformation parameter is difficult to control. Quasi-static protocols should not be applied to NEs whose behavior is significantly affected by dynamic effects, or whose behavior is velocity-sensitive, including strain-rate sensitive NEs.

FEMA 461

FEMA 461 [71] provides a protocol for quasi-static cyclic testing of structural members and NEs. The testing protocol provides technical guidance for the achievement of the following sequential objectives: (a) identification of relevant damage states (DSs); (b) identification of EDPs that are well correlated with DSs identified in (a); and (c) testing of NEs according to a well-defined testing plan and loading protocol to establish quantitative correlations between DS achievement and EDP thresholds. The protocol provides information regarding the following technical aspects: (1) procurement, fabrication, and inspection of testing specimens; (2) extrapolation and interpolation to similar components; (3) laboratory standards, including accreditation criterion, actuators, instruments, data acquisition systems, and safety procedures; (4) test plan and procedures; (5) testing directions and loading control parameters (including de-formation-controlled and force-controlled testing); (6) loading histories, including unidirectional testing, bidirectional testing, and force-controlled loading; and (7) reporting. FEMA 461 protocol could be used to assess fragility data and to derive constituent force-deformation properties and hysteretic data. In the following, deformation- and force-controlled testing protocols are described.

Deformation-controlled testing protocol. Deformation-controlled tests are typically preferred to force-controlled ones since deformation is often better correlated than force with seismic response of displacement-sensitive elements; in particular, differently from force-controlled procedures, deformation-controlled testing typically allows to assess the inelastic response, with particular regard to plastic and degrading behavior. The deformation control EDP may be a displacement or other suitable deformation quantity, e.g., a rotation. This parameter should be correlated with a building deformation parameter, such as interstory drift ratio (IDR), that can be estimated, in terms of seismic demand scenarios, by structural analysis. The testing deformation increment should be selected in a manner that ensures reliability and robustness to the experimental test. Especially, the deformation increment should be sufficiently small that: a) dynamic effects are negligible; b) the value of the deformation parameter, at which onset of the various DSs of interest initiate, is clearly identifiable; c) thermal effects due to work-hardening are not significant, and d) power requirements are reasonable. Moreover, the deformation increment should be sufficiently large that: a) the duration of the test is not excessive; b) material creep is not a significant effect (unless creep is not consistent with investigated DSs), and c) the number of cycles experienced by the component at the onset of significant DSs is of the same order of magnitude as that experienced by real components in buildings subjected to strong earthquake motion. Particular care should be taken to avoid the introduction of low-cycle fatigue behavior that is unlikely to be experienced by real components in buildings.

The parameters required to define the loading history in terms of deformation-controlled testing protocol are the smallest targeted deformation amplitude of the loading history (Δ_0), maximum target deformation amplitude of the loading history (Δ_m), number of steps (or increments) in the loading history (*n*), generally 10 or larger, and amplitude of the cycles (a_i). Δ_0 must be safely smaller than the amplitude at which the lowest significant DSs is first observed; a recommended value (in terms of IDR) is 0.0015. Δ_m is an estimated value of the imposed deformation at which the most severe damage level is expected to initiate; a recommended value for this amplitude (in terms of IDR) is 0.03. The loading history consists of repeated cycles of step-wise increasing deformation amplitudes. Two cycles at each amplitude shall be completed. The amplitude a_{i+1} of the step *i+1* is given by Equation (4.1):

$$a_{i+1} = c\, a_i \tag{4.1}$$

where a_i is the amplitude of the i^{th} and *c* is a parameter suggested to be assumed equal to 1.4.

If the specimen has not reached the final damage state at Δ_m, the amplitude shall be increased further by the constant increment 0.3 Δ_m. Figure 2.2a shows the displacement loading history for the case $a_n = \Delta_m$, $a_1 = 0.0048\ \Delta_m$, and $n=10$. If bidirectional testing is required to evaluate the component performance, the elliptical pattern shown in Figure 2.2b should be followed.

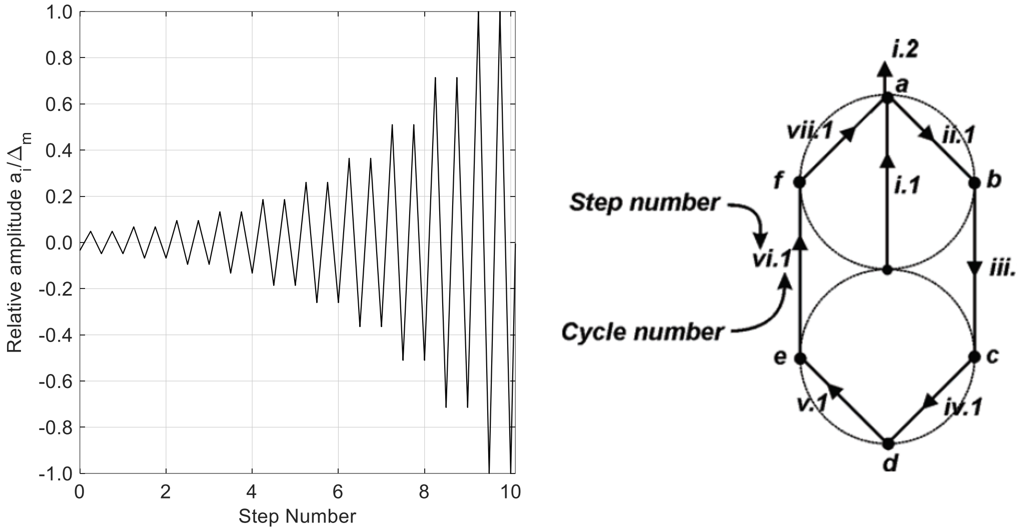

(a) (b)

Figure 2.2: FEMA 461 displacement-controlled quasi-static protocol: (a) loading history considering {a_n,a_1,n} equal to {Δ_m, 0.0048 Δ_m,10} and (b) displacement orbit for bidirectional loading test.

Force-controlled testing protocol. Force-controlled testing should be performed if a force quantity controls the performance of NE, or if a suitable deformation parameter cannot be found/assessed. The force-controlled EDP shall be a measurable and controllable parameter (typically, a force) that relates well to a force-based demand quantity that can be predicted by structural analysis. The force increment should be sufficiently small that: a) dynamic effects are negligible; b) the applied force initiating the various damage states of interest must be identifiable; c) thermal effects due to work hardening are not significant, and d) power requirements are not unreasonable. Finally, the force increment should be sufficiently large that: a) the duration of the test is not excessive, and b) material creep is not a significant effect (unless creep is considered to be part of the damage states of interest).

The reference value on which to base the amplitudes of individual cycles is the maximum force to which NE (or part) may be subjected to in a severe earthquake. Since the force demands strongly depend on characteristics/features of NE, building to NE interaction, building, site, it is impossible to develop a generally applicable force-based loading protocol. Therefore, the following guidelines should be employed to develop case-specific protocols.

Forces are consequences of deformations, and the deformations, in relative magnitude, can be described by Equation (4.1) and Figure 2.3a. If the monotonic force-deformation response of the force-sensitive NE is known (e.g., Figure 2.3a), then the displacement-based loading history (Figure 2.2a) and the NE response can be combined to develop a force-based loading history to be applied to NE (Figure 2.3b).

(a)

(b)

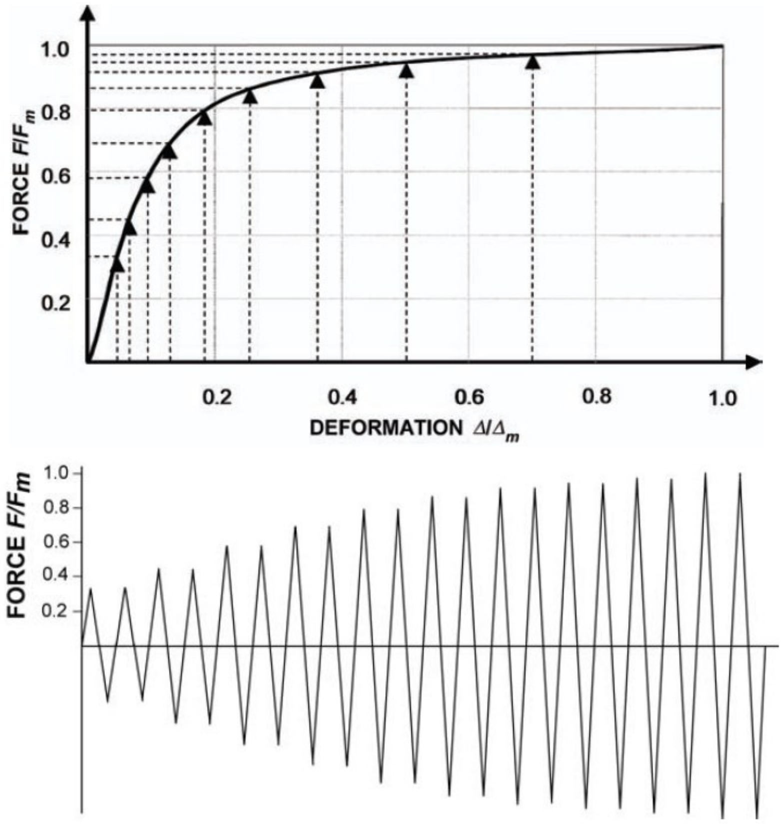

Figure 2.3: FEMA 461 force-controlled quasi-static protocol: (a) force-displacement NE response and (b) de-rived loading history.

CUREE-Caltech

CUREE-Caltech testing protocol [72] was developed by the Consortium of Universities for Research in Earthquake Engineering (CUREE) and California Institute of Technology (Caltech) in the framework of the extensive CUREE-Caltech Woodframe Project. This document provides recommendations for a protocol for quasi-static experimentation on components of wood-frame structures. Materials of interest are wood (for framing and panel elements), plaster and gypsum (for panel elements), and steel (light gauge metal studs, hold-downs, and nails). Testing protocols are generally concerned with the construction and instrumentation of test specimens, the planning and execution of experiments, the loading history to be applied to a test specimen, and the documentation of experimental results. In this document, the emphasis is on the development and documentation of loading histories for deformation and force-controlled component testing. The CUREE-Calthech protocol gives significant importance to the development of loading histories for force- and deformation-controlled tests. The provided data are based on the findings of inelastic time history analysis of hysteretic systems under a wide range of ground motions (ordinary and near-field records). The protocol loading inputs are derived by processing the abovementioned results through damage accumulation concepts and criteria.

The primary aim of this loading history is to evaluate the capacity level seismic performance of NEs subjected to ordinary earthquake records with a probability of exceedance equal to 10% within 50 years. Loading histories associated with smaller events prior to the capacity level event are included in the deformation history. Similarly, to FEMA 461 protocol, deformation-controlled quasi-static cyclic testing should be preferred to force-controlled one, and this latter could be used only for NEs whose behavior is controlled by forces rather than deformations or if a suitable deformation EDP has not been found, which, in general, correspond to NE governed by brittle failure modes; both deformation- and force-controlled protocols are defined.

Figure 2.4 shows the loading protocol associated with a representative cyclic load test. The protocol input is defined by variations in deformation amplitudes, using the reference deformation Δ as an absolute measure of deformation amplitude. The history consists of initiation cycles, primary cycles, and trailing cycles. Initiation cycles are executed at the beginning of the loading history; they serve to check loading equipment, measurement devices, and the force-deformation response at small amplitudes. A primary cycle is a cycle that is larger than all the preceding cycles and is followed by smaller cycles, which are called trailing cycles. All trailing cycles have an amplitude that is equal to 75% of the amplitude of the preceding primary cycle. All cycles are symmetric in terms of positive and negative amplitudes. Deformation control should be considered throughout the experiment.

The reference deformation is the maximum deformation that NE is expected to sustain according to a prescribed acceptance criterion and assuming that the proposed basic loading history has been applied to the test specimen. This is an expected measure of the deformation capacity of the specimen, which should be estimated prior to performing the tests. This capacity could be assessed according to past data or previous experience, monotonic test, or a consensus value that may prove to be useful for comparing tests of different details or configurations. The reference threshold Δ may depend on the specific element to test or may be fixed for a specific testing program according to the following steps. 1) Performing monotonic tests, which provide data on the (monotonic) deformation capacity, Δ_m; this capacity corresponds to the deformation at which the load is reduced by 20% from the maximum applied load, as it is depicted in Figure 2.5 [72]. 2) Using a specific fraction of Δ_m, i.e., $\gamma\Delta_m$, as the reference deformation for the basic cyclic load test. The factor γ accounts for the difference deformation capacity between the monotonic and the cyclic testing procedures in which cumulative damage will lead to earlier deterioration in strength; γ is suggested to be assumed equal to 0.6.

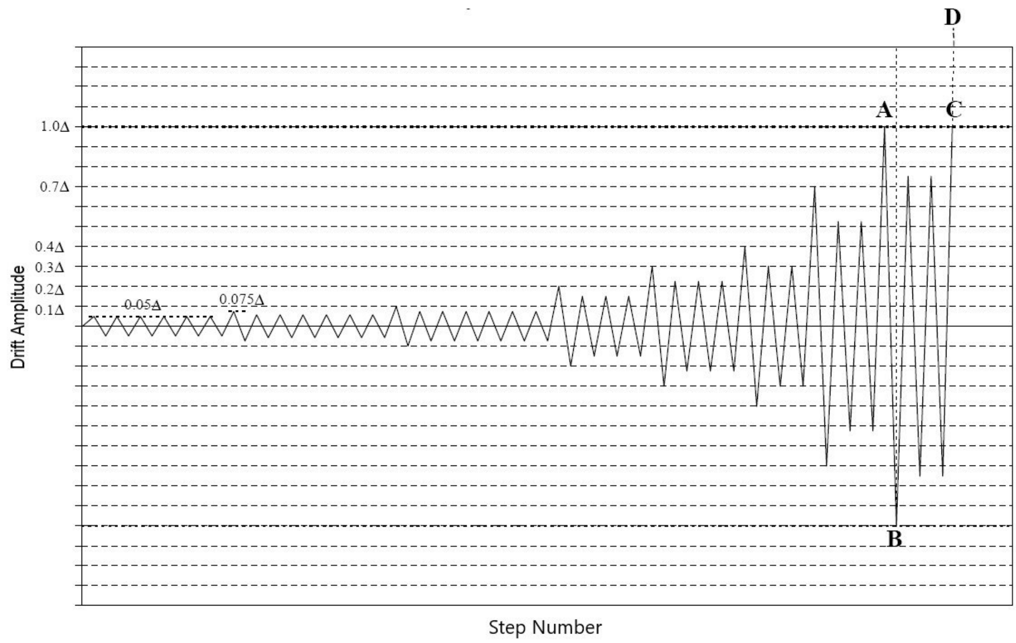

Figure 2.4: Loading history for basic deformation controlled quasi-static cyclic test [72].

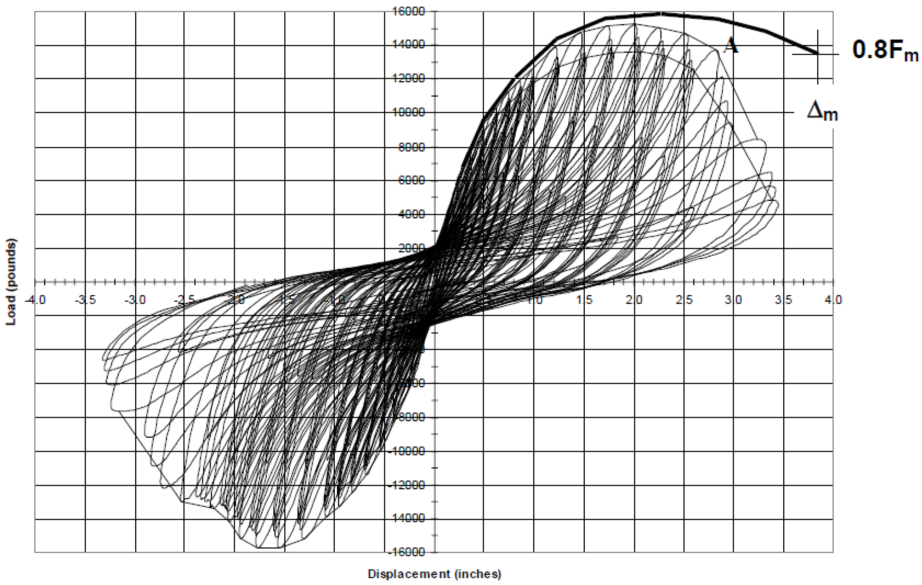

Figure 2.5: Definition of Δm and its relation to a cyclic test [72].

The CUREE protocol proposes three other versions of the loading history protocol: 1) an abbreviated version of the basic protocol input, based on a smaller number of cycles; 2) a simplified version of the basic protocol input, having the same amplitude of the trailing cycles of preceding primary cycle; and 3) a protocol input associated for near-fault records (i.e., seismic hazard with a 2% probability of exceedance within 50 years).

AAMA 501.4 and 501.6

American Architectural Manufacturers Association (AAMA) has developed two test methods: AAMA 501.4 e 501.6 [73]. AAMA 501.4-01 provides a means for evaluating the performance of curtain walls and storefront wall systems when subjected to specified horizontal displacements along the in-plane direction. The method does not account for dynamic, torsional, or vertical response. This method is complementary to AAMA 501.6, which considers ultimate limit state for architectural glass included in the wall or partition system, accounting for fallout from window wall, curtain and storefront walls. Differently, AAMA 501.4 aims to address the seismic serviceability limit state behavior of wall systems and relevant changes or variations in terms of functioning/operation (e.g., air and water leakage rates), as a result of statically applied, in-plane (horizontal) racking displacements.

AAMA 501.4 establishes the procedures to evaluate the performance of curtain walls and storefronts under laboratory conditions, when subjected to horizontal dis-placement intended to represent the effects of an earthquake or a significant wind event. The design displacement shall be determined according to the predicted inter-story deformation of the subject building. For multi-story mock-ups, the displacement between levels may vary due to different story heights. Unless otherwise specified, the design displacement shall be 0.010 times the largest adjacent story heights. The dis-placement shall be measured at the movable floor element, not at the specimen. Prior to conducting the displacement tests, the test specimen shall be, at a minimum, assessed for serviceability by conducting air leakage and water penetration tests. The air leakage and water penetration tests shall be conducted at the differential pressures specified for the application/functioning conditions. Moreover, the air leakage and water penetration tests are repeated after the displacement tests to evaluate the change in functionality of the wall system. In this case, the static displacement is evaluated considering a value equal to 1.5 times the design displacement used in the previous step.

AAMA 501.6 is applicable to any type of glass panel installed within wall system framing members, including the associated glazing elements (setting blocks, gaskets, fasteners, etc.). In the design of building wall system to resist earthquakes, in case glass-to-frame contacts cannot be avoided, or if the glass elements are not highly resistant to earthquake induced glass fallout, ASCE calls for the determination of $\Delta_{fallout}$, i.e., the relative seismic displacement (drift) causing glass fallout from the curtain wall, storefront or partition; $\Delta_{fallout}$ should be estimated through dynamic tests. In particular, this testing method aims at defining a dynamic racking crescendo test for determining $\Delta_{fallout}$. According to the ASCE 7-16, dynamic tests are not required when adequate clearance exists between glass edges and wall frame glazing pockets to prevent contact/interaction under seismic design displacements in the main structural system of the building.

AAMA 501.6 test method involves mounting individual fully glazed wall panel specimens on a dynamic racking test apparatus; the test loads the specimen through sinusoidal racking motions according to gradual progressive increasing racking amplitudes (Figure 2.6). Dynamic racking frequencies are equal to 0.8 Hz at lower racking amplitudes (i.e., ≤ ±75 mm) and equal to 0.4 Hz at higher racking amplitudes (i.e., > ±75 mm). The racking amplitude associated with earlies glass fallout is assumed to de-fine the fallout condition for that test specimen. The lowest value of racking displacement causing glass fallout for the three specimens tested by AAMA 501.6 is the reference value of fallout for that particular wall system glazing configuration. This value of fallout is referred to by ASCE 7-16 for architectural glass.

(a)

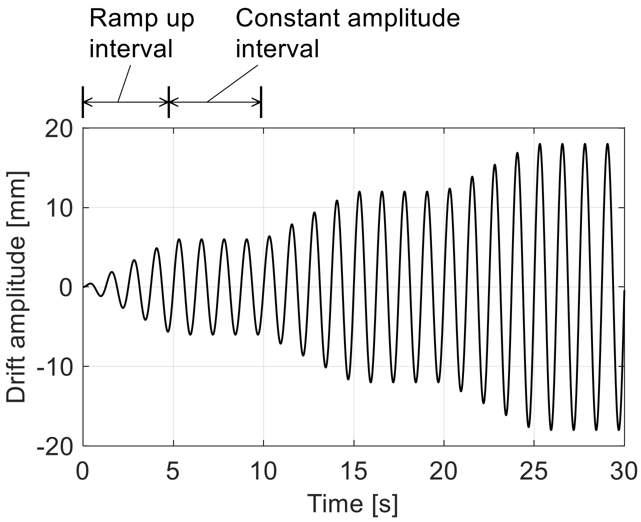

(b)

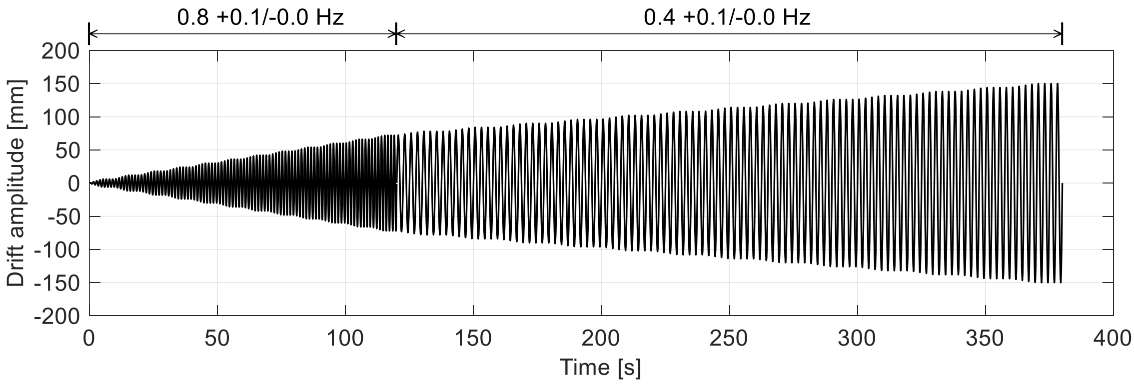

Figure 2.6: Drift time history for dynamic crescendo test: a) first 30 s and b) full time history (AAMA 501.6 2002).

2.3.3 Single-floor dynamic testing protocols

Single-floor dynamic tests are frequently performed to test acceleration-sensitive NEs. Examples of NEs that may be tested in accordance with this protocol include cabinets, storage racks, bookcases, and shelves, appliances (refrigerators, washing machines, diesel generators), hoardings anchored on rooftops, antennas communication towers on rooftops), horizontal projections (sunshades, canopies, and marquees), storage ves-sels, mechanical equipment (boilers and furnaces, HVAC equipment), hospital cabi-nets, and museum artifacts.

Single-floor dynamic tests are generally performed through a shake table or earthquake simulator, which is usually characterized by one or more degrees of free-dom (translational and rotational). Tests are conducted by assigning input signals to the earthquake simulator, which depending on different protocols may be generated differently (artificial or real earthquakes). Earthquake simulators often have perfor-mance limitations in terms of acceleration, velocity, displacement, and frequency range, so the assigned input signals must be adjusted/modified to be compatible with these limitations. However, the input signals must meet spectral compatibility condi-tions required by the testing protocols.

FEMA 461

FEMA 461 [71] establishes a recommended protocol for shake table testing of NEs to determine fragilities according to PBEE approach. This protocol is intended to assess the seismic performance of NEs whose behavior is affected by the dynamic response of the component itself, or whose behavior is velocity-sensitive, or sensitive to strain-rate effects. The protocol includes the procedures and types of testing, test plan, input motion, test equipment and instrumentations, and information on the test report. The first step of the testing procedure includes 1) preliminary inspection and functional verification of the test specimen and 2) definition of functional performance and damage states. In particular, before testing, the test specimen should be examined to verify its functional performance, and appropriate DSs should be defined. Finally, a preliminary estimate should be made of the excitation frequency and intensity expressed in peak spectral acceleration at the component natural frequency, at which each relevant DS is expected to occur.

The test plan of the FEMA 461 protocol includes three types of tests: 1) system identification tests; 2) seismic performance evaluation tests and 3) failure tests. System identification tests should be conducted to identify the dynamic characteristics of the test specimen considering the undamaged conditions (prior to the seismic performance evaluation test) and the evolution along the damage evolution (along the seismic performance evaluation test program). The dynamic properties to estimate include natural frequencies, equivalent fundamental modal viscous damping ratios, and mode shapes. In particular, FEMA 461 protocol establishes that identification tests should be conducted along each principal direction of the test specimen before and after each of the performance evaluation tests and failure tests. The dynamic identification tests can be carried out selecting a test type among four types of tests: white noise tests, single-axis acceleration-controlled sinusoidal sweep tests, resonance tests, and static pull-back tests.

Seismic performance evaluation tests aim at assessing the performance of the specimen with regard to minor to moderate damage conditions, considering an artificial acceleration input and according to an incremental intensity procedure. Failure tests consist of seismic evaluation tests carried out considering higher intensities, in order to assess severe damage and (incipient) failure of the specimen or to assess DSs associated with potential safety risk. Seismic performance evaluation tests and failure tests description and related results should be documented for each intensity level to provide data for fragility assessment.

The input motion parameter used to define intensity should be the peak spectral acceleration corresponding to the natural frequency of the specimen. FEMA 461 protocol establishes that at least three different shaking intensities should be used for the performance evaluation test, and in all cases, a 25% increase in intensity should be the minimum step size between intensity levels. Moreover, the input motions of the performance evaluation and failure tests should be applied along the principal axes of the test specimen by performing triaxial tests or biaxial tests (along a horizontal and vertical direction) considering both horizontal directions (double biaxial tests); if the effect of vertical motion on the seismic response of the test specimen is negligible, biaxial horizontal tests can be performed. The procedure for generating compliant seismic in-puts and provided inputs are based on work done by the U.S. Army Construction Engineering Research Laboratory [74]. In particular, the recommended shake table motions are narrow-band random sweep acceleration records, with scaled amplitudes depending on the sweep frequency, producing motions that have relatively smooth response spectra amplitudes. For records generated for this protocol, the bandwidth is 1/3 octave, and the center frequency of the records sweeps from 0.5 Hz up to 32 Hz, at a rate of 6 octaves per minute or a total signal duration of 60 s. The vertical motion is scaled to have a response spectrum that is approximately 80% of horizontal ones. The response spectra should be defined considering 5% damping. The signal shall be scaled in order to have (a) acceleration response spectra amplitude equal to about 1 g within 2 - 32 Hz and (b) the displacement response spectra would be approximately uniform below 2 Hz. Figure 2.7 shows the shake table motions as they are provided by FEMA 461: (a) horizontal (longitudinal and transversal) and vertical acceleration time histories and (b) related response spectra (5 % damped).

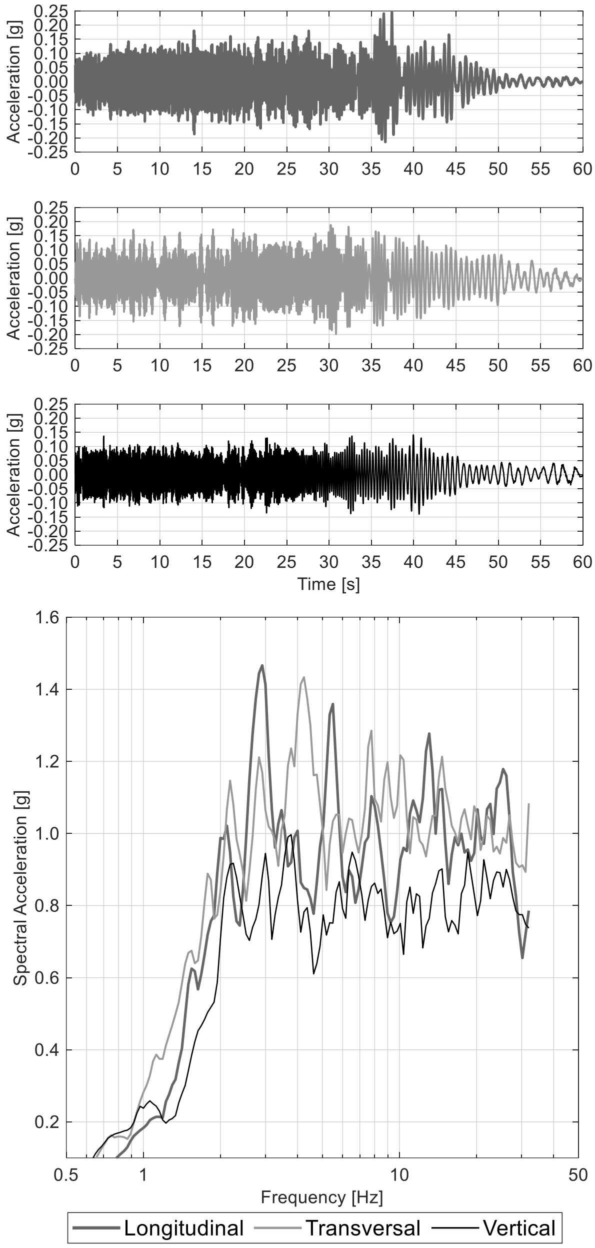

Figure 2.7: Recommended shake table motions according to FEMA 461: a) horizontal (longitudinal and transversal) and vertical input motions and (b) acceleration response spectra, 5% damped.

ICC-ES AC156

The aim of AC156 testing protocol [16] is to establish criteria for seismic qualification/certification of NEs using shake table tests. In particular, these acceptance criteria are applicable for architectural, mechanical, electrical, and other nonstructural systems, components, and elements anchored to structures. This protocol is applicable for shake table testing of NEs that have fundamental frequencies greater than or equal to 1.3 Hz and is not intended to evaluate the effects of relative displacements on NEs. AC156 also reports the formal requirements for issuing the seismic certification.

The testing requirement is to perform qualification testing in all three principal axes. When it is not possible to conduct triaxle testing due to facilities limitations, bi-axial or uniaxial tests may be conducted by the following guidelines. (1) Biaxial tests shall be performed in two phases. One of two horizontal shakings and the vertical shaking of the specimen for a fixed specimen configuration shall be considered in the first phase of the test; in the second phase, the same specimen must be rotated 90 degrees about the vertical axis. (2) Uniaxial tests shall be performed in three distinct, with the test specimen rotated after each phase, such that all three principal axes of the specimen have been tested.

AC156 defines two types of tests: resonant frequency search tests and seismic simulation tests. The former is for determining the resonant frequencies and damping ratios along each orthogonal axis of the test specimen, whereas the latter are for seismic performance evaluation and certification purposes. The input signal of the resonant frequency search test shall be a low-level amplitude single-axis sinusoidal sweep from 1.3 to 33.3 Hz. In particular, the peak input should be 0.1 ± 0.05 g, but a lower input level can be used to avoid specimen damage. Finally, the sweep rate shall be two octaves per minute, or less, to ensure adequate time for maximum response at the resonant frequencies. The input signal for seismic simulation tests shall be determined for replicating the combined effects of the horizontal and vertical earthquakes. Required response spectra (RRS) associated with both horizontal and vertical directions are shown in Figure 2.8; RRS shall be developed based on the formula for total design horizontal force, F_p, provided by ASCE 7-16, shown in Equation (4.2):

$$\frac{F_p}{W_p} = \frac{0.4\, S_{DS}\, a_p}{\frac{R_p}{I_p}}\left(1 + 2\,\frac{z}{h}\right) \tag{4.2}$$

and using a damping value equal to 5 % of critical damping.

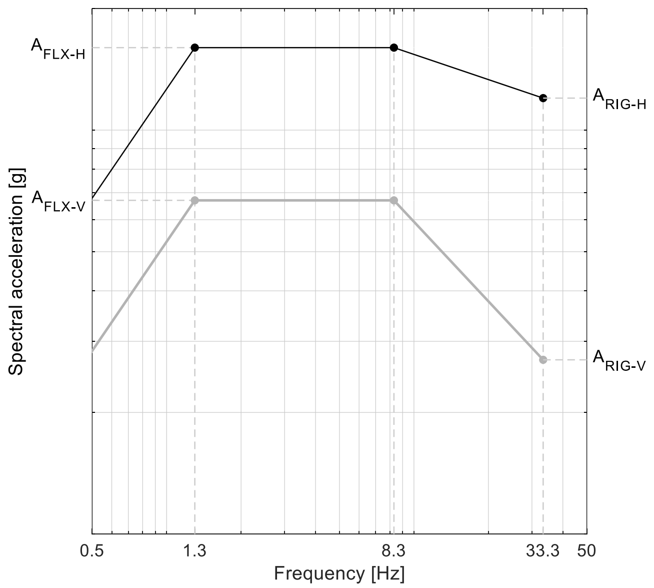

Figure 2.8: Required response spectra in the horizontal (black) and vertical (grey) directions according to AC156, 5% damped.

In Equation (4.2), F_p is total design horizontal force applied in the center of mass or distributed according to the mass distribution of the NEs; W_p is the weight of the NE; Rp/Ip is the ratio of the component response modification factor Rp to the component importance factor Ip. Rp/Ip is considered to be a design reduction factor to account for inelastic response and represents the allowable inelastic energy absorption capacity of the component's force-resisting system; a_p is the component amplification factor that varies from 1.00 to 2.50; *z* is the height in the structure of the point of attachment of the element concerning the base; *h* is the average roof height of the structure for the base. The height factor ratio *z/h* accounts for above grade level component installations within the primary supporting structure and ranges from zero at grade level to one at roof level, essentially acting as a force increase factor to recognize building amplification as you move up within the primary structure; S_{DS} is the design spectral response acceleration parameter at short periods, while the product $0.4\,S_{DS}$ represents the point at period T = 0 s of the design response spectrum. S_{DS} varies depending on geographic location and site soil conditions ASCE 7-16 [3].

During the seismic simulation test, the test specimen will respond to the excitation and inelastic behavior might naturally occur. Therefore, the ratio Rp/Ip shall be generally set equal to 1, which is indicative of an unreduced response. a_p acts as a force increase factor by accounting for probable amplification of response associated with the inherent flexibility of the NEs; this parameter shall be taken from the formal definition of flexible and rigid elements. By definition, NE is considered flexible (maximum amplification $a_p = 2.5$) for fundamental frequencies less than 16.7 Hz, corresponding to the amplified region of the RRS. For fundamental frequencies greater than 16.7 Hz, NE is considered rigid (minimum $a_p = 1.0$), corresponding to the zero peak acceleration (ZPA) range. This results in two normalizing acceleration factors, that when combined, define the horizontal component certification RRS, as reported in Equations (4.3) and (4.4):

$$A_{RIG-H} = 0.4\,S_{DS}\left(1 + 2\frac{z}{h}\right) \tag{4.3}$$

$$A_{FLX-H} = S_{DS}\left(1 + 2\frac{z}{h}\right) \leq 1.6 S_{DS} \tag{4.4}$$

where A_{FLX-H} is limited to a maximum value of 1.6 times S_{DS}.

RRS for the vertical direction shall be developed based on two-thirds of the ground-level base horizontal acceleration. Moreover, *z/h* may be taken to be 0 for all attachment heights, which results in Equation (4.5):

$$A_{RIG-V} = \frac{2}{3}A_{RIG-H} = 0.27 \cdot S_{DS};\; A_{FLX-V} = \frac{2}{3}A_{FLX-H} = 0.67 \cdot S_{DS} \tag{4.5}$$

The input signals for seismic simulation tests shall be nonstationary broadband random excitations having an energy content ranging from 1.3 to 33.3 Hz, and a bandwidth resolution equal to one-third or one sixth-octave, depending on whether the synthesizer is analog or digital, respectively. The total duration of the input motion shall be 30 s, with the nonstationary character being synthesized by an input signal build-hold-decay envelope. The build time includes the time necessary for acceleration ramp-up, the hold time represents the earthquake strong-motion time duration, and the decay time includes the de-acceleration ring down time. The input duration of the time history tests shall contain at least 20 s of strong motion.

AC156 establishes the criteria and rules for the analysis of the test response spectrum (TRS) with regard to RRS, i.e., spectrum-compatibility criteria. TRS shall be computed using either justifiable analytical techniques or response spectrum analysis equipment using the control accelerometers located at the specimen base. TRS shall be calculated using a damping value equal to 5% of critical damping. According to the spectrum-compatibility rules, TRS must envelop the RRS based on a maxi-mum-one-sixth octave bandwidth resolution over the frequency range from 1.3 to 33.3 Hz. It is recommended that the TRS should not exceed the RRS by more than 30% over the amplified region of the RRS. The signal reproduced by the table in the course of the testing, TRS may not fully envelop the RRS. The general requirement for a retest may be exempted if the following criteria are met. In case it can be shown by the use of the resonance search that no resonance response phenomena exist below 5 Hz, TRS is required to envelop the RRS only down to 3.5 Hz (i.e., not along lower frequencies). When resonance phenomena exist below 5 Hz, TRS is required to envelop the RRS only down to 75% of the lowest frequency of resonance. A maximum of two of the one-sixth-octave analysis points of TRS may fall below RRS for each frequency range (i.e., frequencies less than or equal to 8.3 Hz and greater than 8.3 Hz) by 10% or less, provided the adjacent one-sixth-octave points are at least equal to RRS.

AC156 protocol may be also used as multi-floor dynamic testing protocol as performed in [34,35,41,75] and described in Section 2.3.4. This extension could be also applied to other single-floor dynamic testing protocols, implementing procedure consistent with [34,35,41,75].

BS ISO 13033

The British Standards Institution [15] defines the procedures for the definition of the seismic actions and verification of NEs seismic capacity within ISO 13033 standard. ISO 13033 does not specifically cover industrial facilities, including nuclear power plants, since these are addressed by other International Standards. However, the principles in this standard can be applied to the definition of seismic actions for NEs in such facilities. This code establishes that evaluation of NEs for seismic actions is required when any of the following condition applies: a) NEs pose a falling hazard; b) failure of NEs can impede the evacuation of the building; c) NEs contain hazardous materials; d) NEs are necessary to the functioning of essential facilities after the event, and e) damage to NEs represents a significant financial loss. The behavior of NEs shall be evaluated and verified against the specified performance objectives for the ultimate limit state (ULS) and the service limit state (SLS). The following verification methods are allowed: a) design analysis; b) seismic qualification testing; c) procedures that determine acceptable seismic capacity based on documented experience from past earthquakes (experience data); d) a combination of a), b) and c).

To verify the adequacy of NEs by design analysis, a structural analysis of NEs should be performed, including their anchorage and bracing, considering using the design lateral forces defined for ULS and SLS. Each member and connection force resulting from the analysis should be compared with the design capacity of NE individual member, connection brace, or anchorage, provided by regional and national regulations and codes to verify that the capacity exceeds the demand. The design lateral seismic force of NEs attached at level *i* of the building structure for ULS, $F_{D,p,u,i}$, is determined as reported in Equation (4.6):

$$F_{D,p,u,i} = \gamma_{n,E,p} \cdot k_{D,p} \cdot F_{E,p,u,i} \tag{4.6}$$

The design lateral seismic force of NEs attached at level i of the building structure for SLS, $F_{D,p,s,i}$, is determined according to Equation (4.7):

$$F_{D,p,s,i} = \gamma_{n,E,p} \cdot F_{E,p,s,i} \tag{4.7}$$

where $F_{E,p,i}$ is the design lateral seismic force of the NEs attached at level *i* of the building structure for ULS or SLS; $\gamma_{n,E,p}$ is the importance factor related to the required seismic reliability of the NEs; $k_{D,p}$ is NE response modification factor to be specified according to its ductility and overstrength.

The elastic equivalent static seismic forces for ULS and SLS earthquake levels are given as Equation (4.8) reports:

$$F_{E,p,i\ (u\ or\ s)} = k_{I(u\ or\ s)} \cdot k_{H,i} \cdot k_{R,p} \cdot F_{G,p} \tag{4.8}$$

where $k_{I(u\ or\ s)}$ is the ground motion intensity factor to be provided by regional and national standards; $k_{H,i}$ is the floor response amplification factor at the attachment at level *i*; $k_{R,p}$ is the NE amplification factor considering the effect of the natural periods of the NEs and the building; $F_{G,p}$ is the weight (*mg*) on the NEs.

The ground motion intensity factor corresponds to that used for the supporting building. The ground motion intensity factor ($k_{I(u\ or\ s)}$) is given by Equation (4.9):

$$k_{I(u\ or\ s)} = k_Z \cdot k_{E,(u\ or\ s)} \tag{4.9}$$

where k_Z is the seismic zoning factor and $k_{E,(u\ or\ s)}$ is the seismic ground motion intensity for ULS or SLS.

The floor response amplification factor of the building structure at the attachment location at level i ($k_{H,i}$) is related to the ratio between the maximum floor acceleration over the height of the building and the zero-period acceleration at the base of the building. This factor is primarily a function of a) the natural periods of vibration of the building structure; b) the type of building lateral-load resisting system; c) the relative location of the point of attachment of the NEs to the average roof elevation of the structure with respect to grade elevation; and d) the inherent damping and degree of inelastic behavior of the building structure which is dependent on the severity of the ground motion. A trapezoidal distribution of floor accelerations within the supporting building may be assumed when simplified static analysis procedures are implemented. This trapezoidal distribution is expressed by Equation (4.10):

$$k_{H,i} = \left[1 + \alpha \frac{z_i}{H}\right] \tag{4.10}$$

where α is a parameter that is a function of the type of lateral-load resisting system ($\alpha \leq 2.5$); i is the level in the building structure of the point of attachment of the NEs with respect to grade elevation ($0 \leq i/H \leq 1.0$); z_i is the elevation of level i with respect to grade elevation; H is the average roof elevation of the structure with respect to grade elevation.

The verification of the capacity of NEs by shake table testing is accomplished by subjecting the component to either computed or simulated elastic demand floor motions that are compatible with the floor response spectra determined by RRS. The floor response spectrum is the acceleration response spectrum at the point of NEs attachment. This may be used for NEs with natural frequencies greater than a minimum value, f_0, e.g., reasonably assumed to be between 1.3 and 2.5 Hz. A floor response spectrum is typically obtained from a dynamic analysis of the building structure. Alternatively, for a given component frequency, the floor response spectrum ordinate may be estimated as the ratio of the seismic force at level *i* of the building structure ($F_{E,p,i}$) to the weight of the element ($F_{G,p}$), assuming the importance factor ($\gamma_{n,E,p}$) and the NE response modification factor ($k_{D,p}$) equal to one. In particular, using the previous equations, the ordinates of the normalized horizontal floor response spectrum for a NE located at level *i* of the building structure can be determined as given by Equation (4.11):

$$A_i = F_{E,p,i}/F_{G,p} = k_{I(u\ or\ s)} \cdot k_{H,i} \cdot k_{R,p} \tag{4.11}$$

where $A_i \leq A_{flexible}$ for NEs with first-mode frequencies less than f_2 (assumed to be a value between 10 to 16.67 Hz), and $A_i \geq A_{rigid}$ for NEs with first-mode frequencies greater than f_2.

$A_{flexible}$ and A_{rigid} are determined based on information on the building and NEs dynamic characteristics. In particular, when the building dynamic characteristics are not known, these parameters can be estimated according to Equations (4.12) and (4.13):

$$A_{flexible} = k_{I(u\ or\ s)} \cdot k_{H,i} \cdot k_{R,p,flexible} \tag{4.12}$$

$$A_{rigid} = k_{I(u\ or\ s)} \cdot k_{H,i} \cdot k_{R,p,rigid} \tag{4.13}$$

where $k_{H,i}$ is the floor response amplification factor given by Eq. (4.10); $k_{R,p,flexible}$ is the NEs amplification factor for flexible NEs ($k_{R,p,flexible} > 1.0$); and $k_{R,p,rigid}$ is the NEs amplification factor for rigid NEs ($k_{R,p,rigid} = 1.0$).

When the building dynamic characteristics are known, Equations (4.14) and (4.15) can be used:

$$A_{flexible} = A_{D,I} \cdot k_{R,p,i,flexible} \tag{4.14}$$

$$A_{rigid} = A_{D,I} \cdot k_{R,p,i,rigid} \tag{4.15}$$

where $A_{D,I}$ is the acceleration at level *i* obtained from a dynamic analysis procedure (including torsional response) that utilizes an elastic ground motion response spectrum or time-history analysis. A representative damping ratio for this spectrum is 5%.

For determining the vertical response, a fraction of the values from Equation (4.10) may be used, with $k_{H,i}$ evaluated at grade level for all elevations, i.e., z/h equal to zero. For a given NE frequency, the ratio of vertical to horizontal response can be represented by the parameter β, assumed to vary from 1/2 to 2/3. Figure 2.9 shows RRS related to horizontal and vertical directions according to ISO 13033. The plateau of the RRS extends up to frequency value f_1 (assumed to be a value between 7.5 and 8.3 Hz), whereas the ordinate of the normalized floor response spectrum is equal to A_{rigid} at frequency f_3 (assumed to be 33 Hz).

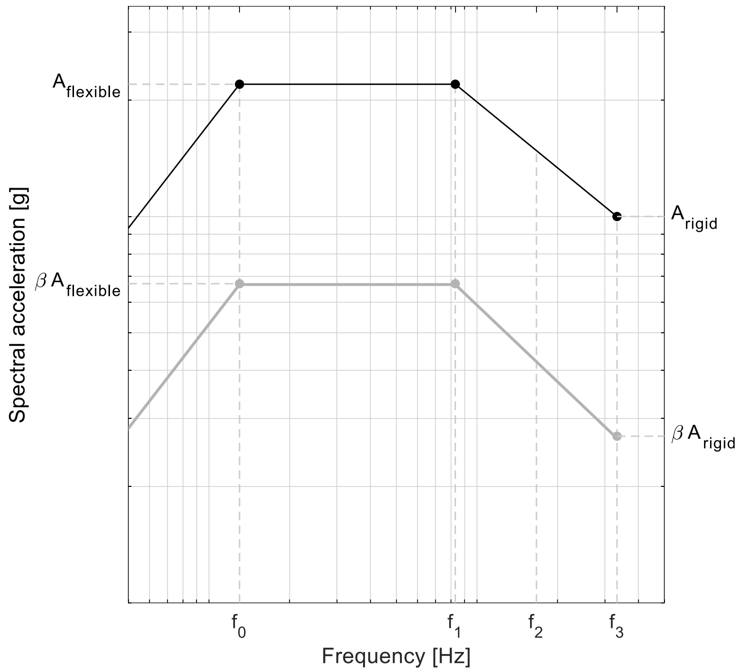

Figure 2.9: Required response spectra in the horizontal (black) and vertical (grey) directions according to ISO 13033, 5% damped.

IEEE 693

The Institute of Electrical and Electronics Engineers and Power & Energy Society (IEEE PES) developed IEEE 693 guidelines [76], which report recommendations for seismic design of substation buildings and structures and seismic design and qualification of substation equipment (i.e., NEs). This code establishes standard methods of providing and validating the seismic capacity and performance of electrical substation equipment. It provides detailed test and analysis methods for selected common equipment types or elements found in substations. IEEE 693 is also intended to provide guidance to the manufacturers of substation equipment regarding seismic design, also with regard to documentation and technical aspects associated with seismic capacity assessment and standardization purposes.

IEEE 693 defines two qualification approaches: performance level qualification approach and design level qualification approach. The response spectra ordinates related to the design level approach are assumed to be half of the performance level ones at any given frequency and level of damping. High, moderate, and low seismic qualification levels are defined for both approaches. Qualification levels are closely related to ZPA, which is assumed to be the acceleration at 33 Hz or greater. For high qualification level, horizontal ZPA associated with the seismic qualification objective is 1.0 g, and the response spectrum associated with the high-performance level is obtained by Equation (4.16):

$$S_a = \begin{cases} 2.288\,\beta\,f \quad for\ 0.0 \le f \le 1.1\ Hz \\ 2.50\,\beta \quad for\ 1.1 < f \le 8.0\ Hz \\ \frac{(26.4\,\beta - 10.56)}{f} - 0.8\,\beta + 1.32 \quad for\ 8.0 < f \le 33\ Hz \\ 1.0 \quad for\ f > 33\ Hz \end{cases}, \tag{4.16}$$

where the factor β is a function of the damping coefficient expressed as a percentage ($d \le 20\%$) and evaluated through Equation (4.17):

$$\beta = \frac{3.21 - 0.68\ \ln(d)}{2.1156} \tag{4.17}$$

For the moderate qualification level, ZPA associated with the seismic qualification objective is 0.5 g and the related response spectrum is assumed to be half the related to the high qualification level. For the low qualification level, there is no horizontal ZPA associated with the seismic qualification level. The low seismic level rep-resents the performance level that can be expected when relatively adequate construction and seismic installation practices are used, when no special consideration is given to the seismic performance of the equipment. The selection of the seismic qualification level is a responsibility of the user and is normally based on an assessment of site geo-physical parameters, risk assessments, and economics. RRS does not include the influence of the dynamic characteristics of the building response. Therefore, one of the following alternatives may be used to account for the effects of building response: 1) de-fining a 2% damped response spectrum that represents the position-specific response within the building to the elastic design spectrum as determined according to the building code; 2) multiplying the RRS by a factor of 2.5. Figure 2.10 shows the RRS for high and moderate seismic performance levels and 5% damped.

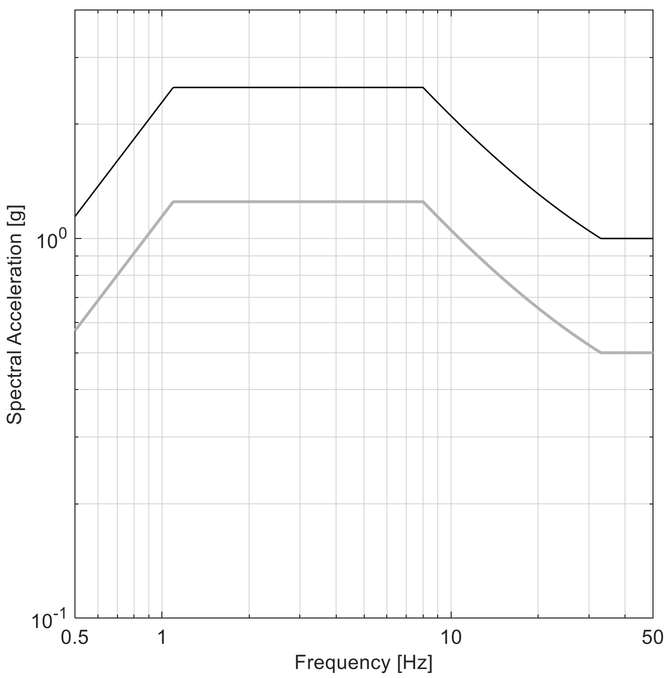

Figure 2.10: Response spectrum required according to IEEE 693 for high (black) and moderate (grey) seismic performance levels, 5% damped.

The equipment or element should be tested/analyzed in its equivalent in-service configuration, including supporting systems. When this is not possible (i.e., in situations that are not practical or economical), a modified input motion or dynamically equivalent structure can be considered. Similarly, to other codes/standard, IEEE 693 defines two types of tests: a) resonant frequency search tests and b) seismic simulation tests. A sine sweep or random noise excitation test shall be used for the frequency search test; frequency search above 33 Hz is not required. No resonant frequency search in the vertical axis is required if it can be shown that no resonant frequencies exist below 33 Hz in the vertical direction. Regarding seismic simulation tests, the test time histories shall be triaxial with the simulation of translational ground accelerations in three orthogonal directions. TRS shall envelop RRS along the two perpendicular horizontal and vertical axes of the equipment, with a response spectrum in the vertical axis that shall have an acceleration of 80% of that in the horizontal axes. The in-put signal of the seismic simulation tests shall have a duration of at least 20 s of strong motion. Acceleration ramp-up time and decay time shall not be included in the 20 s of strong motion. The duration of strong motion shall be defined as the time interval be-tween when the plot of the time history reaches 25% of the maximum amplitude to the time when it falls for the last time to 25% of the maximum amplitude. The theoretical TRS shall be computed at 5% damping and shall include the lower corner point frequency of the RRS (1.1 Hz), for comparison with the RRS. The spectrum matching procedure should be conducted at 24 divisions per octave resolution or higher and shall result in a theoretical response spectrum that is within ±10% of the RRS at 5% damping. The strong part ratio of the table input motion record shall be at least 30% of the total motion duration.

When required to satisfy the operating limits of the shake table, the theoretical input motion record used for testing may be high-pass filtered at frequencies less than or equal to 70% of the lowest frequency of the NE, but not higher than 2 Hz. The table output TRS shall envelop the RRS within a –10%/+50% tolerance band at 12 divisions per octave resolution or higher. A –10% deviation is allowed, provided that the width of the deviation on the frequency scale, measured at the RRS, is not more than 12% of the center frequency of the deviation, and not more than five deviations occur at the stated resolution. For equipment that responds to a single dominant frequency in a given direction, such as instrument transformers, surge arresters, and bushings, TRS spectral acceleration at the equipment as-installed frequency shall not be less than the RRS. Over-testing that exceeds the +50% limit is acceptable in agreement with the equipment manufacturer. Exceedance of the stated upper tolerance limit at frequencies above 15 Hz is generally not of interest and should be accepted unless resonant frequencies are identified in that range.

IEEE 344

IEEE PES provides methods and documentation requirements for seismic qualification of equipment for nuclear power generating stations. In particular, the standard IEEE 344 [14] distinguishes two categories of equipment: seismic Category I and seismic Category II equipment. Seismic Category I equipment is safety-related equipment designed to withstand the effects of the safe shutdown earthquake (SSE) and maintains the specified design function and structural integrity. Seismic Category II equipment is equipment that is not required to function but whose failure could adversely affect the safe shutdown of any Seismic Category I equipment or could result in incapacitating injury to occupants of the control room, which is designed and constructed so that SSE would not cause a failure.

SSE is an earthquake that is based upon an evaluation of the maximum earthquake potential considering the regional and local geology and seismology and specific characteristics of local subsurface material. SSE would produce the maximum vibratory ground motion for which certain structures, systems, and elements are designed to remain functional. These structures, systems, and elements are those necessary to provide reasonable assurance of the following: a) integrity of the reactor coolant pressure boundary; b) capability to shut down the reactor and maintain it in a safe shutdown condition; c) capability to prevent or mitigate the consequences of accidents that could result in potential offsite exposures comparable to applicable regulatory requirements.

IEEE 344 considers multiple methods for seismic qualification purposes, which are grouped into four general categories: a) predict the equipment's performance by analysis; b) test the equipment under simulated seismic conditions; c) qualify the equipment by a combination of test and analysis; d) qualify the equipment through the use of experience data. Each of the abovementioned methods, or other justifiable methods, may be adequate to verify the ability of the equipment to meet the seismic qualification requirements. The choice should be based on the practicality of the method for the type, size, shape, and complexity of the equipment configuration, whether the safety function can be assessed in terms of operability or structural integrity alone and based on the robustness of the conclusions.

This standard includes exploratory vibration tests that are generally not part of the seismic qualification requirements but may be run on equipment to aid in the de-termination of the best test method for qualification or to determine the dynamic characteristics of the equipment. Moreover, the test methods for seismic qualification of the equipment generally fall into three major categories: proof testing, generic testing, and fragility testing. Proof testing is used to qualify equipment for a particular requirement. The equipment shall be subjected to the particular response spectrum, time history, or other parameters defined for the mounting location of the equipment. The equipment is tested to the specified performance requirement and not to its ultimate capability. Generic testing may be considered a special case of proof testing. The objective is to show qualification for a wide variety of applications during one test. The resultant generic RRS typically encompasses a wide frequency bandwidth with relatively high acceleration levels. Finally, fragility testing is used to determine the ultimate capacities of the equipment.

The time history of the input signal for different methods should be stationary, i.e., the frequency/amplitude content of the waveform is statistically constant with time and does not vary significantly during the test. To properly account for vibration build-up and low-cycle fatigue effects, the duration of the strong motion portion of each test should at least be equal to the strong motion portion of the original time his-tory used to obtain the RRS, with a minimum duration of 15 s. For tests using artificial earthquakes, the stationary part of the test defines the strong motion length. The shake table maximum peak acceleration must be at least equal to ZPA of RRS. TRS must envelop RRS over the frequency range for which the particular test is designed to provide a conservative (but not overly so) test-table motion. A 5% damping value is normally assumed. For comparison of the TRS and the RRS (spectrum-compatibility), TRS must be computed with a damping value equal to or greater than that of the RRS and the analysis should be carried out considering 1/6 octave points (or at a narrower band-width resolution). IEEE344 also notes that an input motion that fully envelopes the RRS is occasionally associated with higher acceleration levels at the lowest frequencies, which often require very high shaking table displacement capabilities. Accordingly, the standard proposes that the general requirement for enveloping RRS by TRS can be modified as described in the following. a) If it can be shown by a resonance search that no resonance response phenomena exist below 5 Hz, it is required to envelop the RRS only down to 3.5 Hz. However, excitation must continue to be maintained in the 1 to 3.5 Hz range, also compliance with the capability of the test facility. b) When resonance phenomena exist below 5 Hz, it is required to envelop the RRS only down to 70% of the lowest frequency of resonance. This modification can be made either by high-pass filtering the table motions generated to match the complete RRS or by reducing the RRS at the lower frequencies so that the matching algorithm simply generates a motion without the lower frequency contents [77].

GR-63-CORE Telcordia (ex-Bellcore)

GR-63-CORE testing protocol [78] presents methods, criteria, and rules for seismic tests of telecommunications equipment and systems. During an earthquake, telecommunications equipment is subjected to motions that can over-stress equipment framework, circuit boards, and connectors. The seismic motion and resulting stress on NE depend on the structural characteristics of the building/facility in which NE is contained and the severity of the earthquake. GR-63-CORE shows the map of earthquake risk zones of the U.S. area. In particular, five earthquake risk zones are identified (from 0 to 4, corresponding to no substantial to maximum earthquake risk). The earthquake risk zones are correlated with the expected Richter Magnitude, Modified Mercalli Index, and the expected ground and building accelerations. Seismic qualification tests established by GR-63-CORE follow an approach that takes into account the earthquake risk zone in which the NEs are installed. Thus, NEs that are in earthquake risk zone 4 will need to have a higher level of seismic performance than those that are in lower earthquake risk zones.

The telecommunications equipment shall be tested using a shake table. The acceleration time histories waveform generated by this testing protocol were synthesized from several typical earthquakes and for different building and soil site conditions. The shaking shall be applied in each of the three orthogonal directions of the test specimen, to simulate the conditions that would be encountered in service when building floors apply earthquake motions to the equipment. TRS shall meet or exceed RRS in the frequency range from 1.0 to 50 Hz, considering 2% damping. Moreover, TRS should not exceed RRS by more than 30% in the frequency range of 1 to 7 Hz. A test may be invalid if an equipment failure occurs when the TRS exceeds the RRS by more than 30% in this frequency range. The cut-off of the high-pass filter on the drive signal shall not exceed 0.20 Hz, while the cut-off of the low pass filter on the drive signal shall not be below 50 Hz. TRS shall be verified at one-sixth octave (logarithmically spaced) frequencies from 0.5 to 50 Hz. If a digital analyzer is used, the digitizing rate shall be larger than or equal to 200 Hz with a total storage capacity larger than or equal to 30 s, in real-time. GR-63-CORE defines RRS as a function of the earthquake risk zones considered for seismic qualification of NEs. Figure 2.11 shows RRS for the four earthquake risk zones.

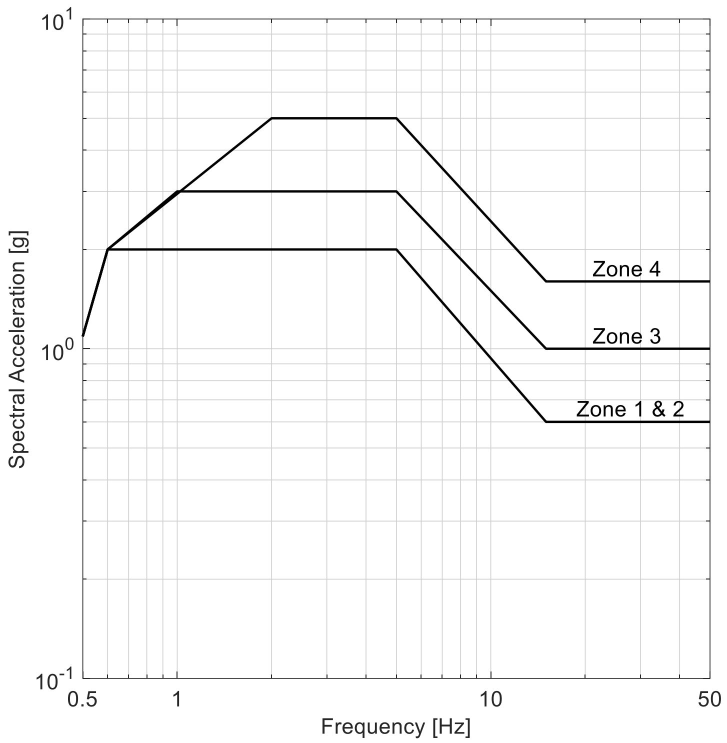

Figure 2.11: Required response spectrum according to GR-63-CORE for the four earthquake risk zones, 2% damped.

RG 1.60

Regulatory Guide 1.60 [79] of the U.S. Nuclear Regulatory Commission (USNRC) establishes a guideline to define target spectra for seismic design of structures, systems, and elements of nuclear power plants. The horizontal and vertical RRS are related to a PGA of 1.0 g and peak ground displacement (PGD) equal to 0.91 m. For different site conditions, RRS should be linearly scaled in proportion to the specified PGA or developed individually, according to the site characteristics (e.g., if the soil site has physical characteristics that could significantly affect the spectral pattern of input motion or in the occurrence of near-field ground motion). RRS are provided for different values of the damping ratio (i.e., 0.5%, 2.0%, 5.0%, 7.0% and 10%). A linear interpolation should be used for values in between the provided ones. Figure 2.12 shows RRS related to PGA of 1.0 g and 5% damped. RG-1.60 does not provide criteria regarding the spectrum matching procedure and definition of input motions for testing.

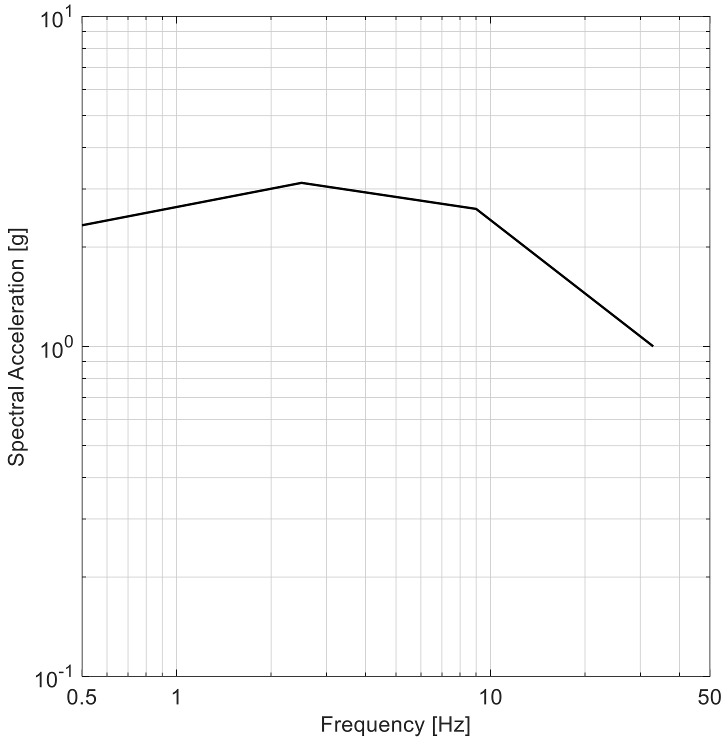

Figure 2.12: Response spectrum required according to RG 1.60 related to the PGA of 1.0 g, 5% damped.

IEC 60068

The international standard IEC 60068-2-57 [80] defines methods and criteria for testing elements, equipment, and electrotechnical products including the testing procedure for seismic applications. The standard outlines the general criteria for seismic testing described in a separate standard, IEC 60068-3-3 [81]. The procedures and methods can also be applied to other elements, and it is intended to evaluate the seismic performance of NEs during an earthquake.

The code defines two seismic classes: a general and a specific seismic class. The specific class is considered when high-reliability safety equipment for a specified environment is required (i.e., equipment in nuclear power plants), otherwise, the general class can be referred to. Equipment service conditions (e.g., electrical, mechanical, thermal pressure, etc.) and the influence of connections, cables, piping, should be replicated in the seismic tests for both classes or their absence justified. Moreover, qualification criteria are provided for classifying the equipment, i.e., a) they experienced no malfunction either during or after the test, b) they suffered a malfunction during the test but reverted to its correct state after the test, and c) they experienced a malfunction during the test and required resetting or adjustment on completion of the test but required no replacement or repair.

IEC 60068-2-57 includes different seismic inputs for seismic testing. In particular, the test inputs are divided into two categories: multifrequency and single-frequency waves. The test waves should a) produce a TRS larger than or equal to RRS, b) possess a maximum peak acceleration value at least equal to the ZPA value, c) reproduce, with a safety margin, the effects of the required earthquake, and d) ideally not include any frequency greater than 35 Hz. The time history obtained according to IEC 60068 shall be generated by the composition of frequencies included within a frequency range from 1.0 to 35 Hz. In some cases, the test frequency range may be extended or reduced depending on the effective value of the cut-off frequency of the ground response spectrum or the critical frequencies of the specimen, but this should be justified. The total duration of the time history shall be about 30 s, of which the strong part shall not be less than 20 s. Three RRS are defined, associated with 2%, 5%, and 10% damping ratio. These RRS have a generalized form that is based on simple correlations among the corner frequencies, depending on assumptions regarding the frequency range of sensitivity of NEs.

The test should be performed through triaxial tests with input motions applied simultaneously along all principal axes of the test specimen, but this does not exclude single-axis or biaxial testing. RRS ordinates associated with the vertical direction of excitation should be 50% of the horizontal RRS ones. IEC 60068 establishes that spectrum-compatibility shall be checked in the specified range at least in one-sixth octave bandwidth resolution in the general case, i.e., specimen damping lying between 2% and 10%. The tolerance to be applied to RRS shall be in a range between 0% and 50%. Moreover, for frequencies larger than the plateau zone, a tolerance of more than 50 % is permitted. Figure 2.13 shows RRS related a frequency range from 1.0 (f_1) to 35 Hz (f_2) and 5% damped.

2.3.4 Multi-floor dynamic testing protocols

Until recently, testing facilities could not easily implement accurate full-scale testing on NEs by means of simultaneous floor accelerations and story deformations loading conditions, reproducing the actual arrangement of NEs housed within multistory buildings and sensitive to both accelerations and displacements (e.g., partition walls, cladding curtain walls, distributed duct, piping, electrical systems, HVAC systems, suspended ceilings, and ceiling mounted equipment).

A brilliant solution, as already discussed in this article, was found by Magliulo et al [34,35,41,75] and Petrone et al [34,35,41,75], where the multi-floor dynamic testing was performed by a test frame, fixed to the shake table, simulating the seismic behavior of a generic story of a building, in which the NEs (i.e., partitions) are installed.

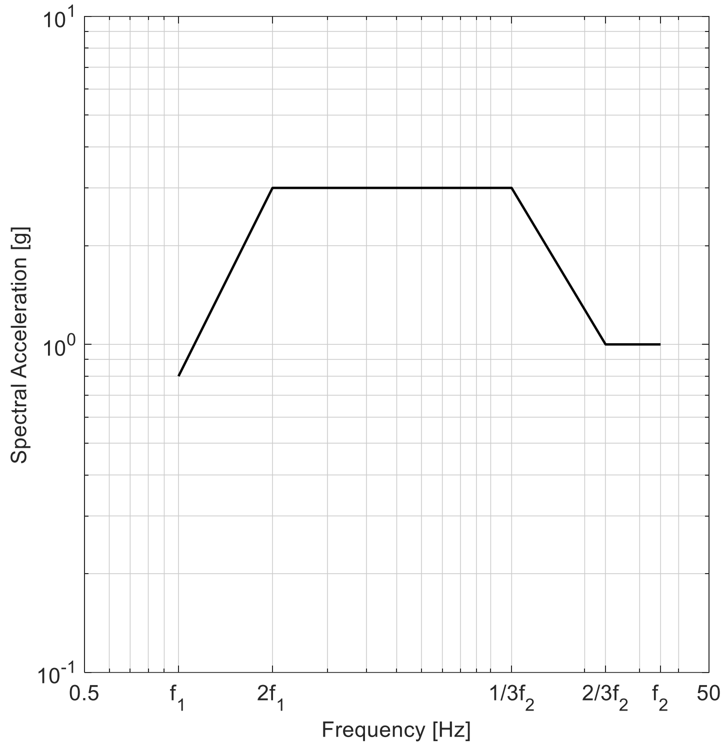

Figure 2.13: Response spectrum required according to IEC 60068 considering a frequency range from 1 (f_1) to 35 Hz (f_2), 5% damped.

The test frame was designed in order to have an assigned drift, i.e., an assigned peak displacement of the top floor, given a peak acceleration at the bottom floor, i.e., at the shake table. The geometry of the test frame was defined taking into account three requirements: (i) realistic value of mass; (ii) realistic interstory height *h*, assumed equal to 2.74 m; (iii) realistic interstory displacement *dr*, assumed equal to *0.005h* for a Damage Limit State (DLS) earthquake with 50-year return period. This strategy allows to assign at the bottom floor a time history according to single-floor dynamic testing protocols, e.g., AC156.

A different solution was found by the University at Buffalo, which commissioned a dedicated Nonstructural Component Simulator (UB-NCS) composed of a two-level testing frame capable of simultaneously subjecting NEs sensitive to both accelerations and displacements to realistic full-scale floor motions expected within multistory buildings also applying story deformation loading conditions. The relevant international reference testing and qualification protocol was developed by Retamales et al [82]. The protocol reduces the minimum testing frequency that can be considered in an experiment from 1.3 Hz, as in the current AC156 procedure, to 0.2 Hz, allowing for more realistic testing of NEs sensitive to low-frequency excitations (e.g., tall slender cantilever type equipment, base-isolated equipment, etc.). The objective of this protocol is not to replace current testing protocols, but rather to enhance the capabilities and the type of equipment that can be tested. Unlike other testing protocols, this protocol is presented as a set of closed-form expressions defining a pair of displacement histories for the bottom and top levels of the UB-NCS that simultaneously matches: (i) a target acceleration response spectrum (either ground or floor response spectra) and (ii) a target generalized interstory drift. Both the target spectral accelerations and drifts can be specified based on the expected values at a given normalized building height h/H, where h is the NE installation height above grade and H is the total building height. This qualification testing protocol considers as variables: (i) the location of the NEs along the height of the building through the parameter h/H; (ii) the range of frequencies to be assessed during testing (f_{min} - f_{max}); and (iii) the ASCE 7-16 design spectral response in the short period range, S_{DS}, and corresponding to 1.0 s period, S_{D1}. The frequency content targeted for the seismic qualification testing protocol covers the range of frequencies between f_{min}= 0.2 Hz and f_{max}= 5.0 Hz. This range corresponds to the operating frequencies of the UB-NCS and the expected fundamental periods of typical multistory buildings, including some higher vibration modes.

2.4 Novel perspectives toward a unified testing approach

2.4.1 Criticalities of existing protocols

The test protocols reviewed here are widely used in the literature, especially AC156 and FEMA 461. AC156, FEMA 461 and ISO 13033 protocols were developed to assess and/or qualify the seismic performance of generic elements, and, among them, AC156 protocol is the only one explicitly aimed at seismic certification. However, few recent research studies pointed out potential criticalities of AC156 protocol, in terms of both spectral demands (RRS) [56,83–85] and damage severity (e.g., for peculiar applications) [86]. The other protocols are intended for systems that are housed within critical facilities (i.e., telecommunications, electrical and nuclear systems) and provide a more standardized qualification approach, e.g., regarding the target performance levels or the seismic zones. Most protocols do not clearly define the applicability conditions with regard to the damage and response sensitivity of NEs. Overall, the aim of the reference protocols is often to assess whether the tested element, subject to a target seismic event (i.e., artificial or natural earthquake), meets certain functionality or stability requirements, i.e., pass or fail qualification outcome. This criterion can be appropriate when the site and the element/building properties are known, which is peculiar to specific NEs (e.g., critical electric equipment for power stations). In different conditions, such as generic qualification of NEs by the manufacturers, this approach cannot be easily applied, and the seismic evaluation of the element cannot be generalized.

2.4.2 Potential improvement interventions

Current regulations and codes often require seismic design and safety verification of NEs. For this purpose, test protocols should include criteria and rules for the estimation of the dynamic properties (DPs) and the significant performance parameters (SPPs) of the NEs to be tested. DPs are mostly required for a relatively accurate evaluation of the seismic demand, in compliance with the regulations/codes (e.g., [1,87]); DPs generally include the fundamental period (T_a), the damping ratio (ξ_a), and the (acceleration) amplification factor (a_p) of the NE.

SPPs represent the quantitative parameters, or measures, to be considered for assessing seismic demands on and capacity of NEs and to verify the safety conditions. SPPs can be considered to be efficient and applicable EDPs, with regard to the specific applications and testing procedures. As was discussed in the previous sections, these parameters depend on (a) the response and damage sensitivity of NEs to seismic actions, including site, building, and relevant interaction responses, and (b) the possibility to robustly assess them through consolidated experimental testing procedures. SPPs can be selected among inertial or deformation measures, or by the combination of them, according to the response/damage mechanisms of interest of the NEs to be tested. Accordingly, both seismic capacity and demand should be estimated considering consistent SPPs. The experimental testing procedures reviewed in this chapter can be used to assess the seismic capacities. The relevant codes/regulations typically define approaches and formulations for defining the seismic demand, which may also depend on the dynamic properties of both buildings and NEs, as it was discussed in the previous sections.

For acceleration-sensitive NEs, the seismic capacity can be expressed in terms of peak floor acceleration (PFA) or peak component acceleration (PCA). PFA is the maximum acceleration obtained on the floor on which the element was installed, while PCA is the maximum acceleration recorded on the component (e.g., in the element's center of mass during the tests). For displacement- or deformation-sensitive elements, the seismic capacity can be expressed in terms of interstory drift ratio (IDR) or target displacement or deformation measures (δ), depending on the applied NE deformations that are relevant to the damage. Finally, for NEs that are sensitive to both acceleration- and deformation-based measures, both types of SPPs should be considered, also accounting for the relevant damage response/mechanisms.

2.4.3 Technical recommendations and final remarks

Technical recommendations are developed for implementing a unified approach for seismic assessment of NEs by means of experimental tests, including seismic qualification purposes. These recommendations were defined in light of the critical review and assessment of current methods and protocols, according to the evidence pointed out in the previous sections. The technical recommendations and innovative perspectives derived in this study aim at improving the seismic assessment and qualification of NEs by means of experimental testing and represent an original literature and practice contribution.

Table 2.1 summarizes these recommendations. In particular, the key parameters/features associated with seismic assessment, qualification, and safety verification of NEs are specified for the most common and representative NEs. The key parameters/features consist of response/damage sensitivity, SPPs, DPs, and recommended test types. No other studies provided a critical review assessment and technical-scientific guidance regarding these applicative aspects, which are essential for implementing relatively reliable and robust assessment and qualification procedures. Table 2.1 represents a reference for both researchers and practitioners, and it might be implemented by codes and regulations.

When multi-floor dynamic tests cannot be performed, quasi-static and single-floor dynamic tests can be conducted separately. An example is the testing procedure adopted by Coppola et al. [88] by means of a special testing facility at the Components and Building Systems Laboratory of the Construction Technologies Institute of National Research Council of Italy (ITC-CNR) in San Giuliano Milanese (Italy). Specifically, the authors conducted quasi-static and dynamic tests for the seismic evaluation of an innovative cladding system. The facility is able to accommodate full size plane elements (partition systems, infill systems, façade systems, etc.) up to 6.3 m wide and up to 8.0 m high. The components can be anchored to the steel supporting frame by means of three beams: one fixed beam at the bottom and two moving beams at the second and third levels. The intermediate and superior beams can be moved, in the plane and out of the plane direction, through six hydraulic actuators, to simulate seismic actions. A mechanical lift system for the moving beams allows for various inter-story heights. The moving beams are supported on low friction rollers and connected to a dynamically controlled hydraulic actuators system. The load cell and transducer of the hydraulic actuator relate to an advanced digital controller that enables the acquisition of real time load and displacement data.

The testing procedure adopted by Coppola et al. [88] consists of cyclic quasi-static tests, performed along in-plane direction according to the loading procedure proposed by FEMA 461, and incremental dynamic tests performed according to AC156.

A unified approach should not be limited to the robust selection of the key parameters and testing approaches/protocols, which already signifies a novel and crucial step in the field. In fact, the selected testing protocols should be applied by maximizing the testing outcomes in terms of systematicity and comprehensiveness. In other words, once the protocol is defined, the testing procedure and program should be implemented in order to identify and characterize the seismic response and damage of tested NEs in a systematic and comprehensive manner. For example, (a) the dynamic properties of the specimen should be estimated corresponding to all relevant DSs, providing useful information regarding the influence of DSs to the dynamic properties, and (b) all relevant DSs, from operativity to ultimate/failure conditions, should be associated with thresholds of SPPs (NE capacity thresholds). However, these experimental correlations should be established by means of standardized approaches, which would allow fully consistent comparisons/extensions and, potentially, generalization. Even though few protocols include directions for implementing a more general and systematic approach, no systematic and standardized recommendations are generally provided. Moreover, most protocols still recommend a pass or fail assessment/qualification approach, which represents a limited application of the potentiality of the abovementioned approach. Therefore, further studies should address the abovementioned issue, by providing a unified approach in terms of testing procedure application and systematicity and comprehensiveness of experimental assessment and qualification of NEs.

2.5 Discussion

The chapter addresses the seismic assessment of nonstructural elements (NEs) by means of experimental testing, with particular focus on testing protocols and seismic qualification. This section reviews the latest literature studies and regulations/codes regarding seismic damage and classification of NEs, providing novel evaluation remarks. The core of the chapter consists of a critical and systematic assessment of the reference international testing protocols and guidelines for seismic assessment and qualification purposes. The scope of the investigation is wide and tends to be comprehensive: quasi-static, single-floor dynamic (shake table), and multi-floor dynamic testing procedures are considered, including multiple protocols, when available.

Table 2.1: Recommended test protocol and DPs and SPPs required for the tested element.

Nonstructural Element	Response/damage Sensitivity			SPPs	DPs	Test
	Acc.	Disp.	Both			
Infill walls, partitions, openings (doors, windows) Facades, glazing systems, and curtains Ceiling systems Systems inside the building (pipes carrying pressurized fluids, fire hydrant piping system, and other fluid pipe systems)			✓	IDR or δ, PFA, PCA	T_a, ξ_a, a_p	Multi-floor dynamic or (secondarily) Quasi-static and Single-floor dynamic
Cabinets, storage racks, bookcases, and shelves Appliances (refrigerators, washing machines, gas cylinders, TVs, diesel generators, water pumps (small), window ACs, wall-mounted ACs) Vertical projections (chimneys & stacks, parapets, water tanks (small), hoardings anchored on rooftops, antennas communication towers on rooftops) Horizontal projections (sunshades, canopies, and marquees) Storage vessels and water heaters (flat bottom containers and vessels, structurally supported vessels) Mechanical equipment (boilers and furnaces, general manufacturing and process machinery, HVAC equipment) Hospital cabinets, museum artifacts, and freestanding objects	✓			PFA, PCA	T_a, ξ_a, a_p	Single-floor dynamic
Systems from within and from outside to inside the building (water supply pipelines, electricity cables & wires, gas pipelines, sewage pipelines, telecommunication wires, rainwater drainpipes, elevators, fire hydrant systems, air-conditioning ducts)		✓		IDR or δ	-	Quasi-static

In the light of the assessment, novel perspectives are developed toward a unified testing approach, and technical recommendations provide guidance for implementing reliable and robust testing procedures. In particular, the relevant parameters and features that are essential for carrying out experimental assessment and qualification procedures are defined for a wide range of NEs, also providing general rules for identifying the relevant NEs in terms of response/damage sensitivity. Furthermore, the appropriate testing method is also recommended, whereas the technical information and evaluation remarks provided regarding the available protocols might be useful for selecting the most appropriate testing protocols.

The chapter contributes to the literature in terms of two key outcomes: technical-scientific review and technical recommendations (unified testing approach). To the knowledge of the author, no other studies carried out a review assessment of the reference testing methods and protocols. Conversely, this section presents a systematic and comprehensive review, which allowed to identify the criticalities and strengths of the available codes/protocols. The technical recommendations provided in the chapter lay the groundwork for more robust and standardized testing and qualification framework. In particular, the provided data might represent the first step for developing code and regulation criteria for seismic assessment and qualification of NEs by means of experimental methods.

2.6 References

[1] Comité Européen de Normalisation (CEN) Eurocode 8: Design of Structures for Earthquake Resistance; 2005.

[2] Ministero delle infrastrutture e dei trasporti Aggiornamento Delle “Norme Tecniche per Le Costruzioni” Decreto 17 Gennaio 2018.; (in italian), 2018; Vol. 20, pp. 23–35.

[3] ASCE 7-16 Minimum Design Loads and Associated Criteria for Buildings and Other Structures; American Society of Civil Engineers (ASCE), 2016; pp. 1–889.

[4] New Zealand Standards New Zealand Standard (NZS): Seismic Performance of Engineering Systems in Buildings. NZS 4219:2009 2009, 1–114.

[5] Instituto Nacional de Normalización NCh3357: Seismic Design of Non-Structural Components and Systems; 2015;

[6] Canadian Commission on Building and Fire Codes National Building Code of Canada 2015; 2015;

[7] Petrone, C.; Magliulo, G.; Manfredi, G. Seismic Demand on Light Acceleration-Sensitive Nonstructural Components in European Reinforced Concrete Buildings. Earthq Eng Struct Dyn 2015, 44, 1203–1217, doi:10.1002/eqe.2508.

[8] Di Domenico, M.; Ricci, P.; Verderame, G.M. Floor Spectra for Bare and Infilled Reinforced Concrete Frames Designed According to Eurocodes. Earthq Eng Struct Dyn 2021, doi:10.1002/eqe.3523.
[9] Abbati, S.; Cattari, S.; Lagomarsino, S. Theoretically-Based and Practice-Oriented Formulations for the Floor Spectra Evaluation. Earthquake and Structures 2018, 15, 565–581, doi:10.12989/eas.2018.15.5.565.
[10] Vukobratović, V.; Fajfar, P. A Method for the Direct Determination of Approximate Floor Response Spectra for SDOF Inelastic Structures. Bulletin of Earthquake Engineering 2015, 13, 1405–1424, doi:10.1007/s10518-014-9667-0.
[11] Filiatrault, A.; Perrone, D.; Merino, R.J.; Calvi, G.M. Performance-Based Seismic Design of Nonstructural Building Elements. Journal of Earthquake Engineering 2021, 25, 237–269, doi:10.1080/13632469.2018.1512910.
[12] Merino, R.J.; Perrone, D.; Filiatrault, A. Consistent Floor Response Spectra for Performance-Based Seismic Design of Nonstructural Elements. Earthq Eng Struct Dyn 2020, 49, 261–284, doi:10.1002/eqe.3236.
[13] Salari, N.; Konstantinidis, D.; Mohsenzadeh, V.; Wiebe, L. Demands on Acceleration-Sensitive Nonstructural Components in Special Concentrically Braced Frame and Special Moment Frame Buildings. Eng Struct 2022, 260, 114031, doi:10.1016/j.engstruct.2022.114031.
[14] IEEE Power and Energy Society Standard for Seismic Qualification of Equipment for Nuclear Power Generating Stations - IEEE 344; Park Avenue, New York, NY 10016-5997, USA , 2013;
[15] British Standards Institution (BSI) Bases for Design of Structures-Loads, Forces and Other Actions-Seismic Actions on Nonstructural Components for Building Applications; British Standard Institution, Ed.; Switzerland, 2013; pp. 1–54.
[16] ICC-ES AC156 Acceptance Criteria for Seismic Certification by Shake-Table Testing of Nonstructural Components; 2012.
[17] Rahmanishamsi, E.; Soroushian, S.; Maragakis, E.M. Analytical Model for the In-Plane Seismic Performance of Cold-Formed Steel-Framed Gypsum Partition Walls. Earthq Eng Struct Dyn 2016, 45, 619–634, doi:10.1002/eqe.2676.
[18] Rahmanishamsi, E.; Soroushian, S.; Maragakis, E.M.; Shirazi, R.S. Analytical Model to Capture the In-Plane and Out-of-Plane Seismic Behavior of Nonstructural Partition Walls with Returns. Journal of Structural Engineering 2017, 143, 04017033, doi:10.1061/(asce)st.1943-541x.0001769.
[19] Petrone, C.; Coppola, O.; Magliulo, G.; Lopez, P.; Manfredi, G. Numerical Model for the In-Plane Seismic Capacity Evaluation of Tall Plasterboard Internal Partitions. Thin-Walled Structures 2018, 122, 572–584, doi:10.1016/j.tws.2017.10.047.

[20] Javid, S.H.; Soroushian, S.; Rahmanishamsi, E.; Maragakis, E.M. Methodology for the Development of Analytical Seismic Fragility for Full Connection Steel-Framed Gypsum Partition Walls. Journal of Earthquake Engineering 2020, doi:10.1080/13632469.2020.1822234.
[21] Shin, D.H.; Kim, H.J. Macro-Modelling Approach for the in-Plane Cyclic Response of Cold-Formed Steel Partition Walls. Applied Sciences (Switzerland) 2020, 10, 1–21, doi:10.3390/app10228163.
[22] Fiorin, L.; Brandolese, S.; Scotta, R. Experimental and Numerical Assessment of Suspended Ceiling Joints. Bulletin of Earthquake Engineering 2021, 19, doi:10.1007/s10518-020-00935-8.
[23] Blasi, G.; Perrone, D.; Aiello, M.A.; Pecce, M.R. Seismic Performance Assessment of Piping Systems in Bare and Infilled RC Buildings. Soil Dynamics and Earthquake Engineering 2021, 149, doi:10.1016/j.soildyn.2021.106897.
[24] Fiorino, L.; Bucciero, B.; Landolfo, R. Evaluation of Seismic Dynamic Behaviour of Drywall Partitions, Façades and Ceilings through Shake Table Testing. Eng Struct 2019, 180, 103–123, doi:10.1016/j.engstruct.2018.11.028.
[25] Fiorino, L.; Pali, T.; Landolfo, R. Out-of-Plane Seismic Design by Testing of Non-Structural Lightweight Steel Drywall Partition Walls. Thin-Walled Structures 2018, 130, 213–230, doi:10.1016/j.tws.2018.03.032.
[26] Macillo, V.; Fiorino, L.; Landolfo, R. Seismic Response of CFS Shear Walls Sheathed with Nailed Gypsum Panels: Experimental Tests. Thin-Walled Structures 2017, 120, 161–171, doi:10.1016/j.tws.2017.08.022.
[27] Pali, T.; Macillo, V.; Terracciano, M.T.; Bucciero, B.; Fiorino, L.; Landolfo, R. In-Plane Quasi-Static Cyclic Tests of Nonstructural Lightweight Steel Drywall Partitions for Seismic Performance Evaluation. Earthq Eng Struct Dyn 2018, 47, 1566–1588, doi:10.1002/eqe.3031.
[28] Hasani, H.; Ryan, K.L. Experimental Cyclic Test of Reduced Damage Detailed Drywall Partition Walls Integrated with a Timber Rocking Wall. Journal of Earthquake Engineering 2021, doi:10.1080/13632469.2020.1859005.
[29] Lee, T.H.; Kato, M.; Matsumiya, T.; Suita, K.; Nakashima, M. Seismic Performance Evaluation of Non-Structural Components: Drywall Partitions. Earthq Eng Struct Dyn 2007, 36, 367–382, doi:10.1002/eqe.638.
[30] Retamales, R.; Davies, R.; Mosqueda, G.; Filiatrault, A. Experimental Seismic Fragility of Cold-Formed Steel Framed Gypsum Partition Walls. Journal of Structural Engineering 2013, 139, 1285–1293, doi:10.1061/(asce)st.1943-541x.0000657.

[31] Kim, H.J.; Shin, D.H. Shake Table Test Program of Cold-Formed Steel in-Plane Partition Walls. Structures 2021, 30, 503–517, doi:10.1016/j.istruc.2021.01.026.
[32] Petrone, C.; Magliulo, G.; Lopez, P.; Manfredi, G. Out-of-Plane Seismic Performance of Plasterboard Partition Walls via Quasi-Static Tests. Bulletin of the New Zealand Society for Earthquake Engineering 2016, 49.
[33] Petrone, C.; Magliulo, G.; Lopez, P.; Manfredi, G. Seismic Fragility of Plasterboard Partitions via In-Plane Quasi-Static Tests. Earthq Eng Struct Dyn 2015, 44, 2589–2606, doi:10.1002/eqe.2600.
[34] Magliulo, G.; Petrone, C.; Capozzi, V.; Maddaloni, G.; Lopez, P.; Manfredi, G. Seismic Performance Evaluation of Plasterboard Partitions via Shake Table Tests. Bulletin of Earthquake Engineering 2014, 12, 1657–1677, doi:10.1007/s10518-013-9567-8.
[35] Petrone, C.; Magliulo, G.; Manfredi, G. Shake Table Tests for the Seismic Assessment of Hollow Brick Internal Partitions. Eng Struct 2014, 72, 203–214, doi:10.1016/j.engstruct.2014.04.044.
[36] Preti, M.; Migliorati, L.; Giuriani, E. Experimental Testing of Engineered Masonry Infill Walls for Post-Earthquake Structural Damage Control. Bulletin of Earthquake Engineering 2015, 13, 2029–2049, doi:10.1007/s10518-014-9701-2.
[37] Hashemi, A.; Mosalam, K.M. Shake-Table Experiment on Reinforced Concrete Structure Containing Masonry Infill Wall. Earthq Eng Struct Dyn 2006, 35, 1827–1852, doi:10.1002/eqe.612.
[38] Nezhad, R.S.; Kabir, M.Z.; Banazadeh, M. Shaking Table Test of Fibre Reinforced Masonry Walls under Out-of-Plane Loading. Constr Build Mater 2016, 120, 89–103, doi:10.1016/j.conbuildmat.2016.05.097.
[39] Di Domenico, M.; Ricci, P.; Verderame, G.M. Experimental Assessment of the Influence of Boundary Conditions on the Out-of-Plane Response of Unreinforced Masonry Infill Walls. Journal of Earthquake Engineering 2020, 24, doi:10.1080/13632469.2018.1453411.
[40] Mulligan, J.; Sullivan, T.J.; Dhakal, R.P. Experimental Seismic Performance of Partly-Sliding Partition Walls. Journal of Earthquake Engineering 2020, doi:10.1080/13632469.2020.1733139.
[41] Petrone, C.; Magliulo, G.; Manfredi, G. Shake Table Tests on Standard and Innovative Temporary Partition Walls. Earthq Eng Struct Dyn 2017, 46, 1599–1624, doi:10.1002/eqe.2872.
[42] Arifin, F.A.; Sullivan, T.J.; Dhakal, R.P. Experimental Investigation into the Seismic Fragility of a Commercial Glazing System; 2020; Vol. 53.

[43] Memari, A.M.; Kremer, P.A.; Behr, R.A. Architectural Glass Panels with Rounded Corners to Mitigate Earthquake Damage. Earthquake Spectra 2006, 22, 129–150, doi:10.1193/1.2164875.
[44] Brandolese, S.; Fiorin, L.; Scotta, R. Seismic Demand and Capacity Assessment of Suspended Ceiling Systems. Eng Struct 2019, 193, 219–237, doi:10.1016/j.engstruct.2019.05.034.
[45] Fiorino, L.; Shakeel, S.; Landolfo, R. Seismic Behaviour of a Bracing System for LWS Suspended Ceilings: Preliminary Experimental Evaluation through Cyclic Tests. Thin-Walled Structures 2020, 155, doi:10.1016/j.tws.2020.106956.
[46] Jun, S.C.; Lee, C.H.; Bae, C.J.; Lee, K.J. Shake-Table Seismic Performance Evaluation of Direct- and Indirect-Hung Suspended Ceiling Systems. Journal of Earthquake Engineering 2020, doi:10.1080/13632469.2020.1845876.
[47] Lu, Y.; Mosqueda, G.; Han, Q.; Zhao, Y. Shaking Table Tests Examining Seismic Response of Suspended Ceilings Attached to Large-Span Spatial Structures. Journal of Structural Engineering 2018, 144, 04018152, doi:10.1061/(asce)st.1943-541x.0002140.
[48] Luo, Z.; Xue, J.; Zhou, T.; Qi, L.; Zhao, X. Shaking Table Tests and Seismic Design Suggestions for Innovative Suspended Ceiling Systems with Detachable Metal Panels. Eng Struct 2021, 232, doi:10.1016/j.engstruct.2020.111830.
[49] Magliulo, G.; Pentangelo, V.; Maddaloni, G.; Capozzi, V.; Petrone, C.; Lopez, P.; Talamonti, R.; Manfredi, G. Shake Table Tests for Seismic Assessment of Suspended Continuous Ceilings. Bulletin of Earthquake Engineering 2012, 10, 1819–1832, doi:10.1007/s10518-012-9383-6.
[50] Patnana, V.; Rai, D.C. Experimental Testing on Nonstructural Continuous Plasterboard Suspended Ceiling Systems under Shake Table-Generated Motions. Earthquake Spectra 2022, 875529302210852, doi:10.1177/87552930221085298.
[51] Aiello, C.; Caterino, N.; Maddaloni, G.; Bonati, A.; Franco, A.; Occhiuzzi, A. Experimental and Numerical Investigation of Cyclic Response of a Glass Curtain Wall for Seismic Performance Assessment. Constr Build Mater 2018, 187, 596–609, doi:10.1016/j.conbuildmat.2018.07.237.
[52] Bianchi, S.; Ciurlanti, J.; Perrone, D.; Filiatrault, A.; Costa, A.C.; Candeias, P.X.; Correia, A.A.; Pampanin, S. Shake-Table Tests of Innovative Drift Sensitive Nonstructural Elements in a Low-Damage Structural System. Earthq Eng Struct Dyn 2021, doi:10.1002/eqe.3452.
[53] Feng, R. qiang; Zhang, L. lin; Wu, Y.; Shen, S. zhao Dynamic Performance of Cable Net Facades. J Constr Steel Res 2009, 65, 2217–2227, doi:10.1016/j.jcsr.2009.06.020.

[54] Sivanerupan, S.; Wilson, J.L.; Gad, E.F.; Lam, N.T.K. In-Plane Drift Capacity of Contemporary Point Fixed Glass Facade Systems. Journal of Architectural Engineering 2014, 20, 04013002, doi:10.1061/(asce)ae.1943-5568.0000130.
[55] Chang, S.J.; Jeong, Y.S.; Eem, S.H.; Choi, I.K.; Park, D.U. Evaluation of MCC Seismic Response According to the Frequency Contents through the Shake Table Test. Nuclear Engineering and Technology 2021, 53, 1345–1356, doi:10.1016/j.net.2020.10.002.
[56] Perrone, D.; Brunesi, E.; Dacarro, F.; Peloso, S.; Filiatrault, A. Seismic Performance of Non-Structural Elements Seismic Assessment and Qualification of Non-Structural Elements in Europe: A Critical Review. 2019, doi:10.7414/4sponse.ID.10.
[57] Kim, S.W.; Jeon, B.G.; Ahn, S.W.; Wi, S.W. Seismic Behavior of Riser Pipes with Pressure and Groove Joints Using an In-Plane Cyclic Loading Test. Journal of Building Engineering 2021, 34, doi:10.1016/j.jobe.2020.101911.
[58] Tian, Y.; Filiatrault, A.; Mosqueda, G. Experimental Seismic Fragility of Pressurized Fire Suppression Sprinkler Piping Joints. Earthquake Spectra 2014, 30, 1733–1748, doi:10.1193/111011EQS278M.
[59] Zaghi, A.E.; Maragakis, E.M.; Itani, A.; Goodwin, E. Experimental and Analytical Studies of Hospital Piping Assemblies Subjected to Seismic Loading. Earthquake Spectra 2012, 28, 367–384, doi:10.1193/1.3672911.
[60] Blasi, G.; Aiello, M.A.; Maddaloni, G.; Pecce, M.R. Seismic Response Evaluation of Medical Gas and Fire-Protection Pipelines' Tee-Joints. Eng Struct 2018, 173, 1039–1053, doi:10.1016/j.engstruct.2018.07.045.
[61] Cosenza, E.; Di Sarno, L.; Maddaloni, G.; Magliulo, G.; Petrone, C.; Prota, A. Shake Table Tests for the Seismic Fragility Evaluation of Hospital Rooms. Earthq Eng Struct Dyn 2015, 44, 23–40, doi:10.1002/eqe.2456.
[62] Di Sarno, L.; Petrone, C.; Magliulo, G.; Manfredi, G. Dynamic Properties of Typical Consultation Room Medical Components. Eng Struct 2015, 100, 442–454, doi:10.1016/j.engstruct.2015.06.036.
[63] Nikfar, F.; Konstantinidis, D. Shake Table Investigation on the Seismic Performance of Hospital Equipment Supported on Wheels/Casters. Earthq Eng Struct Dyn 2017, 46, 243–266, doi:10.1002/eqe.2789.
[64] Fragiadakis, M.; Diamantopoulos, S. Fragility and Risk Assessment of Freestanding Building Contents. Earthq Eng Struct Dyn 2020, 49, 1028–1048, doi:10.1002/eqe.3276.
[65] Neurohr, T.; McClure, G. Shake Table Testing of Museum Display Cases. Canadian Journal of Civil Engineering 2008, 35, 1353–1364, doi:10.1139/L08-084.

[66] Prota, A.; Zito, M.; D'Angela, D.; Toscano, G.; Ceraldi, C.; Fiorillo, A.; Magliulo, G. Preliminary Results of Shake Table Tests of a Typical Museum Display Case Containing an Art Object. Advances in Civil Engineering 2022, 2022, 1–18, doi:10.1155/2022/3975958.
[67] FEMA E-74 Reducing the Risks of Nonstructural Earthquake Damage-A Practical Guide; 2012.
[68] Taghavi, S.; Miranda, E. Response Assessment of Nonstructural Building Elements - PEER 2003/05; 2003.
[69] Di Sarno, L.; Magliulo, G.; D'Angela, D.; Cosenza, E. Experimental Assessment of the Seismic Performance of Hospital Cabinets Using Shake Table Testing. Earthq Eng Struct Dyn 2019, 48, 103–123, doi:10.1002/eqe.3127.
[70] Murty C. V. R.; Rupen Goswami; Vijayanarayanan A. R.; Pradeep Kumar R.; Mehta Vipul V.. Introduction to Earthquake Protection Of-Structural Elements in Buildings. In; Gujarat State Disaster Management Authority (GSDMA), Ed.; 2013; pp. 1–176.
[71] FEMA 461 Interim Testing Protocols for Determining the Seismic Performance Characteristics of Structural and Nonstructural Components; 2007.
[72] Krawinkler, H.; Parisi, F.; Ibarra, L.; Ayoub, A.; Medina, R. Development of a Testing Protocol for Woodframe Structures; 2001.
[73] AAMA "Recommended Static Test Method for Evaluating Curtain Wall and Storefront Systems Subjected to Seismic and Wind Induced Interstory Drift" and "Recommended Dynamic Test Method for Determining the Seismic Drift Causing Glass Fallout from a Wall System Panel,". 2002.
[74] Wilcoski, J.; Gambil, J.B.; Steven, J.S. The CERL Equipment Fragility and Protection Procedure (CEFAPP) - Experimental Definition of Equipment Vulnerability to Transient Support Motions." USACERL. Technical Report 97/58; 1997.
[75] Magliulo, G.; Petrone, C.; Capozzi, V.; Maddaloni, G.; Lopez, P.; Talamonti, R.; Manfredi, G. Shake Table Tests on Infill Plasterboard Partitions. The Open Construction and Building Technology 2012, 6, 155–163.
[76] IEEE Power and Energy Society Recommended Practice for Seismic Design of Substations - IEEE 693; IEEE: Park Avenue, New York, NY 10016-5997, USA , 2018.
[77] Crewe, A.J. Generation of Improved Artificial Earthquakes For Seismic Qualification Testing. In Proceedings of the 15 WCEE; Lisboa, 2012; pp. 1–10.
[78] Network Infrastructure and Operations NEBS Requirements: Physical Protection. Telcordia Technologies Generic Requirements, GR-63-CORE; Piscataway, NJ 08854-41821.866.672.6997 (USA), 2006.

[79] U.S. Nuclear Regulatory Commission (NRC) Regulatory Guide 1.60: Design Response Spectra for Seismic Design of Nuclear Power Plants; U.S., 2014; pp. 1–13.
[80] International Electrotechnical Commission (IEC) Environmental Testing - Part 2-57: Tests - Test Ff: Vibration - Time-History and Sine-Beat Method; Geneva, Switzerland, 2013; pp. 1–43.
[81] International Electrotechnical Commission (IEC) Environmental Testing - Part 3-3: Supporting Documentation and Guidance - Seismic Test Methods for Equipment; Geneva, Switzerland, 2019.
[82] Retamales, R.; Mosqueda, G.; Filiatrault, A.; Reinhorn, A. Testing Protocol for Experimental Seismic Qualification of Distributed Nonstructural Systems. Earthquake Spectra 2011, 27, 835–856, doi:10.1193/1.3609868.
[83] Anajafi, H.; Medina, R.A. Evaluation of ASCE 7 Equations for Designing Acceleration-sensitive Nonstructural Components Using Data from Instrumented Buildings. Earthq Eng Struct Dyn 2018, 47, 1075–1094, doi:10.1002/eqe.3006.
[84] Petrone, C.; Magliulo, G.; Manfredi, G. Floor Response Spectra in RC Frame Structures Designed According to Eurocode 8. Bulletin of Earthquake Engineering 2016, 14, 747–767, doi:10.1007/s10518-015-9846-7.
[85] D'Angela, D.; Magliulo, G.; Cosenza, E. Seismic Damage Assessment of Unanchored Nonstructural Components Taking into Account the Building Response. Structural Safety 2021, 93, doi:10.1016/j.strusafe.2021.102126.
[86] D'Angela, D.; Magliulo, G.; Cosenza, E. Towards a Reliable Seismic Assessment of Rocking Components. Eng Struct 2021, 230, doi:10.1016/j.engstruct.2020.111673.
[87] Ministero delle infrastrutture e dei trasporti Istruzioni per l'applicazione Dell'«Aggiornamento "Norme Tecniche per Le Costruzioni"» Di Cui al Decreto 17 Gennaio 2018; (in italian), 2019; Vol. 11, pp. 23–35.
[88] Coppola, O.; Aiello, C.; Bonati, A.; Caterino, N.; Nuzzo, I.; Occhiuzzi, A. Quasi-static and dynamic tests for the seismic assessment of an innovative cladding system; 2020; 17th World Conference on Earthquake Engineering (17WCEE) Sendai, Japan - September 13th to 18th 2020.

Chapter 3

3 Shake table performance evaluation of an innovative cleanroom with walkable ceiling system under operation conditions

The cleanroom is a controlled atmosphere environment that is increasingly used in the pharmaceutical, food, and micro-electrical industries. The cleanroom is a complex system consisting of architectural, mechanical, and electrical components. Past earthquakes highlighted the vulnerability of the cleanrooms, especially in earthquake-prone countries like Italy; the post-earthquake reconnaissance showed that damage to cleanrooms led to immeasurable economic loss. This chapter investigates the seismic performance of an innovative cleanroom used in the pharmaceutical and healthcare industries. Major modifications within the connections detailing were designed. This chapter reports a series of full-scale shake table tests on an innovative cleanroom, which includes a ventilation system, an electrical equipment, piping, and a walkable ceiling system. The experimental investigation involved 15 shake tests on the cleanroom carried out according to ICC-ES AC156 testing protocol. Both dynamic properties and seismic behavior of the specimen were assessed. Tests showed the excellent seismic behavior of the innovative cleanroom, confirming that simple devices can significantly improve the seismic performance of nonstructural elements.

3.1 Introduction

Cleanroom or white room is an enclosed engineered space/facility having a controlled environment in terms of airborne particles, pressure, relative humidity, and temperature, required to perform specific production and treatment activities that need a strictly-controlled environment [1–3]. Cleanrooms are widely used in pharmaceutical, food, and electronic manufacturing industries [4–6] and in healthcare and hospital facilities (e.g., operating theater) [7,8].

Cleanrooms can be classified as nonstructural elements (NEs) since they are not part of the structural system of buildings and facilities; however, they are very peculiar NEs since consist in complex architectural systems integrating mechanical, electrical, electronic, and hydraulic facilities and equipment [9,10]. Cleanrooms are often highly vulnerable and exposed to damage caused by seismic actions, as highlighted by the 2012 Emilia earthquake [11]. In particular, the cleanroom partitions exhibited major seismic damage, such as cracking and collapse of plaster panels and failure of ceil-mounted equipment. This response caused significant damage to room’s content and required major restoration intervention in terms of facilities and equipment prior to reinstate the production. Therefore, seismic damage of cleanrooms can threaten life safety and can cause severe economic losses due to property loss and downtime [9,12]. For example, microchip manufacturing equipment used in electronic manufacturing facilities is extremely valuable, and total cost of NEs can even be higher than 97% of the total cost of semiconductor fabrication plants [13]. Furthermore, as NEs, cleanrooms are not typically designed considering seismic actions, and relatively frequent earthquakes might even cause significant losses and functioning disruption, which are extremely critical for production and manufacturing facilities.

In the last few decades, several studies investigated architectural NEs such as partitions and ceiling systems [14–22], as well as a growing literature focused on electrical/mechanical/hydraulic equipment and components [23,24], freestanding elements housed within critical facilities [25–28], and objects/contents having historical/cultural significance [28–33]. However, to the author knowledge, no literature studies focused on the seismic performance of complex NEs that integrate architectural and electrical/electronic/mechanical/hydraulic systems, especially under functioning conditions, such as cleanrooms. Despite the recent research efforts towards a reliable seismic assessment and an effective protection of critical systems and components, dynamic properties and seismic vulnerability of cleanrooms is still unknown, and this results in a critical literature gap, as well as it is associated with critical seismic risk.

The chapter represents a first step carried out to address the abovementioned research gap, i.e., an experimental investigation on the seismic performance of a full-scale cleanroom with walkable ceiling system, by means of shake table tests. The cleanroom was designed replicating typical construction practice and technology according to compliant codes, also implementing construction solutions to maximize the seismic performance; the documental compliance reference is associated with ISO Class 7 [3]. The tests were carried out under full functioning conditions, including ventilation, air conditioning, pressure, and electronic opening control. Both dynamic identification and seismic performance evaluation tests were carried out, according to ICC-ES AC156 protocol [34]. The tests represent a seismic qualification of the designed cleanroom. My contribution in this study was to support the design of the innovative cleanroom systems and components, provide support during the execution of the shake table tests and perform the analysis of the recorded data.

3.2 Methodology

Shake table tests of an innovative cleanroom in real scale were carried out at the laboratory of the Department of Structures for Engineering and Architecture of the University of Naples Federico II, Italy. The tests simulated the representative seismic response of a cleanroom installed within a building. Section 2.1 reports the details of the cleanroom specimen, and both experimental facilities and testing setup are defined in Section 2.2; the instrumentation is described in Section 2.3. Section 2.4 reports the testing procedure and loading input, whereas the damage assessment methodology is defined in Section 2.5.

3.2.1 Experimental facilities and testing setup

The shake table has a 3 × 3 m plan dimension and a total height of 1.45 m. It has two (horizontal) degrees of freedom and has maximum payload equal to 200 kN, with an operation frequency range of 0-50 Hz, acceleration peak equal to 1 g (maximum payload), velocity peak equal to 1 m/s, and maximum total displacement equal to 500 mm (±250 mm).

The testing setup was defined in order to replicate a realistic and typical arrangement of the cleanroom within the hosting facility, with particular attention to the functioning/service facilities/systems. It should be recalled that cleanrooms are fixed at their bases to building floors, and they are often located at lower floors of low- or mid-rise buildings. The height of cleanrooms is typically lower than the hosting inter-story height, and a plenum space of variable height (ranging in 40 to 400 cm) is typically arranged between the top of the cleanroom and the upper floor of the building. Most functioning facilities and equipment (e.g., pipeline and electrical networks) are located within this plenum space and connect the external supply to the cleanroom, according to the functioning conditions of the cleanroom.

The shake table was representative of a building floor of installation of the cleanroom. In the following, shake table response is meant as a floor response, and peak table accelerations (PTA) are meant as peak floor accelerations (PFA). In particular, a wood slab was used as an interface between shake table and cleanroom. A steel test frame was designed and constructed to simulate the upper building floor that supports the plenum space facilities and the ceiling of the cleanroom. Figure 3.1 shows the testing setup and the cardinal views.

The steel test frame was designed according to Eurocode 8 [35] and Italian building code NTC 2018 [36]. Design loads consisted of dead loads related to ceiling (0.3 kN/m^2) and pipeline (0.2 kN/m^2) and horizontal load equal to 1.0 kN/m^2. Furthermore, due to the probability of overturning of the panels of the cleanroom, or even the entire specimen, some beam stumps were designed and connected through ropes locked with spring catch. The designed frame consisted in a spatial steel moment-resisting frame (MRF) structure with layout dimensions of 2.60 m (X direction) × 6.21 m (Y direction) × 6.00 m (Z direction). The structure consisted of S355JR circular hollow section CHS 193.7 x 10 mm columns, S275JR HEA 120 mm primary beams, and S235JR rectangular hollow section RHS 9 x 50 x 3 mm secondary beams. The primary to secondary beam connection was achieved through tie type fastening using class 8.8 M12 bolts. The primary beam to column connections were bolted with bolted cover plate splices (moment-resisting connection), and the column to foundation connections were bolted through welded base plate. A finite element (FE) model of the test frame was defined in PROSAP (2S.I. Software e Servizi per l'Ingegneria S.r.l.). In particular, the frame members were modeled as elastic beam elements. The natural vibration periods of the frame were assessed, and the two first translational periods resulted in 0.300 s (3.33 Hz) along X direction and 0.289 s (3.45 Hz) along Y direction.

The cleanroom was connected to the shake table through a wood slab (Figure 3.1a) since this was associated with a clean, rapid, and low-cost installation/transportation condition that was also relatively conservative in terms of connection response. In fact, the cleanroom can be installed on floors of different materials (e.g., reinforced concrete slab) and finishing, and considering a relatively low performing material such as the wood slab represents a conservative testing conditions/arrangement. The wood slab was composed of two layers of poplar plywood, and each layer had a thickness of 35 mm and dimensions of 3 × 3 m. The total weight of the wood slab was about 3.92 kN. To achieve high stiffness in the slab plane, the two layers were installed perpendicularly to each other, in terms of resisting fiber directions. The wood slab was connected to the shake table by equidistance bolts, tight with controlled torque.

The tested cleanroom is classified according to UNI EN ISO 14644-1 [3] of ISO Class 7; at-rest; 0.5 µm. This cleanroom class filtration system must provide filter coverage of 15-25% and a minimum of 60 air changes per hour (ACH). Equivalently, the tested cleanroom is classified as grade C according to good manufacturing practices (GMP) [37] and Class 10,000 according to Federal Standard 209 (FED) [38,39]. The tested cleanroom is known as turbulently-ventilated or nonunidirectional flow. This is of the conventional type, the air being supplied by air supply diffusers or filters in the ceiling similar to that found in offices, shops, etc. However, a cleanroom differs from an ordinary ventilated room in a number of ways: a) increased air supply, b) high-efficiency filters (e.g., high-efficiency particle air (HEPA) filters, or ultra low particle air (ULPA) filters), c) terminal air filters, d) room pressurization and pass-through grilles. Another indication that the room is a cleanroom is the type of surface finish in the room.

Electrical and ventilation systems were installed and made fully operative during the tests to recreate the functioning condition of the cleanroom in realistic conditions (i.e., serviceability) [35]. In particular, a centralized heating, ventilation, and air conditioning (HVAC) filtration system and a control unit implement the functioning conditions of the cleanroom (Figure 3.2 and Figure 3.1a), also including an air handling unit AHU system) provided with high-efficiency particulate air filters (HEPA), a galvanized sheet metal piping system, necessary to circulate air, cleanroom supplies and sensors (pressure control). The system was able to keep the pressure in the cleanroom constantly equal to at about 40 Pascal, with tolerance of ±5 %, so as to ensure an ISO class of air cleanliness of ISO Class 7 according to the relevant requirements [1,3]. The electrical system consisted of a control unit for the operation of the cleanroom opening system (a door and a pass-box), internal pressure sensor, and lighting system. Both service units were placed in an external area that was isolated from the shake table area, and the related network systems were realized through a duct system, flexible pipes, and cable trays. The network system was realized favoring flexible connections among the different components, in order to minimize the transfer of the dynamic actions and the associated deformations from the cleanroom to the units.

The locks of the cleanroom openings (door and pass-box) were electrically controlled in terms of “on” and “off” locking conditions by the central locking system and via an opening keypad, located next to the door. In particular, prior to opening a lock due to a key command, the locking system locks the other one or does not operate if the opening is not in locking position. This is aimed at preventing sudden drops in pressure inside the cleanroom and minimizing the potential contamination of the internal environment. The unlocked/locked condition of the opening is displayed through green/red led lights.

(a)

(b)

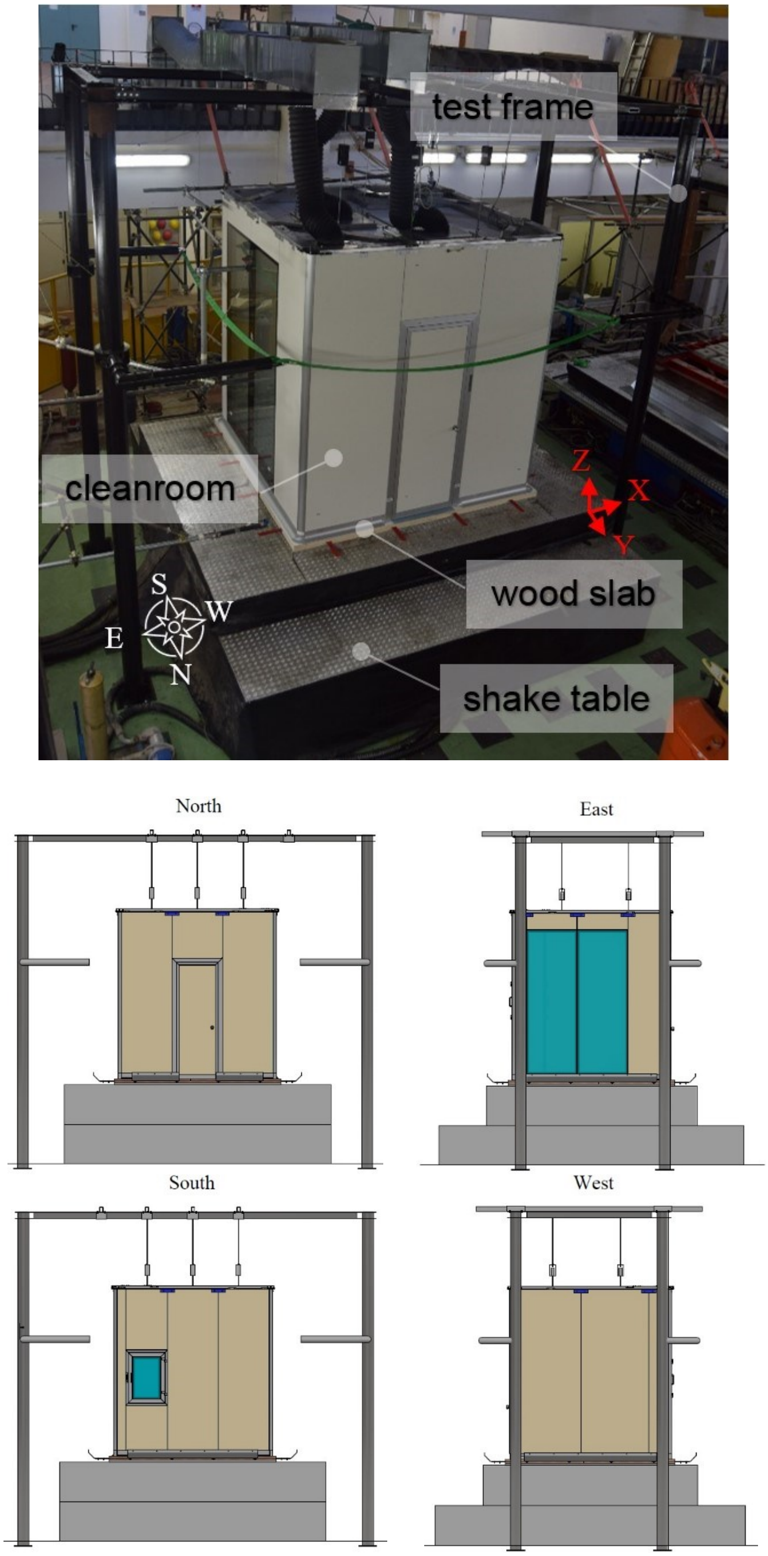

Figure 3.1: Testing setup: (a) global view and (b) cardinal views.

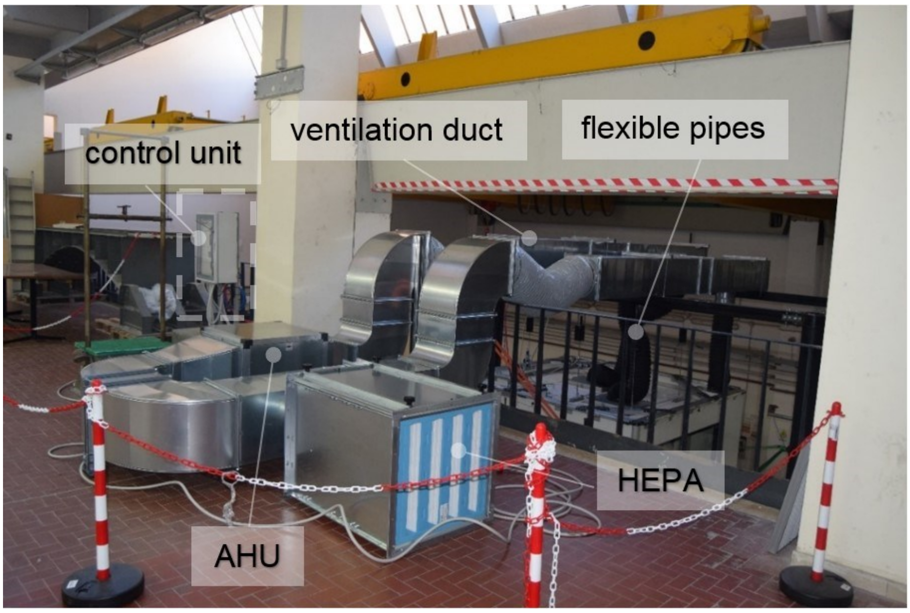

Figure 3.2: ATU system with HEPA filter.

3.2.2 Cleanroom specimen

The specimen was a real-scale cleanroom consisting in the assembly of base/flooring, lateral partition system, ceiling, and electric/ventilation facilities. In the following, the main components of the cleanroom are described, and the mounting procedure is briefly reported. The geometrical details of the elements and the technical specifics of the assembly are omitted for the sake of brevity since they are available within the technical reports [40]. The overall weight of the cleanroom including the weight of the ceiling system (1.96 kN) is 13.4 kN.

Base layout

The base layout of the cleanroom was composed by the assembly of extruded aluminum 6060-T5 elements, i.e., stiffened rectangular cross-section profiles (Figure 3.3a(1)), flanged floor rail profiles (Figure 3.3a(2)), and angular bracket profile elements (Figure 3.3a(3)). Moreover, three innovative components of S275 steel material were introduced: bottom splice (Figure 3.3a(4)), bottom block (Figure 3.3a(5)), and bottom block with thread rod (Figure 3.3a(6)). In particular, these components were designed to connect base layout components to the overall cleanroom and improve its seismic performance. The base layout of the cleanroom is shown in Figure 3.3a(7). The rectangular profiles were fastened to the wood slab with screws passing through fitted holes (Figure 3.3a(8)); these profiles defined the plan layout of the cleanroom, i.e., external cleanroom walls and pass-box/airhole internal cavities (Figure 3.3a(7)). The floor rail profiles were installed on the rectangular profiles and were fastened to them along both lateral surfaces, using both direct screws and angular bracket elements; these latter were screwed to both profiles and wood slab (Figure 3.3a(9)). The connection between the rectangular profiles corresponding to corners of both cleanroom walls and pass-box/airhole elements was implemented by the bottom splice (Figure 3.3a(10)). The bottom block was installed to connect the base of the cleanroom to the vertical splice profiles of the panels of the walls, described in the following subsection. In particular, the bottom block was inserted into the slot of the telescoping track and then fixed with a clamp. Finally, the bottom block was fastened to the vertical splice profiles by bolts (Figure 3.3a(11)). However, when it was not possible to install the vertical splice profile between panels of the walls of the cleanroom, i.e., as for the environment of the pass-box, the bottom block was connected with a threaded rod through a bolt (Figure 3.3a(12)).

Lateral partition system

The lateral partition system included blind and transparent panels, openings (door and pass-box), and various assembly and connection components (Figure 3.1). The lateral partition assembly also included cavities, i.e., the functioning chamber of the pass-box, blind cavities below and above the pass-box, and airhole cavity. The main components of the lateral partition system consist of blind metal panels, transparent (metal-glass) panels, door (and framing), pass-box, and several assembly/construction profiles and elements (i.e., curved angular profiles, (vertical) splice profiles, angular bracket profile elements, π-shaped and H-shaped profiles, single bracket elements, and shell profiles). Moreover, some innovative components were designed and installed to prevent seismic local collapse mechanisms. The main components and innovative components of the lateral partition system of the cleanroom are depicted in Figure 3.3b and Figure 3.4a.

All full-height panels of the cleanroom except openings (door, pass-box, transparent panels) consisted of blind panels. The blind panels (Figure 3.3b(1)) were made by the assembly of two stainless prepainted steel layers on an aluminum frame, with an infilled insulation layer. The aluminum frame of the panels corresponded to the external perimeter of the panels and was infilled within the panel layers; the corners of the aluminum frame profiles were connected and stiffened by internal brackets. The steel layers were bonded to the insulation through a two-part polyurethane adhesives cure (2C PUR).

Two full-height panels included within the east side of the cleanroom (east view, Figure 3.1b) consisted of identical assemblies of a transparent and a blind panel. Transparent (metal-glass) panels (Figure 3.3b(2)) covered the majority of the full height, from the base of the cleanroom, and blind panels were located on the top of them. Transparent panels were made of two layers of laminated glass, glued to an infilled perimetrical aluminum frame, in a configuration similar to the metal panels' one. The openings of the cleanroom consisted of a door and a pass-box (Figure 3.3b(3)). The partition panel with the door (north view, Figure 3.1a) was composed of an aluminum hinged door and a blind panel located above the door. The partition section hosting the pass-box (south view, Figure 3.1c) was composed of a three-dimensional assembly of blind panels defining the cavity in which the (pre-assembled) pass-box chamber was inserted and the construction cavities (below and above the pass-box). The pass-box chamber was delimited by internal and external openings (i.e., pass-box windows).

The curved angular profiles (Figure 3.3b(4)) were installed at the corners of the perpendicular lateral panels and at the corners of the pass-box and airhole panels, and two splice profiles (Figure 3.3b(5)) were prearranged within the slots of each curved profile, as shown in Figure 3.4a(1). In particular, each vertical splice profile was screwed to the curved profile along the height. The panels were connected to the corner vertical splice profiles and were located/arranged along the cleanroom base layout. 4 mm-width gaps were arranged between adjacent in-line panels, and vertical splice profile provided with two gaskets were placed within these gaps. This arrangement was aimed at favoring rapid and economic rearrangement/replacement of the panels. Adjacent perpendicular panels corresponding to pass-box were screwed using angular bracket profile elements (Figure 3.4a(2)). The corner panels of the cleanroom and the pass-box/airhole internal panels were screwed to the flange of the floor rail profiles.

Pass-box was installed on the south side of the cleanroom (Figure 3.1b) after the insertion cavity was arranged; in particular, blind panels were assembled to define the pass-box boundary cavities (below and above the pass-box chamber). The short blind panels (within the cleanroom perimeter) were screw fastened to the perimeter ones by using π-shaped profiles (Figure 3.3b(6)), and these latter profiles were also used to connect the pass-box chamber to the inferior and superior blind panels. Screws and brackets were used to fasten the pass-box chamber to the adjacent panels, as well as perpendicular blind panels were screw fastened through angular bracket profile elements (Figure 3.4a(2)).

The two transparent-blind full-height panels (east view, Figure 3.1b) were pre-assembled prior to be mounted on the floor rail profiles (Figure 3.3a(2)); each metal panel was screw fastened to the transparent panel through a H-shaped profile (along the panels' width, Figure 3.3b(7)) and lateral brackets (Figure 3.3b(8)) (Figure 3.4a(3) and (Figure 3.4a(4)). Two layers of shock absorber were attached to the floor rail profiles prior to arranging the transparent-blind panels in order to minimize the damage to the glass panels (Figure 3.4a(5)). The adjacent two transparent-blind panels were screw fastened using a vertical H-shaped profile.

The frame of the door (north view, Figure 3.1b) was screw fastened to the lateral and top blind panels through π-shaped profiles (Figure 3.3b(6)); two small brackets (screws), located at the bases of the frame, were used to connect (screwing) the door frame to the wood slab and to the lateral panels (Figure 3.4a(6) and Figure 3.4a(7)). The door (including the handle) was pre-assembled and was simply hinged to the frame. The airhole (northeast cleanroom corner, Figure 3.4a(8)) was defined by lateral blind panels, and π-shaped profiles were used to screw fasten the panels among them; the internal corners related to perpendicular panels were screw fastened through angular bracket profile elements. HEPA filter was placed at the bottom of the airhole, and a flexible pipe system was screwed and sealed to the top of the airhole to implement the internal-to-external cleanroom airflow.

The bottom splice systems, described in the previous subsection were connected to the innovative component placed inside the curved angular profile, referred to here as the top splice (Figure 3.3b(9)). In particular, the top splice systems were fastened to the bottom splice systems by a threaded rod (Figure 3.4a(9)). Along the upper perimeter of the partition walls of the cleanroom, an RHS profile of aluminum material was installed (Figure 3.3b(10)). Especially, each end of the RHS profiles was fastened to the top edge splice through screws. Moreover, a T-profile (Figure 3.3b(11)) of aluminum material was placed to connect the side-by-side panels of the walls of the cleanroom, the vertical splice profiles, and the RHS profile (Figure 3.4a(10)). T-profiles were fixed with screws both inside and outside the partition walls. Finally, horizontal braces were installed on the four top corners of the walls of the cleanroom (Figure 3.3b(12)). The horizontal braces consist of an RHS profile of aluminum material and two 45°plate. The latter was needed to connect by screws the horizontal brace to the RHS profile.

Shell profiles were fixed corresponding to both internal and external cleanroom base perimeter defined by the flooring to lateral partition interfaces (Figure 3.4a(11)). These profiles were used for both architectural/aesthetic and technological purposes. In particular, they favor laminar airflow within the cleanroom, minimizing the airflow turbulence. The shell profiles were fixed to the angular profile elements by using silicone sealant. All interfaces between panels and other components were fully sealed by silicone sealant to prevent air pressure loss in the cleanroom. The floor finishing covered all internal floor of the cleanroom and shell profiles (Figure 3.4a(12)); this consisted in consisted in 2-3 mm-thick PVC flooring, bonded to the wood slab by using adhesive glue.

Ceiling system

The ceiling system was walkable and included lighting and ventilation system. In particular, two lights were integrated in the ceiling, as well as supply and recovery ventilation ports. The finish level of the ceiling corresponded to 2.8 m height (from cleanroom flooring), at a level lower than the height of the partition system. The components of the ceiling diaphragm included extruded aluminum 6060-T5 elements: T-shape profiles (Figure 3.4b(1)), angular joint connectors (Figure 3.4b(2)), loadbearing panels (Figure 3.4b(3)), H-shaped profiles (Figure 3.3b(7)), stiffened suspension connection profile elements (Figure 3.4b(4)), angular profile elements (Figure 3.3a(3)).

The ceiling hanger-suspension devices consisted in six threaded rods (Figure 3.4b(5)) integrated with hinges (at the extremities) (Figure 3.4b(6)) and spring devices (in the internal part) (Figure 3.4b(7)); the extremities of suspension devices were fastened to the test frame (superiorly) and to the ceiling diaphragm (inferiorly, to stiffened suspension connection profile elements) after the ceiling diaphragm was assembled. The hinge devices allowed rotation along both horizontal directions, whereas spring devices allowed elongation of the suspension devices (horizontal displacements of the ceiling system) minimizing the suspension reactions associated with axial deformation of the rods; the spring devices consisted in a series of two spring elements (Figure 3.4b(7)) (designed according to maximum expected seismic demand deformations). The lighting system, consisting in two lights, and the ventilation system, consisting in airflow supply and recovery ports, were integrated within the panels after their assembly.

T-shape profiles defined the perimetrical support of the ceiling system over the lateral partition system and were screw fastened to the vertical panels (Figure 3.4b(8) and Figure 3.4b(9)); adjacent perpendicular T-shape profiles were connected through angular joint connectors. Loadbearing panels were placed on and fixed to the T-shape profiles along north-south direction; H-shaped profiles were used to screw fasten adjacent panels; these profiles were inserted within the panel-to-panel gaps (Figure 3.4b(4)) and the panels were screwed to them; stiffened suspension connection profile elements were inserted within panel-to-panel profile connections Figure 3.4b(10)) and superiorly screwed to the panels (and H-shaped profiles) Figure 3.4b(11)), to also strengthen the panel-to-panel connection. Superiorly to the panels, angular profile elements were screwed to both panels and the vertical panels along the perimeter of the ceiling system (Figure 3.4b(12)). Figure 3.5 depicts the assembled ceiling system from (a) the top and (b) the inside of the cleanroom.

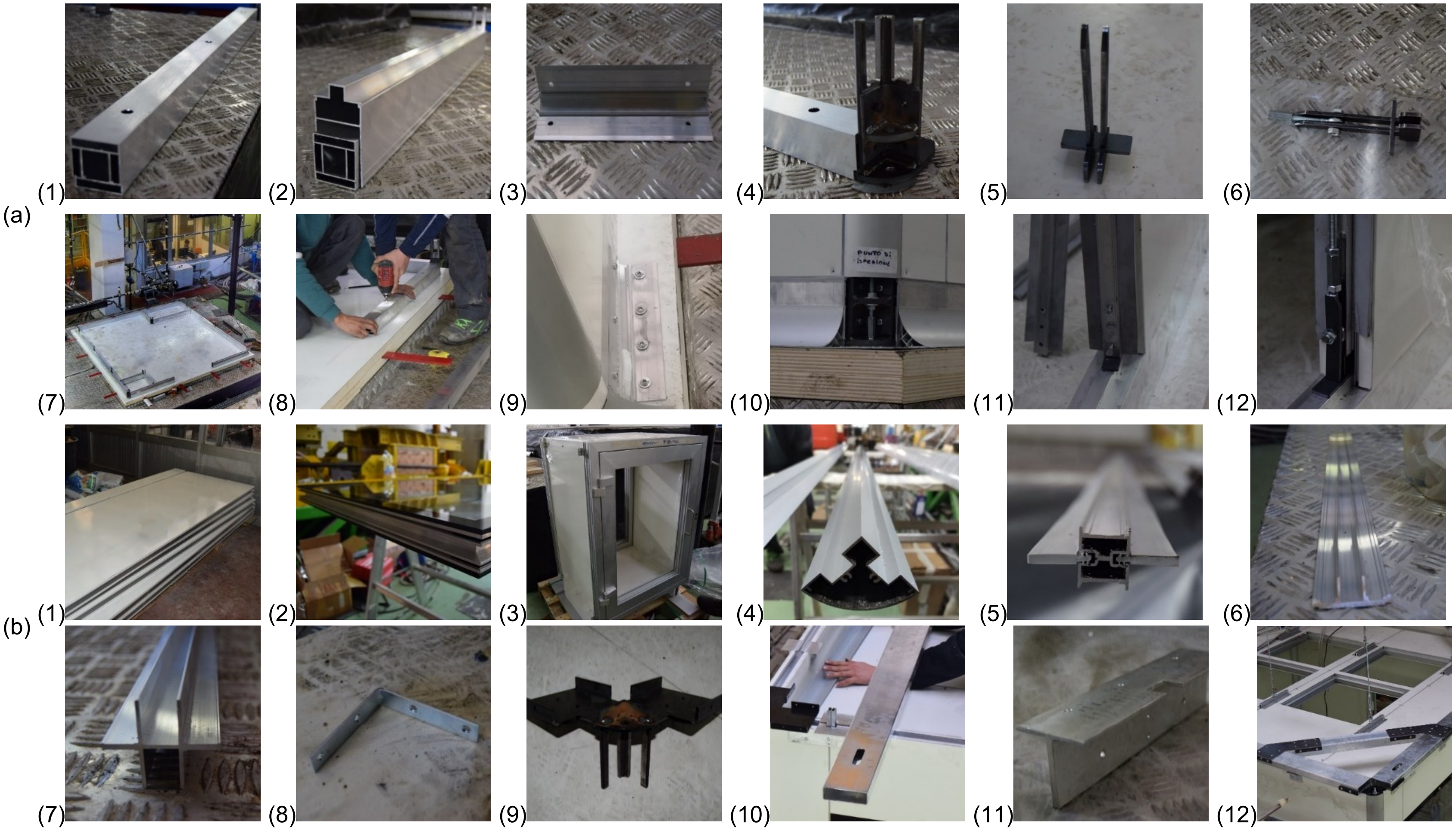

Figure 3.3: Details of cleanroom components; (a) base layout: (1) stiffened rectangular cross-section profile, (2) flanged floor rail profiles, (3) angular bracket profile element, (4) bottom splice, (5) bottom block, (6) bottom block with thread rod, (7) base layout, (8) rectangular profile to wood screw fastening, and (9) floor rail (and rectangular) profile(s) to wood slab screw fastening using angular bracket element, (10), detail of the bottom splice connection, (11) fastened to the vertical splice profiles, and (12) connected with a threaded rod; (b) lateral partition system: (1) blind metal panels, (2) transparent (metal-glass) panels, (3) pass-box chamber, (4) curved angular profiles, (5) (vertical) splice profiles, (6) π-shaped profiles, (7) H-shaped profiles, (8) single bracket elements, (9) top splice, (10) RHS profile, (11) T-profile, and (12) horizontal brace.

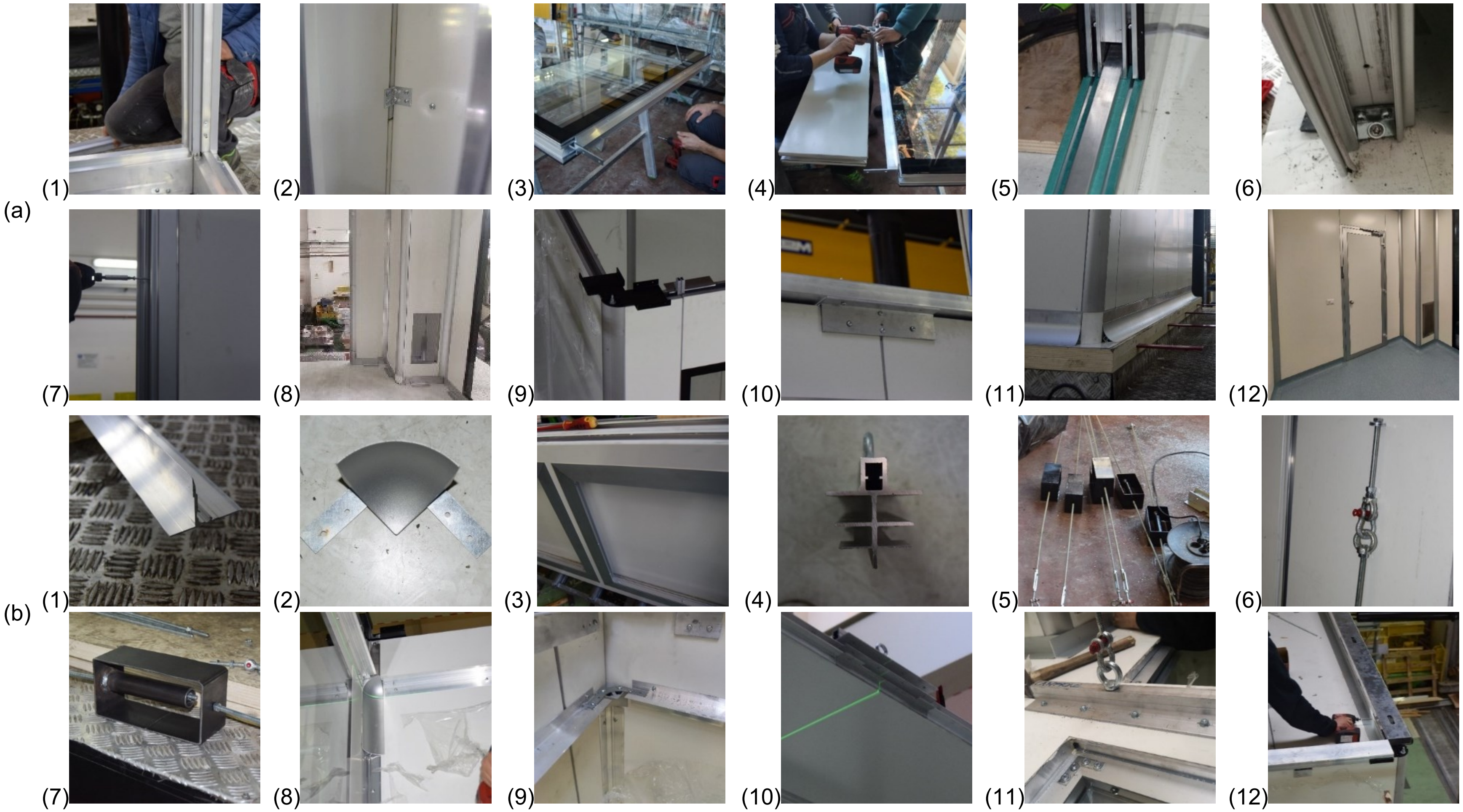

Figure 3.4: Details of cleanroom components; (a) lateral partition system: (1) curved angle to and splice profiles assembly, (2) perpendicular blind panels bracket fastening, transparent to blind panels connection: (3) H-shaped profile and brackets and (4) panels' assembly, (5) shock absorber on floor rail profile, (6) door frame screw fastening, (7) bracket connecting door frame bases to wood slab and adjacent panels, (8) airhole, (9) detail of the top splice connection, (10), detail of the T-profile connection, (11), shell profiles, and (12) internal floor of the cleanroom; (b) ceiling system: (1) T-shape profiles, (2) angular joint connector, (3) loadbearing panels, (4) stiffened suspension connection profile elements, (5) hanger-suspension devices, (6) detail of (superior) hinge device (suspension), (7) detail of spring device (suspension), (8) fastening of the T-shape profiles to the vertical panels, (9) adjacent perpendicular T-shape profile fastening through angular joint connectors, (10) detail of connection among panel, H-shaped profile, and stiffened suspension connection profile element, (11) fastening of stiffened suspension connection profile elements to panels, and (12) fastening of angular profile elements to vertical panels.

(a) (b)

Figure 3.5: View of the assembled ceiling system: (a) from the top and (b) from the inside the cleanroom.

3.2.3 Monitoring Instrumentation

Monitoring instrumentation consisted of eleven accelerometers (Acc), eight displacement laser sensors (Las), four wire potentiometers (WPot), and four video cameras (Figure 3.6a). The accelerometers were three-axis piezoelectric devices, with a measurement range of ±10 g and a sampling rate of 100 Hz. Four accelerometers (Acc662, Acc766, Acc050, and Acc053) were positioned at the middle point of the cardinal side lateral panels of the cleanroom, on the external side. Three accelerometers (Acc763, Acc818, and Acc766) were located at the top of the lateral panels (middle width), corresponding to south, east, and west side panels; an additional accelerometer (Acc765) was installed on the west side panel, corresponding to the bottom of the lateral panel (middle width). An accelerometer (Acc762) was installed on the wood slab (middle width), corresponding to the west side. Two accelerometers (Acc052 and Acc056) were placed on the ceiling system, i.e., corresponding to (Acc052) suspension connection element and (b) panel frame. The shake table was monitored by internal accelerometers (AccTX and AccTY, not depicted in Figure 3.6a). “Luchsinger” e “Wenglor” type laser sensors were used (LasL and LasW); the former (latter) had a measurement range of 600 (200) mm at high resolution, i.e., 80 μm (50 μm), with maximum sampling frequency equal to 1.5 kHz (100 Hz); both sensor types were unaffected by materials, colors, and brightness issues. Five laser sensors were installed on the south side (LasL1, LasL2, LasW1, LasW2, and LasW4) and two on the east side (LasL3 and LasW6); displacement of the shake table along X and Y direction were monitored by LasW3 and LasW5, respectively (not depicted in Figure 3.6a). LasL (LasW) sensors were 400 (250) mm distant from the specimen. The top displacements of the test frame were monitored by four wire potentiometers (WPot1, WPot2, WPot3, and WPot4, Figure 3.6b); WPot1, WPot2, and WPot3 (WPot 4) had a measurement range equal to 300 (150) mm.

The pressure within the cleanroom was monitored in real time by means of air pressure sensors with accuracy of up to ± 0.5 Pa and measurement of minimal differential pressures from 0 to 50 Pa, according to UNI EN ISO 14644-3 41], considering ISO Class 7 requirements [1,3]. In particular, a differential pressure transducer connected externally to the control unit was installed inside the cleanroom.

3.2.4 Testing procedure and loading inputs

Both dynamic identification and seismic performance evaluation tests were carried out through mono- and bi-directional shake table testing, respectively. Dynamic identification tests were performed considering 60-s low-amplitude random vibration signals [42] (i.e., maximum acceleration not exceeding 0.2 g), which were obtained by a uniform random stationary process [43]. The shake table input to perform seismic performance evaluation tests was developed according to the ICC-ES AC156 protocol [34]; the procedure implemented to generate the signal can be found in [44]. Seismic performance evaluation tests were carried out through incremental tests (AC tests), by scaling the reference seismic input up to peak table accelerations larger than 2.0 g. Dynamic identification tests were performed prior to and after the incremental procedure, and in-between all incremental steps.

Design spectral acceleration at short periods S_{DS} was used as a reference intensity measure for scaling the intensity of the incremental tests. Figure 3.7 shows (a) acceleration time history and (b) response spectra associated with the reference seismic inputs along both horizontal directions considering S_{DS} equal to 1.50 g. In particular, test response spectra (TRS) and required response spectra (RRS) are depicted in Figure 3.7b, considering one-sixth-octave bandwidth resolution along the ordinate axis.

Table 3.1 reports the loading program, including both RAN and AC tests, maximum corresponding accelerations recorded on shake table (PFA_t) and wood slab (PFA_s) along horizontal directions, and percentage variation (V).

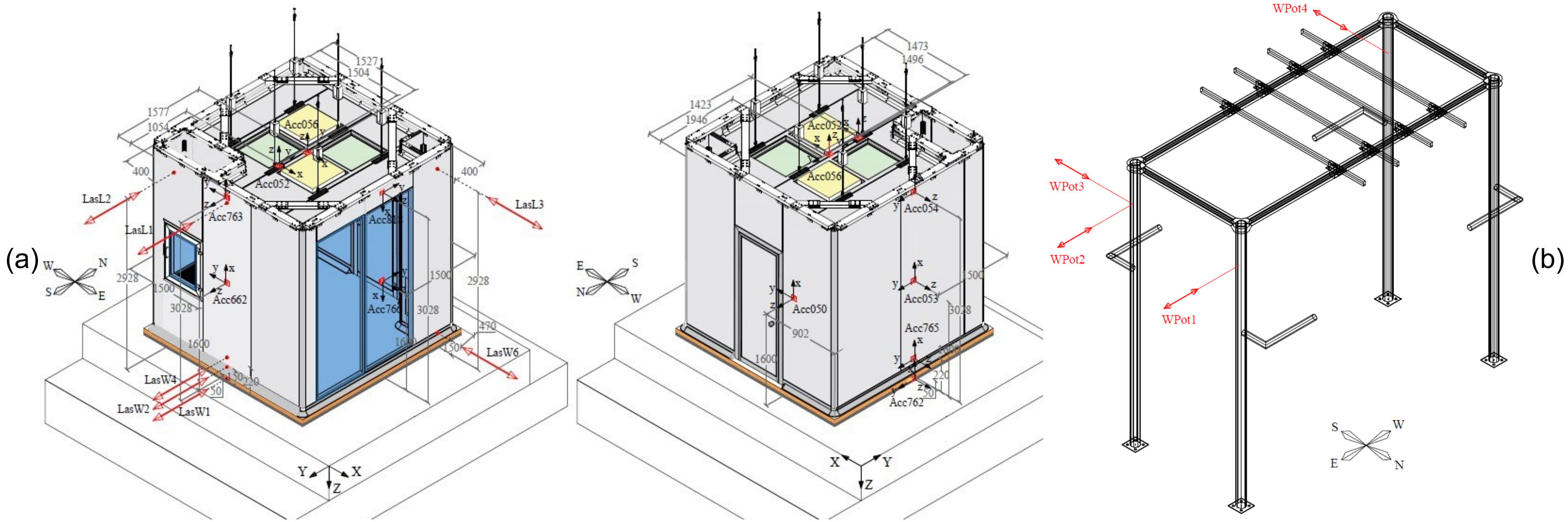

Figure 3.6: Perspective view of the instrumentation arrangement: (a) specimen and (b) test frame.

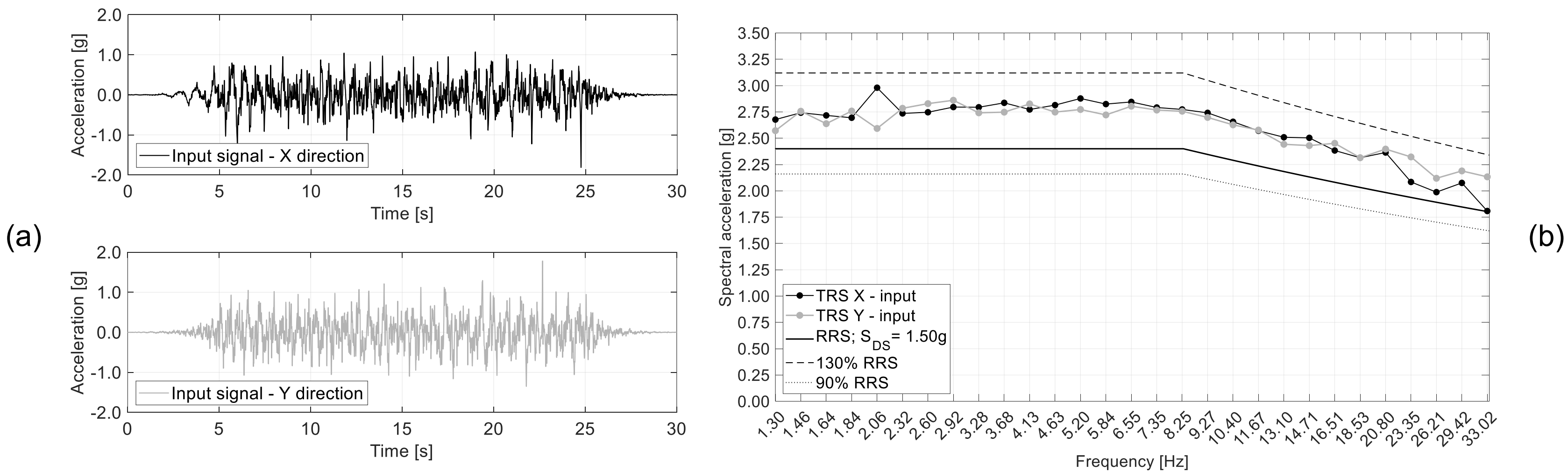

Figure 3.7: AC156 testing input corresponding to SDS equal to 1.50 g: (a) acceleration time histories and (b) acceleration response spectra (i.e., test response spectra (TRS) and required response spectra (RRS)).

Table 3.1: Testing program (AC test parameters and sequence of tests), maximum accelerations recorded on shake table (PFAt) and wood slab (PFAs), and (V) percentage variation.

test ID	S_{DS}	PFA_{tx}	PFA_{ty}	PFA_{sx}	PFA_{sy}	V_x	V_y
	[g]	[g]	[g]	[g]	[g]	[%]	[%]
AC01	0.10	0.12	0.11	0.12	0.11	-0.6	-1.2
AC02	0.20	0.25	0.25	0.25	0.25	0.1	0.8
AC03	0.30	0.38	0.37	0.38	0.37	-0.5	0.9
AC04	0.40	0.50	0.48	0.50	0.48	-0.2	0.0
AC05	0.50	0.64	0.58	0.62	0.58	-2.0	-0.1
AC06	0.60	0.75	0.64	0.74	0.64	-1.0	-1.5
AC07	0.70	0.85	0.76	0.86	0.75	1.0	-1.5
AC08	0.80	1.01	0.85	0.99	0.86	-2.4	1.5
AC09	0.90	1.09	1.03	1.13	1.03	3.9	0.3
AC10	1.00	1.27	1.12	1.26	1.11	-0.7	-1.0
AC11	1.10	1.42	1.51	1.42	1.61	-0.1	6.4
AC12	1.20	1.50	1.72	1.53	1.79	1.9	3.8
AC13	1.30	1.58	1.87	1.73	1.94	9.9	3.4
AC14	1.40	1.86	2.06	1.88	2.12	1.1	3.1
AC15	1.50	1.96	2.20	2.05	2.27	4.7	3.2
Testing program (sequence of AC and RAN tests)							
RAN1000, RAN2000, AC01, AC02, AC03, AC04, RAN1003, RAN2003, AC05, RAN1004, RAN2004, AC06, AC07, AC08, RAN1007, RAN2007, AC09, RAN1008, RAN2008, AC10, RAN1009, RAN2009, AC10bis, RAN1009bis, RAN2009bis, AC11, RAN1010, RAN2010, AC12, RAN1011, RAN2011, AC13, RAN1012, RAN2012, AC14, RAN1013, RAN2013, AC15							

3.2.5 Dynamic identification

The dynamic properties of the cleanroom were assessed by using the transfer function method [43]. In particular, the transfer curves and associated vibration modes of the specimen were assessed considering RAN tests. The natural frequencies (local peak frequencies) and damping ratios were estimated, and their evolution along the incremental tests was assessed. The transfer functions were defined as the ratio of the Fourier transforms related to acceleration time histories recorded at the cleanroom top and on the shake table. Acc054z and Acc054y were considered as output accelerometers for X and Y directions, respectively, whereas AccT was considered as input accelerometers (Figure 3.6). The equivalent damping ratio was evaluated according to the half-power bandwidth method [43,45], typically used to assess structures and components assumed to have linear viscous damping [42,46]. The damping ratio associated with the first mode of the cleanroom was evaluated by assessing the transfer functions obtained by RAN tests.

3.2.6 Damage states

Damage assessment was performed considering the following damage states (DSs): DS0 (absent damage), DS1 (minor damage), DS2 (moderate damage), and DS3 (major damage). Generally, a DS can be achieved by each (significant) component of a specimen in the course of a seismic test, and, in this context, the most severe DS achieved by (at least) a component over an incremental test is meant as a global DS achieved by the specimen from that increment on. DS1 achievement implies the need to implement minor repair/rearrangement actions restore the original conditions (of the component). Typically, achievement of DS1 is associated with violation of full operativity conditions, especially for cases in which minor damage can affect the functioning of the facility, e.g., hospitals and medical equipment. DS2 achievement implies that the component is moderately damaged so that it needs to be partially replaced or moderately repaired/rearranged. DS3 implies that the damage level is such that (a) the component needs to be totally replaced or heavily repaired/rearranged and/or (b) life safety is not ensured.

The quantitative technical correlation scheme that associates the exhibited/expected physical damage/response of the components/specimen to the DS occurrence (namely, damage scheme) is typically based on the damage/response significance expressed in terms of three “D” losses contributions [9], i.e., human casualties (Deaths), direct economic loss due to the repair or replacement of the NEs (Dollars), and occupancy or service loss (Downtime). The damage scheme implemented in this section is reported in Table 2; this was assessed according to current practice and past studies [18]. It is worth noting that the inside-to-outside cleanroom differential pressure is a key parameter regarding the functioning of cleanroom environments. In particular, a differential pressure lowering below a threshold limit, associated with residual conditions after seismic excitation, is considered as a sufficient condition for achieving DS1. The assumed target differential pressure within the cleanroom was set equal to 40 Pa, whereas the required minimum value was set equal to 25 Pa [1,3].

Seismic response and damage of the components/specimen were checked during the tests by real-time physical inspections and recorded data observation, including the real-time monitoring of both peak and residual differential pressure over the tests. These real-time assessment results were collected in prearranged damage surveys sheets. The survey sheets were checked in the data analysis and elaboration phases, referring to video/picture and instrumental data recording. Finally, the achievement of the relevant DSs was identified according to Table 2.

Table 3.2: Damage scheme for the correlation between the recorded damage in each component of the cleanroom and the attained damage state.

Damage type	Need to repair or replace a percentage of components larger than		
Dollars	10%	30%	50%
Downtime	-	Moderate (1-2 days)	Significant (≥3 days)
Death	-	Limited	Significant
Components	DS 1	DS 2	DS 3
Ceiling System	Localized damage to some panels	Damage to the panels and slight/moderate damage to the connection, plasticization of the spring of the hanger, slight/moderate damage to the wall trim	Fall of the panels and serious damage to the connection, breakage of the spring of the hanger, severe damage and total detachment of the wall trim
Steel panels	Slight rotation out of the plane or in the plane of the panel, sealant de-bonding	Out-of-plane rotation of the panel, local plastic strains	Overturning of the panel, widespread plastic strains
Glass panels	Slight rotation out of the plane or in the plane of the panel, sealant de-bonding	Out-of-plane rotation of the panel, cracking and local disconnections, detachment or damage shock absorber	Overturning of the panel, severe or widespread cracking
T-profile, 45° and T plate	Minor/moderate damage	Severe damage and total detachment	-
Screws	Unscrewing/failure of 10% of the screws	Unscrewing/failure of 30% of the screws	Unscrewing/failure of 50% of the screws
Mechanical fasteners for use in wood slab, L-profile, shell profile	Detachment of the shell profile (external detachment), slight damage of the L-profile	Moderate damage of the L-profile	Pull-out of the wood slab screws, severe damage and total detachment of the L-profile
Angle and vertical splice profile	Slight damage to the splice and its connections	Moderate damage to the splice and its connections	Severe damage/collapse of the splice and its connections
Rectangular profile, telescoping track, bottom and top edge splice, bottom block	Minor damage	Moderate damage	Severe damage and total detachment
Ventilation and electrical system	Slight damage to components such as lights, filter, system malfunction, breakage of suspension hooks, air control (< 25 Pa), slight damage to pipes and their connections	Moderate damage to light supports and filter, serious damage/collapse of pipes and their connections	Severe damage and total detachment of lights supports and filter
Door, pass-box	Opening, minor damage to the lock, pass-box locked	Moderate damage	Severe damage, door overturning, pass-box ejection

3.3 Results and remark

3.3.1 RRS to TRS spectrum-compatibility

The spectrum-compatibility was evaluated considering all performed tests according to AC156, assuming a one-sixth-octave bandwidth resolution and damping value equal to 5% of critical damping. Spectrum-compatibility was checked for input theoretical signals (i.e., assigned to the table) and for signals recorded on (a) shake table (AccT) and (b) wood slab (Acc762) along both directions. Spectrum-compatibility was verified in all cases, and representative results are depicted in Figure 3.8, corresponding to (a) AC04 (S_{DS} equal to 0.40 g) and (c) AC15 (S_{DS} equal to 1.50 g) tests along (1) X and (2) Y directions; TRS and RRS are test response spectra and required response spectra, respectively. In particular, even in the very few cases in which TRS fall below RRS (e.g., Figure 3.8b(2), corresponding to frequencies equal to 10.4 and 13.1 Hz), the compatibility is confirmed since (a) TRS ordinate is not lower than 90% RRS ordinate and (b) adjacent one-sixth-octave points ordinates are at least equal to RRS ones. In some cases, TRS exceed RRS by more than 30 percent (e.g., Figure 3.8a(1), corresponding to frequencies equal to 9.27 and 10.40 Hz), not following the code recommendations. However, TRS upper limitation can be considered to be a desired condition rather than a strict requirement, since higher spectral ordinates are associated with higher acceleration demand severity.

3.3.2 Observed damage and critical response

No damage or critical response of the cleanroom was observed over all tests except for AC10 test. In fact, the opening of the doors of the pass-box was observed in the course of this latter test, resulting in a sudden drop (to zero) of differential pressure within the cleanroom, below the required minimum threshold. In particular, Figure 3.9 shows the evolution of the cleanroom differential pressure over the incremental tests, where both recorded initial and recorded minimum (shaking and post-shaking) pressure values are reported, together with target and required minimum thresholds. It is recalled that the differential pressure should be larger than or equal to a required minimum value (25 Pa) to guarantee the facility operativity (DS0) (Table 2). In all cases, initial differential pressure was within 37 - 40 Pa, whereas the minimum value of shaking pressure was typically between 30 and 35 MPa, except for AC10 test (as previously described). It should be noted that the post-shaking differential pressure was always larger than the recorded minimum one, reaching values similar to the initial pressures.

The opening of the doors was caused by the functioning disruption of the locks; this was probably due to the demagnetization of the lock components caused by the dynamic excitation of the metal powder particles deposited within the pass-box profiles/components; this potential cause was also supported by the expert electricians of the manufacturer.

After AC10 test, the lock was repaired and the functioning was fully restored (Figure 3.10), and test AC10 was repeated (AC10bis). No functioning disruption was observed (e.g., pass-box window opening not occurred); the repetition of test AC10 was associated with a similar response of the cleanroom. No damage or critical response (including electric/electronic issues) was observed for the following tests.

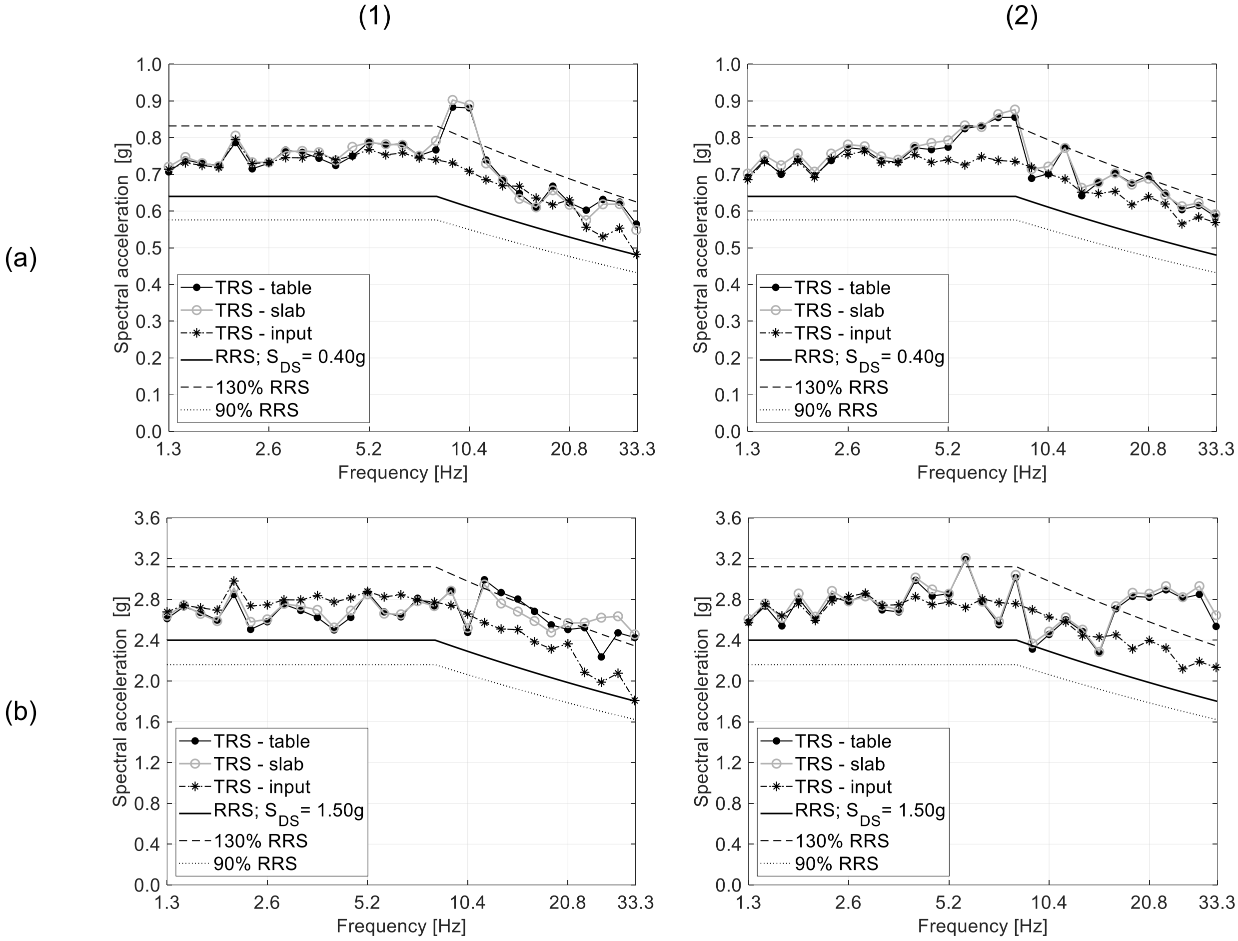

Figure 3.8: Spectrum-compatibility results: required response spectra (RRS) and test response spectra (TRS) along (1) X and (2) Y directions. The results are related to tests (a) AC04 (SDS equal to 0.40 g) (b) and (c) AC15 (SDS equal to 1.50 g). TRS - table, TRS - slab, and TRS – input correspond to TRS associated with records on table, records on wood slab, and input (theoretical) signal.

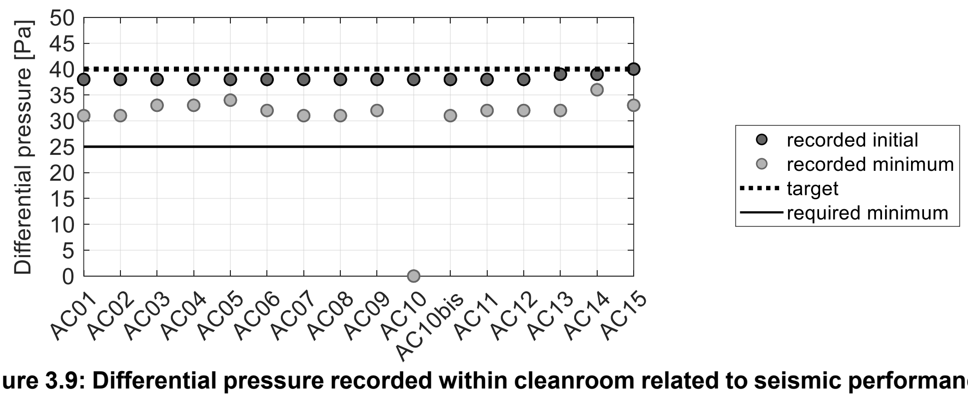

Figure 3.9: Differential pressure recorded within cleanroom related to seismic performance (AC) tests: recorded initial, recorded minimum (shaking and post-shaking), target, and required minimum values.

Strictly speaking, the response observed in AC10 test should be associated with DS1, whereas all other test responses should be associated with DS0 (i.e., full operativity). However, test AC10, or more generally, seismic intensity related to tests AC10, might be associated with DS0. In fact, the test was repeated (AC10bis) and no damage or critical response of the cleanroom components (including pass-box windows) was identified. Moreover, the opening of the doors was more associated with an electromagnetic issue rather than to a structural behavior. Having said that, the evidence stressed the need for further investigation into the response of metal electronic locks under dynamic actions, behind the structural performance.

Figure 3.10: Damage of the electromagnetic lock of the inside door of pass-box, ID 110 test.

3.3.3 Dynamic identification

Prior to presenting the results of the dynamic identification, it should be noted that the cleanroom consists in the assembly of multiple components, implementing by means of non-standard connections, according to nonsymmetrical layouts and peculiar arrangements. The lateral partition sides are different among them and include various elements and parts in addition to the metal panels (e.g., transparent panels, pass-box, door). This geometrical and assembly complexity is necessarily associated with a complex and relatively irregular dynamic response, even considering the elastic vibration properties. Therefore, the dynamic identification results should be interpreted in the light of this complexity, recalling that the vibrational response of the cleanroom might be reasonably conditioned by both local and global modes, even according to relatively irregular patterns. Despite that, the author tried to identify clear and univocal trends in terms of dynamic properties and seismic response of the specimen, which could be reasonably extended to cleanroom systems manufactured by using the described materials/components and implementing the relevant construction and assembly procedures.

Figure 3.11 shows the dynamic identification results: (a) transfer functions (RAN test functions) and (b) peaks of the first fundamental vibration mode associated with (1) X and (Y) directions. The transfer functions associated with the different tests are very similar among them along both directions, in terms of both peak frequencies and peak amplitudes; this strengthens the robustness of the methodology. Over a reasonably significant frequency range (0 to 35 Hz), two main relatively regular vibration modes (frequency peaks) can be identified along Y direction (20.3 and 27.9 Hz, corresponding to 4.09 and 2.45 amplitudes, respectively; Figure 3.11a(2)), whereas the frequency response is more complex along X direction. In particular, the lowest frequency mode exhibited frequency peak (10.9 Hz) with an amplitude ordinate (1.71) significantly lower than the larger frequency mode (4.54) (Figure 3.11a(1)); therefore, this latter represents the fundamental vibration mode. Frequencies related to about 20-21 Hz are significant for both direction responses, and the related vibration modes might be associated with the mutual X-Y direction vibration, possibly representing similar vibration modes. Further relatively sensitive response, was also observed corresponding to about 20.7 and 27.9 Hz, along X and Y direction, respectively, even though this response was associated with lower amplitudes.

The fundamental peak frequency does not essentially vary over the incremental tests along both directions, as it can be seen in Figure 3.11b (RAN tests were performed prior to and after each incremental tests). Accordingly, it might be derived that the main elastic properties of the system (including the connections) are not conditioned by the effects of the incremental testing procedure, which are necessarily not associated with damage or degradation of the specimen parts. The very minor peak frequency variations identified along both directions (along X direction, maximum positive (negative) variation for following tests equal to 4.40% (-1.10%) and total variation equal to 5.49%, and along Y direction, maximum positive (negative) variation for following tests equal to 1.98% (-2.88%) and total variation equal to -0.96%) are reasonably due to very minor rearrangements among parts and connections (e.g., bolt connection loosening or sealing adjustment), which do not sensibly affect the properties of the cleanroom. The natural frequency of the cleanroom associated with undamaged conditions was equal to 17.8 (20.3) Hz along X (Y) direction, i.e., RAN1000 (RAN2000) test curve in Figure 3.11a(1) (Figure 3.11a(2)).

Figure 3.11c depicts the evolution of damping ratio of first vibration mode along RAN tests, along (1) X and (2) Y directions. The initial damping ratio (associated with RAN1000 and RAN2000 tests along X and Y direction, respectively) is quite similar for X and Y directions (equal to X% and Y%, respectively). Damping ratio in X direction does not significantly vary along incremental tests (maximum positive (negative) variation for following tests equal to 13.3% (-5.21%) and total variation equal to 15.3%), whereas ratio in Y direction gradually increases as the test intensity grows (maximum positive (negative) variation for following tests equal to 21.5% (-1.97%) and total variation equal to 66.7%). This latter response might be due to the slight variation of the specimen connections' arrangements, which increase their damping capacity as the testing intensity increases. The estimated damping ratios are consistent with values assessed in the literature for similar components [38], even though it is not possible to make quantitative comparisons given the unicity of the tested specimen.

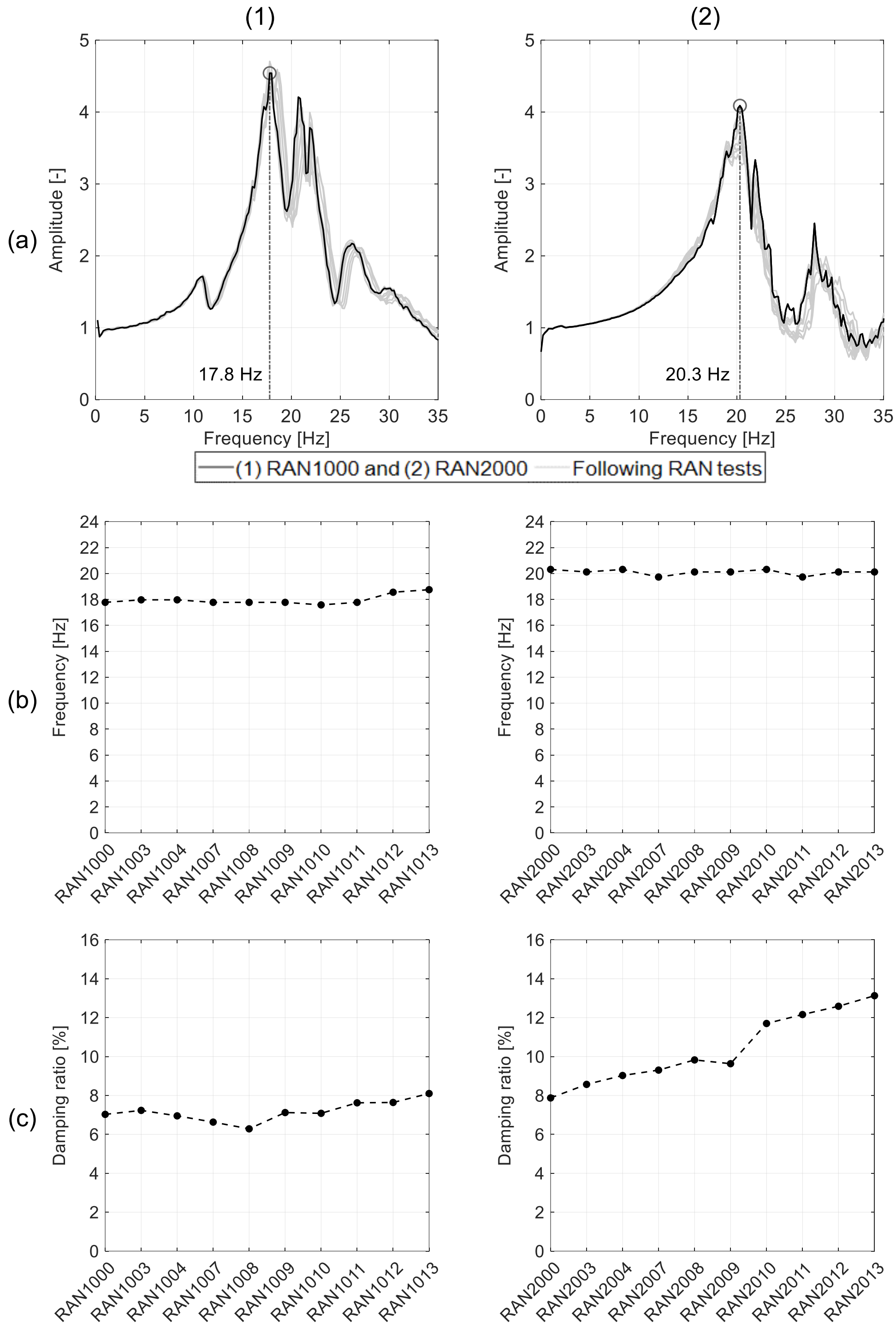

Figure 3.11: Dynamic identification results (RAN tests): (a) amplitude transfer functions, (b) evolution of first vibration mode frequency peaks, (c) evolution of damping ratio of first vibration mode, along (1) X and (2) Y directions.

3.3.4 Acceleration response

PFA (recorded on the shake table), peak component acceleration (PCA), and component amplification factor (CAF), i.e., PCA to PFA ratio, were estimated and associated with the incremental test intensities (AC tests), as well as CAF was also estimated considering the dynamic identification tests (RAN tests). Figure 3.12 depicts PCA measured corresponding to (a) cleanroom top (top of lateral partition) (Acc054), (b) ceiling system (next to the hanger-suspension device) (Acc052), (c) lateral partition panels (out of plane direction, Acc050 (blind panel, north), Acc766 (glass panel, east), Acc662 (blind panel, south), and Acc053 (blind panel, west)), and PFA (AccTX and AccTY), along both horizontal directions.

PCA associated with cleanroom top (lateral partition) (Figure 3.12a) and ceiling system (hanger-suspension device) (Figure 3.12b) are approximately the same, implying that the ceiling system is essentially rigid and that is rigidly connected to the lateral partition system. In particular, PCA (approximately) grows linearly as PFA increases, with very similar gradient along X and Y direction, according to testing PFA (Figure 3.12d). PFA was approximately the same along X and Y direction up to AC10 test, with PFA slightly larger along X, whereas PFA along Y became larger from tests following AC10.

The trend of the out of plane PCA (Figure 3.12c) is more irregular than the one associated with top responses (Figure 3.12a and b), especially considering north partition panel. Up to PFA equal to about 0.75 g east (west) panels PCA are almost identical to north (south) ones, whereas, for larger intensities. For larger intensities, east (glass panel) PCA values are significantly larger than north (blind panel) ones and even larger than other panels' PCA. It should be recalled that PFA along X and Y direction presented some differences along the incremental testing procedure, especially for relatively large intensities, i.e., X direction PFA were slightly larger than Y ones over medium intensities and an opposite trend was observed for larger intensities (Figure 3.12d). Therefore, the interpretation of PCA results should be also based on estimation of CAF.

Figure 3.13 shows CAF related to (a) cleanroom top (Acc054), (b) ceiling frame (hanger-suspension device) (Acc052), and (c) lateral partition panels ((out of plane direction, Acc050 (blind panel, north), Acc766 (glass panel, east), Acc662 (blind panel, south), and Acc053 (blind panel, west)), and PFA (AccTX and AccTY). In particular, CAF was assessed considering (1) incremental tests and PFA as an x-axis reference and (2) dynamic identification tests and RAN test ID as an x-axis reference. As a first comment, it can be observed that CAF associated with RAN tests is quite more regular over the different tests than CAF related to incremental tests. RAN-based CAF values are overall larger than CAF associated with incremental tests and are overall constant as the testing procedure proceeds.

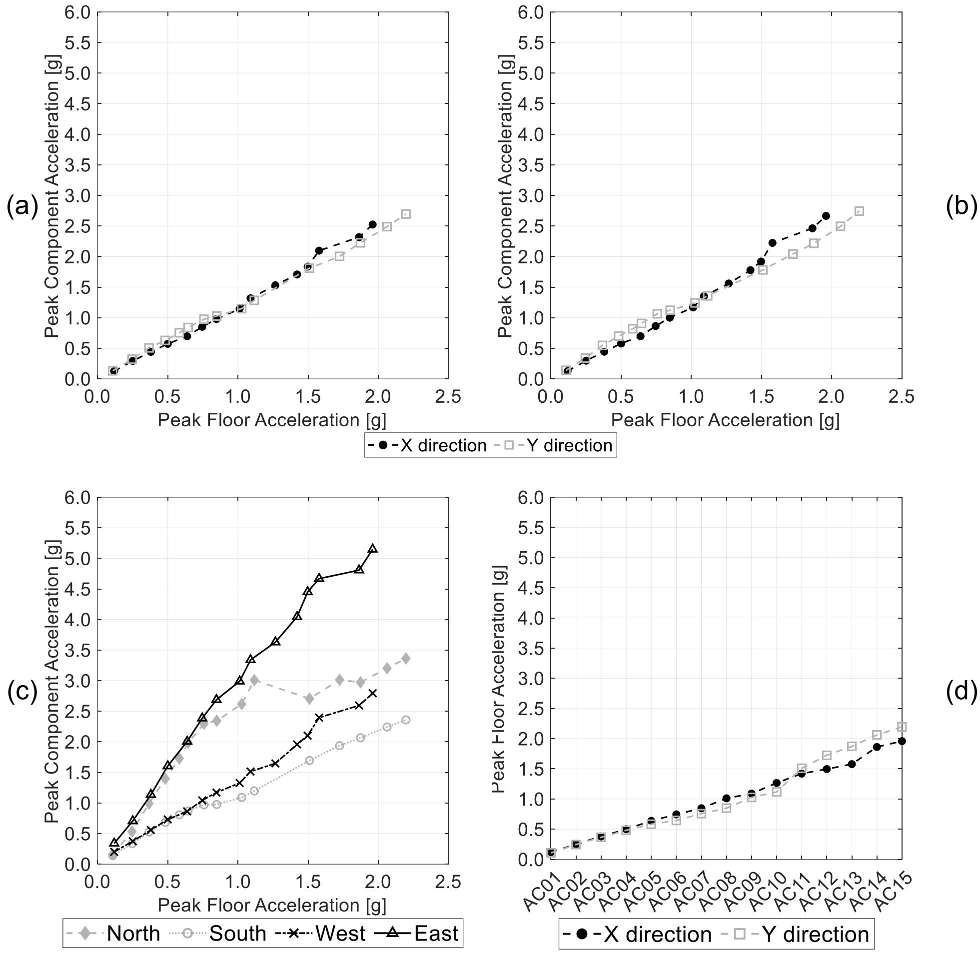

Figure 3.12: Acceleration response: peak component acceleration (PCA) evolution over the incremental test peak floor acceleration (PFA) values, associated with (a) cleanroom top (lateral partition), (b) ceiling panel (hanger-suspension device), (c) lateral partition panes (out of plane directions), and testing PFA.

The out of plane response of the panels is associated with CAF values larger than global response of the cleanroom, and the former is representative of local vibration modes and response. For both incremental and RAN tests, blind panels are associated with maximum CAF values equal to about 3.0 – 3.5, showing a relatively large dispersion over the different panels. Considering the glass panel, CAF values derived considering RAN tests are significantly larger than CAF values related to incremental tests, even doubling it. This evidence stresses the potential of RAN tests as a means for exciting the maximum elastic amplification response. However, this extremely amplified response might not be representative of actual amplification scenarios, i.e., associated with real or realistic seismic loading histories.

The maximum CAF related to global response of the cleanroom are overall lower than typical values recommended by building codes (e.g., 2.5 according to ASCE 7-16 [10]), especially the ones related to display case top. A value equal to 2 might be considered as a conservative reference. CAF values equal to about 3 might be considered reliable for local design/assessment of blind panels, whereas larger values could be representative of glass panel, even though extremely large values (e.g., equal to 6) might be excessively conservative, as previously discussed.

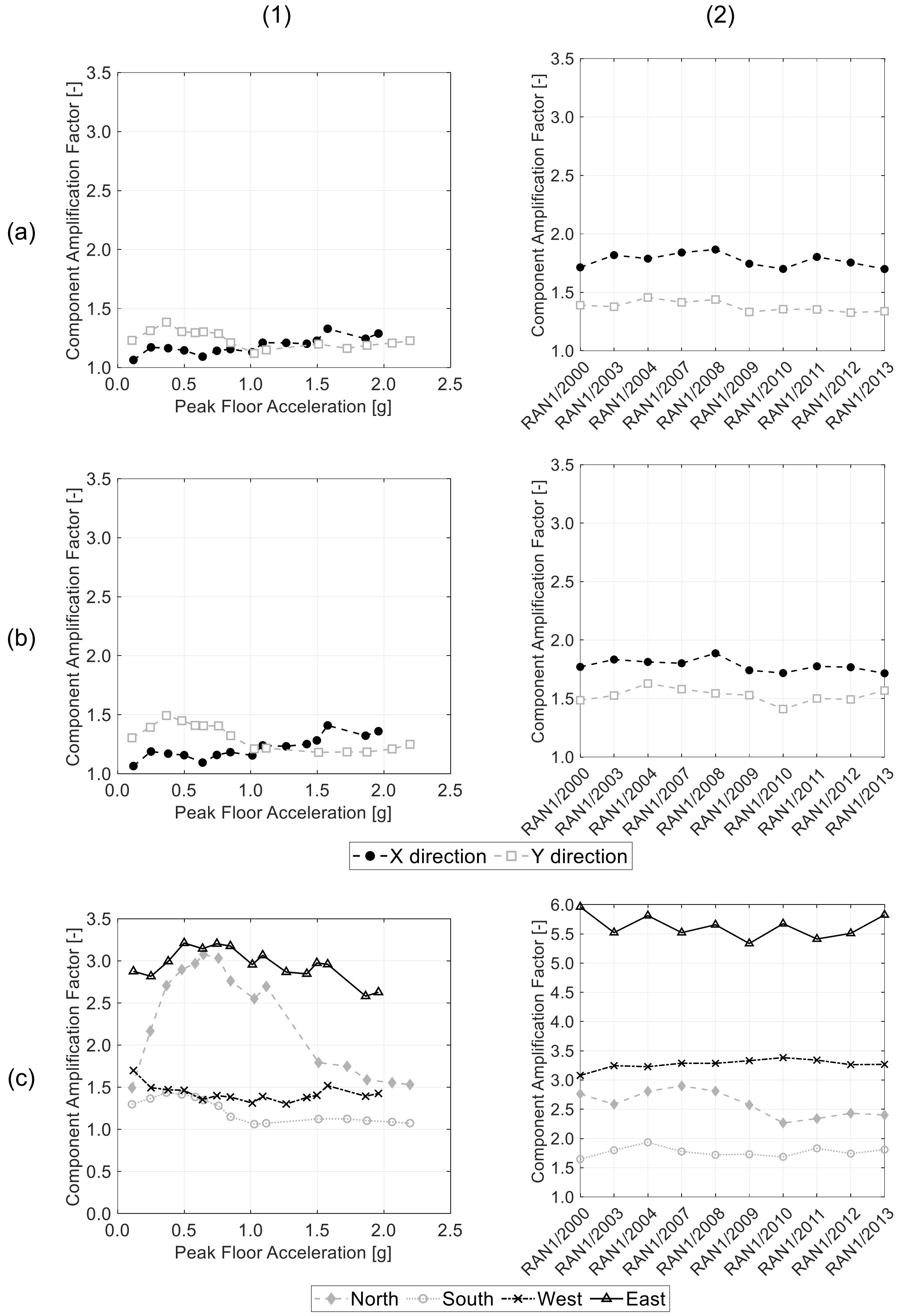

Figure 3.13: Acceleration response: component amplification factor (CAF) evolution associated with (a) cleanroom top (lateral partition), (b) ceiling frame (hanger-suspension device), and (c) lateral partition panels (out of plane directions), considering (1) incremental tests, as a funcion of PFA, and (2) dynamic identification tests, as a functon of RAN test IDs.

3.3.5 Displacement response

Two measures of displacements are assessed under functioning conditions: (D1) relative horizontal displacement between story of the test frame and top of the cleanroom (i.e., lateral panels' top) and (D2) relative horizontal displacement between top of the cleanroom (i.e., lateral panels' top) and the shake table. D1 informs regarding the transversal deformation capacity of the suspensions system and cleanroom plenum, whereas D2 is associated with the transversal deformation capacity of the cleanroom itself (including the cleanroom base to shake table interations). Figure 3.14a depicts the peak values of D1, normalized considering the distance between cleanroom top and the test frame top, i.e., expressed an interstory drift ratio (namely, IDR1), as a function of the incremental test PFA values, along both directions. D1 was assessed considering the average between the two available measures, i.e., WPot1 to L3 instruments and WPot2 to L3 instruments along X direction and WPot3 to L1 instruments and WPot4 to L1 instruments along Y direction.

IDR1 (Figure 3.14a) increases as PFA grows following an approximately linear pattern, even though response along X direction is more regular than along Y direction. In particular, the suspensions system and cleanroom plenum were found to be more deformable along Y direction (i.e., larger IDR1 for given PFA), especially within 0.4 – 1.5 g; for lower and higher intensities, IDR1 is more comparable along X and Y directions. The suspensions system and plenum are found to be able to accommodate extremely large relative horizontal displacements between the top of the cleanroom and the frame story (e.g., up to IDR1 equal to 10%), without transferring interaction forces from the test frame to the cleanroom top, and, more importantly, without affecting the cleanroom functioning (if the anomaly related to test AC10, previously discussed, is neglected). Therefore, the cleanroom system can be assumed to be fully uncoupled from the test frame, and, generally, from the top story of the building floor in which the cleanroom is housed.

Figure 3.14b depicts the peak values of D2, normalized considering the distance between shake table/cleanroom base and cleanroom top, i.e., expressed as an interstory drift ratio (namely, IDR2), as a function of the incremental test PFA values, along both directions. The absolute displacements for estimating D2 were obtained by double integrating acceleration time histories associated with the relevant accelerometers; as a matter of fact, some laser sensors went out of scale for relatively high intensities. Acc052x to AccTX instruments were considered along X direction and Acc052y to AccTY instruments along Y direction to assess the relative displacement between top of the cleanroom and the shake table, respectively.

IDR2 (Figure 3.14b) linearly grows as PFA increases; the response is almost identical in X and Y direction up to about PFA equal to 1.3 g; for higher intensities, IDR2 related to X direction is larger than along Y direction. Overall, the cleanroom was found to have a relatively stiff response considering IDR2, especially the deformability of the suspensions system and plenum of the cleanroom is considered as a reference. For example, IDR2 was lower than 0.15% (0.5%) under PFA equal to about 0.5 g (2.0 g), showing a gradient that is not affected by the test intensity (e.g., linear elastic response). It is recalled that no damage or performance/functioning disruption were observed up to the maximum intensities (if the anomaly related to test AC10, previously discussed, is neglected). Accordingly, the cleanroom system remained fully functioning up to IDR2 values equal to 0.5%.

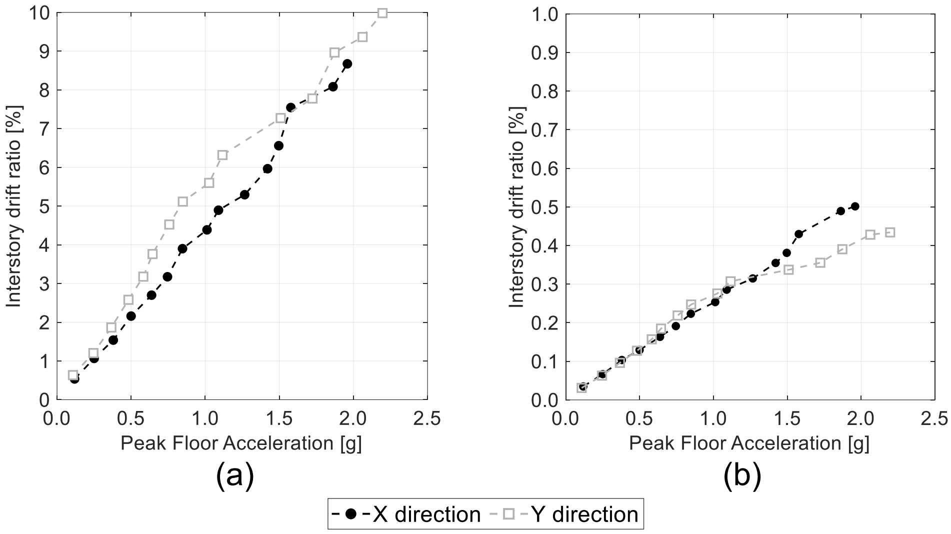

Figure 3.14: Displacement response: (a) peak relative displacement between test frame story and cleanroom top (D1), normalized considering cleanroom top to test frame story distance, expressed as an interstory drift ratio (IDR1), and (b) peak relative displacement between cleanroom top and cleanroom base/shake table (D2), normalized considering cleanroom height, expressed as an interstory drift ratio (IDR2), both as a function of incremental test PFA values.

3.4 Discussion

The main dynamic properties of the specimen were estimated, with particular regard to transfer functions, vibration modes, fundamental frequencies, and damping ratios. The acceleration response was characterized in terms of time histories, peak values, and component amplification ratios, considering accelerograms recorded over several cleanroom locations/components; both peak values and amplification ratios were correlated with testing intensity. The deformability of the system was assessed considering relative displacements and interstory drift, associating peak values to the testing intensity. In particular, the deformability of both suspensions system-cleanroom plenum system and whole cleanroom was estimated and correlated with testing intensity. The following main conclusion remarks can be drawn.

- The cleanroom was found to be fully operational under extremely high seismic intensities, e.g., peak floor accelerations significantly higher than those associated with high seismicity (e.g., in Italy and Europe).

- The suspensions system-cleanroom plenum system was able to uncouple the response of the cleanroom from the test frame story, representative of the top story of installation building floor. In other words, the cleanroom would not be affected by extremely large potential building deformation due to seismic actions (e.g., interstory drift).
- The lateral response of the cleanroom was found to be relatively stiff, and this would preserve the functioning conditions in case of significant seismic actions.
- Seismic design and assessment methods and recommendations are provided; the fundamental component frequencies, damping ratios, and acceleration amplification factors are provided.
- Technical and constructive requirements and innovation technologic solutions are supplied for the enhancement of the seismic performance of cleanrooms. In particular, innovation components and connection arrangements are illustrated, and their efficiency is experimentally proven.

3.5 References

[1] Yang Z, Hao Y, Shi W, Shao X, Dong X, Cheng X, et al. Field test of pharmaceutical cleanroom cleanliness subject to multiple disturbance factors. Journal of Building Engineering 2021; 42: 103083. DOI: 10.1016/j.jobe.2021.103083.

[2] Liu J, Zhang L, Yang J, Chen Y, Zhang X. Study on pressure control and energy saving of cleanroom in purification air conditioning system. Energy and Buildings 2021; 253: 111502. DOI: 10.1016/j.enbuild.2021.111502.

[3] European Committee for Standardization (CEN). Cleanrooms and associated controlled environments - Part 1: Classification of air cleanliness by particle concentration. Brussels, Belgium: https://store.uni.com/; 2016.

[4] Meghea A, Weissieker H. Identification of environmental sensors for cleanroom monitoring and control strategy. vol. 68. 2006.

[5] Shao X, Hao Y, Liang S, Wang H, Liu Y, Li X. Experimental characterization of particle distribution during the process of reducing the air supply volume in an electronic industry cleanroom. Journal of Building Engineering 2022; 45: 103594. DOI: 10.1016/j.jobe.2021.103594.

[6] Loomans MGLC, Ludlage TBJ, van den Oever H, Molenaar PCA, Kort HSM, Joosten PHJ. Experimental investigation into cleanroom contamination build-up when applying reduced ventilation and pressure hierarchy conditions as part of demand controlled filtration. Building and Environment 2020; 176: 106861. DOI: 10.1016/j.buildenv.2020.106861.

[7] Andersson AE, Bergh I, Karlsson J, Eriksson BI, Nilsson K. Traffic flow in the operating room: An explorative and descriptive study on air quality during orthopedic trauma implant surgery. American Journal of Infection Control 2012; 40(8): 750–755. DOI: 10.1016/j.ajic.2011.09.015.
[8] Can A, Divarci HÖ, Buyruk E. Design principles of the hospital clean rooms. Transactions of FAMENA Special Issue 1 2021; XLV(1): 1–15. DOI: https://doi.org/10.21278/TOF.45Si1008521
[9] FEMA E-74. Reducing the Risks of Nonstructural Earthquake Damage-A Practical Guide. 2012.
[10] ASCE 7-16. Minimum Design Loads and Associated Criteria for Buildings and Other Structures. American Society of Civil Engineers (ASCE); 2016. DOI: 10.1061/9780784414248.
[11] Petruzzelli F. Seismic risk assessment of an industrial plant struck by the Emilia 2012 earthquakes. vol. 3. 2016.
[12] Taghavi S, Miranda E. Response Assessment of Nonstructural Building Elements - PEER 2003/05. 2003.
[13] Hwang JS, Wang SJ, Huang YN, Chen JF. A seismic retrofit method by connecting viscous dampers for microelectronics factories. Earthquake Engineering & Structural Dynamics 2007; 36(11): 1461–1480. DOI: 10.1002/eqe.689.
[14] Jun SC, Lee CH, Bae CJ. Shake table testing of braced and Friction-Added suspended ceilings and associated numerical study. Engineering Structures 2022; 252: 113724. DOI: 10.1016/j.engstruct.2021.113724.
[15] Qi L, Kurata M, Ikeda Y, Kunitomo K, Takaoka M. Seismic evaluation of two-elevation ceiling system by shake table tests. Earthquake Engineering and Structural Dynamics 2021; 50(4): 1147–1166. DOI: 10.1002/eqe.3390.
[16] Mulligan J, Sullivan TJ, Dhakal RP. Experimental Seismic Performance of Partly-Sliding Partition Walls. Journal of Earthquake Engineering 2020. DOI: 10.1080/13632469.2020.1733139.
[17] Arifin FA, Sullivan TJ, Dhakal RP. Experimental investigation into the seismic fragility of a commercial glazing system. vol. 53. 2020.
[18] Petrone C, Magliulo G, Manfredi G. Shake table tests on standard and innovative temporary partition walls. Earthquake Engineering and Structural Dynamics 2017; 46(10): 1599–1624. DOI: 10.1002/eqe.2872.
[19] Magliulo G, Petrone C, Capozzi V, Maddaloni G, Lopez P, Manfredi G. Seismic performance evaluation of plasterboard partitions via shake table tests. Bulletin of Earthquake Engineering 2014; 12(4): 1657–1677. DOI: 10.1007/s10518-013-9567-8.
[20] Magliulo G, Pentangelo V, Maddaloni G, Capozzi V, Petrone C, Lopez P, et al. Shake table tests for seismic assessment of

suspended continuous ceilings. Bulletin of Earthquake Engineering 2012; 10(6): 1819–1832. DOI: 10.1007/s10518-012-9383-6.
[21] Shin DH, Kim HJ. Macro-modelling approach for the in-plane cyclic response of cold-formed steel partition walls. Applied Sciences (Switzerland) 2020; 10(22): 1–21. DOI: 10.3390/app10228163.
[22] Javid SH, Soroushian S, Rahmanishamsi E, Maragakis EM. Methodology for the Development of Analytical Seismic Fragility for Full Connection Steel-Framed Gypsum Partition Walls. Journal of Earthquake Engineering 2020. DOI: 10.1080/13632469.2020.1822234.
[23] Butenweg C, Bursi OS, Paolacci F, Marinković M, Lanese I, Nardin C, et al. Seismic performance of an industrial multi-storey frame structure with process equipment subjected to shake table testing. Engineering Structures 2021; 243: 112681. DOI: 10.1016/j.engstruct.2021.112681.
[24] Ghalibafian H, Bhuyan GS, Ventura C, Rainer JH, Borthwick D, Stewart RPB, et al. Seismic Behavior of Flexible Conductors Connecting Substation Equipment—Part II: Shake Table Tests. IEEE Transactions on Power Delivery 2004; 19(4): 1680–1687. DOI: 10.1109/TPWRD.2004.832387.
[25] Filiatrault A, Kuan S, Tremblay R. Shake table testing of bookcase – partition wall systems. Canadian Journal of Civil Engineering 2004.
[26] Wittich CE, Hutchinson TC. Shake table tests of unattached, asymmetric, dual-body systems. Earthquake Engineering & Structural Dynamics 2017; 46(9): 1391–1410. DOI: 10.1002/eqe.2860.
[27] D'Angela D, Magliulo G, Cosenza E. Seismic damage assessment of unanchored nonstructural components taking into account the building response. Structural Safety 2021; 93. DOI: 10.1016/j.strusafe.2021.102126.
[28] Di Sarno L, Magliulo G, D'Angela D, Cosenza E. Experimental assessment of the seismic performance of hospital cabinets using shake table testing. Earthquake Engineering and Structural Dynamics 2019; 48(1): 103–123. DOI: 10.1002/eqe.3127.
[29] Prota A, Zito M, D'Angela D, Toscano G, Ceraldi C, Fiorillo A, et al. Preliminary Results of Shake Table Tests of a Typical Museum Display Case Containing an Art Object. Advances in Civil Engineering 2022; 2022: 1–18. DOI: 10.1155/2022/3975958.
[30] Blasi G, Aiello MA, Maddaloni G, Pecce MR. Seismic response evaluation of medical gas and fire-protection pipelines' Tee-Joints. Engineering Structures 2018; 173: 1039–1053. DOI: 10.1016/j.engstruct.2018.07.045.

[31] Tran TT, Salman K, Kim D. Distributed plasticity approach for nonlinear analysis of nuclear power plant equipment: Experimental and numerical studies. Nuclear Engineering and Technology 2021. DOI: 10.1016/j.net.2021.03.017.
[32] Soroushian S, Maragakis EM, Jenkins C. Capacity evaluation of suspended ceiling components, Part 1: Experimental studies. Journal of Earthquake Engineering 2015; 19(5): 784–804. DOI: 10.1080/13632469.2014.998354.
[33] Tian Y, Filiatrault A, Mosqueda G. Seismic response of pressurized fire sprinkler piping systems I: Experimental study. Journal of Earthquake Engineering 2015; 19(4): 649–673. DOI: 10.1080/13632469.2014.994147.
[34] ICC-ES AC156. Acceptance criteria for seismic certification by shake-table testing of nonstructural components. 2012.
[35] Comité Européen de Normalisation (CEN). Eurocode 8: Design of structures for earthquake resistance. 2005.
[36] Ministero delle infrastrutture e dei trasporti. Aggiornamento delle “Norme tecniche per le costruzioni” Decreto 17 gennaio 2018. vol. 20. (in italian); 2018.
[37] European Commission enterprise and industry directorate-general. Good Manufacturing Practice Medicinal Products for Human and Veterinary Use (GMP) Annex 1: Manufacture of Sterile Medicinal Products. Brussels, Belgium: EU Guidelines; 2008.
[38] U.S. General Services Administration. Federal Standard 209E: Airborne Particulate Cleanliness Classes in Cleanrooms and Clean Zones. 1992.
[39] U.S. General Services Administration. Appendix 1 Federal Standard 209D: cleanroom and work station requirements, controlled environment. 1992.
[40] G. Magliulo. Prove su tavola vibrante per l’analisi della prestazione sismica di una cleanroom serie 62 acciaio (in Italian). Naples: 2021.
[41] European Committee for Standardization (CEN). Cleanrooms and associated controlled environments - Part 3: Test methods. European Committee for Standardization (CEN): https://store.uni.com/; 2019.
[42] Di Sarno L, Petrone C, Magliulo G, Manfredi G. Dynamic properties of typical consultation room medical components. Engineering Structures 2015; 100: 442–454. DOI: 10.1016/j.engstruct.2015.06.036.
[43] Clough RW, Penzien J. Dynamics of Structures. 2003.
[44] Magliulo G, Maddaloni G, Petrone C. A procedure to select time-histories for shaking table tests on nonstructural components. Proceedings of the 4th ECCOMAS Thematic Conference on Computational Methods in Structural Dynamics and Earthquake Engineering, 2013.

[45] Chopra AK. Dynamics of Structures. Prentice Hall 1995.
[46] Papagiannopoulos GA, Hatzigeorgiou GD. On the use of the half-power bandwidth method to estimate damping in building structures. Soil Dynamics and Earthquake Engineering 2011; 31(7): 1075–1079. DOI: 10.1016/j.soildyn.2011.02.007.

Chapter 4

4 Shake table tests of a typical museum display case containing an art object

The seismic response of freestanding elements is typically extremely critical, and this is associated with a high seismic risk in the case of museum objects and artefacts. This chapter reports the preliminary results of an experimental testing campaign aimed at assessing the dynamic properties and the seismic performance of museum objects and artefacts. Shake table tests of a typical museum display case containing a representative art object (vase) are performed. Both dynamic properties and seismic behavior of the specimens were assessed. Tentative damage assessment correlations are developed. The chapter sheds lights on the critical behavior of the tested specimens, stressing the need for further studies towards a more comprehensive assessment of freestanding museum objects and artefacts.

4.1 Introduction

The seismic response of engineering systems governed by rigid motion (e.g., freestanding or unanchored elements) is typically extremely critical [1–4]. In many cases, rigid-dominated systems are nonstructural elements [5–8]. The seismic risk associated with these systems can be high, especially if they are housed within critical facilities (e.g., hospital or laboratory equipment [9,10] or nuclear facilities [11,12]) or have historical/cultural significance (e.g., art objects) [13–15]. In the light of that, several studies recently provided guidance for mitigating the seismic vulnerability of freestanding valuable and museum systems and objects [16–18]. However, current arrangements for those systems housed in critical facilities and museums typically do not include protection systems, except for few peculiar cases.

Freestanding systems typically exhibit significant rocking-sliding motion under relatively low seismic intensity excitations [19–21]. Several studies assessed the seismic response of critical freestanding (or unanchored) elements through experimental testing [9,22–26] and numerical analysis [12,20,27–30]. Dar et al [12] assessed the reliability of simplified method provided by ASCE 43-05 for the assessment of freestanding elements. It was found that this method provides unreliable estimations, recommending the use or more refined analysis methodologies (nonlinear dynamic analyses). Fragiadakis and Diamantopoulos [29] developed a simplified approach to assess the fragility of freestanding building contents and provided quantitative results promising for risk estimates regarding a case study application (four-story reinforced concrete building). Huang et al. [31] performed free-rocking tests on freestanding elements accounting for variation in center of gravity location. Particular focus was on rocking response and dynamic properties and on the influence of the center of gravity variation on these parameters. The study highlighted potential discrepancies between analytical estimations and experimental response, providing an accurate equivalent rectangular rigid block model.

Despite the copious literature addressing the seismic response of freestanding elements, a reduced number of studies focused on museum objects and artefacts. Berto et al. [32] investigated the seismic behavior of six Michelangelo's sculptures by means of rigid block and finite element analysis. They highlighted the weakness of the investigated statues regarding their seismic performance and provided technical insights towards the mitigation of the seismic risk associated with art objects. Sorace and Terenzi [17] carried out finite element analysis of a marble statue housed in a castle in Italy through an incremental procedure, assessing both dynamic behavior and stress distribution. The case study was representative of a wide range of scenarios. They developed assessment criteria and suggested possible isolation solutions for an effective seismic protection of art objects. Wittich and Hutchinson [24] performed shake table tests on statue-pedestal unattached systems, varying geometry (including asymmetry), loading history, and friction coefficient. They stressed the complexity of the dynamic response of dual body unanchored systems, characterized by both significant sliding and rocking, multi-modal interaction, and three-dimensional response.

Very few studies focused on freestanding display cases/cabinets containing unanchored art objects or valuable components. This configuration is typically quite critical since both the container (e.g., display case) and the content (e.g., art object) may exhibit rigid-dominated response, associated with major motion and resulting in high seismic risk. Moreover, most of small and medium size objects and components are often contained in such display cases or cabinets, and this makes this configuration quite common in museums and critical facilities. Neurohr and McClure [33] performed shake table testing of high density fiberboard display cases with plexiglas covers containing art objects. They assessed the influence of seismic input, floor height, surface friction, and mass of art objects on the vulnerability of the investigated specimens. Cosenza et al. [19] and Di Sarno et al. [9] performed shake table tests of freestanding hospital cabinets containing unanchored containers and phials. They investigated the influence of the contents on the dynamic properties and seismic performance of the cabinets and assessed the seismic fragility of both cabinets and contents.

Despite the recent research efforts towards a reliable seismic assessment and an effective protection of freestanding components and art objects, dynamic properties and seismic vulnerability of the most common configurations of museum systems and objects are still unknown. The chapter represents a first step carried out to fill the abovementioned research gap. In particular, shake table tests of a steel-glass display case containing an unanchored art object (vase) are performed, and preliminary results are reported in this section. The specimens represent a very common museum configuration, potentially associated with a high vulnerability. The specimens were provided by the National Archaeological Museum of Naples (MANN), Italy. The dynamic properties and seismic behavior of both display case and art object are assessed. A preliminary damage assessment is also performed in the light of the observations and the data analysis. My contribution in this study was to provide support during the execution of the vibration table tests and perform the analysis of the recorded data.

4.2 Display case and art object

The tested display case is part of the exhibition equipment of the MANN (Figure 4.1). The dimensions of the assembled display case are a 92 × 92 × 244.5 cm. The display case is composed of several components that were assembled on the shake table by specialized workers. The display case assembled on the shake table is depicted in Figure 4.2a. The steel base frame has dimensions 92 × 92 × 12 cm (width × length × height) and weight of 46.2 kg (Figure 4.2b). Four corner supports are screwed below the base frame, and each support is made of a steel threaded rod having a circular base pin, covered in plastic (Figure 4.2c); the supports have 1.5 cm height. A cover plate is simply supported by the internal part of the base frame. The plate consists of an internal wood plate covered by a steel shelter; the plate has dimensions 84 × 84 × 1.8 cm (width × length × thickness) and weight of 16.3 kg. The lateral surface of the case consists of three fixed panels and a front rotating door panel (Figure 4.2a). Both fixed panels and door panel are made of double-glass panels fixed to an inferior and a superior thin steel runner. Each glass panel has dimensions of 88.5 × 234 × 1.1 cm (width × height × thickness) and mass of about 55 kg. The door rotates about two hinges, fastened to the top and base frame; the door has an inferior and superior locker, fixing the runners to the base and top frames (Figure 4.2a). Both top and bottom door runners have dimensions equal to 92 × 2 cm (length × thickness) and mass of about 10.5 kg. The four lateral panels are connected to a top frame, having mass of 58.8 kg, that also incorporates the superior lighting system (Figure 4.2d); the top cover frame has height equal to 12 cm, equal to the height of the base frame. The glass panels, including the opening glass panel, are fixed to the bottom and top elements by friction. In particular, both bottom and top elements (corresponding to the runners) have a bucket (with seals) that is made by two flanges connected by a screw and two bolts (Figure 4.2e); the glass panels are inserted within this bucket, and the applied torque (fastening the screw/bolts) provides the friction to fix the glass panels to those flanges, providing their fastening to base and top elements.

A pedestal is located within the case and is simply supported by the internal cover plate (Figure 4.2a). The pedestal is made of a welded steel frame and thin steel cover surfaces; the frame consists of welded square hollow thin sections with dimensions 3 × 3 cm; the top and lateral pedestal steel covers are welded to the frame and have 2 cm width, whereas the base frame does not have a cover. The pedestal has dimensions of 60 × 60 × 88 cm (width × length × height) and mass of 45.8 kg. An art object was placed on the artefact support (Figure 4.2e); the object consisted in a ceramic vase, having base diameter and maximum diameter plus handles equal to about 22 and 42 cm, respectively, height equal to about 29 cm, and mass equal to about 7 kg.

The display case, including the art object, consists in the assembly of several parts. The base and top frames of display case are relatively rigid and are interconnected through the lateral glass panels (including the door). The glass panels are fastened to the base and top frame runners by means of friction bucket connections, which might allow a relatively reduced amount of free (relative) rotation. The components located inside the display case, i.e., basement, pedestal, and art object are not fastened among them (they are just freestanding to each other), and the basement is not fastened to the display case frame (just freestanding). Therefore, basement, pedestal, and art object are expected to be governed by a rigid block response; in particular, the basement is expected to exhibit a sliding response due to the very reduced slenderness; the pedestal is expected to be mostly governed by sliding due to reduced friction (smooth contact surfaces); the art object is expected to exhibit sliding due to reduced slenderness and reduced friction. The whole display case system is expected to exhibit a mixed sliding-rocking response, given the relatively slender geometry (rocking) and the relatively reduced friction (sliding). The sliding response might be more significant than the rocking one. The display case is also expected to exhibit minor elastic vibrational response (especially glass vibrations out of their plane). The dynamics of the internal components might condition the overall response of the system, especially the rigid-dominated motion. This description is only meant to ease the interpretation of the experimental results and does not involve numerical modeling or analysis.

Figure 4.1: Arrangement of the tested display case within the National Archaeological Museum of Naples (MANN), Italy.

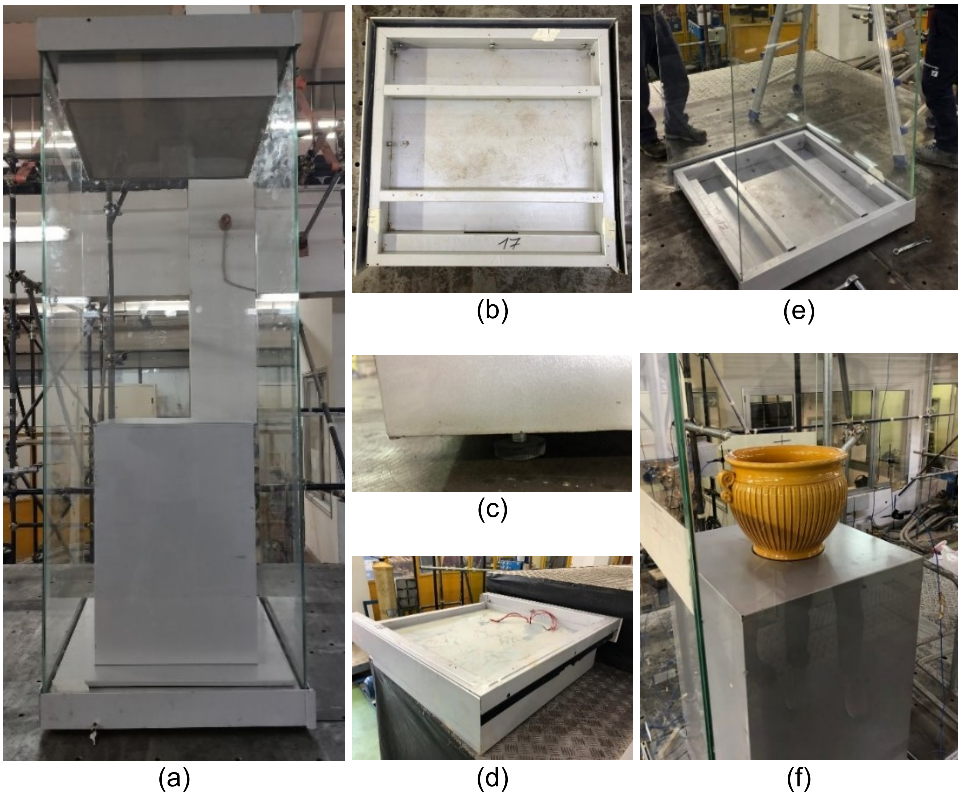

(a) (b) (c) (d) (e) (f)

Figure 4.2: Details of the tested specimen: (a) assembled display case, (b) base frame, (c) detail of the base frame support, (d) upside down top frame, (e) detail of the glass to frame connections, (f) detail of pedestal and art object (vase).

4.3 Shake table testing

4.3.1 Testing set-up and instrumentation

The display case was simply supported by the shake table steel floor, and the door panel was facing north side. Shake table and tested specimens were monitored by accelerometers (Acc), displacement laser sensors (Las), and video cameras (Figure 4.3). Four triaxial accelerometers (Acc054, Acc658, Acc766, and Acc056) were installed at the center of the double-glass panels, on the external surface of the glass. Two triaxial accelerometers (Acc052 and Acc053) were installed at the center of the east and south sides of the base frame. On south and west sides, two triaxial accelerometers (Acc765 and Acc763) were positioned at the center of the top frame. A triaxial accelerometer (Acc050) was installed on south side to measure the response of the bottom portion of the double-glass panel with respect to the two flanges. Two triaxial accelerometers (Acc762 and Acc818) were placed on the artefact support and base frame cover plate, respectively. The accelerations of the table were monitored by an internal accelerometer (AccT). Six displacement laser sensors were installed on south side (LasL2, LasW3, and LasW2) and east side (LasL3, LasW6, and LasW5). Two sensors (LasW1 and LasW4) were placed on south and east sides respectively, in order to record the displacement of the shake table in both horizontal directions. A safety scaffolding structure was built around the display case to protect the instruments and prevent critical displacement/overturning. The structure was 25 cm distant from the display case.

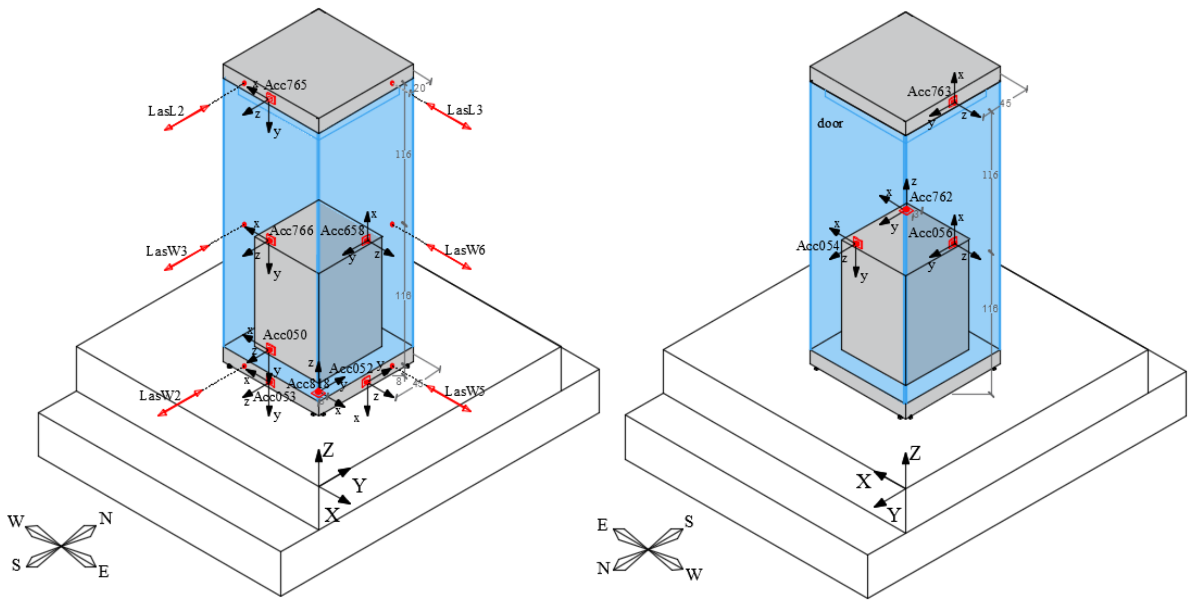

Figure 4.3: Perspective view of the instrumentation arrangement. The internal shake table accelerometer and laser sensors LasW1 and LasW4 are not depicted.

4.3.2 Testing input and program

Shake table testing represents the most reliable method for seismic assessment of acceleration sensitive elements such as freestanding systems [1,24,34]. Seismic assessment and qualification of acceleration-sensitive elements is typically performed through two types of testing: dynamic identification and seismic performance assessment [35,36]. Both dynamic identification and seismic performance tests were performed through mono- and bi-directional shake table testing, respectively. Low-amplitude random vibration signals (i.e., maximum acceleration not exceeding 0.1 g) were used to perform the dynamic identification tests (RAN tests) [9]. The seismic performance tests were carried out according to an incremental procedure, whereas the dynamic identification tests were performed prior to, during, and after the incremental tests. The shake table input related to the incremental tests (AC tests) was developed according to the ICC-ES AC156 protocol [36], which represents the international reference for seismic qualification and certification of acceleration-sensitive nonstructural components [1]. The procedure developed in [37] was used to generate/process the testing signals; this was already used in other experimental studies carried out by the authors (e.g., [38–41]); further details are omitted as the procedure is well described in the abovementioned literature studies. It should be noted that AC156 protocol is not aimed to assess freestanding elements but generic acceleration-sensitive elements, which are typically meant to be single-point attached/fastened to the structure. However, this protocol is typically used in literature and practice also for these components [9,19,34,42–44] since no alternative reference protocols exist to assess and qualify freestanding elements. For more details regarding this issue, please, refer to [1,30].

The design spectral acceleration at short periods S_{DS} was used as a reference intensity measure for scaling the intensity of the incremental tests. The acceleration time history and the response spectra associated with the defined AC156 input along both horizontal directions are depicted in Figure 4.4a and Figure 4.4b, respectively, considering S_{DS} equal to 0.45 g. In particular, test response spectra (TRS) and required response spectra (RRS) are depicted in Figure 4.4b considering sixths of octave as a unit reference along the ordinate axis. Please refer to [40] for further details regarding the development of the testing inputs.

Table 4.1 reports the testing program, including both dynamic identification (RAN) and seismic performance (AC) tests. The table maximum accelerations recorded along both horizontal directions, meant as a peak floor acceleration (PFA), are also reported in Table 4.1.

4.3.3 Analysis and assessment methodology

The spectrum-compatibility between TRS and RRS was assessed according to the procedure defined by AC156 protocol [36,45]. The dynamic identification of the specimens was carried out, and both natural frequencies and damping ratios of the specimens were assessed [46–48]. The transfer function method was used to estimate the natural frequency of the tested museum display case. In particular, the transfer function of the tested museum display case was obtained as the ratio of the Fourier transforms related to acceleration time histories recorded at the display case top and at the shake table.

Table 4.1: Testing program and maximum recorded accelerations: dynamic identification (RAN) and seismic performance (AC) tests.

test ID	direction(s)	S_{DS} [g]	PFA_x [g]	PFA_y [g]
RAN1000	X	-	0.05	-
RAN2000	Y	-	-	0.03
AC01	X,Y	0.05	0.05	0.08
AC02	X,Y	0.10	0.10	0.18
RAN1001	X	-	0.10	-
RAN2001	Y	-	-	0.06
AC03	X,Y	0.15	0.17	0.30
RAN1002	X	-	0.10	-
RAN2002	Y	-	-	0.08
AC04	X,Y	0.20	0.24	0.38
RAN1003	X	-	0.10	-
RAN2003	Y	-	-	0.08
AC05	X,Y	0.25	0.31	0.43
RAN1004	X	-	0.11	-
RAN2004	Y	-	-	0.08
AC06	X,Y	0.30	0.36	0.50
RAN1005	X	-	0.11	-
RAN2005	Y	-	-	0.08
AC07	X,Y	0.35	0.42	0.54
RAN1006	X	-	0.10	-
RAN2006	Y	-	-	0.08
AC08	X,Y	0.40	0.47	0.59
RAN1007	X	-	0.11	-
RAN2007	Y	-	-	0.08
AC09	X,Y	0.45	0.54	0.63
RAN1008	X	-	0.10	-
RAN2008	Y	-	-	0.07

The equivalent damping ratio was evaluated according to the half-power bandwidth method [48,49], typically used to assess structures and components assumed to have linear viscous damping [46,50]. The damping ratio associated with first mode of the display case was evaluated by data from each frequency response obtained by dynamic identification tests. As these tests were performed considering relatively low intensity shaking levels, the display case did not exhibit rigid motion but only elastic response, behaving as it was fixed at its base. Accordingly, the application of half-power bandwidth method is reasonably consistent. The time history accelerations recorded on both table and display case components were assessed, and the peak values, i.e., PFA and peak component acceleration (PCA) were associated with the incremental test intensities. The component amplification factor, defined as the ratio between PCA and PFA, was computed considering multiple components of the display case and associated with incremental tests. The time history displacements recorded on table and display case were assessed, including both absolute and relative displacement measures; the peak relative displacements is associated with the incremental test intensity.

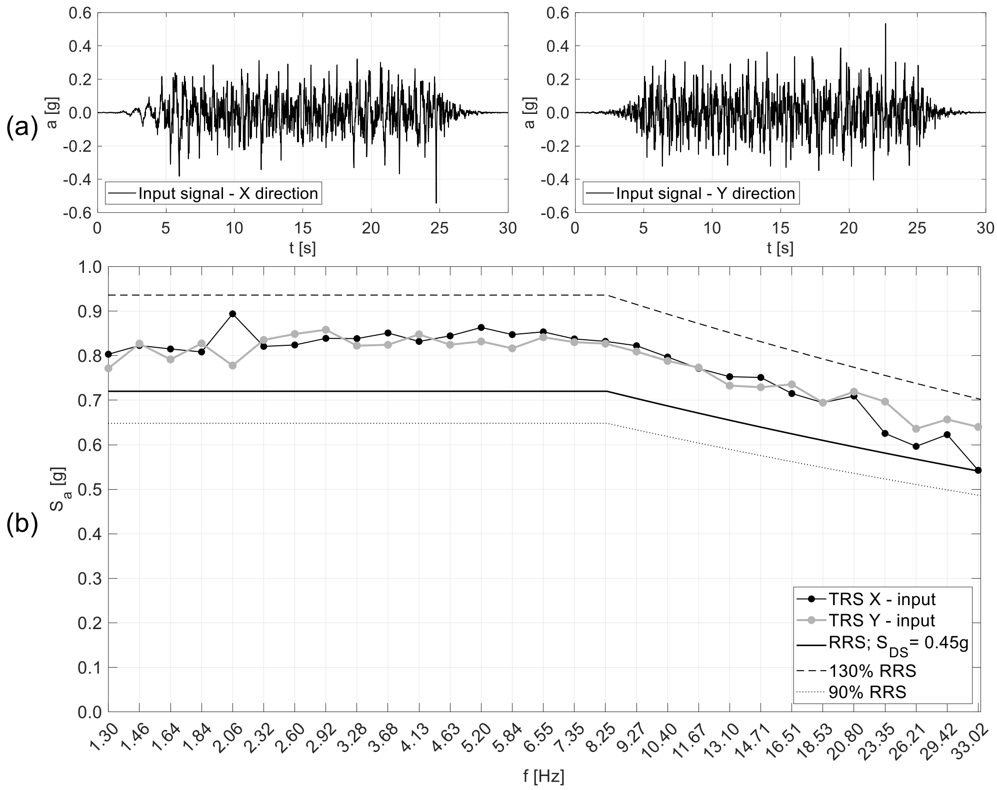

Figure 4.4: AC156 testing input corresponding to S_{DS} equal to 0.45 g: (a) acceleration time histories and (b) acceleration response spectra (i.e., test response spectra (TRS) and required response spectra (RRS)).

A preliminary damage assessment was performed considering the following damage states (DSs): DS0 (absent damage), DS1 (minor damage), DS2 (moderate damage), and DS3 (major damage) (e.g., [19,41]). DS1 achievement implies the need to reposition the specimen or art object in order to restore its original condition; DS2 achievement implies the need to partially replace the components of the specimen; DS3 implies the complete replacement of the specimen, and the life safety is not ensured. Usually, the difference from DS2 to DS3 is due to significant damage that could result in loss of life [5,51]. In the case of extremely valuable components (e.g., museum art object), significant motion and/or large residual displacement of the component could even be associated with DS3, even though this response is not associated with loss of life. In fact, this response could result in critical economic and cultural losses. It should be noted that the damage correlations should also depend on the desired level of safety and on importance of the building, and that the assessment of museum facilities and art object should follow more conservative rules. The correlation between the exhibited damage and the DS occurrence (namely, damage scheme) was assessed according to past studies [19] and abovementioned consideration. After each shaking level, the damage was observed by inspecting the physical conditions of the components of the display case and art object. The damage level required to reach a given DS was identified for each component of the display case and art object; obviously, the DS is the maximum between the different DS recorded in each component. In particular, the damage exhibited by the specimens was assessed by both observational checks and data analysis. The observational assessment was carried out during the tests and by checking the recorded videos, whereas a more quantitative assessment was performed through the analysis of the testing output data. The results reported in the following sections should be considered as preliminary findings, and the damage assessment should not be considered exhaustive.

4.4 Results and remark

4.4.1 RRS to TRS spectrum-compatibility

Figure 4.5 depicts the RRS to TRS spectrum-compatibility related to tests (a) AC01, (b) AC05, and (c) AC09 (X direction), corresponding to S_{DS} equal to 0.10, 0.25, and 0.45 g, respectively. The recorded (test) TRS was quite similar to the RRS one, and the spectrum-compatibility was verified for all tests. In particular, even in the only case in which the TRS spectrum falls below RRS (e.g., Figure 4.5a, corresponding to frequency between 18.5 and 20.8 Hz), the compatibility is confirmed since (a) TRS ordinate is not lower than 90% RRS ordinate and (b) TRS exceeds or equals the RRS corresponding to the superior and inferior adjacent sixth of octave [36].

4.4.2 Dynamic identification

The dynamic identification results are shown in Figure 4.6: (a) transfer curves (RAN test curves and median curves), (b) peaks of first fundamental vibration mode, and (c) damping ratios, associated with (1) X and (Y) directions. In particular, Acc765z and Acc763z were considered as output accelerometers for X and Y directions, respectively, whereas AccT was considered as input accelerometer. RAN1000 and RAN2000 results are not depicted as the tests did not produce consistent transfer functions, and this was reasonably due to the too low intensity amplitude of the random signals (Table 4.1). It should be noted that the specimen exhibited a complex frequency response (i.e., irregular and multiple vibration modes, Figure 4.6a), and the frequency peaks associated with first modes (Figure 4.6b) cannot fully describe the dynamic properties of the specimen. This points out that the system represents a multiple-degree of freedom system. Considering X direction, two sets or families of transfer curves can be identified (Figure 4.6a.1): (1) RAN1001, RAN1002, and RAN1006; (2) RAN1003, RAN1004, RAN1005, RAN1007, and RAN1008. Set 1 curves are quite similar among them and exhibit two significant frequency peaks, corresponding to about 8 Hz (fundamental frequency) and 13 Hz and associated with transfer function ordinates equal to about 3.5 and 3.0, respectively. Set 2 curves present fundamental peak frequencies lower than Set 1 ones, corresponding to about 6 Hz, with lower transfer function ordinates; the second peak frequency related to set 2 curves corresponds to about 18 Hz and is associated with ordinates equal to about 1. Each curve/frequency set might be associated with a different arrangement/settlement/adjustment condition of the specimen components, activated by the course of the incremental tests. Along Y direction, the transfer curves are more similar among them, identifying similar fundamental peaks and transfer curve ordinates (Figure 4.6a.2). In particular, the fundamental peak frequencies are equal to about 7 Hz and correspond to transfer curve ordinates equal to about 4. A second peak frequency can be identified, corresponding to about 11 Hz and transfer function ordinates ranging between 2 and 2.75.

The fundamental frequency overall decreases as the incremental tests proceed along X direction, and the only anomaly is associated with RAN1006 case, where the fundamental frequency exceeds RAN1001 and RAN1002 ones (Figure 4.6b.1). Despite this anomaly, it might be hypothesized that the progress of the incremental tests determines deformation/adaptation conditions that, even though minor, affect the elastic properties of the specimens in terms of fundamental frequency. In fact, this influence is not actually likely to be associated with damage condition, but to different arrangements of the parts and connections of the specimens. A more regular and gradual decrease in fundamental frequency is observed along Y direction (Figure 4.6b.2). The anomaly related to RAN1006 (Figure 4.6b.1) might be by a change in arrangement/settlement/adjustment condition of the specimen due to incremental test preceding test RAN1006. To interpret this anomaly, it should also be recalled that the specimen consists in a complex system of several components connected among them through non-controlled constraints, and this is associated with an extremely complex and irregular elastic response. For example, a temporary loosening or tightening condition of an intra- or inter-component connection might have affected the elastic vibration of the component. However, in this preliminary stage, it is not possible to provide more definite comments.

The damping ratio associated with X (Y) direction ranges in about 16 – 25% (10 – 13%), showing that the specimen has higher damping properties along X direction. The evolution of the damping ratio over the incremental tests is non-monotonic; in particular, the ratio overall increases along both X and Y directions, even though the increment related to Y direction is less significant than along X direction. Given the unicity of the tested specimen, it is not meaningful to make quantitative comparisons with literature results. However, the trends and the ranges of the fundamental periods and damping ratios are consistent with previous literature studies (e.g., [46]).

(a)

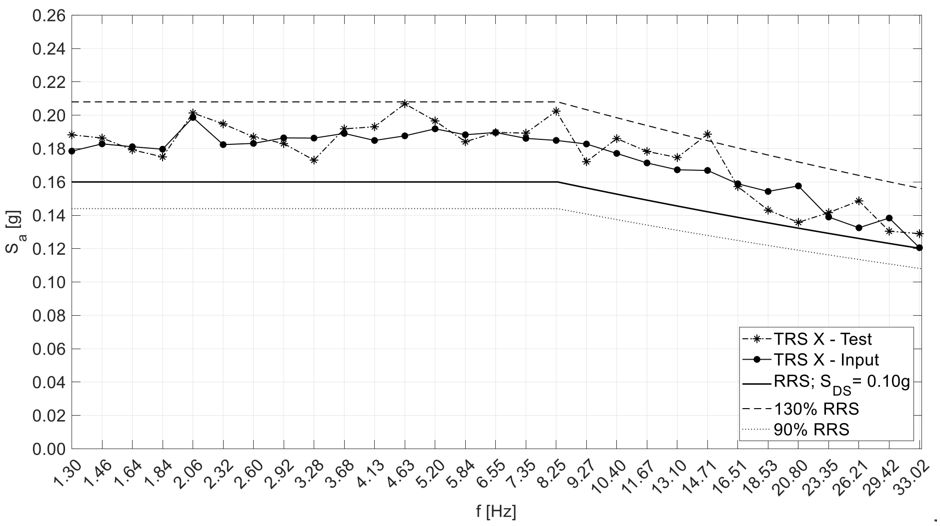

(b)

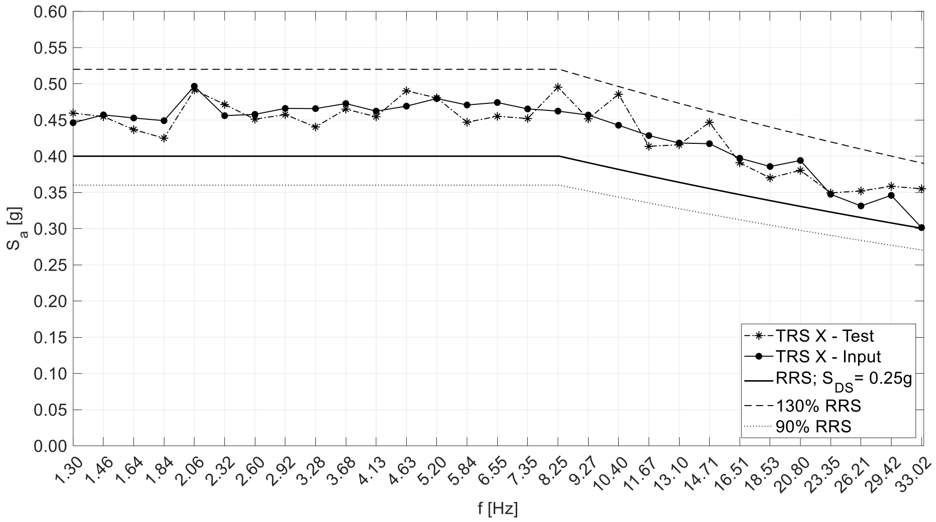

(c)

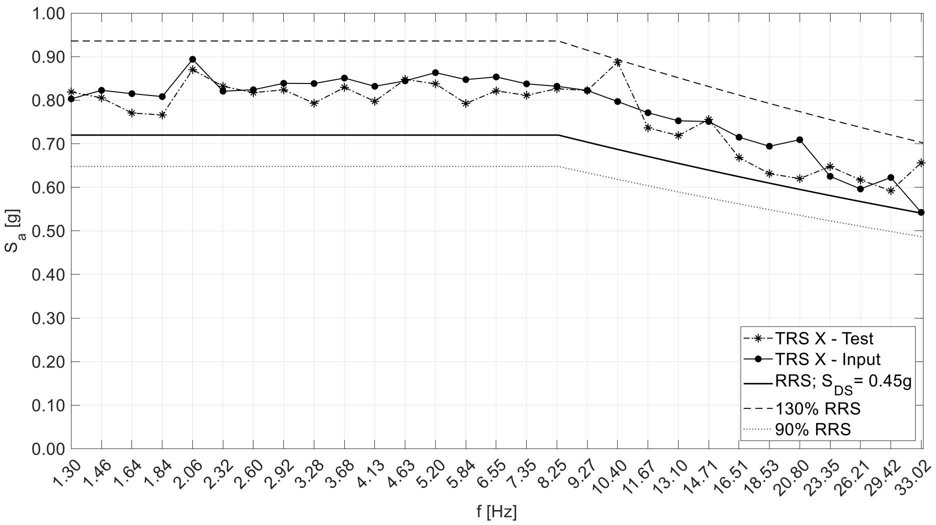

Figure 4.5: Spectrum-compatibility analysis: required response spectra (RRS) and test response spectra (TRS) along X direction. The results are related to tests (a) AC02 (S_{DS} equal to 0.10 g), (b) AC05 (S_{DS} equal to 0.25 g), and (c) AC09 (S_{DS} equal to 0.45 g). "TRS X - Test" and TRS X - Input" spectral correspond to recorded test signal and assigned input signal.

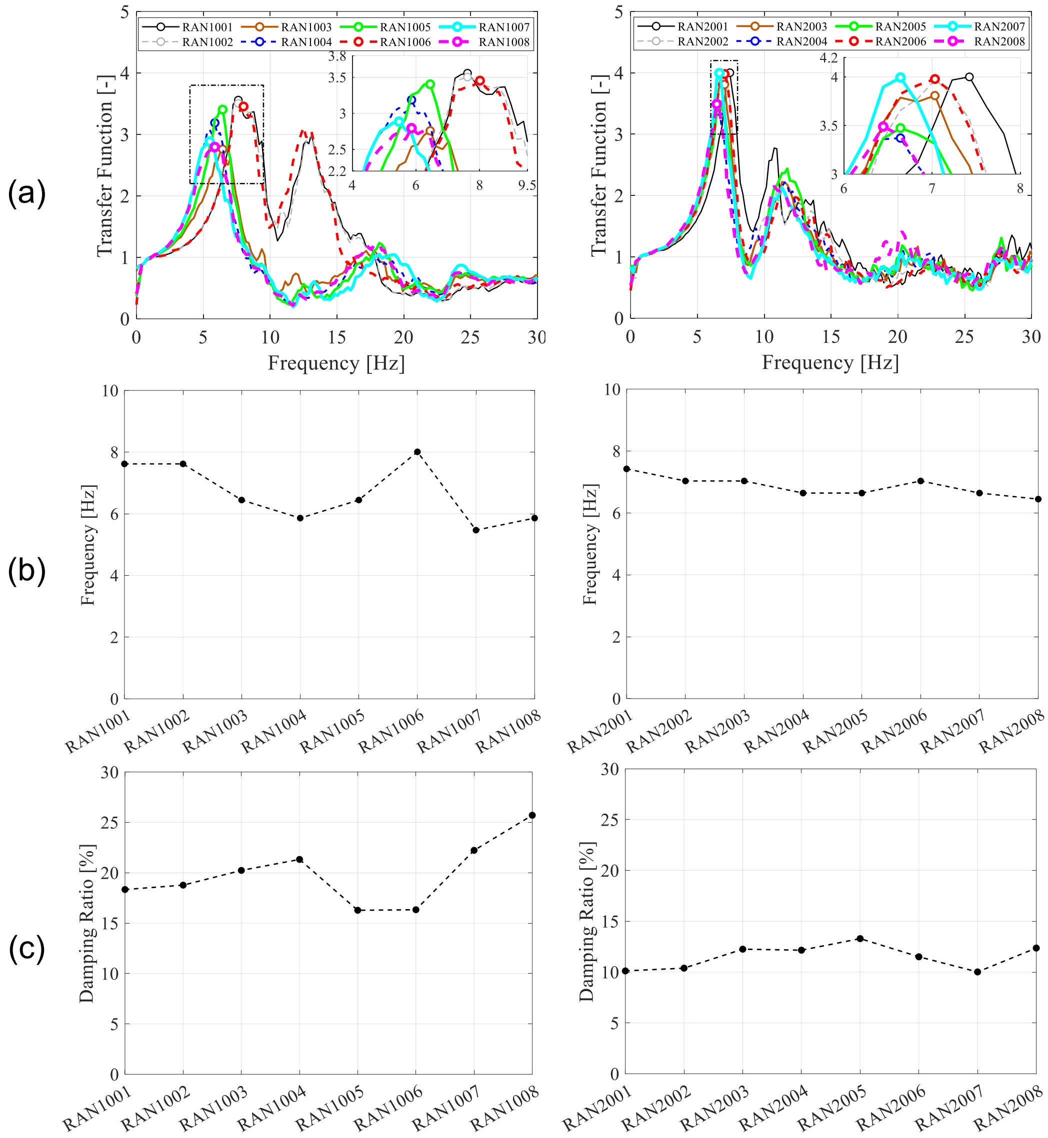

Figure 4.6: Dynamic identification: (a) transfer curves related to all dynamic identification (RAN) tests and (b) the frequency peaks associated with first vibration mode and (c) damping ratios evolution over RAN tests, estimated along (1) X and (2) Y directions.

4.4.3 Acceleration response

For the sake of brevity, only the time histories related to a representative test are depicted in the chapter, whereas peak accelerations related to all tests are shown. Figure 4.7 depicts the time history accelerations related to test AC05, associated with S_{DS}, PFAx, and PFAy equal to 0.25, 0.31, and 0.43 g, respectively. AC05 test is representative since it is threshold between the minor elastic response of the display case (for lower intensities) and the onset of significant the rigid motion (from test AC05 on). In Figure 4.7, the accelerations are related to both horizontal directions and correspond to (a) top of the display case, (b) top of pedestal, (c) middle point of representative glass panels, and (d) shake table. In particular, the accelerations of the glass panels are related to their out-of-plane directions. Therefore, X and Y results are associated with different glass panels, as also specified in Figure 4.7. As a matter of fact, the out-of-plane accelerations of the panels are typically more significant than the in-plane ones. Significantly high accelerations were recorded in both directions along the out-of-plane direction of the glass panels (Figure 4.7c), especially considering the shake table accelerations (Figure 4.7d); this evidences the considerable acceleration amplification associated with the behavior of the glass panels. The accelerations measured at the top of the display case are also significant, but they are lower than the ones recorded on the pedestal. The vase, supported by the pedestal, was subjected to accelerations significantly larger than the shake table ones, with extremely high peaks.

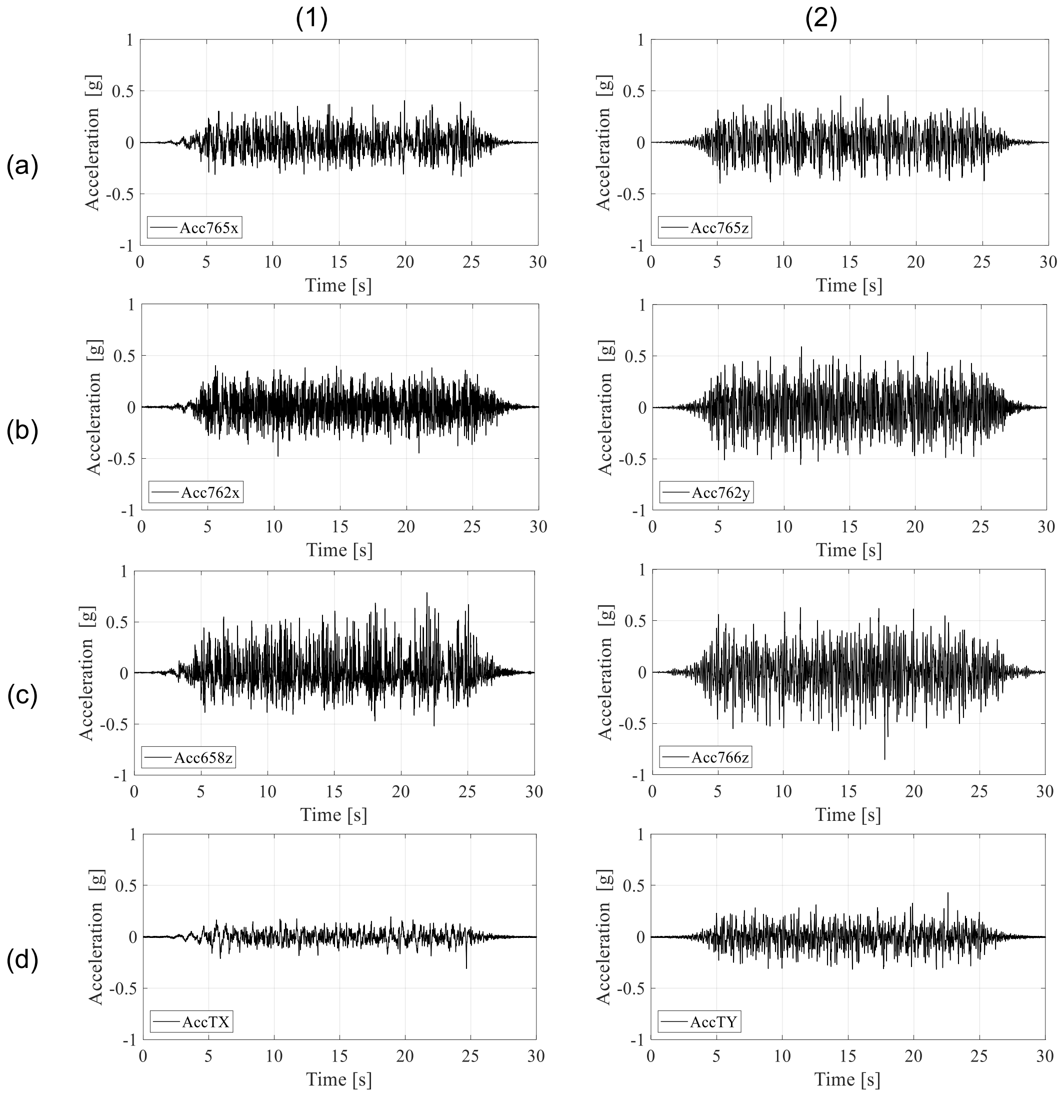

Figure 4.7: Acceleration time histories related to AC05 test, corresponding to (a) display case top, (b) pedestal top, (c) glass panels middle point, and (d) shake table, along (1) X and (2) Y directions.

Figure 4.8 shows the peak component acceleration (PCA) evolution over the incremental tests, related to (a) display case top, (b) pedestal top, (c) glass panels middle point, and (d) shake table, along both horizontal directions. PCA evolution related to both display case top (Figure 4.8a) and pedestal (Figure 4.8b) is more regular than the ones recorded on the glass panels (Figure 4.8c). In the former cases (Figure 4.8a and Figure 4.8b), there is an increase over the incremental tests that is relatively similar to the one associated with the accelerograms recorded on the shake table (Figure 4.8d). The acceleration peaks related the glass panels (Figure 4.8c) are more irregular as the testing intensity grows (Figure 4.8d). Considering both display case top and pedestal top accelerometer, the acceleration peaks related to Y direction are higher than the ones associated with X direction, similarly to the shake table acceleration peaks, whereas, for glass panel acceleration, the peak related to the horizontal directions are overall more similar among them. The glass acceleration peaks are significantly higher than the ones recorded on the other components. In some cases, extremely high acceleration (e.g., much greater than 1.0 g) peaks were recorded on the components; these peaks were determined by a significant interaction between the monitored component and the adjacent parts (i.e., test AC08 on glass panel and test AC09 on pedestal). In particular, the significant out-of-plane motion of the glass panels and the hammering against the adjacent (perpendicular) glass panels, determined extremely high and sudden acceleration peaks. These responses were not considered in a quantitative manner in this section.

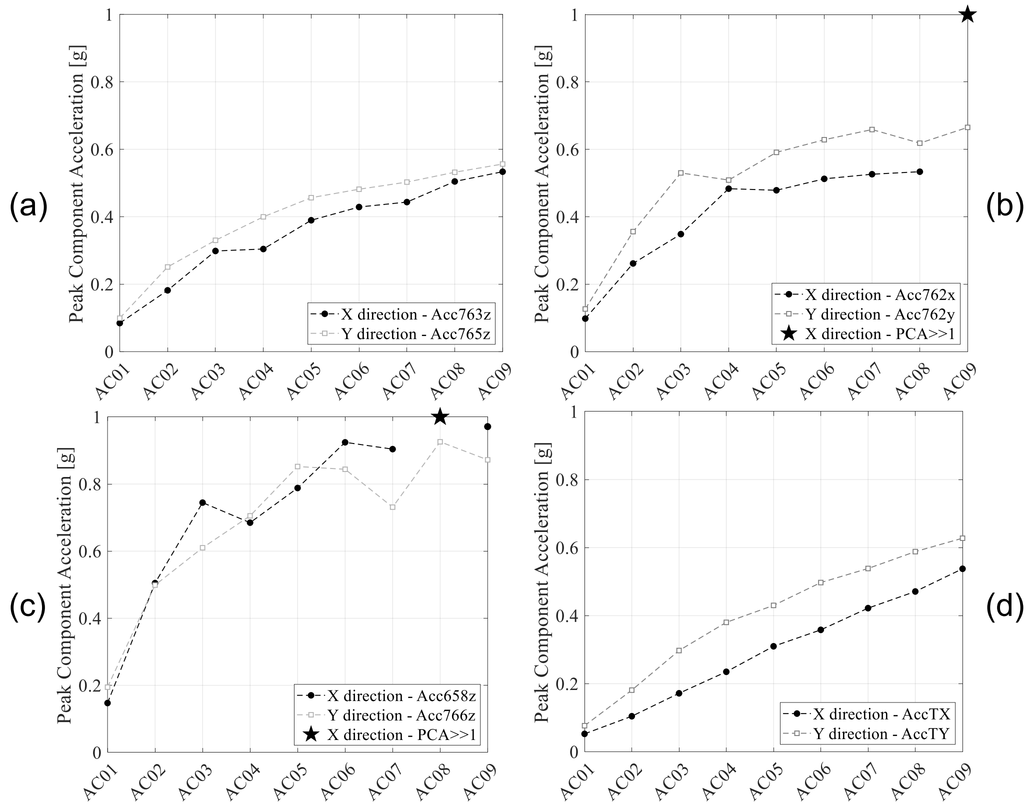

Figure 4.8: Peak component acceleration (PCA) evolution over the seismic performance tests corresponding to (a) display case top, (b) pedestal top, (c) glass panels middle point, and (d) shake table, along both horizontal directions.

The evolution of the component amplification factor over the PFA is depicted in Figure 4.9, corresponding to (a) display case top, (b) pedestal top, and (c) glass panels middle point, along both horizontal directions. The PFA is considered as abscissa axis since X and Y PFA are relatively different over same AC tests (Figure 4.8d); accordingly, the influence of the intensity can be directly assessed on component amplification factor. The trend of the component amplification factor over the incremental tests is similar over the different components of the display case, even though significant ordinate values are observed among the different components, especially along X direction. Overall, component amplification factor along X direction is larger than Y direction one over low intensity tests, especially for glass panel (Figure 4.9c) recording.

The maximum component amplification is always associated with test AC02 (PFA equal to about 0.10 g), whereas the minimum values are related to highest intensity tests. This points out that the most significant elastic response of the display case components is associated with about 0.10 g PFA intensities, when the specimen does not exhibit rigid motion, whereas the less significant elastic response is related to tests corresponding to which the specimen exhibit a significant rigid motion. It is recalled that dynamic identification tests were performed considering this intensity, to maximize the relevance of the elastic vibrational response. The maximum component amplification related to and display case top (Figure 4.9a) and pedestal top (Figure 4.9b) are overall lower than typical values recommended by building codes (e.g., 2.5 according to ASCE 7-16 [45]), especially the ones related to display case top. Conversely, maximum component amplification factor on the glass panels (Figure 4.9c) (e.g., equal to about 5 for X direction and AC02 test) is larger than these values, especially over low intensities.

(a)

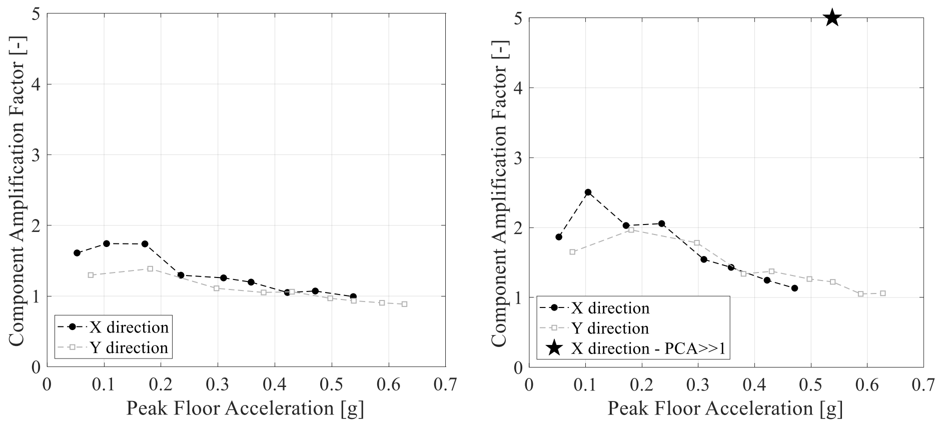

(b)

(c)

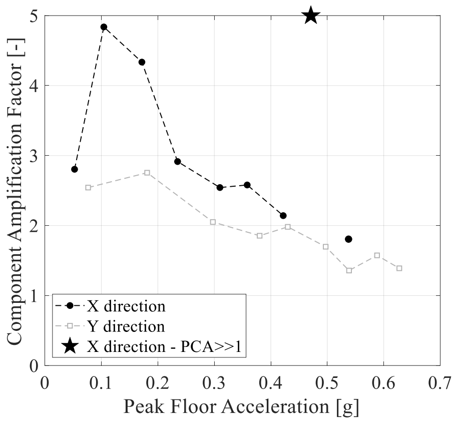

Figure 4.9: Component amplification factor evolution over the seismic performance tests corresponding to (a) display case top, (b) pedestal top, and (c) glass panels middle point, along both horizontal directions.

4.4.4 Displacement response

The displacement time histories related to AC05 test are depicted in Figure 4.10: (a) absolute displacement of the display case top, (b) absolute displacement of the shake table, (c) relative displacement of the display case assessed between display case top and shake table (L3-W4 along X direction and L2-W1 along Y direction), and (d) relative displacement of the display case assessed between display case top and bottom (L3-W5 along X direction and L2-W2 along Y direction). The display case exhibited a complex (rigid) rotational-translational motion, in addition to the minor elastic response. The response of the display case started to become more significant and more complex after the first 5-7 seconds, which correspond to the end of the triggering part and the onset of the strong motion part of the acceleration input. This can be derived by comparing the absolute displacements at the display case top (Figure 4.10a) and the shake table displacements (Figure 4.10b) or by assessing the relative displacement (Figure 4.10c). In particular, the rotational-oscillatory and translational contribution of the case motion can be clearly observed in Figure 4.10c. After 5-7 seconds, the time history begins to deviate from the zero-displacement axis This deviation results in significant residual displacements of the display case in both directions (i.e., about -21 and +26 mm along X and Y directions, respectively). The rotational-oscillatory motion of the specimen can be identified in Figure 4.10d, as the depicted relative displacement accounts for the horizontal projection of the inclination of the display case, which is associated with rotational-oscillatory motion. This relative displacement is not significantly large if compared with the one associated with translational motion (Figure 4.10c). It can be concluded that the sliding response is more significant than the rocking one.

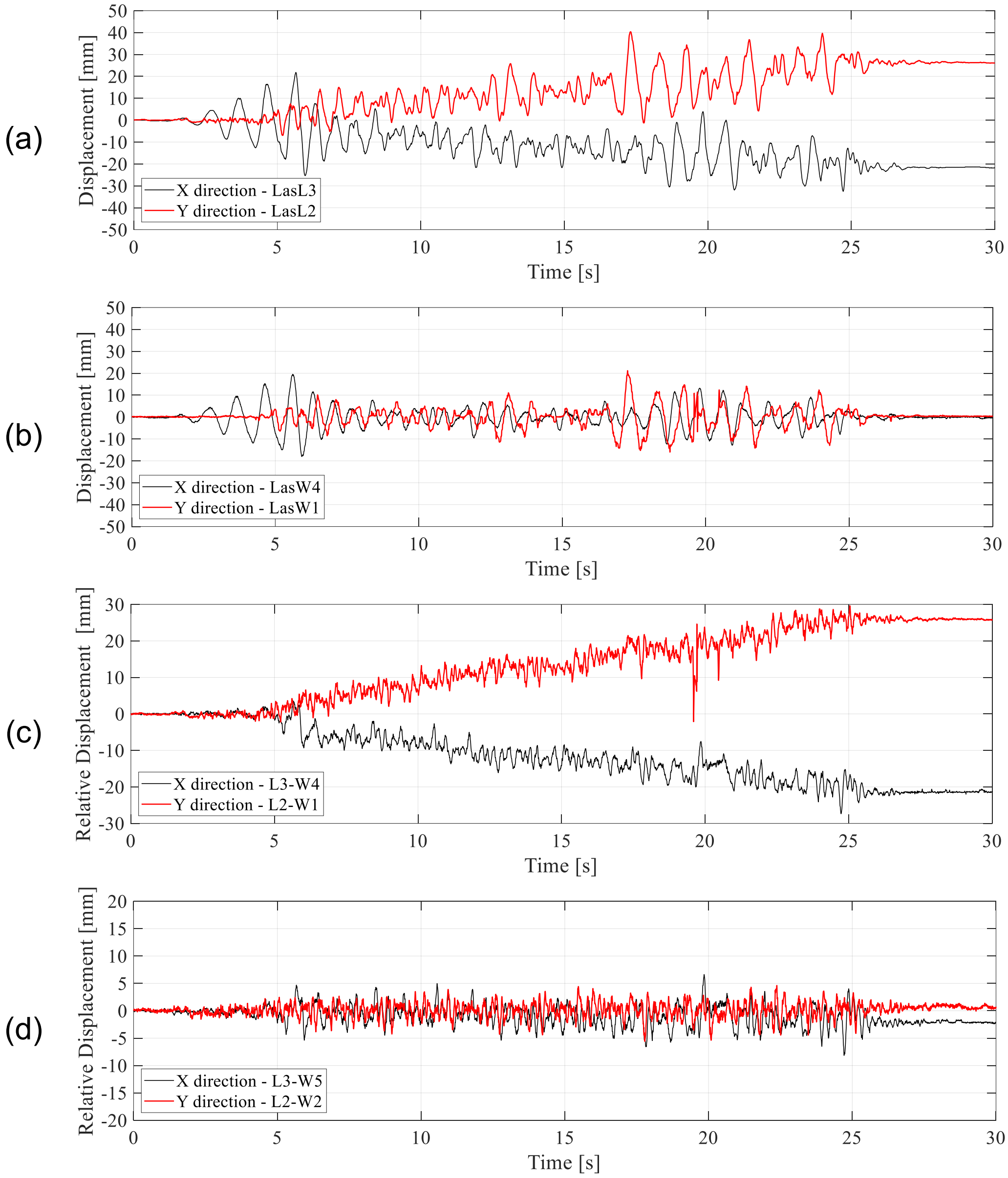

Figure 4.10: Displacement time histories related to AC05 test: (a) absolute displacement of display case top, (b) absolute displacement of shake table, (c) relative displacement of the display case assessed between display case top and shake table (L3-W4 along X direction and L2-W1 along Y direction), and (d) relative displacement of the display case assessed between display case top and bottom (L3-W5 along X direction and L2-W2 along Y direction).

In order to assess the significance of the rotational-oscillatory motion over the incremental tests, the peak relative displacement evaluated between top and base of the display case is shown in Figure 4.11; AC09 Y result is not depicted in Figure 4.11 as one of the lasers went out of scale. The peak relative displacement is comparable along X and Y directions and approximately increases as the test intensity grows. Even for significant testing intensities, the peak relative displacement is not critically large, especially if it is compared with relative displacement between display case top and shake table and with height of the specimen. This stresses the relevant of the sliding response of the display case over the rocking one.

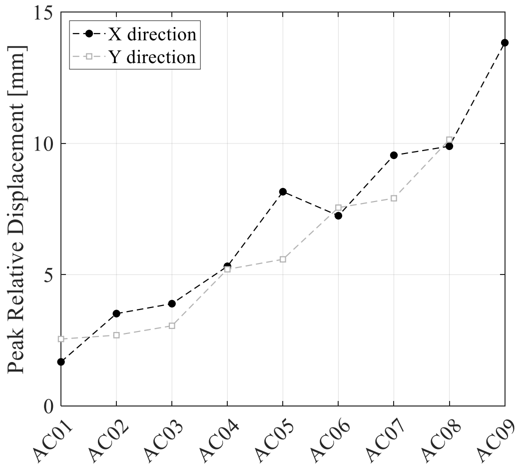

Figure 4.11: Peak relative displacement evolution over the seismic performance tests, evaluated between the top and base of the display case (L3-W5 along X direction and L2-W2 along Y direction).

4.4.5 Preliminary damage assessment

Prior to presenting the damage assessment results, it is recalled that this section was not aimed at assessing in a quantitative and accurate manner the damage exhibited by both display case and vase. Therefore, the following assessment results should be considered as preliminary and tentative estimations, only aimed to shed lights on the critical behavior of the tested specimens. A tentative correlation between the seismic tests and the occurred DSs is reported in Table 4.2, including preliminary information regarding the component motion and the residual displacements. Moreover, the correlation between an engineering demand parameter (EDP) and the occurred DSs is presented. Two EDPs were chosen: PFA and PCA (recorded on the top of the display case). The damage identification reported in Table 4.2 is based on the assessment of two component response parameters, i.e., component motion and residual displacement, related to each seismic performance test. In particular, three levels of severity are defined for each parameter, i.e., minor, moderate, and major. The occurred DS related to each test is identified according to the detected levels of severity and assuming that the art object has an extremely significant economic and cultural value.

The damage assessment associated with AC01, AC02, and AC03 resulted in DS0. In particular, the specimen did not exhibit appreciable motion and damage, except for the glass panels, which exhibited a minor to moderate out-of-plane motion (oscillation) during the shaking; minor to moderate glass motion does not reasonably produce any damage or disruption. AC04 test excitation determined minor to moderate motion of the components, with minor residual displacement of the vase. Accordingly, DS1 was assumed to be achieved. In the context of valuable items, even minor motion or residual displacement can be considered to be associated with DS1. For higher intensities, i.e., for AC05 to AC09 test, major component motion and major residual displacement were observed. The glass panels strongly hammered against the adjacent perpendicular glass panels, producing significant impacts. The art object exhibited a major sliding motion from AC05 test on (included), resulting in residual displacement comparable with the semi-dimension of the pedestal’s top support surface. However, the object did not fall from the pedestal or impact against the glass panels. No significant permanent damage/deformation of both vase and display case components was observed. Therefore, focusing on the specific and peculiar outcome of the present test, DS2 could be reasonably be assumed. However, in the context of valuable components as art objects, the responses corresponding to AC05 to AC09 tests (i.e., significant motion and large residual displacements) could be reasonably associated with DS3. In fact, a slightly different arrangement or a less stable or more fragile art object could have potentially been damaged by the significant motion observed in the course of these tests: this would have caused extremely significant economic and cultural losses, also compatible with DS3 achievement. Therefore, both DS2 and DS3 are associated with AC05 to AC09 tests, according to the abovementioned motivations, and given that the damage scheme also depends on desired level of safety and building/component type/importance. Finally, the author recall that the damage assessment results are to be meant as preliminary and not exhaustive.

Table 4.2: Preliminary damage assessment.

test ID	min (PFA_x,PFA_y)	min (PCA_x, PCA_y)	DS	component motion				residual displacement		
	[g]	[g]		display case	pedestal	glass	vase	display case	pedestal	vase
AC01	0.05	0.09	DS0	-	-	-	-	-	-	-
AC02	0.10	0.18	DS0	-	-	*		-	-	-
AC03	0.17	0.30	DS0	-	-	**	-	-	-	-
AC04	0.24	0.30	DS1	*	*	**	*	-	-	*
AC05	0.31	0.39	DS2/DS3	***	*	***	***	*	-	***
AC06	0.36	0.43	DS2/DS3	***	*	***	***	***	-	***
AC07	0.42	0.44	DS2/DS3	***	***	***	***	***	***	***
AC08	0.47	0.51	DS2/DS3	***	***	***	***	***	***	***
AC09	0.54	0.53	DS2/DS3	***	***	***	***	***	***	***

*: minor; **: moderate; ***: major.

4.5 Discussion

The chapter reported the preliminary results of an experimental campaign aimed at assessing the dynamic properties and the seismic performance of museum objects and artefacts. A typical museum display case was tested on shake table, including the presence of a representative art object (ceramic vase). The main dynamic properties of the specimen were estimated, and both accelerations and displacements recorded on the specimen were assessed, estimating the peak values. Rocking and sliding response of the display case was identified, and component amplification factors associated with both display case and pedestal were assessed. A tentative damage assessment of both display case and vase was carried out. The following main conclusion remarks can be drawn.

- The display case did not show damage (DS0) up to a PFA of 0.172 g in the X direction and 0.297 g in the Y direction, and PCA at the top of 0.299 g and 0.330 g in the X and Y directions, respectively.
- The value of the fundamental period of the display case corresponding to DS0 was found to be 0.125 s (8.0 Hz) in the X direction and 0.143 s (7.0 Hz) in the Y direction. Thus, in a simplified way, it can be assumed that the period of the tested display case varies in the range 0.125 s - 0.143 s.
- The value of the damping ratio of the display case corresponding to DS0 is approximately 20.0 % in the X direction and approximately 12.0 % in the Y direction. Thus, in a simplified way, it can be assumed that the damping of the tested display case varies in the range of 12.0 % - 20.0 %.
- The value of the CAF, understood as the ratio between the PCA recorded at the top of the display case and the PFA recorded at the base of the shake table during the tests, corresponding to SD0, was approximately equal to 1.75 in the X direction and 1.30 in the Y direction. Even higher values of local amplification were recorded but they were associated with local dynamic response and modes. It can be assumed that the tested case is characterized by an amplification coefficient of 1.75.

4.6 References

[1] D'Angela D, Magliulo G, Cosenza E. Towards a reliable seismic assessment of rocking components. Engineering Structures 2021;230:111673. https://doi.org/10.1016/j.engstruct.2020.11167

[2] Dimitrakopoulos EG, Paraskeva TS. Dimensionless fragility curves for rocking response to near-fault excitations. Earthquake Engineering & Structural Dynamics 2015;44:2015–33. https://doi.org/10.1002/eqe.2571

[3] Klaboe K, Pujol S, Laughery L. Seismic Response of Rocking Blocks. Earthquake Spectra 2018;34:1051–63. https://doi.org/10.1193/060517EQS107DP

[4] Purvance MD, Anooshehpoor A, Brune JN. Freestanding block overturning fragilities: Numerical simulation and experimental validation. Earthquake Engineering & Structural Dynamics 2008;37:791–808. https://doi.org/10.1002/eqe.789

[5] Taghavi S, Miranda E. Response Assessment of Nonstructural Building Elements. PEER Report 2003/05. Pacific Earthquake Engineering Research Center: University of California at Berkeley, Berkeley, California; 2003.

[6] Fierro EA, Miranda E, Perry CL. Behavior of Nonstructural Components in Recent Earthquakes, American Society of Civil Engineers; 2011, p. 369–77. https://doi.org/10.1061/41168(399)44

[7] Achour N, Miyajima M, Kitaura M, Price A. Earthquake-Induced Structural and Nonstructural Damage in Hospitals. Earthquake Spectra 2011;27:617–34. https://doi.org/10.1193/1.3604815
[8] Yön B, Onat O, Öncü ME. Earthquake Damage to Nonstructural Elements of Reinforced Concrete Buildings during 2011 Van Seismic Sequence. J Perform Constr Facil 2019;33:04019075. https://doi.org/10.1061/(ASCE)CF.1943-5509.0001341
[9] Di Sarno L, Magliulo G, D'Angela D, Cosenza E. Experimental assessment of the seismic performance of hospital cabinets using shake table testing. Earthquake Engineering & Structural Dynamics 2019;48:103–23. https://doi.org/10.1002/eqe.3127
[10] Konstantinidis D, Makris N. Experimental and analytical studies on the response of freestanding laboratory equipment to earthquake shaking. Earthquake Engng Struct Dyn 2009;38:827–48. https://doi.org/10.1002/eqe.871
[11] Saraswat A, Reddy GR, Ghosh S, Ghosh AK, Kumar A. Seismic stability of a standalone glove box structure. Nuclear Engineering and Design 2014;276:178–90. https://doi.org/10.1016/j.nucengdes.2014.04.031
[12] Dar A, Konstantinidis D, El-Dakhakhni WW. Evaluation of ASCE 43-05 Seismic Design Criteria for Rocking Objects in Nuclear Facilities. J Struct Eng 2016;142:04016110. https://doi.org/10.1061/(ASCE)ST.1943-541X.0001581
[13] Makris N, Kampas G. Size Versus Slenderness: Two Competing Parameters in the Seismic Stability of Free-Standing Rocking Columns. Bulletin of the Seismological Society of America 2016;106:104–22. https://doi.org/10.1785/0120150138.
[14] Gesualdo A, Iannuzzo A, Monaco M, Penta F. Rocking of a rigid block freestanding on a flat pedestal. J Zhejiang Univ Sci A 2018;19:331–45. https://doi.org/10.1631/jzus.A1700061
[15] Costa AA, Arêde A, Penna A, Costa A. Free rocking response of a regular stone masonry wall with equivalent block approach: experimental and analytical evaluation. Earthquake Engineering & Structural Dynamics 2013;42:2297–319. https://doi.org/10.1002/eqe.2327
[16] Di Egidio A, Contento A, Olivieri C, de Leo AM. Protection from overturning of rigid block-like objects with linear quadratic regulator active control. Structural Control and Health Monitoring 2020;27:e2598. https://doi.org/10.1002/stc.2598
[17] Sorace S, Terenzi G. Seismic performance assessment and base-isolated floor protection of statues exhibited in museum halls. Bull Earthquake Eng 2015;13:1873–92. https://doi.org/10.1007/s10518-014-9680-3
[18] Di Egidio A, Contento A, De Leo AM, Gardoni P. Dynamic and Seismic Protection of Rigid-Block-Like Elements and Structures on Deformable Ground with Mass-Damper Dynamic

Absorbers. J Eng Mech 2020;146:04020046. https://doi.org/10.1061/(ASCE)EM.1943-7889.0001782
[19] Cosenza E, Di Sarno L, Maddaloni G, Magliulo G, Petrone C, Prota A. Shake table tests for the seismic fragility evaluation of hospital rooms. Earthquake Engineering & Structural Dynamics 2015;44:23–40. https://doi.org/10.1002/eqe.2456
[20] Bao Y, Konstantinidis D. Dynamics of a sliding-rocking block considering impact with an adjacent wall. Earthquake Engng Struct Dyn 2020;49:498–523. https://doi.org/10.1002/eqe.3250
[21] Gesualdo A, Iannuzzo A, Minutolo V, Monaco M. Rocking of freestanding objects: theoretical and experimental comparisons. Journal of Theoretical and Applied Mechanics 2018;56:977–91. https://doi.org/10.15632/jtam-pl.56.4.977
[22] Filiatrault A, Kuan S, Tremblay R. Shake table testing of bookcase – partition wall systems. Canadian Journal of Civil Engineering 2004;31:664–76. https://doi.org/10.1139/l04-031
[23] Vassiliou MF, Broccardo M, Cengiz C, Dietz M, Dihoru L, Gunay S, et al. Shake table testing of a rocking podium: Results of a blind prediction contest. Earthquake Engng Struct Dyn 2021;50:1043–62. https://doi.org/10.1002/eqe.3386
[24] Wittich CE, Hutchinson TC. Shake table tests of stiff, unattached, asymmetric structures: Shake Table Tests of Stiff, Unattached, Asymmetric Structures. Earthquake Engineering & Structural Dynamics 2015;44:2425–43. https://doi.org/10.1002/eqe.2589
[25] Vassiliou MF, Broccardo M, Cengiz C, Dietz M, Dihoru L, Gunay S, et al. Shake table testing of a rocking podium: Results of a blind prediction contest. Earthquake Engng Struct Dyn 2021;50:1043–62. https://doi.org/10.1002/eqe.3386
[26] Wittich CE, Hutchinson TC. Rocking bodies with arbitrary interface defects: Analytical development and experimental verification. Earthquake Engng Struct Dyn 2018;47:69–85. https://doi.org/10.1002/eqe.2937
[27] Vassiliou MF, Mackie KR, Stojadinović B. Dynamic response analysis of solitary flexible rocking bodies: modeling and behavior under pulse-like ground excitation. Earthquake Engng Struct Dyn 2014;43:1463–81. https://doi.org/10.1002/eqe.2406
[28] Petrone C, Di Sarno L, Magliulo G, Cosenza E. Numerical modelling and fragility assessment of typical freestanding building contents. Bulletin of Earthquake Engineering 2017;15:1609–33. https://doi.org/10.1007/s10518-016-0034-1
[29] Fragiadakis M, Diamantopoulos S. Fragility and risk assessment of freestanding building contents. Earthquake Engng Struct Dyn 2020;49:1028–48. https://doi.org/10.1002/eqe.3276
[30] D’Angela D, Magliulo G, Cosenza E. Seismic damage assessment of unanchored nonstructural components taking into

account the building response. Structural Safety 2021;93:102126. https://doi.org/10.1016/j.strusafe.2021.102126
[31] Huang B, Pan Q, Lu W, Shen F. Free-rocking tests of a freestanding object with variation of center of gravity. Earthquake Engng Struct Dyn 2021:eqe.3498. https://doi.org/10.1002/eqe.3498
[32] Berto L, Favaretto T, Saetta A, Antonelli F, Lazzarini L. Assessment of seismic vulnerability of art objects: The “Galleria dei Prigioni” sculptures at the Accademia Gallery in Florence. Journal of Cultural Heritage 2012;13:7–21. https://doi.org/10.1016/j.culher.2011.06.005
[33] Neurohr T, McClure G. Shake table testing of museum display cases. Can J Civ Eng 2008;35:1353–64. https://doi.org/10.1139/L08-084
[34] Burningham C, Mosqueda G, Saavedra RR. Comparison of seismic fragility of free standing equipment using current testing protocols and recorded building floor motions. Proceedings, Earthquake Engineering Symposium for Young Researchers, Seattle, WA: 2007.
[35] Federal Emergency Management Agency (FEMA). Interim protocols for determining seismic performance characteristics of structural and nonstructural components through laboratory testing. Report No. FEMA 461. Washington D.C., USA: 2007.
[36] International Code Council Evaluation Service (ICC-ES). AC156 Acceptance Criteria for the Seismic Qualification of Nonstructural Components. Brea, California, USA: 2012.
[37] Magliulo G, Maddaloni G, Petrone C. A procedure to select time-histories for shaking table tests on nonstructural components. Proceedings of the 4th ECCOMAS Thematic Conference on Computational Methods in Structural Dynamics and Earthquake Engineering, vol. Paper n. 1720, Kos Island, Greece: M. Papadrakakis, V. Papadoupolus, V. Plevris (eds.); 2013. https://doi.org/10.13140/2.1.4693.8881
[38] Di Sarno L, Magliulo G, D’Angela D, Cosenza E. Experimental assessment of the seismic performance of hospital cabinets using shake table testing. Earthquake Engineering & Structural Dynamics 2019;48:103–23. https://doi.org/10.1002/eqe.3127
[39] Petrone C, Magliulo G, Manfredi G. Shake table tests on standard and innovative temporary partition walls. Earthquake Engineering & Structural Dynamics 2017;46:1599–624. https://doi.org/10.1002/eqe.2872
[40] Magliulo G, Pentangelo V, Maddaloni G, Capozzi V, Petrone C, Lopez P. Shake table tests for seismic assessment of suspended continuous ceilings. Bulletin of Earthquake

Engineering 2012;10:1819–32. https://doi.org/10.1007/s10518-012-9383-6
[41] Petrone C, Magliulo G, Manfredi G. Shake table tests for the seismic assessment of hollow brick internal partitions. Engineering Structures 2014;72:203–14. https://doi.org/10.1016/j.engstruct.2014.04.044
[42] Chai JF, Lin FR. Seismic retrofit and shaking table test of medical equipment in a hospital. Ninth Pacific Conference on Earthquake Engineering Building an Earthquake-Resilient Society, Auckland, New Zealand: 2011.
[43] Huang B, Günay S, Lu W. Seismic Assessment of Freestanding Ceramic Vase with Shaking Table Testing and Performance-Based Earthquake Engineering. Journal of Earthquake Engineering 2021:1–23. https://doi.org/10.1080/13632469.2021.1979132
[44] Mahdi T, Mahdi A. Sliding Fragility of Restrained and Unrestrained Block-Type Nonstructural Components. Asian Journal of Civil Engineering 2013;14:545–55.
[45] American Society of Civil Engineers, editor. ASCE 7-16. Minimum design loads for buildings and other structures. Reston, Va: American Society of Civil Engineers : Structural Engineering Institute; 2017.
[46] Di Sarno L, Petrone C, Magliulo G, Manfredi G. Dynamic properties of typical consultation room medical components. Engineering Structures 2015;100:442–54. https://doi.org/10.1016/j.engstruct.2015.06.036
[47] Bracci JM, Reinhorn AM, Mander JB. Seismic resistance of reinforced concrete frame structures designed only for gravity loads: part I – design and properties of a one-third scale model structure. Technical Report NCEER-92-0027. State University of New York at Buffalo, NY, US; 1992.
[48] Clough RW, Penzien J. Dynamics of structures. New York: McGraw-Hill; 1975.
[49] Chopra AK. Dynamics of structures: theory and applications to earthquake engineering. 3rd ed. Upper Saddle River, N.J: Pearson/Prentice Hall; 2007.
[50] Papagiannopoulos GA, Hatzigeorgiou GD. On the use of the half-power bandwidth method to estimate damping in building structures. Soil Dynamics and Earthquake Engineering 2011;31:1075–9. https://doi.org/10.1016/j.soildyn.2011.02.007
[51] Federal Emergency Management Agency (FEMA). Reducing the Risks of Nonstructural Earthquake Damage – A Practical Guide. Report No. FEMA E-74. Washington D.C., USA: 2012.

Chapter 5

5 A novel shake table protocol for seismic assessment and qualification of acceleration-sensitive nonstructural elements

A novel shake table protocol for seismic assessment and qualification of acceleration-sensitive nonstructural elements is developed. The chapter firstly critically reviews existing protocols and highlights their criticalities, pointing out the need for the development of novel assessment and qualification approaches and protocols. The novel protocol is developed in the light of these criticalities, considering the most recent advances in the field and the specific expertise of the research team. The most significant and contributing parts of the developed protocol consist in the definition of novel required response spectra and generation of signals for seismic performance evaluation tests. The reliability and robustness of the protocol is evidenced in the chapter considering real floor motions as a reference, also proving the superiority of the developed protocol with respect to the reference alternatives. The defined approach and procedures are generally applicable and easily extendable to different case studies as the process is highly versatile and modifiable. The implementation of the developed approach and protocol in the literature and in practice will significantly enhance seismic assessment and qualification of acceleration-sensitive nonstructural elements, possibly having a strong impact in public safety and economy.

5.1 Introduction

5.1.1 Technical background

The estimation and mitigation of the effects of catastrophic events such as earthquakes on infrastructural and structural systems are among the most challenging aims of the modern era and are increasingly pushing researchers and engineers to develop innovative solutions [1]. Design and assessment of nonstructural elements (NEs) according to current regulations, codes, and guidelines are typically based on Performance-Based Earthquake Engineering (PBEE) [2-8]. These documents often provide methods and criteria for both behavior assessment and performance evaluation of NEs; seismic qualification and certification procedures are also defined in ASCE 7-16 [2]. Seismic performance evaluation of NEs typically consists in (a) assessing the nonstructural element (NE) seismic capacity associated with relevant damage states (DSs) and (b) correlating this capacity to consistent measures of seismic demand or targets, often defined by regulations/codes. The definition of both seismic capacity and demand is based on the performance levels of interest. The capacity to demand evaluation is typically performed via statistical-based approaches, possibly accounting for relevant uncertainty sources, considering effective engineering demand parameters (EDPs) for the quantitative assessment. Seismic qualification of NEs is an assessment and evaluation process aimed at satisfying specific NE performance levels, according to strict requirements and rules typically defined by regulations and codes. The seismic qualification process includes the assessment of the seismic behavior of the NEs, involving the dynamic identification of NEs, which is an essential task for robust seismic assessment of engineering systems [9,10]. Seismic certification procedure typically includes seismic qualification processes carried out according to specific certification requirements and criteria, aimed at achieving the highest possible level of credibility, operated through the intervention of subjects accredited by the institutions/authorities that regulate and issue the certifications. Seismic certification, meant as the outcome of a certification procedure, is a standardized certificate recognized by the reference institutions. ASCE 7-16 establishes requirements and criteria for performing (special) seismic certification (SSC) of NEs. In particular, mechanical and electrical equipment that has to be functioning under the design earthquake ground motion, NEs with hazardous substances, and NEs with importance factor equal to 1.5 (§13.1.3, [2]) shall be certified by the manufacturer considering operativity/functioning as a performance level. Other national regulations and industrial codes define requirements and criteria for seismic performance evaluation and certification of NEs [11,12]. Overall, seismic qualification, or seismic certification, when required, shall be carried out via one of the following methods: (a) analysis, (b) (experimental) testing, (c) experience data, (d) a combination of methods (a), (b) and (c).

Experimental testing (i.e., method (b)) is the most common method to qualify/certify NEs as this is typically considered to be the most reliable and robust. Experimental qualification is performed according to strict protocols and requirements. Quasi-static and dynamic testing procedures are typically associated with qualification of displacement- and acceleration-sensitive NEs, respectively. However, dynamic testing is generally preferred (a) for NEs that show marked sensitivity to multiple demand parameters (e.g., both acceleration- and displacement-sensitive) and (b) in the case of NEs expected to exhibit a complex and irregular dynamic response that can (only) be identified and characterized through dynamic loading procedures, which are more representative of actual seismic demand. Dynamic testing also allows assessing the dynamic properties of the elements (e.g., dynamic identification). Shake table testing represents the state-of-the-art for dynamic testing [13-23].

Numerical/analytical assessment of NEs is typically complex but represents a powerful method, often economic and fast, and easily implementable if the relevant models are effective and relatively reliable. However, these conditions are not often verified due to limited use and inadequate knowledge. According to IEEE 344 [12], analysis is not recommended for equipment and systems that cannot be modeled in an adequate manner. Similar provisions are supplied in ASCE 7-16 [2] regarding active mechanical and electrical equipment. Qualification through experience data is even less typical than using analysis methods. As a matter of fact, there are very limited supporting data and information, especially considering the wide variability of the characteristics of NEs, buildings, and ground motions. Therefore, experimental testing is generally preferential and considered to be more reliable and applicable among the qualification methods.

5.1.2 Inadequacy of existing shake table protocols

The technical definition of both loading and testing protocols is of paramount importance for seismic qualification of NEs through shake table testing. However, both regulation provisions and literature criteria defining loading/testing protocols for NEs are inadequate, as it is motivated in the following.

As a first comment, it should be noted that, seismic demands on nonstructural elements became a topical issue for research only in the very last years. Before, the existence of seismic demand formulations, despite these were reliable or not, was already an achievement since nonstructural elements were meant to be objects of “second rank” of interest. In particular, the existing shake table protocols used for seismic assessment and qualification of nonstructural elements were often developed considering insolated and self-referential approaches, often associated with peculiar applications (e.g., specific type of equipment).

Both response and performance of NEs subjected to seismic events is significantly conditioned by loading history, which cannot generally be univocally correlated with given values of intensity measures (IMs) associated with the seismic events (e.g., peak accelerations) [24]. The seismic input properties significantly affect the response of NEs. For example, the time-varying frequency content may have a significant effect on the system response, and a nonstationary earthquake ground motion model could guarantee a relatively reliable seismic assessment, capturing the temporal nonstationarity of realistic earthquake scenarios [25,26].

The definition of the protocols, with particular regard to required response spectra (RRS), was often not based on the evaluation of the pre-existing methods/formulations, and in many cases, it did not even consider reference responses to calibrate these formulations. Conversely, safe, consistent, and updated formulations of the seismic demand need to be considered to develop reliable qualification protocols, with particular regard to RRS. The existing protocols and reference RRS except AC156 [27] are not clearly associated with real or analytical demand formulations, also taking into account potential building scenarios (e.g., [28,29]). Perrone et al. [30] modified ISO 13033 [11] formulation in order to be compliant with the Eurocode 8 [3] in terms of seismic demand on NEs, even though they considered AC156 provisions for the corner frequencies. Their study stresses the lack of adherence between the protocol and the compliant seismic demand formulations and highlights the need for further studies. AC156 RRS, or equivalently, ASCE 7-16 seismic demand formulation, was found to potentially underestimate the seismic demands on building acceleration-sensitive NEs [30-32]. Furthermore, standards and specific rules should be defined by the protocols in order to guarantee analysis, finalization, and extension of qualification outcomes in a robust and reliable manner. The existing protocols do not often provide univocal and consistent rules and criteria (e.g., [11]) or provide extremely complex procedures that are difficultly implementable (e.g., [28]), especially regarding the generation and processing of the protocol-compliant testing protocol and program. However, baseline generation and signal processing procedures define the features of the seismic inputs and appropriate generation/processing methods/techniques allow to characterize and enhance the key characteristics of the seismic inputs (e.g., [33]). For example, the analytical procedures for enforcing the spectrum compatibility are rarely defined within the protocols, especially regarding the signal processing/adjustment methods and techniques [34,35].

Finally, the seismic qualification is typically referred to specific critical elements (e.g., telecommunication equipment [29]), and, more importantly, the relevant rules are not general and strongly depend on the developer’s discretion. In the opinion of the author, this should not be acceptable for seismic qualification procedures. These should be as general and universal as possible. Qualification should be possibly applicable to any NE and the related protocols should be provided by minimizing any conflict of interest. Both loading inputs and testing protocols should be validated considering their representativeness and reliability with regard to severe real ground and floor motions, as these latter represent the most essential reference for comparison purposes. Accordingly, current approaches for performing seismic qualification need major revision and testing/loading protocols urge technical updating and significant enhancement.

5.1.3 Aim, objectives, and organization of the chapter

This chapter is motivated by both the inadequacy of the existing protocols and the critical need for reliable and consistent protocols. After a technical review of existing protocols, a novel assessment and qualification protocol is developed in this section. The loading input and testing procedure are defined to solve the criticalities associated with the current codes, considering (a) a novel assessment and qualification approach recently implemented in the literature, (b) a consistent code-compliant formulation of the seismic demand on acceleration-sensitive NEs, (c) a series of technical consolidated rules and criteria for developing and filtering the loading input, and (d) an evaluation and validation process.

Section 5.2 reports a solid and robust technical background/methodology description, from the elementary ingredients to the newly defined methodology framework. The literature contribution associated with this section is expressed in terms of original synthesis, assessment, evaluation, discussion, and validation of the state of the art of shake table qualification of nonstructural elements, with particular regard to the methodological and procedural levels. Section 5.3 defines a novel code-compliant shake table protocol, by particularizing the methodology framework representing an outcome in terms of valuable product/outcome/item. Signal-based evaluation and validation of the developed protocol is reported in Section 5.4, where alternative protocols and real floor motions are considered as a reference.

5.2 Methodology

5.2.1 Case study nonstructural elements and shake table protocols

The case study nonstructural elements consist in linear elastic single degree of freedom (SDOF) systems, which are assumed to not interact with the structure (and with the shake table). Obviously, the protocol is suitable for real acceleration-sensitive elements, which might be associated with complex and nonlinear responses. The interaction between the shake table and the tested nonstructural elements is typically not accounted for or neglected since the basic hypothesis of no expected interaction is often reasonably assumed to be valid. However, depending on the mass and stiffness, and, more generally, dynamic properties of the nonstructural element, and on the element to shake table connections, a non-negligible interaction might be exhibited in real cases. With regard to experimental testing, the assessment of the interaction is investigated in terms of actual experimental response, whereas the shake table protocols do not account for the interaction. Therefore, the application can be considered as reliable in this context.

Floor response spectra and shake table protocols generally assume nonstructural elements as linear elastic SDOF systems Indeed, acceleration-sensitive nonstructural elements are generally meant to be SDOF systems in the literature [36-38], and the assessment methodology, also including the seismic demand estimation, is based on SDOF hypotheses and spectral responses according to most authoritative national and international regulations and codes [2,6,11]. Representative examples of nonstructural elements compatible with

SDOF systems include but are not limited to operating lights, projectors, antennas, base-anchored cabinets, and museum artifacts.

AC156 [27] is intended to support data for seismic certification of systems that are sensitive to the accelerations, i.e., architectural, mechanical, electrical, and other nonstructural systems attached to structures. FEMA 461 [28] establishes a protocol for shake table testing of structural members and NEs that are sensitive to the dynamic effects of motion transferred to the component through a single point of attachment (acceleration-sensitive); the protocol also includes the methodology for PBEE assessment via fragility estimation. ISO 13033 [11] defines the procedure to derive seismic actions and seismic performances of NEs. This code is not intended for mechanical and electrical equipment of industrial facilities, including nuclear power plants. However, the standard might be applied for these facilities.

AC156, FEMA 461, and ISO 13033 are intended for generic (acceleration-sensitive) NEs, whereas other protocols describe methods and criteria for seismic qualification of specific or peculiar NEs, such as mechanical and electrical equipment. GR-63-CORE [29] provides a protocol for shake table testing of telecommunications equipment, systems, or service facilities. IEEE 344 [12] describes methods for seismic qualification of nuclear power plant equipment. The protocol can be used to perform the seismic/dynamic evaluation of NEs: from the tests to the analysis, up to the experienced-based evaluations. The code encloses common methods currently used in the seismic qualification. IEEE 693 [39] provides the minimum requirements for seismic qualification of electrical substation equipment. Regulatory Guide 1.60 [40] (referred to below as RG-1.60) of the U.S. Nuclear Regulatory Commission (USNRC) establishes design response spectra for the seismic design of nuclear power plants. The international standard IEC 60068-2-57 [41] outlines methods and standards for testing components, equipment, and electrotechnical products including the testing procedure for seismic applications. It extends the general requirements on seismic testing described in a separate standard, IEC 60068-3-3 [42].

5.2.2 Loading input

Outline

The definition of input signals according to assessment and qualification/certification protocols and compliant codes/guidelines is a complex process that often involves several phases and multiple key parameters and features. Typically, shake table signals are artificially obtained [27,28], but they can also be defined following empirical approaches [39,41]. For, example, two groups of strong ground motion records and one group of artificial waves were used for the input excitations by Lu et al. [43] and Luo et al. [19]. In Takhirov et al. [44], a set of earthquake and synthetic strong-motion records were generated IEEE 693-spectrum-compatible to the seismic qualification of NEs.

The definition process of artificially obtained shake table inputs is generally based on the definition of the following features: (a) IM, (b) baseline signal, (c) RRS, (d) compliance/compatibility criteria and rules, and (e) instrument characteristics and capacities. It should be mentioned that no studies or literature documents define or describe these features, which were systematically defined and discussed in this section, according to personal experience regarding shake table testing and literature/code references.

Intensity measure (IM)

The most common IM typically consists in peak table acceleration (PTA), and this is representative of peak ground acceleration (PGA) or peak floor acceleration (PFA). The reference IM of the input test signal defined according to AC156 is the design earthquake spectral response acceleration parameter at short periods, i.e., S_{DS} [2]. FEMA 461 recommends the use of the spectral acceleration at the appropriate natural frequency of the NE as an IM, i.e., ($S_a(T_a)$). IEEE 693 employs the site-specific hazard method, considering PGA. GR-63-CORE supplies four earthquake risk zones as a parameter to be used for defining input test signal intensity level.

Baseline signal

The main features of the baseline signal are discussed in the following reference protocols and literature. (1) The baseline time interval envelope typically includes (a) acceleration ramp-up or rise part (RP), (b) hold time or strong motion part (SMP), and (c) de-acceleration ring downtime or decay part (DP). AC156 and IEEE 693 require that the total duration of the input motion shall have at least 20 s of SMP, whereas signal duration should be equal to 60 and 32 s according to FEMA 461 and GR-63-CORE, respectively. IEC 60068 requires duration of SMP to be a given percentage of the total duration, whereas the typical total duration is 30 s with a minimum SMP duration equal to 20 s. (2) Fixed sampling rate/frequency is typically assumed for the baseline; AC156 and IEEE 693 do not define that, whereas FEMA 461 and GR-63-CORE recommend a sampling rate equal to 100 Hz and equal to or larger than 200 Hz, respectively. (3) The energy content [45] of the theoretical input signal is typically associated with given frequency ranges and resolutions. Energy content should be ranging from 1.3 to 33.3 Hz with one-third-octave and one-sixth-octave bandwidth resolution corresponding to analog and digital synthesis equipment, respectively, for AC156, whereas FEMA 461 provides signals with frequency contents ranging in 0.5 – 32 Hz and one-third-octave bandwidth resolution. IEEE 693 requires that the input motion includes the lower corner point frequency of the RRS equal to 1.1 Hz. GR-63-CORE inputs should have frequency contents ranging in 0.5 – 50 Hz. The time history obtained according to IEC 60068 shall be generated by composition of frequencies included within a specified range (typically frequency range from 1 to 35 Hz [46]) and through an appropriate resolution as a function of the specimen damping: the larger the specimen damping the lower the frequency resolution.

Required response spectra (RRS)
Required response spectra (RRS) or target spectra can be obtained through empirical, analytical, and standard code approaches. Empirical methods consist of assessing reference RRS according to (ground or floor) time histories recorded during the seismic events [44,46]. The analytical approach typically involves numerical analysis of structures and/or NEs for the estimations of RRS [47,48]. Finally, the approach based on standard code provisions uses closed-form RRS formulations, depending on relevant parameters of buildings and/or NEs and often also referred to for NE design purposes; this latter approach is the one typically recommended by shake table protocols [11,27]. The procedure used to define standard code RRS is not typically described/provided by the relevant codes and guidelines. It should be noted that code-based floor demand estimations might not be reliable according to recent studies, where numerical estimations [49-52] or real records [31,53,54] were considered as a reference, stressing the need for technical revision of code prescriptions.

AC156 defines 5%-damped RRS according to the formulation of the horizontal seismic design force and the definition of flexible and rigid NEs provided by ASCE 7-16. RRS were defined considering two regions: amplified region and zero period acceleration (ZPA) region, separated by 8.3 Hz; for the computation of the spectral demand acceleration, 16.7 Hz is considered as a threshold for defining flexible and rigid NEs; however, this discrepancy only seems to be formal and does not affect the RRS. FEMA 461 does not define RRS but provides some rules regarding the response spectra of the input signals. The response spectra should be defined considering 5% damping. The signal shall be scaled in order to have (a) acceleration response spectra amplitude equal to 1 g within 2 - 32 Hz and (b) the displacement response spectra would be approximately uniform below 2 Hz. IEEE 693 supplies two RRS, associated with high and moderate-performance levels; these spectra are provided as a function of the NE damping, considering a range of values ranging in 2 – 20%. GR-63-CORE provides RRS associated with four earthquake zones (Zone 1 to 4 in the US), considering a damping value equal to 2%. Unlike other cases, GR-63-CORE RRS spectra have shapes varying for different areas. ISO 13033 follows an approach similar to the one recommended in AC156 for the definition of RRS; however, the former can also be extended to other regulations and building codes. For example, in Perrone et al. [30], the approach proposed by ISO 13033 was modified to provide RRS compatible with the design horizontal equivalent static force evaluated according to Eurocode 8 [3]. RG-1.60 provides RRS associated with five damping ratios, i.e., 0.5%, 2.0%, 5.0%, 7.0% and 10% (for different damping ratios, a linear interpolation should be used). These

RRS correspond to a PGA equal to 1.0 g and peak ground displacement (PGD) equal to 0.91 m. For different design earthquakes, the RRS can be linearly scaled in proportion to the specified PGA (e.g., PGA=0.5 g). IEC 60068 defines three RRS, associated with 2%, 5% and 10% damping ratio. These RRS exhibit a generalized form that is based on simple correlations among the corner frequencies, and the specific corner frequencies depend on assumptions regarding the frequency range of sensitivity of the NE.

Figure 5.1a shows a comparison among the response spectra related to the protocols of interest, where FEMA 461 long and trans stand for FEMA 461 signals along horizontal longitudinal and transversal directions. All spectra but GR-63-CORE RRS (a) are related to 5% damping and (b) were computed considering PGA equal to 0.50 g and assuming a building acceleration amplification factor according to the specific protocol (a value equal to 2.5 was assumed for FEMA 461, which does not provide this ratio). Both z/H equal to zero and one conditions are depicted for AC156 and ISO 13033 RRS. IEEE 693 RRS is associated with moderate performance level and FEMA 461 spectra were obtained by scaling the protocol input signals. In particular, these latter were provided by the protocol considering specific levels of acceleration (e.g., PFA equal to about 0.2 - 0.25) and, in this section, these signals were scaled in order to obtain PGA equal to 0.50 g (Figure 5.1a) and spectral ordinate Sa corresponding to 32 Hz equal to 1.0 g (Figure 5.1b). GR-63-CORE RRS are associated with 2% damping, as the protocol only considers this damping condition. For this latter protocol, RRS spectra associated with earthquake risk zones 3 and 4 are depicted, which correspond to expected PGA in the range of 0.2 - 0.4 g and 0.4 - 0.8 g, respectively.

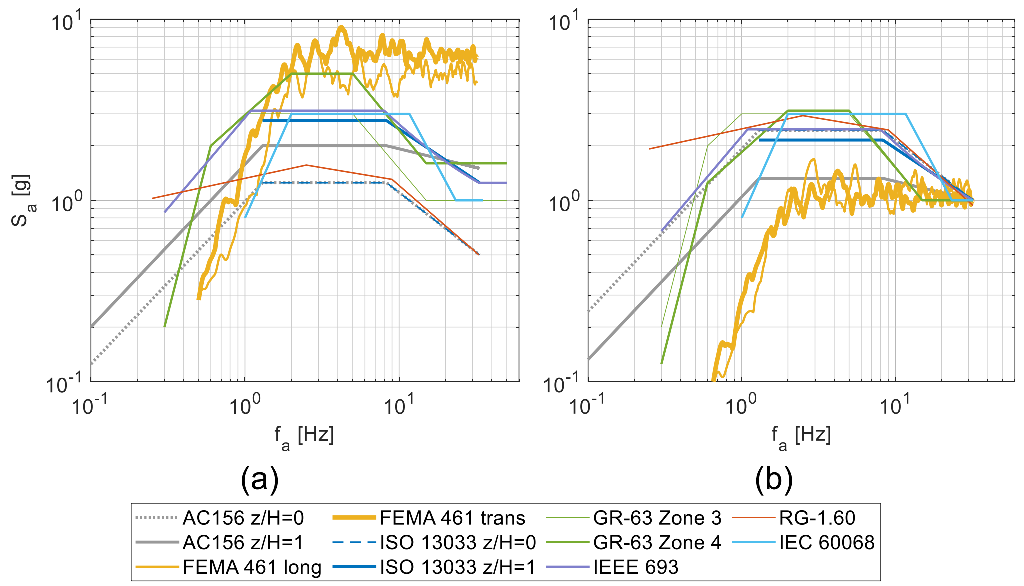

Figure 5.1: Comparison among RRS and input response spectra related to reference protocols considering (a) PGA equal to 0.50 g and (b) spectral ordinate Sa corresponding to 32 Hz equal to 1.0 g.

FEMA 461 spectra exhibit higher spectral ordinates than all other RRS for frequencies higher than about 2 Hz, whereas for lower frequencies, they cross all other RRS and become the lowest spectra over the lowest frequencies (e.g., lower than 0.7 – 1.0 Hz). AC156 and ISO 13033 are identical for z/H equal to zero condition, whereas ISO 13033 presents significantly higher ordinates for z/H equal to one condition. In particular, z/H equal to zero spectra present the lowest ordinates, for frequencies larger than about 1 Hz. GR-63-CORE and IEEE 693 RRS are the most amplified spectra over most frequencies, but it is recalled than the former is associated with 2% damping whereas the other spectra with 5%. The spectral shape is quite similar among the different RRS, whereas FEMA 461 inputs present a different trend of the ordinates over the frequencies. Sections of the response spectra can be identified for FEMA 461 signals: (a) increasing branch up to about 2 Hz and (b) plateau for larger frequencies. The increasing branch crosses all other spectra, whereas the plateau has ordinates significantly larger than the other RRS ones.

Figure 5.1b depicts a comparison among the protocol spectra considering a different comparison criterion. In particular, the spectra are calculated under the assumptions described regarding Figure 5.1a, but they are scaled in order to have spectral ordinate equal to 1.0 g corresponding to 32 Hz, which represents the highest frequency (lowest period) common to all protocols. The spectral response associated with this frequency is related to the response of an approximately rigid NE. Accordingly, Figure 5.1b highlights the spectral amplification associated with the flexible to rigid response of NEs. All spectra but FEMA 461 and AC156 z/H = 1 ones are quite similar among them, whereas these latter provide significantly lower ordinates. GR-63-CORE spectra (2% damping) and IEC 60068 present the highest plateau ordinate, while IEEE 693, AC156 z/H=0 and ISO 13033 spectra (5% damping) present a similar, lower, ordinate, still significantly larger than AC156 z/H=1 and FEMA 461 ones. Further comments are omitted for the sake of brevity.

Spectrum-compatibility

Test response spectra (TRS) should be compatible with RRS in order to satisfy specific target levels, considering both theoretical signals and recorded signals. IEEE 693 supplies different compatibility rules for theoretical and recorded inputs. For all other protocols, no distinction is made between theoretical and recorded input compatibility rules. In general, the spectrum compatibility rules include: (a) the spectral resolution definition of TRS, (b) the frequency range against which to perform the spectrum compatibility check, (c) spectrum ordinate amplitude tolerance range, expressed in terms of RRS, that quantifies the compatibility spectrum ordinate check for TRS (e.g., inferior or superior ordinate tolerance). The spectral resolution represents the interval between two frequency data points of spectral analysis. AC156 protocol states that TRS must envelop the RRS at 5% damping based on a maximum-one-sixth octave bandwidth resolution over the frequency range from 1.3 to 33.3 Hz. TRS should not exceed the RRS by more than 30 percent over the amplified region of the RRS (i.e., frequencies lower than or equal to 8.3 Hz). The protocol provides exemption rules applicable to both amplified region and ZPA region (i.e., frequencies larger than or equal to 8.3 Hz).

Theoretical TRS to RRS compatibility should be checked at 24 divisions per octave resolution or higher, and TRS ordinate should be within ±10% of the RRS at 5% damping; TRS shall include the lower corner point frequency of the RRS (1.1 Hz), for comparison with the RRS. IEEE 693 defines compatibility criteria less restrictive for recorded inputs. In particular, the shake table output TRS shall envelop the RRS within a –10%/+50% tolerance band at 12 divisions per octave resolution or higher. Exemptions are provided regarding both upper and lower limitations. According to GR-63-CORE, TRS must meet or exceed RRS for the applicable earthquake risk zone in the range from 1.0 to 50 Hz. In particular, TRS evaluated considering 2% damping should not exceed RRS by more than 30% in the frequency range 1 to 7 Hz. A test may be invalid if an equipment failure occurs when the TRS exceeds the RRS by more than 30% in this frequency range. ISO 13033 and RG-1.60 do not provide criteria regarding the spectrum compatibility. IEC 60068 establishes that the TRS shall be checked in the specified range at least in one-sixth octave bandwidth resolution in the general case, i.e., specimen damping lying between 2% and 10%. The tolerance to be applied to the RRS shall be in a range between 0% and 50%. Moreover, after the plateau zone of the RRS a tolerance more than 50% is permitted.

While protocols often provide spectrum-compatibility verification rules, the procedure to achieve or enforce this condition is not typically addressed. In order to achieve the best possible spectrum-compatibility, Crewe [55] recommends that (a) the iterative matching process for each time history should be continued beyond initial convergence to capture later iterations that may be a much closer match to the RRS, (b) the spectra matching procedure should be always conducted at a minimum of one-twenty-fourth-octave points, (c) high-pass filtering of input motions should not be used to limit the demand placed on the shake table by TRS, and (d) matching over a reduced frequency range is more effective and results in a TRS that matches the RRS more closely.

The response spectrum compatibility is often performed in the literature using software products and tools based on the analytical methods and formulations. Zaghi et al. [56] and Tran et al. [57] generated an artificial earthquake using the SIMQKE software [58]. In Magliulo et al. [59] and Di Sarno et al. [60], the signal was enhanced using the spectrum-matching procedure of the RSPMatch software [35]. Yazdani & Takada [61] developed a method for modifying many realistic earthquake ground motions through linear/nonlinear response spectra and energy matching.

Amiri et al. [62] introduced a method to generate a suite of artificial near-fault ground motion time histories for specified earthquakes based on the superposition of a coherent extracted velocity pulse with a random acceleration record corresponding to a wavelet-based nonstationary model and multiplied by a time-modulating envelope function. Several other authors carried out shake table tests and implemented artificial acceleration time histories using the STEX program of MTS [46,63].

Signal processing and instrumentation compatibility
Capacities and limitations of shake table and testing instrumentation must be met by the spectrum-compatible signals, and this should be checked prior to performing the tests. Among the possible parameters to be checked, maximum accelerations, velocities, and displacements expected to be achieved by the table should be assessed and compared to the shake table and instrumentation capacities. For example, low frequency content in the input signal typically imposes large displacement demands on the table, which can often exceed the shake table displacement capacity; this limitation is typically critical to verify [44]. If the capacity compatibility is not achieved, the input signal might be adjusted. In particular, the acceleration time history of the theoretical input motion could be filtered to meet the capacities of the shake table.

AC156 recommends that the general requirement for enveloping RRS by the TRS can be modified under certain conditions. When no resonance response phenomena exist below 5 Hz, TRS is required to envelop the RRS down to 3.5 Hz (instead of 1.3 Hz), whereas TRS is required to envelop the RRS only down to 75% of the lowest frequency of resonance (instead of 1.3 Hz) if resonance below 5 Hz exists. According to IEEE 693, the theoretical input may be high-pass filtered at frequencies lower than or equal to 70% of the lowest fundamental frequency of the specimen, but not higher than 2 Hz. The lowest fundamental frequency of the specimen should be assessed through experimental tests (i.e., dynamic identification tests, as described in following sections). GR-63-CORE requires that the cutoff of the high-pass filter does not exceed 0.20 Hz, while the cutoff of the low-pass filter should not be below 50 Hz. FEMA 461 and ISO 13033 do not establish a procedure to process the signals to obtain the compatibility with the shake table limitations. However, FEMA 461 provides a procedure for filtering input motions to remove energy contents close to the excitation frequency that has already caused a DS to occur or, more generally, that is not of interest (i.e., notch filtering).

The filtering procedure used to reduce shake table displacement demands often consists in applying a high-pass filter in the frequency domain. However, it might be necessary to also reduce the high frequency contents of the input signals according to other capacities and limitations of the shake table (e.g., 50 Hz). Therefore, a band-pass filter is often applied to solve both problems of maximum displacements and high frequency contents. In several studies [16,59,64], the acceleration time histories were filtered through low-pass and band-pass filters in order to meet the instrument and facility capacities, e.g., to reduce the maximum shake table displacements. Takhirov et al. [44] proposed several filtered options suitable for most of the shake tables worldwide to the seismic qualification of NEs according to IEEE 693.

Analytical and experimental validation

The final step of the loading input definition should be the signal verification and the validation of the experimental procedure, especially if further filtering procedures were implemented. Generally, the adherence of both theoretical and recorded signals is considered to be sufficient for verifying and validating the experimental qualification procedure, and this is based on spectrum-compatibility criteria. However, the protocol compliance of (recorded) signals might be critical since shake table and testing instrumentation might not generally reproduce a compliant signal given to instrumental and diverse reasons, and this stresses the need for strict verification and validation rules and criteria (e.g., [65]).

5.2.3 Testing procedure

Outline

The testing program typically involves pretest and testing phases. For the pretest phase, FEMA 461, AC156, IEEE 693 and GR-63-CORE require pretest inspection and functional verification to be documented. The testing phase generally consists of dynamic identification tests and seismic performance evaluation tests. FEMA 461 includes an additional testing type, named failure tests. Failure tests are carried out to induce DSs that could pose life safety risks and DSs corresponding to the incipient failure of the test specimen. Failure tests are typically performed as part of the performance evaluation tests.

The current testing protocols implicitly define that the dynamic identification tests should be performed prior to seismic performance evaluation tests. However, FEMA 461, which recommends an incremental performance evaluation test procedure, establishes that dynamic identification tests should be conducted prior to and after each performance evaluation tests. In literature, several studies followed this approach. For example, in Cosenza et al. [66] and Petrone et al. [64], the dynamic identification was carried out over the incremental tests and both dynamic properties and exhibited damage were correlated to the testing intensities.

Dynamic identification tests

To perform an exhaustive assessment, vibration modes, fundamental periods/frequencies, and damping ratios evolution should be associated with the damage process evolution, considering undamaged, partially, and fully damaged conditions (or at least all the DSs reached during the tests). Another parameter that also accounts for the dynamic properties of NEs is the dynamic component amplification factor, often defined a_p by regulations and codes [2-8]. In most regulations and codes, a_p is a key parameter for computing seismic demand forces on NEs [2-8]. This parameter is typically defined by conservative expressions and is rarely assessed with regard to specific NEs through experimental or numerical procedures. Reference shake table protocols do not require estimations of this parameter even though it is essential for reliable estimations of RRS or seismic demands.

Disregarding a_p, the input of the dynamic identification tests is generally expressed by a low-intensity acceleration time history signal, which is defined by the reference protocol in some cases. FEMA 461 establishes that single-axis identification tests should be carried out along each principal direction of the test specimen, considering four alternative types of test: white noise tests, single-axis acceleration-controlled sinusoidal sweep tests, resonance tests, and static pull-back tests. AC156 and GR-63-CORE recommend single-axis acceleration-controlled sinusoidal sweep tests, IEEE 693 indicates sine sweep or random noise excitation test, and ISO 13033 includes the dynamic tests but does not describe the testing procedure and input.

Several testing methods were used in the literature to identify the dynamic characteristics of NEs. Random noise excitation tests [16,19,21,43,60, 64,66,67] and sine sweep tests [17,18,68,69] are among the most used ones, even though no studies, to the knowledge of the author, identified the differences among the different methods in terms of dynamic properties assessment results or supplied motivations for preferring the use of one specific method. Even though the methods defined within the relevant protocols or in the literature can be considered to be relatively reliable, the absence of a preferred method and the lack of standardized definitions might condition the robustness of the estimations, especially considering comparison purposes. This stresses the need for defining a unique reliable and robust dynamic identification test method, that is compliant with specific technical procedures for defining the input signal, that minimizes the analyst bias, also being widely applicable, strengthening the accuracy of the estimations and favoring consistent comparisons and result extrapolations.

Seismic performance evaluation tests

According to most protocols, seismic performance evaluation tests are defined by the tests performed considering the seismic intensity associated with target performance level(s) that the specimen should meet. ISO 13033, AC156, IEEE 693 and GR-63-CORE do not specify a minimum number of performance evaluation tests to perform or do not provide recommendations for defining a testing program. Conversely, FEMA 461 supplies criteria to define the testing program according to an incremental approach. In particular, this protocol requires at least three different shaking intensities and indicates that the intensities of the performance evaluation tests should be defined in order to induce relevant DS occurrence, i.e., functioning interruption and repair/replacement intervention, for seismic performance evaluation tests, and severe damage, incipient failure, and risk of life threatening, for failure tests. FEMA 461 also defines the minimum intensity step increment between consecutive intensity level tests, which is equal to 25%.

Seismic performance evaluation tests are generally carried out by applying the input motions simultaneously along the principal axes of the specimens. In particular, AC156, IEEE 693, GR-63-CORE and FEMA 461 establish that the performance evaluation tests (and failure tests for FEMA 461) should be performed through triaxial tests with input motions applied simultaneously along all principal axes of the test specimen; alternatively, multiple biaxial tests can be used (along horizontal and vertical directions) according to an exhaustive approach. FEMA 461 states that horizontal tests (biaxial or uniaxial) could be performed if the effect of vertical motion on the seismic response of the test specimen is negligible; the other protocols do not address this condition, which can be quite common for typical NEs (e.g., partitions or infill panels). In particular, FEMA 461 recommends that this condition may be acceptable if the vertical fundamental frequency of vibration of the test specimen is at least 10 times larger than horizontal fundamental frequencies or if the vertical natural frequency of the test specimen falls outside the frequency range of the input motions. AC156 allows uniaxial tests, which should be performed along each of the three principal directions of the specimens.

In several literature studies, shake table tests were performed through incremental procedures despite only FEMA 461, among several protocols, recommends performing multiple (incremental) tests for assessing the seismic performance and qualifying NEs. It is worth recalling that this latter protocol is not intended for seismic certification, and therefore, this approach (i.e., incremental tests) is not required to be applied for seismic certification purposes. In some literature studies, shake table inputs compliant with protocols other than FEMA 461 (e.g., AC156) were scaled according to relatively dense incremental procedures [20,60,64,67], i.e., FEMA 461 approach was applied considering seismic inputs other than this latter approach. This stresses the lack and inconsistency of the current seismic qualification approaches and protocols. In particular, they do not seem to give significance to incremental procedures, which are certainly associated with more reliable and robust assessment and evaluation, also compliant with PBEE approach [70].

Representativeness of qualification and certification

The test specimens should effectively represent the class or type of components intended to be qualified/certified by the manufacturer in order to achieve the target representativeness of the qualification/certification; this representativeness strongly depends on the objective of the assessment or qualification. A relatively adequate number of shake table tests should be performed considering a minimum number of test specimens. AC156 provides the criteria for defining test specimen configuration requirements for an element product line. The selection can be achieved based on the least seismic capacity offered by the structural configurations, mounting configurations, mass distribution, and specimen components and subassemblies. Other current protocols do not provide requirements or information on the representativeness of the qualification/certification procedure. GR-63-CORE only provides recommendations regarding installation conditions for equipment and systems. Only FEMA 461 recommends a minimum number of specimens to test, which is equal to three.

5.2.4 Critical evaluation of existing protocols

Table 5.1 summarizes the key parameters and features that are essential for the definition and implementation of qualification procedures defined by the reference protocols. Most of parameters reported in Table 5.1 were described and discussed in previous sections; therefore, redundant comments are omitted for the sake of brevity, and the focus of this section is on most significant comparisons and critical evaluation. AC156, FEMA 461, and ISO 13033 are intended for any type of elements (i.e., generic NEs), whereas IEEE 693, GR-63-CORE and RG-1.60 are defined for specific equipment or systems. However, it is not clear how the type of target specimens conditioned the definition of the protocol characteristics, especially for the specific equipment protocols. Even regarding the sensitivity of the target specimens, there are not clear requirements for several protocols (e.g., specific equipment protocols). However, the author believe that there is a common skepticism for using shake table testing (protocols) to assess and qualify NEs that are (also) sensitive to displacements/drifts, as it can also be identified in AC156 criteria. Indeed, the fact that shake table testing is the best option to assess dynamic effects/response should not limit the use of the reference protocols to assess NEs that are also sensitive to drifts/deformations or that, more generally, have a complex response that can only be reasonably assessed through dynamic tests. This critical issue will be addressed further in the following section, where the proposed approach and the novel protocol are described. Regarding the boundary conditions of the target specimens, most protocols are intended to provide criteria for anchored or attached elements. However, due to the absence of reliable protocols intended for unanchored or freestanding equipment, the reference protocols were often used in the literature also to assess these peculiar NEs (e.g., [15,60,71-73]).

Sinusoidal sweep and white noise tests are the most referenced by the protocols, and these methods are the most used in the literature, as previously discussed. However, the protocols do not provide clear information and technical guidance on how to develop the dynamic identification test inputs, or rather they do not follow general and widely applicable approaches.

Regarding RRS, the reference protocols provide quite dispersed and varied requirements and information, which are associated with significant differences among the protocols. These differences might be significant in terms of RRS details/specification/information, site-dependency, scalability of RRS, frequency range and corner frequencies, and component and floor amplification factors.

This parameter variability might significantly condition the reliability of the protocols as tools to qualify the NEs. For example, the plateau to ZPA amplification provided by AC156 RRS (related to z/h) is significantly lower than the one related to other protocols. This was already proven to underestimate seismic demands associated with strong floor motions [53]. This is likely due to an upper limitation criterion defined by the protocol, which was already criticized by literature studies [30,50,74]. Another critical definition of RRS is related to IEEE 693 criteria, which seem to not intrinsically account for the building acceleration amplification, which should be included by RRS amplifications by the signal analysts.

RRS definition should be based on consolidated and consistent formulations of seismic ground and building demands on NEs, which should be reported by the protocols and proven to be reliable and robust, but also relatively simple to implement.

A significant variability is also associated with the protocol definition of the test input to perform seismic performance evaluation tests, and, similarly to the case of RRS, this can significantly affect the reliability of assessment, qualification, or certification procedure. The present chapter has already stressed the significance of the seismic loading history characteristics on the reliability of the seismic evaluation. The spectrum-compatibility criteria are more comparable among the different protocols and follow more common approaches. However, some non-negligible differences can also be identified, as it can be seen in Table 5.1.

As a conclusive comment, the author believe that seismic performance of NEs should be assessed through incremental procedures of excitation, by scaling the input signals to be representative of the seismic scenario actions that would potentially excite the specimen at the structure-to-element interfaces. This is compliant with PBEE approaches and is recommended in FEMA 461. In particular, it is desirable that the results of the qualification tests are documented for each significant intensity level and regarding relevant DSs and used for fragility or vulnerability assessment. These aspects are not addressed by reference protocols except FEMA 461. Therefore, novel approaches and protocols should be defined to favor reliable and robust assessment, qualification, and certification procedures according to incremental procedures and evaluations based on PBEE.

Table 5.1: Comparison among reference protocols considering most significant features and parameters.

		AC156	FEMA 461	ISO 13033	IEEE 693	GR-63-CORE	RG-1.60	IEC-60068
Target specimens	Type	Any	Any	Any	Electrical substation equipment	Telecommunications network equipment	Nuclear power plants equipment	Components, equipment, and electrotechnical products
	Behavior/EDP sensitivity	Not specified[1]	Dynamic effects, velocity, strain-rate effects	Acceleration/ displacement	Not specified	Not specified	Not specified	Not specified
	Boundary conditions	Anchored[2]	Anchored	Anchored	Anchored	Anchored	Not specified	Not specified
Dynamic identification test	Sinusoidal sweep	**X**	**X**	-	**X**	**X**	-	
	White noise		**X**		**X**			
	Resonance		**X**					**X**
	Static pull-back		**X**					
RRS	Damping level, ν [%]	5	Not applicable	5	2÷20	2	0.5,2,5,7,10	2,5,10
	Site-Dependency	**X**		**X**				
	Maximum building acceleration amplification factor	1.6	Not applicable	Not applicable	2.5	Included	Not applicable	2.0
	Frequency range [Hz]	0.1-33.3	Not applicable	1.3-33.3	0.3-50	0.3-50	0.25-33.0	1-35
	Plateau range [Hz]	1.3-8.3	Not applicable	1.3÷2.5 -7.5÷8.3	1.1-8.0	2.0-5.0 (Zone 4)	2.5-9.0	2-11.7
	Spectral acceleration at plateau, in fractions of ZPA	f(z/h): 2.5(z/h=0)	Not applicable	2.5	f(ν): 3.24(ν=2%)	f(Zone): 3.13 (Zone 4)	f(ν): 2.9[3] (at 5%)	f(ν): 3.0 (at 5%)
Seismic performance evaluation test input	Total (strong motion) duration [sec]	30±6 (20 +6/-0)	60	Not applicable	(≥20)	32	Not applicable	30
	Strong part to duration ratio [%]	Not applicable	Not applicable	Not applicable	≥30	Not specified	Not applicable	25,50,75
	Sampling rate [Hz]	Not applicable	100	Not applicable	Not specified	>200	Not applicable	Not specified
	Energy content [Hz]	1.3-33.3	0.5-32	Not applicable	1.1-33	Not specified	Not applicable	Not specified
	Resolution bandwidth [octave]	1/3 or 1/6	1/3	Not applicable	Not specified	1/6	Not applicable	Not specified
Spectrum-compatibility	Tolerance above RRS [%]	30	Not applicable	Not applicable	50[4]	30	Not applicable	50
	Tolerance below RRS [%]	10[5]	Not applicable	Not applicable	10[6]	0	Not applicable	0
	Tolerance range applicability [Hz]	1.3-8.3	Not applicable	Not applicable	<15	1.0-7.0	Not applicable	Not specified
	Tolerance resolution [octave]	1/6	Not applicable	Not applicable	1/12[7]	1/6	Not applicable	f(ν): 1/6(ν=2-10%)
	Compatibility range applicability [Hz]	75% f_a[8] (or 3.5) - 33	Not applicable	Not applicable	70% f_a[8] (or 2) - 33	1.0-50.0	Not specified	Not specified

[1]The protocol is not intended to evaluate effects of relative displacements on NEs.
[2]The protocol is intended for anchored elements but this is not clearly and univocally stated within the document.
[3]The plateau spectral ordinate varies from 3.13–2.61 (average).
[4]The tolerance above RRS for the theoretical response spectrum is equal to 10%.
[5]In both the ZPA region and the amplified region of RRS a maximum of two individual points up to 10% below the RRS can be acceptable provided the adjacent 1/6 octave points are at least equal to the RRS.
[6]A –10% deviation is allowed, provided that the width of the deviation on the frequency scale, measured at the RRS, is not more than 12% of the center frequency of the deviation, and not more than five deviations occur at the stated resolution.
[7]The spectrum matching procedure should be conducted at one-24th octave resolution or higher for the theoretical response spectrum
[8] f_a is the natural frequency of NE.

5.3 Definition of a novel code-compliant testing protocol

5.3.1 Outline

A novel code-compliant shake table testing procedure, namely testing protocol, is defined in this section. The protocol defines the procedure and requirements for seismic assessment of acceleration-sensitive NEs by shake table testing, with particular reference to seismic qualification and certification processes. The protocol is applicable for NEs having fundamental frequencies greater than or equal to 1.0 Hz. In the following, the seismic input used for the seismic performance evaluation test is also referred to as loading protocol, as this represents the most significant feature of the testing protocol.

5.3.2 Seismic qualification approaches

Two different approaches can be considered for qualifying NEs: (a) specific performance level qualification and (b) extensive qualification. The first approach is inspired by the procedure typically referred to by existing shake table protocols [11,27,29,39]. In particular, according to this approach, the qualification is aimed at checking whether the component fulfills (or not) a specific performance level, associated with a target level of a relevant (seismic) intensity parameter. The seismic intensity parameter and the relevant target levels are typically defined by regulations or codes. Acceleration spectral response S_a is typically considered as a seismic intensity parameter for assessment of acceleration-sensitive elements and is referred to within several national and international codes [2-8]. However, PGA or PFA might also be considered, if appropriate, as they might be equally reliable as seismic intensity demands. Target seismic intensity parameters should not be confused with testing IMs, even though testing IMs might also be considered as seismic intensity parameters, when possible and appropriate. It is fundamental that the target intensity parameter measures are established from the basic parameters (e.g., hazard or soil conditions) following consistent and robust approaches and formulations/specifications, which should also be compatible with the qualification protocol. In particular, the target levels can be defined according to specific site-building-component scenarios or can be more general and referred to entire regions and wide representative scenarios. For example, if the building site and NE installation height (over building height) are known, NE could be qualified considering the specific scenario associated with this location, according to reference seismic demand formulations. A regional or national maximum demand scenario is typically considered for the identification of the qualification intensity level, especially if the qualification is carried out by manufacturers. Further comments on target seismic intensity parameters are omitted as their definition should be addressed, through conventional decisions, by regulation, codes, and technical guidelines.

The extensive qualification reflects the technical-scientific requirement for a more exhaustive assessment and evaluation of the seismic performance of NEs, not only meeting a conventional requirement target, but developing novel technical and applicative knowledge. This approach was developed in the light of the recent literature in the field, where incremental complex shake table procedures were implemented [15,17,22,56,60,66,67]. In particular, the extensive qualification is aimed at characterizing the behavior and the damage response of NEs considering multiple incremental intensity levels, identifying the NE capacity thresholds corresponding to the significant performance levels. Target levels of seismic intensity parameters should be defined for the relevant performance levels as it is described for specific performance level qualification.

The extensive qualification is a complete and exhaustive identification and characterization of the NE in terms of seismic behavior, capacity, and performance, providing robust and reliable capacity thresholds to evaluate the fulfillment of the target performance levels, whereas the specific performance level qualification is only associated with the fulfillment of a conventional performance level requirement. The use of one approach over another should be regulated by national and international regulations and qualification or certification rules/standards. In particular, the importance and representativeness of the NE should be among the most significant key parameters for providing these criteria.

The manufacturer could prefer to perform an extensive qualification even if a specific performance level is required by the relevant regulatory requirements, as this would shed light on the complete performance of the NE, providing significant additional technical information to the specific performance level check. For example, the specific performance level qualification does not allow determining the safety conditions regarding the performance level demand, as the result of this qualification process is checking that the performance level is satisfied, without quantifying the capacity and safety margins. This specific margin quantification could be considered to be of primal importance, for example, in the case of nuclear power facilities or hospitals, where safety is expected to matter more than the economic aspects. Moreover, identifying the capacity margins associated with the relevant performance levels would be essential for an efficient design of the NE. Finally, an incremental qualification procedure would also allow the assessment of the seismic fragility and vulnerability associated with NE, essential features for PBEE. For these and other reasons, particular focus is given to the extensive qualification approach in this section.

5.3.3 Damage states and limit states

Four representative damage states (DS) associated with the NE can be defined in order to perform seismic qualification through both possible approaches: absent damage DS0, minor damage DS1, moderate damage DS2, and major damage DS3. DS1 achievement implies the need for minor repair interventions and/or rearrangement of specimens to restore the original conditions; in general, DS1 does not affect the functioning of the element. DS2 implies that the test specimen is damaged so that it should be partially replaced, and this results in loss of functioning. DS1 and DS2 are typically associated with serviceability limit states (SLSs) [3]. DS3 implies that the damage level is such that the test specimen needs to be totally replaced/repaired and life safety is not ensured. DS3 is typically associated with ultimate limit states (ULSs) [3].

The technical definition of the damage level associated with DS, which is defined by damage-to-DS criteria or correlations (namely, damage scheme), strongly depends on the type, features, and arrangement of NEs. An example of the DS definition for seismic qualification of temporary partition wall was proposed in Petrone et al. [64]. In this context, DS definition and related consequences are based on the definition given by Taghavi & Miranda [75]. In particular, the correlation between each DS and the loss can be expressed in terms of the three "D" [76]: (a) human casualties (Deaths), (b) direct economic loss due to the repair or replacement of NCs (Dollars), and (c) occupancy or service loss (Downtime). Damage schemes should be defined for each type of damage and for each significant component of the test specimen (e.g., panels, studs, horizontal element, rails, screws, in Petrone et al. [64]). The more damage scheme is defined by quantitative and univocal engineering parameters and measures, the more this is efficient and robust.

Regarding shake table tests, damage of NEs should be observed after each seismic performance evaluation test by inspecting the physical conditions of the test specimen, and an appropriate damage survey form should be compiled. The achievement of DSs should be identified by analysis of the damage survey forms according to the criteria defined within the damage scheme, and the DSs should be correlated to efficient intensity parameter measures that are representative of the seismic demands. The limit state verifications should be performed according to the qualification approach and the compliant regulations.

5.3.4 Test specimens and loading program

The selection of the test specimen should follow the aim of the manufacturer and the requirements of the relevant regulations. In particular, the test specimen should be more or less representative of a production line according to the expected wideness and representativeness of the qualification results. Generally, the test specimen should represent a conservative condition to obtain the least seismic capacity associated with the system of interest. The number of specimens to be tested should also be compliant with the relevant requirements and should reasonably depend on (a) desired qualification robustness and (b) potential uncertainty associated with the production and response of the specimen.

The loading program consists of a series of dynamic tests, including both dynamic identification tests and seismic performance evaluation tests. According to the extensive qualification approach, the seismic performance evaluation tests should be performed through an incremental procedure. The initial, incremental, and final testing IM level should be chosen according to the expected behavior and damage exhibited by the specimen with regard to the performance target (e.g., operativity conditions) and should be compatible with the capacities of shake table and instrumentation. Before and after each significant performance evaluation test, a dynamic identification test should be conducted along each principal direction of the test specimen. Generally, the performance evaluation tests should be performed via triaxial tests, with motions applied in the principal directions of the NEs. However, biaxial (horizontal) tests may be carried out if the element can be reasonably assumed to be not sensitive to the accelerations along the vertical direction; this condition could be considered to be applicable if the vertical fundamental period is at least an order of magnitude lower than a maximum horizontal fundamental period or if the vertical fundamental period is outside the significant frequency range of the signal.

5.3.5 Dynamic identification tests

White noise tests are recommended in this section to identify natural frequencies and damping of the test specimen [16,19-21,43,66,67,77]. In practice, white noise is a theoretical idealization since no system can generate a uniform spectrum for all frequencies extended from zero to infinity. In real applications, white noise signals present spectral ordinates having values oscillating around the reference spectral value over a range of frequencies. Typically, the white noise signals present greater amplitude at low frequencies and a smaller amplitude tending to zero at higher frequencies [45].

The random noise excitation should be obtained by a uniform random stationary process [78]. The acceleration peaks of the signal shall be at most of 0.10 ± 0.05 g; this intensity threshold should prevent from causing damage to the specimen, however, in some cases, a lower (or higher) intensity might be considered. The signal should have a significant energy content ranging from 1 to 32 Hz, a minimum duration of 60 s, and a sampling frequency of 200 Hz. The baseline can be filtered in order to provide the abovementioned frequency contents to the random noise excitation or to eliminate frequencies not compatible with the instrumental facility capacity; in this latter case, it should be verified that the cut of the critical frequencies do not affect the reliability of the signal and the robustness of the dynamic identification (e.g., by proving that the specimen does not exhibit significant sensitivity to those frequencies). In particular, a fourth order low-pass Butterworth filter with a cut-off frequency of 40 Hz was used in the context of the proposed protocol, according to the literature review and expertise of the author. The signal was then modified with a window function to have a rise time and decay time equal to 5% of the signal duration.

Figure 5.2a shows a representative random noise excitation developed according to this procedure. Figure 5.2b shows the corresponding Fourier amplitude spectrum [26] that extends from 1.0 Hz to 40 Hz and envelopes the frequency range of interest.

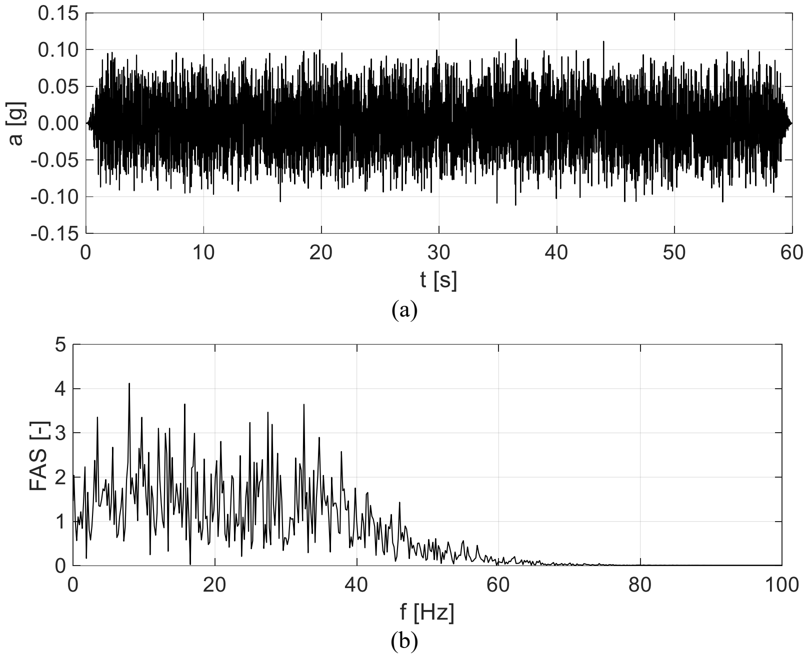

Figure 5.2: Example of random noise excitation history: (a) acceleration time history; (b) Fourier amplitude spectrum (FAS).

5.3.6 Seismic performance evaluation tests

Required response spectra

The proposed RRS was developed according to the NTC 2018 [6] formulation and literature studies [38,74]. NTC 2018 defines the total design horizontal force on NE, F_a, defined as

$$F_a = \frac{S_a \cdot W_a}{q_a} \tag{5.1}$$

In particular, F_a is the horizontal seismic design force applied at the component's center of gravity and distributed relative to the component's mass distribution, S_a is the horizontal spectral design acceleration of the NE attached at level *i* of the building structure for the limit state in question, W_a is the weight of the NE, and q_a is the NE response modification factor or behavior factor, i.e., a factor aimed at reducing the elastic design forces accounting for the expected inelastic response; q_a can be specified according to the ductility and overstrength overstrength of the NE, referring to regulations/codes [2,3,6] and/or literature studies [79-81].

The floor response spectrum (S_a) used to calculate the horizontal equivalent static force is given by:

$$S_a = \begin{cases} \max\left\{\alpha S\left(1+\frac{z}{H}\right)\left[\frac{a_p}{1+(a_p-1)\left(1-\frac{T_a}{a\cdot T_1}\right)^2}\right], \alpha S\right\} & \text{for } T_a < aT_1 \\ \alpha\cdot S\left(1+\frac{z}{H}\right)a_p & \text{for } aT_1 \leq T_a < bT_1 \\ \max\left\{\alpha S\left(1+\frac{z}{H}\right)\left[\frac{T_1}{1+(a_p-1)\left(1-\frac{T_a}{b\cdot T_1}\right)^2}\right], \alpha S\right\} & \text{for } T_a \geq bT_1 \end{cases} \tag{5.2}$$

according to NTC commentary [82]; this formulation was derived from [38,74] and was already proven to be reliable by recent literature studies, considering bare and infilled RC buildings as a reference [49,51]. In particular, α is the ratio between the design peak ground acceleration on stiff soil for the relevant limit state and acceleration of gravity, S is the soil amplification factor, z is the height of the building point of attachment of component, measured from the foundations, H is the average roof height of the building measured from the foundations, T_a the fundamental period of the component-attachment system, T_1 is the fundamental period of the building, and a, b and a_p are parameters defined according to the fundamental period of the building (Table C7.2.II §C7.2.3 NTC commentary [82]).

If the dynamic proprieties of the building are not defined, it is not possible to evaluate the RRS through Equation (5.2). In particular, regarding (generic) seismic qualification, NEs should be assumed to be installed in different types of buildings, and the RRS should not depend on specific dynamic characteristics of the building. In order to supply a valid and applicable qualification, a novel RRS formulation was developed considering a wide and representative range of building fundamental periods, i.e., from 0.1 to 2.0 s; this range was defined according to representative European building scenarios [83,84]. Figure 5.3 shows the dimensionless floor response spectra for $z/H = 1.0$, obtained considering the range of periods of interest (5% damping). The proposed RRS envelopes 0.1 to 2.0 s building period floor response spectra evaluated according to:

$$\frac{S_a}{(\alpha S)} = \begin{cases} 4\,(1+z/H) + \frac{(1+z/H)}{(f_1-f_0)}(f_a - f_0) & \text{for } f_a < f_1 \\ 5\,(1+z/H) & \text{for } f_1 \leq f_a < f_2 \\ \left[\frac{5\,(1+z/H)}{1+4\left(1-\frac{f_2}{f_a}\right)^2}\right] & \text{for } f_a \geq f_2 \end{cases} \tag{5.3}$$

as it is depicted in Figure 5.4. The formulation is reported in Equation (5.3), where f_0, f_1, and f_2 are set equal to 1.00, 1.40, and 12.5 Hz, respectively.

Considering the most relevant *z/H* condition (i.e., equal to unity), the proposed RRS is compared with reference protocol RRS and input spectral responses (for FEMA 461) in Figure 5.5, following the same comparison approach used in Figure 5.1. Considering PGA equal to 0.50 g, the proposed RRS is the most conservative RRS, whereas it is among the most conservative RRS if PFA equal to 1.0 g is considered. The plateau frequency range of the proposed RRS is larger than other protocols. Even if few reference RRS provide slightly higher ordinates corresponding to narrow frequency ranges, the proposed RRS is overall the most conservative one, especially considering the reference RRS envelope and both PGA equal to 0.50 g (Figure 5.5a) and Sa(32 Hz) equal to 1.0 g (Figure 5.5b) conditions. In fact, the reference spectra that exceed the proposed RRS ordinates in some regions are associated with significantly lower responses in other regions. It should be noted that the proposed RRS matches significantly well the plateau of FEMA 461 input spectra. The proposed RRS associated with z/H equal to zero is also more severe than other reference protocol RRS, especially considering PGA equal to 0.50 g condition (Figure 5.5a).

Seismic performance evaluation test input

The generation and processing of the seismic performance evaluation test input in terms of acceleration time history was implemented considering the RRS described in previous section. In this specific case, the RRS provided by Formula (5.3) was detailed assuming 5% damping, z/H = 1.0 and $\alpha \cdot S$ = 0.4 g, which is representative of high seismicity in Italy. However, the procedure is general and easily applicable considering different seismic demand formulations or RRS.

An artificial procedure was carried out through three phases: (1) *baseline generation*, (2) *RRS spectrum-compatibility enforcement*, and (3) *further signal processing*, including (4) *exceptions*, which is described in the following.

The procedure is described with regard to horizontal components, but it is generalizable for the vertical direction. According to the literature, the author recommend that, if triaxial tests are to be performed, the response spectra of the vertical input should be compatible with 80% of the horizontal RRS.

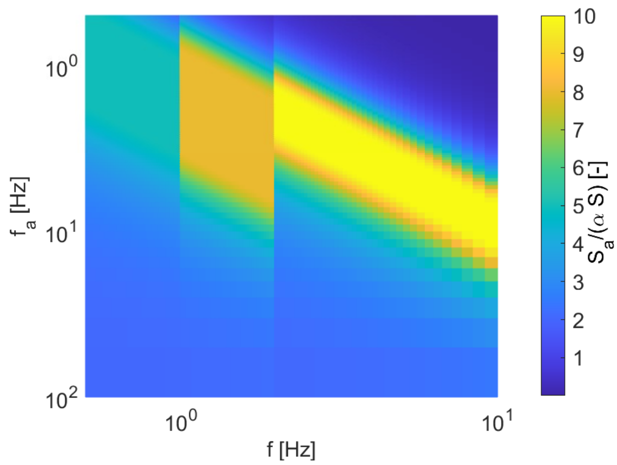

Figure 5.3: Dimensionless response spectra for the range building fundamental periods from 0.1 to 2.0 s, expressed as a function of fundamental NE frequency (fa) and fundamental frequency of primary structure (f).

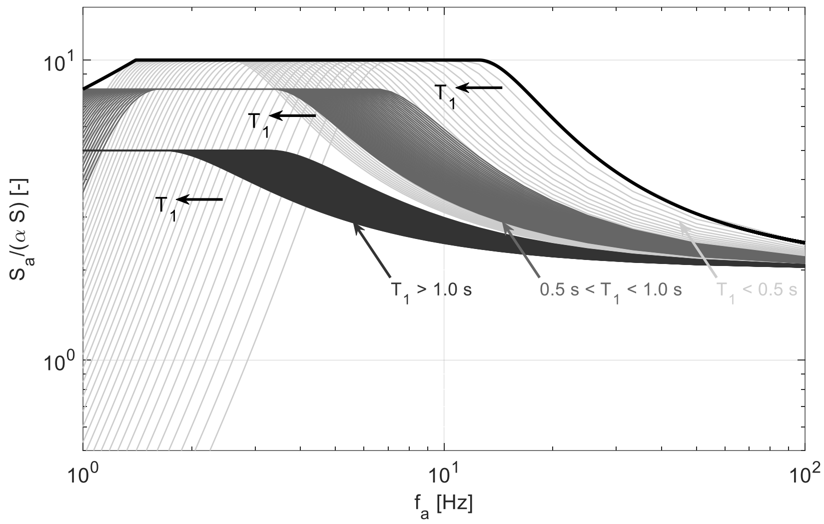

Figure 5.4: Required response spectra (RRS) (5% damping) derivation according to the proposed protocol.

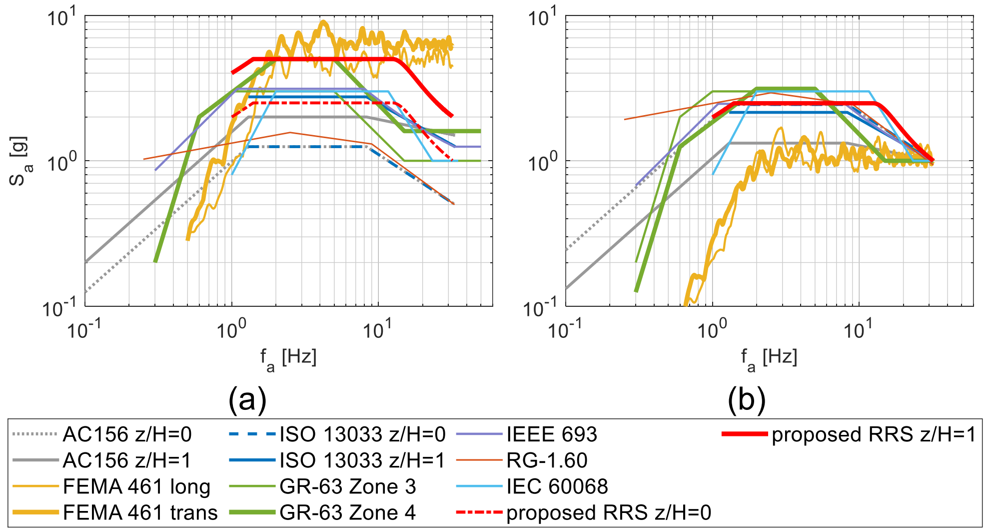

Figure 5.5: Comparison between proposed RRS and RRS and input response spectra related to reference protocols considering (a) PGA equal to 0.50 g and (b) spectral ordinate corresponding to 32 Hz (Sa(32 Hz)) equal to 1.0 g.

1. Baseline generation. The baseline signal was generated with the following features: nonstationary random signal with an energy content ranging from 1.0 to 32.0 Hz; one-sixth octave bandwidth resolution, i.e., for each octave, two consecutive frequencies have a ratio equal to $2^{1/6}$; sampling rate of 400 Hz; total duration equal to 30 seconds; at least 20 seconds of strong motion; non-stationary time history with rise (RP), strong motion (SMP) and decay (DP) parts of 5, 20, and 5 s, respectively. For each frequency (f_i) a sinusoidal wave with a duration of 30 seconds was defined as follows:

$$x_i(t) = A \cdot \sin(2\pi f_i \cdot t + \varphi_i) \tag{5.4}$$

In particular, A is the amplitude of the sinusoidal wave; the time step (t) is the reciprocal of the sampling rate, i.e., equal to 0.0025 seconds; φ_i is the phase angle of the sinusoidal wave, defined according to:

$$\varphi_{i+1} = \frac{a \cdot \pi}{n_f} + \varphi_i. \tag{5.5}$$

The phase angle of the first sinusoidal wave was set equal to $\varphi_1 = a\pi/n_f$ where n_f is the number of frequencies in the range from 1.0 to 32.0 Hz and a is a harmonizing factor that modifies the phase of the strong motion of baseline. In particular, a defines the quantitative manner of combination of the elementary frequency contents in terms of harmonic functions. This parameter is responsible for the unicity of the baseline and accounts for the "random" character. The value of a for each baseline was assumed through implementing a random function in Matlab, which selects, randomly, real numbers. Please, find further details regarding this issue in [78,85]. This factor allows to obtain a smooth signal and to avoid abrupt discontinuities of the baseline. The baseline was obtained by adding the three parts, i.e., RP, SMP, and DP: SMP ($y_{SMP}(t)$) was determined as the mean of all sinusoidal waves for each time step in the range from 5 to 25 seconds; RP was defined with a growth exponential signal in the range from 0 to 5 seconds, according to:

$$y_{RP}(t) = \frac{y_{SMP}(t)e^t}{b} \tag{5.6}$$

where, b is the harmonizing factor of the rise part of the baseline; finally, DP was defined with a negative exponential signal in the range from 25 to 30 seconds, using:

$$y_{DP}(t) = \frac{y_{SMP}(t)e^{-(t-25)}}{c} \tag{5.7}$$

where, c is the harmonizing factor of the decay part of the baseline.

Figure 5.6 shows an example of a baseline signal, where RP and DP are depicted in gray and SMP in black. Figure 5.7 shows the spectrogram (power spectral density (PSD)) of the baseline highlighting how the frequency content varies with time. The maximum spectral power is concentrated in the frequency range of interest and in the SMP.

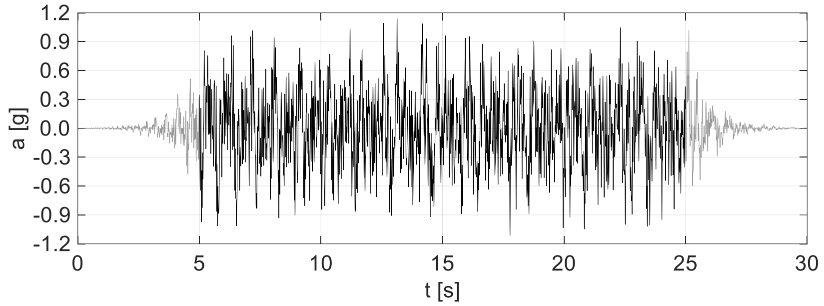

Figure 5.6: Example of baseline for developing a seismic performance evaluation test input. The gray part represents RP and DP parts of the signal, whereas the black one represents the SMP part.

2. RRS spectrum-compatibility enforcement. The spectrum-compatibility enforcement was carried out using RSPMatch [35]. In particular, the procedure was applied through a time-domain modification of the baseline signal to enforce the RRS spectrum-compatibility. The RSP match signal processing procedure was implemented according to the recommendations provided by Hancock et al. [35]. In particular, some wavelets were added to the signal acceleration time history in the time domain, according to Suárez & Montejo [86], i.e., sinusoidal corrected displacement compatible wavelet using explicit integration (model 14, according to RSPMatch manual).

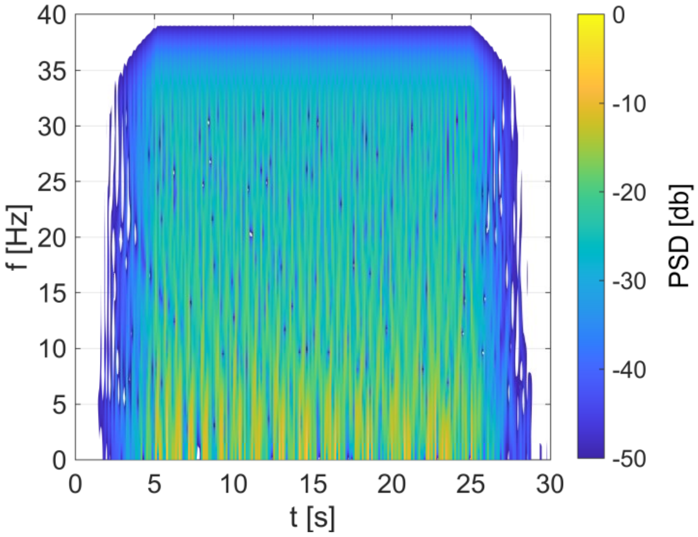

Figure 5.7: Power spectral density (PSD) of the baseline.

The spectrum-compatibility was enforced by considering the frequency sixths octave used to generate the baseline to optimize the procedure. In particular, the seismic performance evaluation test input should be associated with response spectra that envelope RRS considering a maximum one-sixth-octave bandwidth resolution over the frequency range from 1 to 32 Hz. The amplitude of each matched spectrum ordinate should be independently adjusted until the response spectrum envelopes the RRS. The response spectrum ordinates should not be lower than RRS and larger than 1.3 times RRS. For these reasons, the RSPMatch reference RRS was obtained by considering a 10% increase of the RRS described in previous section.

The spectrum-compatibility should be checked considering both signals to assign to the table (theoretical signals) and signals recorded by the table in the course of the seismic performance evaluation tests (actual signals). In particular, theoretical signals that produce spectra that fall below the RRS ordinates are generally not acceptable, whereas the spectrum-compatibility criteria of the actual signals are less stringent. In this latter case, a maximum of two of the one-sixth octave analysis points may be below RRS, in terms of spectral ordinate, by 10% or less, provided that, for each point, the adjacent one-sixth-octave points are at least equal to RRS. This condition can occur in both the amplified region of the RRS (frequencies less than or equal to 12.5 Hz) and ZPA region (frequencies greater than 12.5 Hz).

3. Further signal processing. The maximum accelerations, velocities, and displacements associated with the theoretical inputs should be estimated considering the maximum expected levels of shaking intensity defined in the loading program. These estimations should be compared with the capacities of the instrumentation and shake tables to guarantee consistent tests and to provide reliability to the results. In the case of exceedance of the capacity thresholds, the input might be subjected to further filtering processing. The filtering procedure is described in the following considering a representative case study application.

4. Exceptions. There might be cases in which signal processing procedures are not able to guarantee a full compatibility of the signal with the limitations/capacities/features and the signal cannot be adequately reproduced by the shake table (i.e., theoretical signal is spectrum-compatible and reproduced signal is not). These difficulties might be associated with two main issues: significantly larger peak displacements of the tables and/or major resonance of the shake table with testing facilities or infrastructures. When the filtering procedures do not solve the abovementioned problems, a novel approach could be used to operatively solve the problem. The first step is the detection of the unique frequency range that is associated with the abovementioned problems, if it exists, e.g., typically lower frequencies for higher displacements or facility/infrastructure fundamental frequencies for resonance issues. Once the frequency range is identified, if this is sufficiently reduced, i.e., it does not exceed one-sixth octave interval, the baseline can be generated by assuming a parameter A corresponding to these two one-sixth octave elementary harmonics that is lower than the value assumed for all other harmonics; this value might even be set equal to zero. The spectrum-matching procedure is then carried out considering the modified baseline as an input, and, if the spectrum-compatibility is fully achieved, the output signal could be fully considered to be compliant with the protocol. As a matter of fact, pilot studies carried out by the Author found that this procedure lowers the Fourier transform amplitude corresponding to the critical frequencies (for maximum two one-sixths octave) still enforcing the full spectrum-compatibility. In particular, the matching procedure adds wavelets also corresponding to the two critical one-sixths octave, in order to achieve the compatibility. Lowering the transform amplitudes eases the reproducibility of the signal since the energy content associated with the critical frequencies is lower, even though the signal is fully compliant with the RRS. In particular, the lowering of A should be balanced by an enhancement of the signal reproducibility by the shake table. The value of parameter A to assume depends on the criticality of the reproducibility issues and should be calibrated by iterative signal generation processes and experimental calibrations/tests, at the discretion of the analysts. This exception does not affect the signal severity since the presence of the energy contents related to the critical frequencies is guaranteed (wavelets added by matching procedure) and the spectrum-compatibility is achieved.

Considering the present application and with regard to the facilities of the Laboratory of the University of Naples Federico II (Italy), the maximum displacement limits were assumed to be equal to ±25.0 cm. These limits are likely to be compatible with most shake tables and earthquake simulators [44]. However, the procedure described in the following is generalizable and applicable to different capacity limits. Since displacement time histories typically present peaks due to long-period components of the accelerograms, a low-cut filter can be applied to the signals in order to reduce maximum displacements [87]. The obtained matched record was, then, filtered with a band-pass Butterworth filter, order equal to four, over the range of frequency 0.4 ÷ 40 Hz. This filter is among the most used in literature, as well as it can be considered among the most effective and robust ones for reducing the long-period noise in accelerograms [88]. The need to keep the signal energy content ranging from 1.0 to 32.0 Hz justified the use of a band-pass filter. In particular, the lower cutoff frequency was determined by the need to correct the signal according to the procedure by Boore & Bommer [88] and to keep the energy content from 1 Hz; whereas the higher cutoff frequency was determined considering the frequency limit of the shake table (in this specific case equal to 50 Hz) and the upper limit of the energy content of the signal. The acausal filter was used to not produce any phase distortion in the signal [88]. Moreover, the low-frequency content was eliminated from the test signals records for not exceeding the displacement and velocity capacities of the shake table.

The definite signals should be verified to be spectrum-compatible, and preliminary (empty table) tests should be performed to fully check the experimental reproducibility. In case the conditions associated with

Exceptions apply, the previously proposed procedure can be used to foster the generation of fully reproducible signals.

Acceleration, velocity, and displacement time histories of the test signal before and after the filtering procedure are shown in Figure 5.8. The difference between filtered and unfiltered velocities and accelerations is negligible, while the maximum displacement was reduced to about 200 mm, lower than the table limit, and the mean deviation was zeroed. Figure 5.9 depicts the spectrum-compatibility check performed with respect to the protocol requirements, considering baseline, signal after spectrum-compatibility, and signal after further filtering.

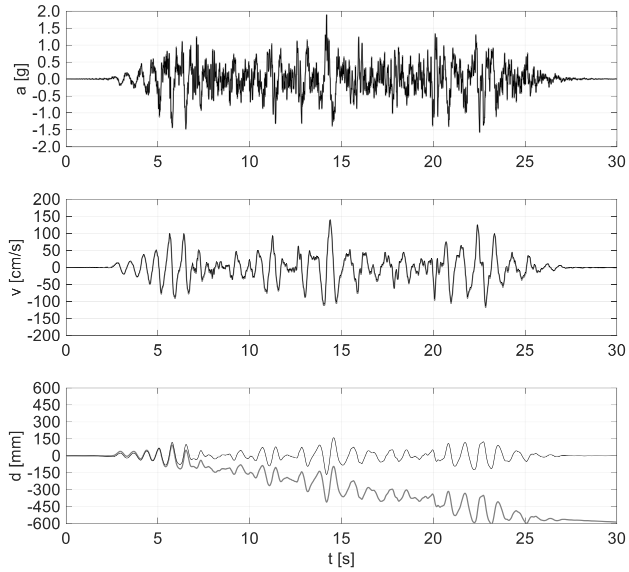

Figure 5.8: Acceleration, velocity, and displacement time histories of the test signal: output by RSPMatch (gray), and output after the filtering procedure (black).

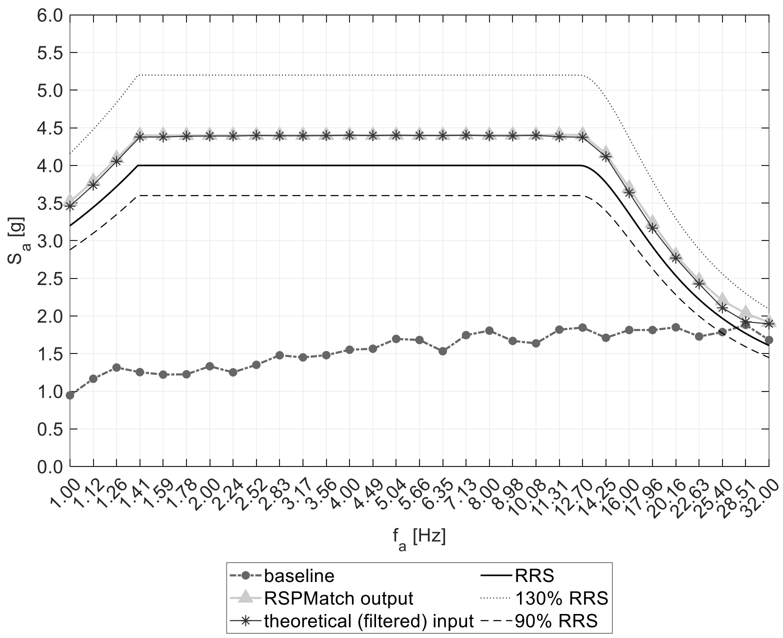

Figure 5.9: Spectrum-compatibility check of the test response spectrum TRS with RRS and RRS limits: TRS of the baseline signal, TRS of the RSPMatch output signal and TRS of the (further) filtered signal.

5.4 Evaluation and validation

5.4.1 Methodology

In this section, the proposed protocol is evaluated and validated considering a set of seven representative performance evaluation test acceleration signals. These signals are referred to as novel protocol (acceleration) signals (NPSs). NPSs are tested through a multi-level criteria approach, which is associated with signal-based assessment.

Time history assessment. Acceleration, velocity, and displacement time histories of NPSs are analyzed, also referring to their spectral response.

Seismic parameter assessment. Representative seismic parameters typically correlated with seismic damage of dynamic systems are computed for NPSs, and they are assessed considering representative real floor motions as a reference, referred to as FMs. In particular, Table 5.2 reports the seismic parameters considered for the analysis, i.e., strong floor motion duration (*SFMD*) [84,89], peak floor velocity to peak floor acceleration ratio (*PFV/PFA*) [53,90], specific energy density (*SED*) [24,91], and predominant period (T_m) [91,92]. These parameters were generally found to be well correlated with both (seismic) damage potential and exhibited damage of structures and NEs, even though they cannot be considered to be exhaustive.

Spectral assessment. Elastic acceleration response spectra of NPSs are assessed considering FMs and alternative protocols as a reference, considering 5% damping. Time history and seismic parameter assessment do not imply the assumption of specific models for the case study acceleration-sensitive elements, whereas the spectral assessment procedure implicitly assumes a linear elastic SDOF response, which is consistent with the case study elements (please, see Section 5.2.1). It should be mentioned that a damage-based evaluation should be carried out and an experimental validation should be performed.to fully validate the protocol for regulation/code implementation purposes. FMs are signals recorded in instrumented US buildings and derived from CESMD database [93]; for each seismic event and building, the most amplified (acceleration) response was selected over the building floors. In particular, reinforced concrete buildings designed/built from 1923 to 1975 are considered as a reference. Two sets of FMs are considered for both seismic parameter and spectral assessment: (set 1 FMs) 24 records related to an equal number of low-, medium-, and high-rise buildings, equally including near and far field ground motions, with PGA ranging in 0.05 to 0.45 g; (set 2 FMs) seven records related to low-, medium-, and high-rise buildings, including both near and far field ground motions, with PGA larger than 0.20 g. Set 2 is included within set 1. Further details on the selected floor motions are omitted as the same FM sets were used in D'Angela et al. [53].

Table 5.2: Definition of SFMD, SED, and T_m. T_D is the total duration of the signal, I_a is the Arias intensity [94], C_i are the Fourier amplitude coefficients, and f_i are the discrete Fast Fourier Transform (FFT) frequencies between 0.25 and 20 Hz.

$\mathbf{SFMD} = \mathbf{t_{95}} - \mathbf{t_5}$	$\mathbf{t_X} = \bar{\mathbf{t}} \mid \mathbf{I_a}(\bar{\mathbf{t}}) = \frac{\mathbf{X}}{\mathbf{100}} \mathbf{I_a}(\mathbf{T_D})$
	$I_a(\bar{t}) = \frac{\pi}{2g} \int_0^{\bar{t}} [a(t)]^2 dt$
$\mathbf{SED} = \int_0^{T_D} [\mathbf{v}(\mathbf{t})]^2 \mathbf{dt}$	
$\mathbf{T_m} = \frac{\sum_i \mathbf{C_i^2}(\mathbf{1}/\mathbf{f_i})}{\sum_i \mathbf{C_i^2}}$	

5.4.2 Results

Figure 5.10a depicts a representative NPS (#1) expressed in terms of acceleration, velocity, and displacement time histories; the other reference NPSs are reported in the Appendix A. The response spectra associated with the developed time histories are shown in Figure 5.10b. NPSs are developed considering PGA equal to 0.40 g and assuming z/h equal to one. Qualitatively, the time histories are not dissimilar to real ground and floor records [53], as well as they are quite similar to the ones developed according to other protocols, such as AC156 ones [17,19,64]. RP, SMP, and DP are quite regular, and several significant peaks are observed in SMP, especially in the first and last part. The time histories have (multiple) significantly high peaks; PFA, peak floor velocity (PFV), and peak floor displacement (PFD) range in 1.45 - 1.88 g, 1.15 – 1.40 m/s, and 0.146 – 0.184 m, with median values equal to 1.76 g, 1.21 m/s, and 0.156 m, and coefficient of variation equal to 0.098, 0.076, and 0.081, respectively. The response spectra are overall relatively smooth, even though a minor (genuine) dispersion can be observed among the different spectra, especially in the amplified frequencies region. The spectrum-compatibility criteria determine spectral ordinates overall slightly larger than RRS ones.

Figure 5.11 depicts the comparison between NPSs and (set 1 and set 2) FMs in terms of (a) SFMD, (b) PFV/PFA, (c) SED, and (d) T_m. The results are reported considering each signal and percentile/median thresholds for NPSs and FMs, respectively. Considering all parameters, NPSs provide values larger (smaller) than median (86^{th} percentile) related to set 1 FM ones, whereas NPS values match very well (are larger than) median values of set 2 FM considering PFV/PFA and T_m (SFMD and SED). A higher parameter value is typically associated with higher damage potential for the investigated parameters. NPSs provide a reduced dispersion, associated with a limited uncertainty and variability due to the signal generation/development process. These findings confirm the reliability of the protocol procedure and prove that the protocol loading histories are potentially associated with relatively high and representative damage severity, according to efficient seismic parameters.

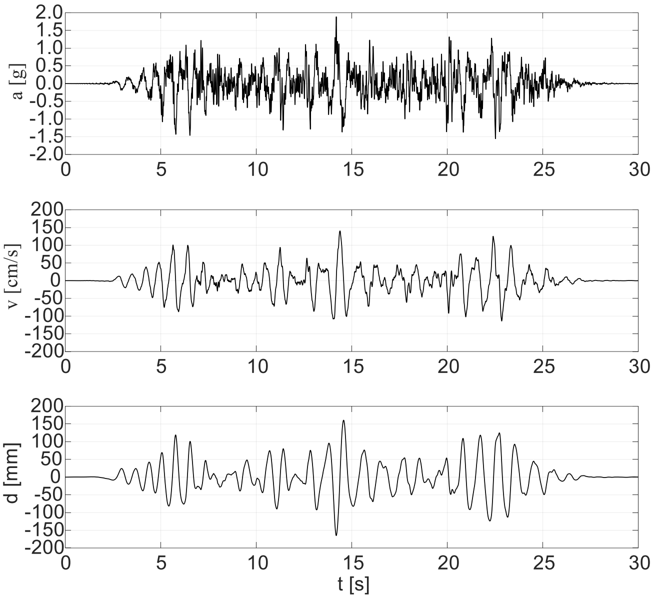

(a)

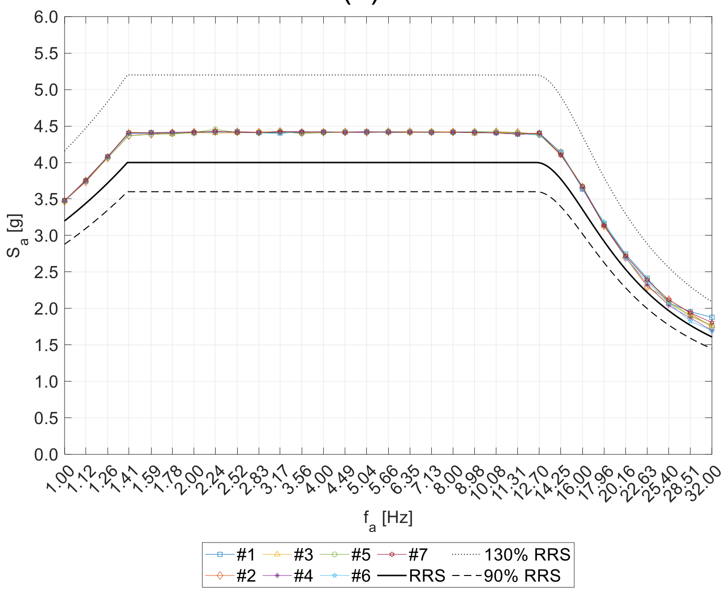

(b)

Figure 5.10: (a) Acceleration, velocity, and displacement time histories related to NPS #1 and (b) response spectra related to reference protocol signals (time histories NPS #2 to #7 are reported in the Appendix A). NPSs are related to RRS having PGA equal to 0.40 g and assuming z/h equal to one.

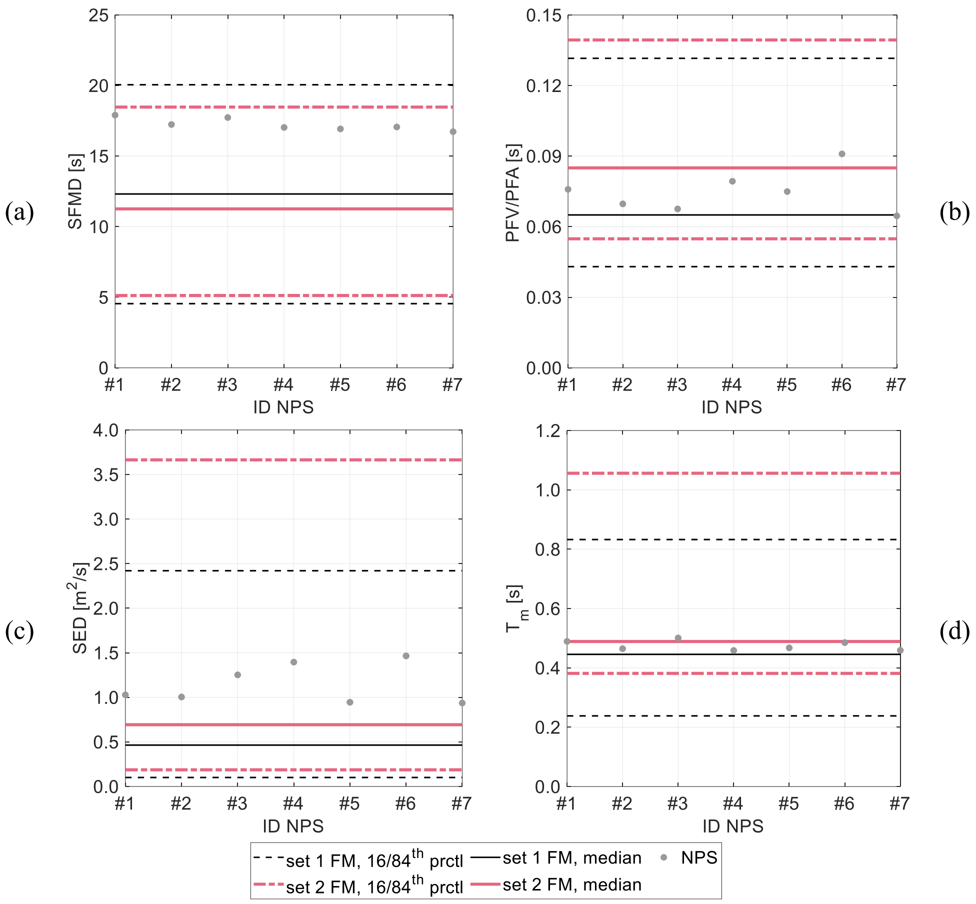

Figure 5.11: Comparison between NPSs and (set 1 and set 2) FMs considering (a) SFMD, (b) PFV/PFA, (c) SED, and (d) T_m.

Figure 5.12 shows the acceleration response spectra of NPSs normalized considering (a) PFA and (b) PGA, compared with (1) set 1 and (2) set 2 FMs, respectively, whereas Figure 5.13 depicts the spectral comparisons among reference protocol inputs, NPSs, and FMs (PGA equal to 0.50 g). Considering the component amplification, i.e., looking at spectral response normalized using PFA, the response spectra related to NPSs envelope very well the median spectrum of set 1 FMs (Figure 5.12a1); moreover, they also envelope the 84th percentile spectrum except for few peak responses, associated with 1.59 to 4 Hz. However, enveloping 84th percentile would certainly be too conservative, as the median spectral response (over seven spectra) is typically considered as reliable for (structural assessment) spectrum-compatibility (e.g., [3]). Therefore, NPSs are conservative but not in an excessive manner, accounting for a wide and representative range of low-to-high seismicity hazard, building, site, soil type scenarios. Regarding set 2 FMs, median FM spectra exceed NPS spectra only in the narrow vicinity of 3 Hz, even though with a magnitude not larger than 20% (Figure 5.12a2); in other frequency ranges, NPS spectra are significantly higher than median FM ones. However, it is to be noted that unscaled (natural) set 2 FMs are associated with an average PGA equal to 0.32 g, which is consistent with high-to-very high seismicity in Europe. Set 2 FM PGA is 88% higher than the value associated with set 1 FMs. Furthermore, unscaled (natural) set 2

FM also present PGV, PFA and PFV 120%, 76% and 100% larger than related values of set 1 FMs. For further details regarding set 1 and set 2 FMs, please, refer to [53].

Considering both building and component amplification, i.e., looking at spectral response normalized considering PGA, NPS spectra present ordinates significantly higher than both set 1 (Figure 5.12b1) and set 2 (Figure 5.12b2) FMs, whereas FM 84th percentiles slightly exceed and exceed NPS spectra in the narrow vicinity of 3 Hz considering set 1 and set 2 FM, respectively. Further comments on the conservativity associated with 84th percentiles of FMs are omitted as this was previously discussed.

The safe compatibility between NPSs and FM stresses the reliability of the developed protocol also with regard to seismic and building scenarios considered to develop the seismic demand associated with RRS. Moreover, this evidence proves the generality and wide applicability of the developed protocol. Extensive comparisons between RRS of NPSs and alternative reference protocols were reported in the previous sections. However, as an additional evaluation and validation means, reference protocol spectra (RRS and input spectra) are compared with NPS spectra and FMs in Figure 5.13a and 13b, respectively.

GR-63-CORE RRS is not reported as this is defined for 2% damping (and all other spectra, including NPS ones refer to 5% damping). The spectra are reported considering PGA equal to 0.50 g since this allows assessing both building and component amplification response. Reference protocols provide spectral ordinates significantly lower than NPS ones (Figure 5.13a) and, in some cases, lower than set 1 and set 2 FM median responses. This points out the superiority of the developed RRS and NPSs, and, overall, of the developed protocol.

5.5 Discussion

A protocol is developed for seismic assessment and qualification purposes through shake table testing. The protocol development is based on the synthesis among (a) technical critical evaluation of reference existing protocols, (b) recent advances in the field, also accounting for latest literature studies and testing applications, and (c) expertise and experience gained in the field by the research team.

Novel testing approaches are developed towards seismic assessment and qualification performed following performance-based earthquake engineering (PBEE). Technical criteria are developed for defining a robust qualification protocol. This protocol is demonstrated to provide more reliable testing procedures, promisingly associated with more robust assessment and qualification outcomes.

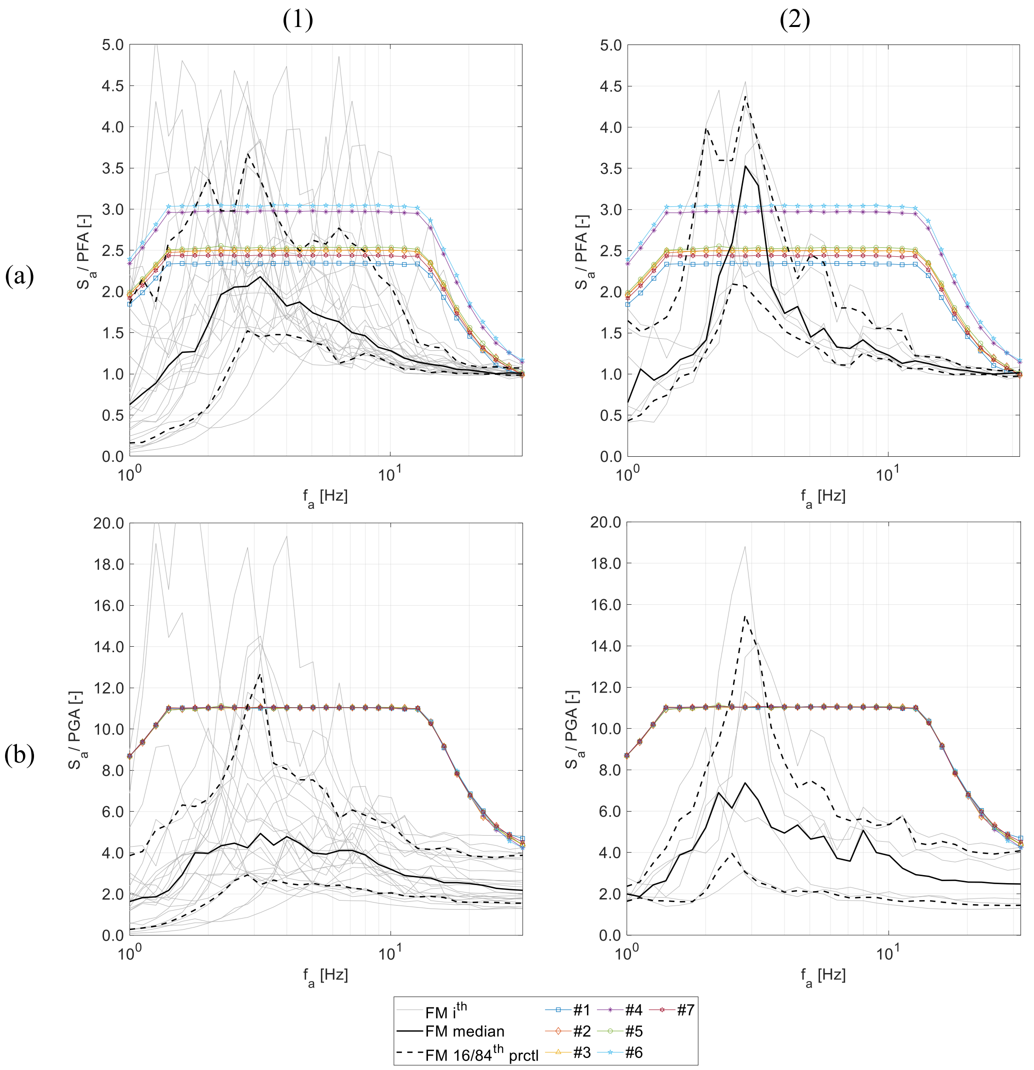

Figure 5.12: Acceleration response spectra of NPSs normalized considering (a) PFA and (b) PGA, compared with (1) set 1 and (2) set 2 FMs. All spectra are related to 5% damping.

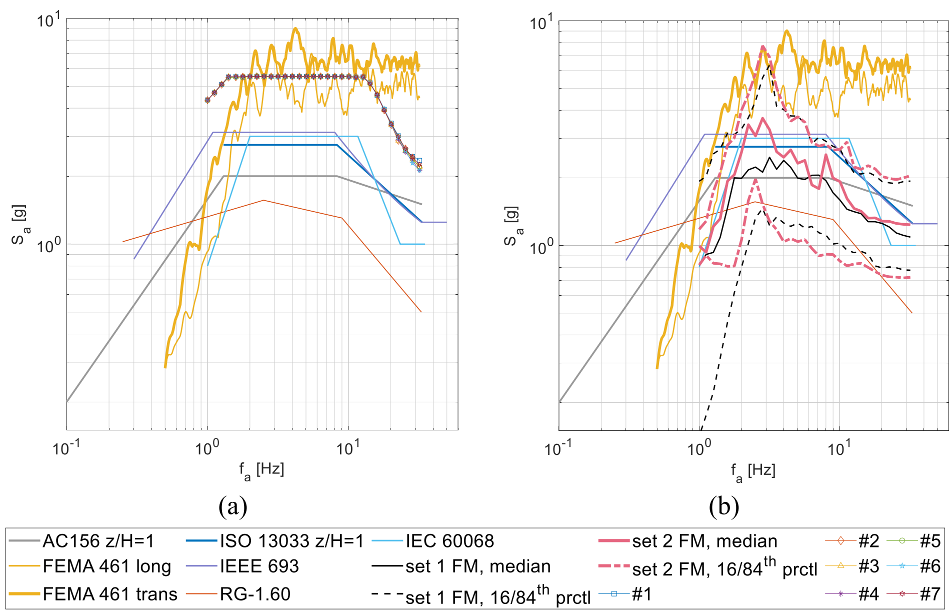

Figure 5.13: Comparison between RRS/input response spectra related to reference protocols and (a) NPS spectra and (b) FM spectra, considering PGA equal to 0.50 g. All spectra are related to 5% damping.

The most significant and substantial feature of the protocol is associated with a consistent code-compliant definition of the loading histories to perform seismic evaluation tests. This definition follows the extension of a recently developed seismic demand formulation, which is compliant with reliable estimations and proven reliability. In particular, this formulation is implemented considering an innovative approach, which accounts for a wide variability of building periods. The most critical part of the seismic signal development is associated with the analysis and processing procedures, which are carried out through consolidated methodologies, which are clearly described and discussed in the chapter, also providing technical and detailed guidance for implementation.

5.6 References

[1] Javadinasab Hormozabad, S., Gutierrez Soto, M., & Adeli, H. (2021). Integrating structural control, health monitoring, and energy harvesting for smart cities. Expert Systems, 38(8).

[2] ASCE 7-16. (2016). Minimum Design Loads and Associated Criteria for Buildings and Other Structures. Minimum Design Loads and Associated Criteria for Buildings and Other Structures, American Society of Civil Engineers (ASCE), 1–889.

[3] Comité Européen de Normalisation (CEN). (2005). Eurocode 8: Design of structures for earthquake resistance. British Standards Institution.

[4] National Research Council of Canada (NRCC). (2015). National Building Code of Canada, vol. 1.

[5] Instituto Nacional de Normalización (INN). (2015). NCh3357: Seismic design of non-structural components and systems (in Spanish).

[6] Ministero delle Infrastrutture e dei Trasporti (MIT). (2018). Aggiornamento delle Norme tecniche per le costruzioni Decreto 17 gennaio 2018, 23–35 (in Italian).

[7] New Zealand Standard (NZS). (2009). Seismic performance of engineering systems in buildings. NZS 4219:2009, 1–114.

[8] Universitatea Tehnica de Constructii Bucuresti (UTCB). (2013). Cod de proiectare seismică. partea i – prevederi de proiectare pentru clădiri. P100-1. Bucharest, Romania (in Romanian).

[9] Amezquita-Sanchez, J. P., H. S. Park, & Adeli, H. (2017). A novel methodology for modal parameters identification of large smart structures using MUSIC, empirical wavelet transform, and Hilbert transform. Engineering Structures, 147: 148–159.

[10] Perez-Ramirez, C. A., J. P. Amezquita-Sanchez, H. Adeli, M. Valtierra-Rodriguez, D. Camarena-Martinez, & R. J. Romero-Troncoso. (2016). New methodology for modal parameters identification of smart civil structures using ambient vibrations and synchrosqueezed wavelet transform. Engineering Applications of Artificial Intelligence, 48: 1–12.

[11] British Standards Institution (BSI). (2013). Bases for design of structures-Loads, forces and other actions-Seismic actions on nonstructural components for building applications. (British Standard Institution, ed.), Switzerland, 1–54.
[12] IEEE Power & Energy Society (IEEE PES). (2013). Standard for Seismic Qualification of Equipment for Nuclear Power Generating Stations - IEEE 344. IEEE Std 344-2013 (Revision of IEEE Std 344-2004), Park Avenue, New York, NY 10016-5997, USA.
[13] Bianchi, S., Ciurlanti, J., Perrone, D., Filiatrault, A., Costa, A. C., Candeias, P. X., Correia, A. A., & Pampanin, S. (2021). Shake-table tests of innovative drift sensitive nonstructural elements in a low-damage structural system. Earthquake Engineering & Structural Dynamics, 50(9), 2398-2420.
[14] Filiatrault A, K. S. T. R. (2004). Shake table testing of bookcase – partition wall systems. Canadian Journal of Civil Engineering, 31(4).
[15] Ghith, A., Ezzeldin, M., Tait, M., & El-Dakhakhni, W. (2019). Shake Table Seismic Performance Assessment of Auxiliary Battery Power Systems Using the FEMA 461 Protocol. Journal of Structural Engineering, 145(8), 04019080.
[16] Jun, S. C., Lee, C. H., Bae, C. J., & Lee, K. J. (2020). Shake-Table Seismic Performance Evaluation of Direct- and Indirect-Hung Suspended Ceiling Systems. Journal of Earthquake Engineering.
[17] Kim, H. J., & Shin, D. H. (2021). Shake table test program of cold-formed steel in-plane partition walls. Structures, 30, 503–517.
[18] Lee, S. M., & Jung, W. Y. (2020). Evaluation of anchorage performance of the switchboard cabinet under seismic loading condition. Advances in Mechanical Engineering, 12(5).
[19] Luo, Z., Xue, J., Zhou, T., Qi, L., & Zhao, X. (2021). Shaking table tests and seismic design suggestions for innovative suspended ceiling systems with detachable metal panels. Engineering Structures, 232.
[20] Magliulo, G., Petrone, C., Capozzi, V., Maddaloni, G., Lopez, P., & Manfredi, G. (2014). Seismic performance evaluation of plasterboard partitions via shake table tests. Bulletin of Earthquake Engineering, 12(4), 1657–1677.
[21] Qi, L., Kurata, M., Ikeda, Y., Kunitomo, K., & Takaoka, M. (2021). Seismic evaluation of two-elevation ceiling system by shake table tests. Earthquake Engineering & Structural Dynamics, 50(4), 1147–1166.
[22] Tian, Y., Filiatrault, A., & Mosqueda, G. (2015). Seismic response of pressurized fire sprinkler piping systems I:

Experimental study. Journal of Earthquake Engineering, 19(4), 649–673.
[23] Zhou, T., Wang, X., Liu, W., Zhang, Z., Ma, B., & Tan, W. (2021). Shaking table tests on seismic response of discontinuous suspended ceilings. Journal of Building Engineering, 43, 102916.
[24] Cao, V. van, & Ronagh, H. R. (2014). Correlation between seismic parameters of far-fault motions and damage indices of low-rise reinforced concrete frames. Soil Dynamics & Earthquake Engineering, 66.
[25] Li, Y., Conte, J. P., & Barbato, M. (2016). Influence of time-varying frequency content in earthquake ground motions on seismic response of linear elastic systems. Earthquake Engineering & Structural Dynamics, 45(8), 1271–1291.
[26] Zhou, Z., & Adeli, H. (2003a). Wavelet energy spectrum for timefrequency localization of earthquake energy. International Journal of Imaging Systems & Technology, 13(2), 133–140.
[27] ICC-ES. (2012). AC156 Acceptance criteria for seismic certification by shake-table testing of nonstructural components.
[28] FEMA 461. (2007). Interim Testing Protocols for Determining the Seismic Performance Characteristics of Structural and Nonstructural Components.
[29] Telcordia Technologies (2006). NEBS Requirements: Physical Protection. Telcordia Technologies Generic Requirements, GR-63-CORE. Piscataway, NJ 08854-41821.866.672.6997 (USA).
[30] Perrone, D., Brunesi, E., Dacarro, F., Peloso, S., & Filiatrault, A. (2019). Seismic Performance of Non-Structural Elements Seismic Assessment and Qualification of Non-structural Elements in Europe: a Critical Review. SPONSE 2019 Conference.
[31] Anajafi, H., & Medina, R. A. (2018). Evaluation of ASCE 7 equations for designing acceleration-sensitive nonstructural components using data from instrumented buildings. Earthquake Engineering & Structural Dynamics, 47(4), 1075–1094.
[32] D'Angela, D., Magliulo, G., & Cosenza, E. (2021a). Incremental Dynamic Analysis of Rigid Blocks Subjected to Ground and Floor Motions and Shake Table Protocol Inputs. Bulletin of the New Zealand Society for Earthquake Engineering, 55.
[33] Zhou, Z., & Adeli, H. (2003b). Time-Frequency Signal Analysis of Earthquake Records Using Mexican Hat Wavelets. Computer-Aided Civil & Infrastructure Engineering, 18 (5): 379–389.
[34] Amiri, G. G., Abdolahi Rad, A., Aghajari, S., & Khanmohamadi Hazaveh, N. (2012). Generation of Near-Field Artificial Ground Motions Compatible with Median-Predicted Spectra Using PSO-Based Neural Network and Wavelet Analysis.

Computer-Aided Civil & Infrastructure Engineering, 27(9), 711–730.
[35] Hancock, J., Watson-Lamprey, J., Abrahamson, N. A., Bommer, J. J., Markatis, A., McCoy, E. M. M. A., & Mendis, R. (2006). An improved method of matching response spectra of recorded earthquake ground motion using wavelets. Journal of Earthquake Engineering, 10, 67–89.
[36] Akkar, S., & J. J. Bommer. (2007). Prediction of elastic displacement response spectra in Europe and the Middle East. Earthquake Engineering & Structural Dynamics, 36 (10): 1275–1301.
[37] Merino, R. J., Perrone, D., & Filiatrault, A. (2020). Consistent floor response spectra for performance-based seismic design of nonstructural elements. Earthquake Engineering & Structural Dynamics, 49 (3): 261–284. John Wiley and Sons Ltd.
[38] Petrone, C., Magliulo, G., & Manfredi, G. (2015). Seismic demand on light acceleration-sensitive nonstructural components in European reinforced concrete buildings. Earthquake Engineering & Structural Dynamics, 44(8), 1203–1217.
[39] IEEE Power & Energy Society (IEEE PES). (2018). IEEE Recommended Practice for Seismic Design of Substations. IEEE 693-2018, Park Avenue, New York, NY 10016-5997, USA.
[40] U.S. Nuclear Regulatory Commission (NRC). (2014). Regulatory Guide 1.60: design response spectra for seismic design of nuclear power plants. U.S., 1–13.
[41] International Electrotechnical Commission (IEC). (2013). Environmental testing - Part 2-57: Tests - Test Ff: Vibration - Time-history and sine-beat method. Geneva, Switzerland, 1–43.
[42] International Electrotechnical Commission (IEC). (2019). Environmental testing - Part 3-3: Supporting documentation and guidance - Seismic test methods for equipment. Geneva, Switzerland.
[43] Lu, Y., Mosqueda, G., Han, Q., & Zhao, Y. (2018). Shaking Table Tests Examining Seismic Response of Suspended Ceilings Attached to Large-Span Spatial Structures. Journal of Structural Engineering, 144(9), 04018152.
[44] Takhirov, S. M., Fujisaki, E., Power, B., Vancouver, A., Riley, W. M., & Low, B. (2017). PEER Report No. 2017/10 Development of Time Histories for IEEE693 Testing and Analysis (Including Seismically Isolated Equipment). University of California, Berkeley.
[45] Luise, M., & Vitetta, G. M. (2009). Teoria dei segnali. (McGraw-Hill, ed.), Paolo Roncoroni, Milano (in Italian).
[46] Takhirov, S. M., Fenves, G. L., Fujisaki, E., & Clyde, D. (2004). PEER Report No. 2004/07 Ground Motions for Earthquake

Simulator Qualification of Electrical Substation Equipment. University of California, Berkeley.
[47] Blasi, G., Perrone, D., Aiello, M. A., & Pecce, M. R. (2021). Seismic performance assessment of piping systems in bare and infilled RC buildings. Soil Dynamics & Earthquake Engineering, 149.
[48] Singh, S., & Gupta, A. (2021). Seismic response of electrical equipment subjected to high–frequency ground motions. Nuclear Engineering & Design, 374.
[49] Chichino, B., Peloso, S., Bolognini, D., Moroni, C., Perrone, D., & Brunesi, E. (2021). Towards Seismic Design of Nonstructural Elements: Italian Code-Compliant Acceleration Floor Response Spectra. Advances in Civil Engineering, 2021, 1–18.
[50] D’Angela, D., Magliulo, G., & Cosenza, E. (2021b). Towards a reliable seismic assessment of rocking components. Engineering Structures, 230.
[51] Di Domenico, M., Ricci, P., & Verderame, G. M. (2021). Floor spectra for bare and infilled reinforced concrete frames designed according to Eurocodes. Earthquake Engineering & Structural Dynamics, 50(13), 3577-3601.
[52] Salari, N., D. Konstantinidis, V. Mohsenzadeh, & L. Wiebe. (2022). Demands on acceleration-sensitive nonstructural components in special concentrically braced frame and special moment frame buildings. Engineering Structures, 260: 114031.
[53] D’Angela, D., Magliulo, G., & Cosenza, E. (2021c). Seismic damage assessment of unanchored nonstructural components taking into account the building response. Structural Safety, 93.
[54] Pürgstaller, A., P. Quintana Gallo, S. Pampanin, & K. Bergmeister. (2020). Seismic demands on nonstructural components anchored to concrete accounting for structure-fastener-nonstructural interaction (SFNI). Earthquake Engineering & Structural Dynamics, 49 (6): 589–606.
[55] Crewe, A. J. (2012). Generation of Improved Artificial Earthquakes For Seismic Qualification Testing. 15 WCEE, Lisboa, 1–10.
[56] Zaghi, A. E., Maragakis, E. M., Itani, A., & Goodwin, E. (2012). Experimental and analytical studies of hospital piping assemblies subjected to seismic loading. Earthquake Spectra, 28(1), 367–384.
[57] Tran, T. T., Salman, K., & Kim, D. (2021). Distributed plasticity approach for nonlinear analysis of nuclear power plant equipment: Experimental and numerical studies. Nuclear Engineering & Technology, 33(9), 3100-3111.
[58] Gasparini, D. A., & Vanmarcke, E. H. (1976). Simqke: A program for artificial motion generation. User’s manual and documentation. Cambridge, Massachusetts.

[59] Magliulo, G., Pentangelo, V., Maddaloni, G., Capozzi, V., Petrone, C., Lopez, P., Talamonti, R., & Manfredi, G. (2012). Shake table tests for seismic assessment of suspended continuous ceilings. Bulletin of Earthquake Engineering, 10(6), 1819–1832.
[60] Di Sarno, L., Magliulo, G., D'Angela, D., & Cosenza, E. (2019). Experimental assessment of the seismic performance of hospital cabinets using shake table testing. Earthquake Engineering & Structural Dynamics, 48(1), 103–123.
[61] Yazdani, A., & Takada, T. (2009). Wavelet-Based Generation of Energy- and Spectrum-Compatible Earthquake Time Histories. Computer-Aided Civil & Infrastructure Engineering, 24(8), 623–630.
[62] Amiri, G. G., Rad, A. A., & Hazaveh, N. K. (2014). Wavelet-Based Method for Generating Nonstationary Artificial Pulse-Like Near-Fault Ground Motions. Computer-Aided Civil & Infrastructure Engineering, 29(10), 758–770.
[63] Jeon, B. G., Son, H. Y., Eem, S. H., Choi, I. K., & Ju, B. S. (2021). Dynamic characteristics of single door electrical cabinet under rocking: Source reconciliation of experimental and numerical findings. Nuclear Engineering & Technology, Korean Nuclear Society.
[64] Petrone, C., Magliulo, G., & Manfredi, G. (2017). Shake table tests on standard and innovative temporary partition walls. Earthquake Engineering & Structural Dynamics, 46(10), 1599–1624.
[65] Maddaloni, G., Ryu, K. P., & Reinhorn, A. M. (2011). Simulation of floor response spectra in shake table experiments. Earthquake Engineering & Structural Dynamics, 40(6), 591-604.
[66] Cosenza, E., Di Sarno, L., Maddaloni, G., Magliulo, G., Petrone, C., & Prota, A. (2015). Shake table tests for the seismic fragility evaluation of hospital rooms. Earthquake Engineering & Structural Dynamics, 44(1), 23–40.
[67] Fiorino, L., Bucciero, B., & Landolfo, R. (2019). Evaluation of seismic dynamic behaviour of drywall partitions, façades and ceilings through shake table testing. Engineering Structures, 180, 103–123.
[68] Lin, F. R., Chai, J. F., Lai, Z. Y., Chou, P. F., & Wu, Y. C. (2014). Experimental study for seismic demands on in-cabinet equipment in NPPs. Journal of the Chinese Institute of Engineers, Transactions of the Chinese Institute of Engineers, Series A, 37(7), 833–844.
[69] Son, H., Park, S., Jeon, B. G., Jung, W. Y., Choi, J., & Ju, B. S. (2020). Seismic qualification of electrical cabinet using high-fidelity simulation under high frequency earthquakes. Sustainability (Switzerland), 12(19), 1–14.

[70] Porter, K. (2020). A Beginner's Guide to Fragility, Vulnerability, and Risk. Denver CO USA.
[71] Huang, B., Günay, S., & Lu, W. (2021). Seismic Assessment of Freestanding Ceramic Vase with Shaking Table Testing and Performance-Based Earthquake Engineering. Journal of Earthquake Engineering, 1–23.
[72] Prota, A., Zito, M., D'Angela, D., Toscano, G., Ceraldi, C., Fiorillo, A., & Magliulo, G. (2022). Preliminary Results of Shake Table Tests of a Typical Museum Display Case Containing an Art Object. Advances in Civil Engineering, 2022, 1–18.
[73] Wittich, C., & Hutchinson, T. (2014). Development Of A Rocking-Period Centered Protocol For Shake Table Testing Of Unattached Stiff Components. Tenth U.S. National Conference on Earthquake Engineering. Frontiers of Earthquake Engineering, Anchorage, Alaska.
[74] Petrone, C., Magliulo, G., & Manfredi, G. (2016). Floor response spectra in RC frame structures designed according to Eurocode 8. Bulletin of Earthquake Engineering, 14(3), 747–767.
[75] Taghavi S. & Miranda E. (2003). Response Assessment of Nonstructural Building Elements - PEER 2003/05.
[76] FEMA E-74. (2012). Reducing the Risks of Nonstructural Earthquake Damage-A Practical Guide.
[77] Di Sarno, L., Petrone, C., Magliulo, G., & Manfredi, G. (2015). Dynamic properties of typical consultation room medical components. Engineering Structures, 100, 442–454.
[78] Clough, Ray W, & Joseph Penzien. (2003). Dynamics of Structures. Berkeley, CA, USA: Computers & Structures, Inc.
[79] NIST GCR 18-917-43. (2018). Recommendations for improved seismic design and installation of nonstructural components. Redwood, CA: Applied Technology Council.
[80] Johnson, T. P., & R. K. Dowell. (2017). Evaluation of the overstrength factor for nonstructural component anchorage into concrete via dynamic shaking table tests. Journal of Building Engineering, 11: 205–215.
[81] Kazantzi, A. K., E. Miranda, & D. Vamvatsikos. (2020). Strength-reduction factors for the design of light nonstructural elements in buildings. Earthquake Engineering & Structural Dynamics, 49 (13): 1329–1343.
[82] Ministero delle Infrastrutture e dei Trasporti (MIT). (2019). Istruzioni per l'applicazione dell'«Aggiornamento delle Norme tecniche per le costruzioni» di cui al decreto ministeriale 17 gennaio 2018, 23–35 (in Italian).
[83] Housner, G. W., Martel, R. R., & Alford, J. L. (1953). Spectrum analysis of strong-motion earthquakes. Bulletin of the Seismological Society of America, 43(2), 97–119.

[84] Rodriguez, D., Perrone, D., Filiatrault, A., & Brunesi, E. (2021). A probabilistic strong floor motion duration model for seismic performance assessment of non-structural building elements. Earthquake Engineering & Structural Dynamics, 50(15), 4161-4179.
[85] Bendat, J. S., & Piersol, A. G. (2010). Random Data: Analysis and Measurement Procedures. Fourth Edition, Wiley, ed. 1-600.
[86] Suárez, L. E., & Montejo, L. A. (2005). Generation of artificial earthquakes via the wavelet transform. International Journal of Solids & Structures, 42(21–22), 5905–5919.
[87] Trifunac, M. D. (1971). Zero baseline correction of strong-motion accelerograms. Bulletin of the Seismological Society of America, 61(5).
[88] Boore, D. M., & Bommer, J. J. (2005). Processing of strong-motion accelerograms: Needs, options and consequences. Soil Dynamics & Earthquake Engineering, 25(2), 93–115.
[89] Trifunac, M. D., & Brady, A. G. (1975). A study on the duration of strong earthquake ground motion. Bulletin of the Seismological Society of America, 65(3), 581–626.
[90] Kramer, S. L. (1996). Geotechnical earthquake engineering. (Prentice Hall, ed.), New Jersey.
[91] Nguyen, D.-D., Thusa, B., Han, T.-S., & Lee, T.-H. (2020). Identifying significant earthquake intensity measures for evaluating seismic damage and fragility of nuclear power plant structures. Nuclear Engineering & Technology, 52(1), 192-205.
[92] Rathje, E. M., Faraj, F., Russell, S., & Bray, J. D. (2004). Empirical Relationships for Frequency Content Parameters of Earthquake Ground Motions. Earthquake Spectra, 20(1), 119–144.
[93] Partner Data Centers & Networks. (2017). Center for Engineering Strong Motion Data (CESMD). https://www.strongmotioncenter.org/
[94] Arias, A. (1970). A measure of earthquake intensity in Seismic Design of Nuclear Power Plants. (R. J. Hansen, ed.), Massachusetts Inst. of Tech., Cambridge. Univ. of Chile, Santiago de Chile.

Chapter 6

6 Reliability of existing shake table protocols for seismic assessment and qualification of acceleration-sensitive systems and estimation of reliability-targeted capacity safety factors

Nonstructural elements (NEs) are typically associated with major seismic risk, as several post-event surveys and literature studies highlighted in the last few decades. NE seismic risk is often expressed in terms of critical functioning disruption, economic losses, and casualties, and this might be significant even in the case of low seismicity sites. In particular, seismic risk can be more critical for NEs than for structural parts, especially frequent seismic events. Shake table testing represents the most reliable method for seismic assessment and qualification of NEs that are sensitive to accelerations (i.e., acceleration-sensitive NEs). However, several protocols and testing inputs were defined in literature and codes but none of them has been assessed in terms of seismic scenario representativity and reliability.

The present chapter reports the methodology and the results of an extensive investigation into the seismic assessment and qualification of NEs through experimental methods and shake table testing. Existing reference shake table protocols defined by regulations/codes are assessed in terms of seismic damage potential/severity, modeling NEs modeled as inelastic single degree of freedom (SDOF) systems. The reliability index associated with the investigated protocols is considered as an evaluation parameter. The operative outcome of the chapter is associated with the accurate estimation of the reliability index of the reference protocols and with the development of applicative safety coefficients towards a reliability-targeted assessment of nonstructural elements. Novel perspectives for developing more reliable shake table protocols and seismic inputs are traced in the light of the preliminary results.

6.1 Introduction

NEs are generally particularly sensitive to seismic actions and may exhibit a critical behavior also under relatively low intensity earthquakes [1-3], especially if they were not designed at all or with regard to seismic actions. NE seismic behavior typically affects facility functioning and can be associated with significant economic losses; moreover, damage of NEs might even cause human losses. Therefore, the seismic assessment of NEs is an issue of paramount importance, especially regarding NEs that are housed within critical facilities [1,4].

The seismic capacity and performance of NEs can be generally assessed by means of analytical, numerical, experimental, observational, and mixed methods. NEs that are critical in terms of their functioning and stability with regard to seismic actions, such as fire sprinkler systems [5] or medical equipment [6], should be preferably assessed via experimental methods (e.g., [7]), and quasi-static and shake table testing are generally considered to be optimal for assessing displacement-sensitive and acceleration-sensitive NEs, respectively (e.g., [8]). Generally, NEs are typically sensitive to both displacements and accelerations, and shake table testing can be reasonably considered to be the best option if the testing setup is able to reproduce realistic NE installation arrangements.

In order to supply robust and representative results, shake table tests are often performed considering seismic inputs compliant with reference testing protocol; this is strictly required when seismic qualification or certification are carried out. As a matter of fact, the seismic response of NEs is strongly conditioned by the record characteristics, and shake table protocol are supposed to provide seismic inputs associated with relatively severe and representative responses. AC156 [9] and FEMA 461 [8] protocols represent the state of the art for seismic assessment and qualification/certification of acceleration-sensitive elements. Other protocols exist but are meant to be used to assess/qualify specific components and equipment, e.g., power substation equipment [10] or telecommunication equipment [11]. However, the level of reliability of existing protocols is not reported or discussed by the protocols, as well as this issue was not systematically addressed in the literature, except for a very few studies, that focused on peculiar applications (e.g., [12,13]).

The present chapter reports the results of an extensive research project aiming at evaluating the current approaches and methods for seismic assessment and qualification of NEs. The reliability of AC156 [9], FEMA 461 [8], IEEE 693 [10] and Zito et al. [14] protocols is assessed with regard to the seismic severity in terms of damage potential of NEs. Elements that can be modeled by SDOF systems are considered as a case study; these elements correspond to most studied and common acceleration-sensitive elements (e.g., [15,16]). Incremental dynamic analyses (IDAs) are performed to assess the seismic response and damage of several case study models. The reliability index associated with the investigated protocols is estimated considering real floor motions as a reference, according to a recently developed methodology [13]. By evaluating the reliability index of the reference protocols and comparing them with target indexed (assessed in the study), safety factors associated with investigated protocols, models, and DS are provided. These coefficients are aimed at reducing the seismic capacity estimated through the application of the reference protocols (shake table testing) by enforcing a target reliability, based on robust assumptions. Novel perspectives for more reliable seismic assessment of acceleration-sensitive are traced, according to the reliability assessment results.

6.2 Methodology

6.2.1 Outline

The methodology flowchart is depicted Figure 6.1 and described in the following. Reference shake table protocols (STPs) were selected within current regulations/codes and relevant literature studies (Section 6.2.2); acceleration loading histories were defined considering both reference STPs (input generation and processing) and real records (input selection and processing) (Section 6.2.3). Case study NEs were defined favoring representativeness and generalizability (Section 6.2.4), advanced numerical modeling was implemented, performing IDAs (Section 6.2.5). Engineering demand parameters (EDPs) and relevant damage states (DSs) were defined (Section 6.2.6), and both damage (fragility) and reliability assessment were performed considering a newly defined perspective and according to literature methods (Section 6.2.7). Finally, reliability-targeted safety factors were estimated according to a newly proposed method, favoring the applicative optimization (Section 6.2.8).

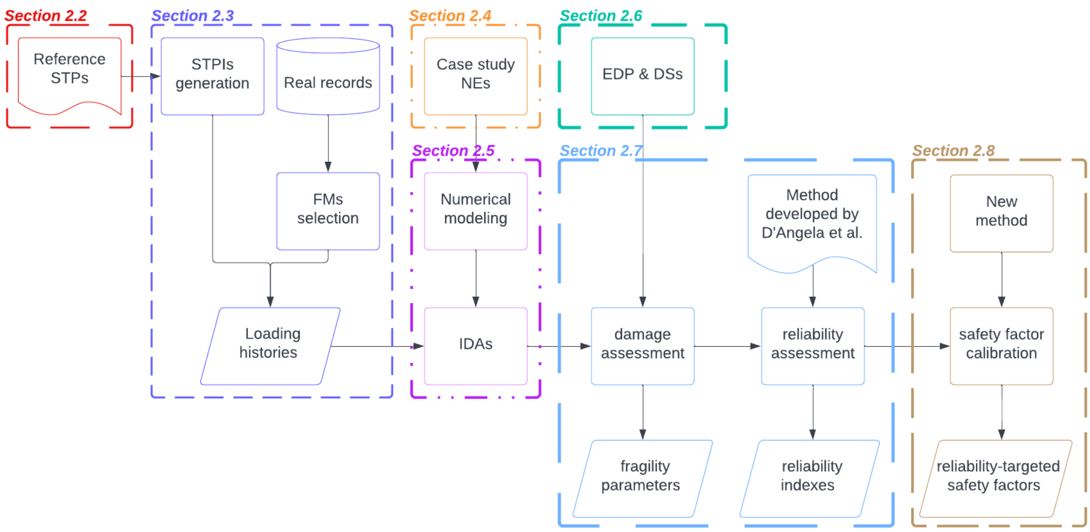

Figure 6.1: Methodology flowchart.

6.2.2 Reference shake table protocols (STPs)

Shake table protocols (STPs) investigated in this chapter are AC156 [9], AC156w/o, FEMA 461 [8], IEEE 693 [10], Zito et al. [14]; AC156w/o protocol is a modified version of AC156, developed in this study and described in the following. AC156 protocol establishes the rules and criteria for seismic certification of NEs that have fundamental frequencies larger than 1.3 Hz. This protocol is considered as the international reference for seismic certification of NEs, in compliance with International Building Code [17] and ASCE 7 [7]. Two categories of tests are defined in the protocol, i.e., resonant frequency search and seismic simulation tests. The former tests are aimed at determining the resonant frequencies and damping of the test specimen, whereas the latter tests allow the assessment of the seismic capacity of the specimen, essential for the seismic certification. The input signal for the seismic simulation tests consists of nonstationary broadband random excitations having energy content ranging from 1.3 to 33.3 Hz and a bandwidth resolution equal to one-third for analog systems and one-sixth octave for digital ones. The input duration shall contain at least 20 seconds of strong motion. The input signal shall be compatible, in terms of test response spectrum (TRS), with a required response spectrum (RRS) according to strict criteria. AC156 RRS is compliant with the design horizontal force provided by ASCE 7 [7], and this is defined by two acceleration thresholds: A_{FLX}, i.e., plateau spectral ordinate over 1.3 to 8.3 Hz, and (b) A_{RIG}, i.e., spectral ordinate at 33.3 Hz; RRS is log linear between 8.3 and 33.3 Hz. RRS is also defined for frequencies lower than 1.3 Hz, but this is not to be considered for spectral compatibility analysis. RRS is defined for horizontal and vertical directions according to the formulations provided for {A_{FLX-H}, A_{RIG-H}} and {A_{FLX-V}, A_{RIG-V}}, respectively. The key parameters for determining RRS are S_{DS}, i.e., design spectral response acceleration parameter at short periods, and z/h, i.e., ratio between the height location of NE (z) and the building height (h).

AC156 protocol assumes an upper bound limit for A_{FLX-H}, equal to $1.6\ S_{DS}$. AC156 RRS with and without limitation is show in Figure 6.2a. This limitation was derived from the provisions for the evaluation of the seismic demand force on NEs [7]. A_{FLX-H} reduction associated with this limitation increases linearly from z/h equal to 0.3 (null reduction) to z/h equal to one (47% reduction), as observed in the Figure 6.2b. This limitation might significantly affect the severity of the compliant seismic input and might even result in unsafe capacity estimations, as recent studies pointed out [13,18-20], e.g., Petrone et al. [19] proved that such a limitation generates RRS that might underestimate the floor response spectra related to a representative set of generic frame structures. Accordingly, a modified version of AC156 protocol, namely AC156w/o, was considered in this section. In particular, AC156w/o RRS coincides with AC156 RRS without applying the abovementioned limitation to A_{FLX-H}, and AC156w/o signal generation procedure is the same implemented for AC156.

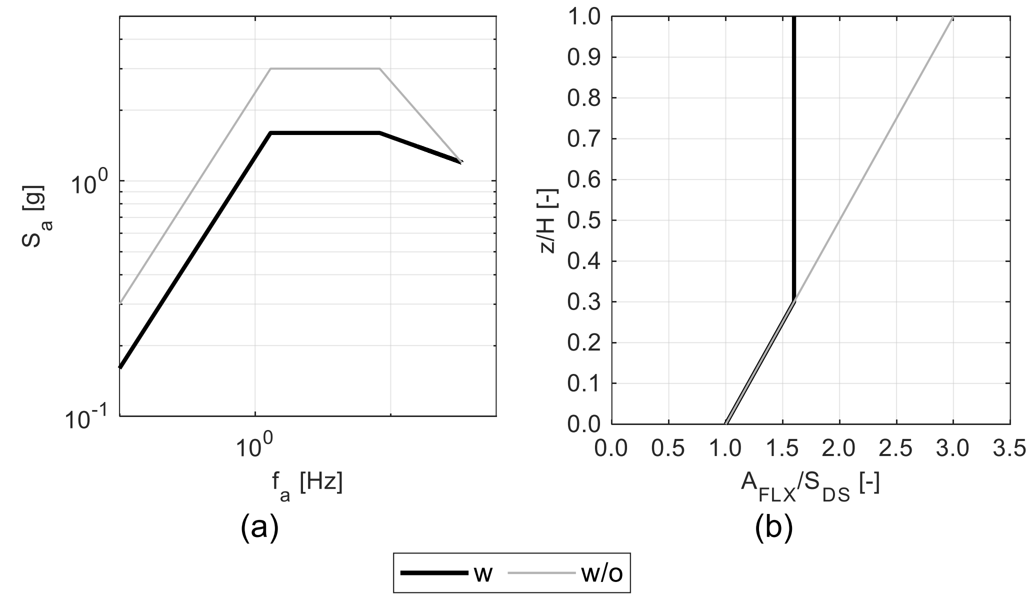

Figure 6.2: AC156 protocol with and without upper bound limit for A_{FLX}: a) required response spectra, and b) A_{FLX}/S_{DS} ratio as a function of z/h ratio.

FEMA 461 protocol provides methods for seismic evaluation of structural and NEs, identifying shake table testing as the most preferred method for assessment of acceleration-sensitive elements. The shake table testing protocol is designed for testing elements that are sensitive to the velocity and dynamic effect of motion imparted at a single point of attachment. The seismic performance of the test specimen is evaluated under input motions of increasing intensities representative of the motion at the single level of a building structure on which the test specimen is located. The development procedure and the seismic inputs used to assess the capacity of NEs were developed by Wilcosky et al. [21]. The test input consists of a 60-s narrowband random sweep excitation signal, with a center frequency of the sweeps ranging from 32 Hz to 0.5 Hz, at a rate of six octaves per minute, having a bandwidth resolution equal to a one-third octave. FEMA 461 does not provide the RRS, but only some representative cases, and generic spectral indications: TRS should be relatively smooth with the acceleration response spectra amplitude equal to 1 g within 2 and 32 Hz and with a uniform displacement response spectrum below 2 Hz. The spectral ordinate of the TRS at the resonant frequency of the NE (i.e., $S(T_a)$) is considered as an intensity parameter. The protocol also defines a procedure for the generation and the filtering of the shake table input; however, the use of the provided signals is implicitly suggested.

IEEE 693 protocol establishes criteria for seismic design and qualification of electrical substation equipment, according to three seismic qualification levels (low, moderate, and high). Qualification levels are defined according to zero period acceleration (ZPA) of RRS, i.e., high and moderate levels are associated with horizontal ZPA equal to 1.0 and 0.5 g, respectively, whereas no specific ZPA value is associated with low level. IEEE 693 RRS does not account for the influence of the hosting building, which can be considered by amplifying RRS by 2.5. The input signal of the seismic simulation tests shall have a duration of at least 20 s of strong motion. Theoretical TRS (i.e., related to assigned signal) shall be computed at 5% damping and shall meet RRS from the lower corner point frequency of the target response spectra (1.1 Hz). Unlike other protocols, IEEE 693 supplies different spectrum-compatibility rules for theoretical and recorded inputs. The protocol provides several spectrum-compatible seismic inputs. In particular, Takhirov et al. [22] developed several time histories according to IEEE 693 protocol. The seismic inputs were generated considering different earthquake type, i.e., crustal, subduction, and artificial ones.

Zito et al. protocol [14] defines criteria for seismic qualification/certification of (acceleration-sensitive) NEs that have fundamental frequencies greater than 1.0 Hz. The loading program consists of a series of dynamic tests, including both dynamic identification tests and seismic performance evaluation tests. This protocol considers two approaches: specific performance level qualification and extensive qualification. The former is intended to verify whether the component fulfills a specific performance level, associated with a target level of a relevant (seismic) intensity parameter defined by regulations or codes. The latter qualification consists in an incremental testing procedure encompassing low to high seismic intensities and minor to major damage DSs. Zito et al. RRS was derived from the formulation provided by the Italian building code [23,24] for frame buildings, which was developed in [25] and assessed in several studies (e.g., [26,27]); in particular, RRS was defined by implementing a general and site-building independent approach, favoring a generalizable and representative formulation. Zito et al. [14] also provides exception rules/criteria to be applied when the signal cannot be adequately reproduced by the shake table due to instrumental issues, e.g., exceeded peak displacement capacities or instrumental dynamic resonance issues, despite consolidated filtering procedures have been implemented. In this study, it is hypothesized that frequencies in the vicinity of 1.0 Hz are critical for the testing facility, and Zito et al. exceptions are applied accordingly, defining Zito et al. exception protocol. It should be mentioned that the investigated exception might be consistent with several testing facilities since low frequencies are often critical in terms of spectrum-compatibility and signal reproduction by shake tables [22,28].

6.2.3 Loading histories

Two types of acceleration records were selected for the numerical analyses: floor motions (FMs) and shake table protocol inputs (STPIs). FMs were provided by CESMD database and consist in real accelerograms recorded in US instrumented buildings. FMs are related to ground motions having PGA not smaller than 0.05 g, and they are always associated with higher intensity response over the building floors (mostly recorded at the roof level). The case study buildings consist in RC buildings designed within 1923 – 1975. In particular, 18 FMs were considered in this section, deriving them from the 24 FMs selected by D'Angela et al. [20]. In particular, FMs #4, #8, #11, #16, #20, and #24 considered in this latter section were not included in the present chapter. As a matter of fact, a pilot study showed that these records were extremely mild for the case study NE models. The considered FM set (FM#1 to FM#18) is widely representative in terms of (a) recorded PGA and PFA distribution, (b) near and far field records, and (c) low-, medium-, and high-rise buildings. For the sake of brevity, further FM details are not reported in this section since they are provided in the abovementioned chapter.

STPIs are artificial inputs derived compliant with the most authoritative STPs for seismic evaluation and qualification/certification of acceleration-sensitive elements. STPIs were generated or derived according to STPs described in section 6.2.2. Seven acceleration time histories were generated according to AC156 (AC set: AC#1 to AC#7), according to [28,29]; z/h was set equal to one to consider the most severe NE location condition as well as to consider the highest upper cut spectral limitation [13,18]. Seven inputs were generated according to AC156w/o (ACw/o set: ACw/o#1 to ACw/o#7), i.e., considering the procedure related to AC156 without applying the A_{FLX-H} upper bound limit. Three inputs developed according to FEMA 461 were considered (FEMA set: FEMA#1 to FEMA#3): FEMA#1 and FEMA#2 were provided by FEMA 461 (i.e., recommended longitudinal and transversal records) and FEMA#3 was generated in D'Angela et al. [13], according to the commentary of FEMA 461 and the procedure developed by Wilcoski et al. [21]. It was verified that AC, ACw/o, and FEMA set signals were compatible with representative shake table testing facilities, considering a spectral acceleration response at rigid periods equal to 1.0 g as a reference. In particular, the signals met the capacity limits of the shake tables of the University of Naples (e.g., [30]), and the most severe limitations were associate with peak displacement and upper frequency limit (capacity thresholds equal to 250 mm and 50 Hz, respectively).

Ten acceleration time histories were selected according to IEEE 693 (IEEE#1 to IEEE#7), also considering the study by Takhirov et al. [22]. IEEE#1 to IEEE#5 inputs were obtained by considering empirical time histories as a baseline (i.e., El-Centro, CA (1940), Landers, CA (1992), and El Mayor-Cucapah, Mexico (2010)), whereas the others were artificially generated. IEEE#4 to IEEE#7 were selected among the filtered versions of IEEE-spectrum compatible time histories and with peak displacements limitations of 200 mm, developed by Takhirov et al. [22]. This limit was considered to be compliant with the abovementioned shake table limitations. IEEE#1 to IEEE#3 were filtered in this chapter considering a band-pass Butterworth filter over the range of frequency 0.5 ÷ 35 Hz to meet the same displacement limit [30].

Seven inputs were developed according to Zito et al. protocol (NPS set: NPS#1 to NPS#7), according to the procedure defined in [14], not reported here for the sake of brevity. In particular, the signals were artificially generated as of nonstationary random signal with an energy content ranging from 1.0 to 32.0 Hz and a duration of 30 s. The theoretical spectra of the signal inputs were matched to the RRS defined with PGA equal to 0.4 g and the height ratio *z/H* equal to one. RRS was developed by generalizing and extending the formulation of the seismic demands on NEs provided by Italian building code [23,24]. The acceleration time histories were filtered with a band-pass filter to be compatible with the facilities limits previously described [30]. Another seven inputs (NPS exception set: NPSe#1 to NPSe#7) were generated according to Zito et al. protocol following the exceptions procedures describe by the authors (defined in section 6.2.2, referred to as Zito et al. exception).

The time history inputs related to STPIs are depicted in the Appendix B. Figure 6.3 shows the spectral acceleration response (Sa) as a function of frequency (f_a) associated with FM and STPI sets, assuming PFA equal to 1.0 g. Both (a) median and (b) 84th percentile spectra are depicted.

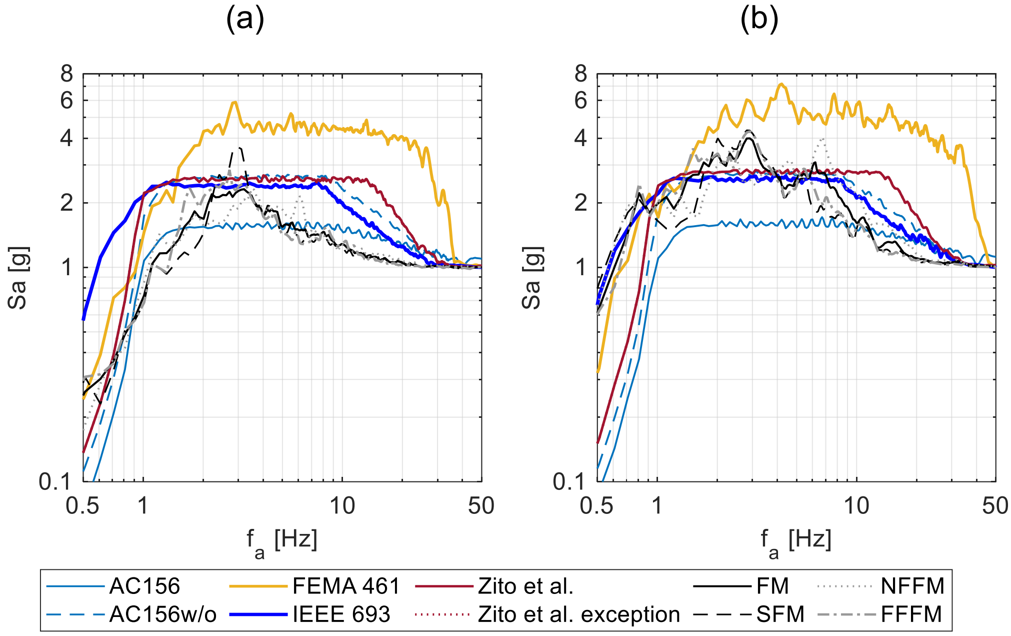

Figure 6.3: Spectral acceleration response (Sa) over frequency f_a associated with FM and STPI sets: (a) median curves and b) 84th percentile curves. The spectra were computed considering PFA equal to 1.0 g.

6.2.4 Case study models

NEs of interest are acceleration-sensitive elements that can be modeled by SDOF systems. In particular, case studies consist in cantilever elements with lumped mass at the free end. This model was chosen since it is representative of the dynamic behavior of wide range of acceleration-sensitive NEs, such as operating lights, projectors, antennas, base-anchored cabinets, and museum artifacts. Figure 6.4 depicts a representative example of critical nonstructural element that can be modeled by SDOF systems, i.e., a part of an historical structure and related supports exposed at the National Archeological Museum of Naples (MANN), Italy. Indeed, acceleration-sensitive NEs are generally meant to be SDOF systems in the literature (e.g., [15,16,25]), and the assessment methodology, including seismic demand estimation, is based on SDOF hypotheses and spectral responses [7,24,31].

Figure 6.4: A part of an historical structure and related supports exposed at the National Archeological Museum of Naples (MANN), Italy, which can be reasonably modeled by SDOF systems.

A set of 12 models was considered to account for various NEs over a wide range of elastic frequencies and geometric/structural properties. All models were made of steel S275 square hollow sections (SHS). In fact, acceleration-sensitive NEs are often provided by a supporting/resisting system (or structure) composed by steel elements, often box/tubular sections or profiles. Table 6.1 reports the geometrical/structural details of the case study models, including elastic frequencies (f_a). The models were defined by varying cross-section dimensions (i.e., size b and thickness t), mass m, and elevation height H. In particular, the models cover a wide range of elastic frequencies (approximately from 1 to 9 Hz) that is representative of most NEs (e.g., [7]). In particular, four ranges of elastic frequency (f_a) ranges were defined, i.e., (range 1) ~1.0 Hz, (range 2) ~1.5 Hz, (range 3) ~3.0 Hz, and (range 4) > ~3.0 Hz; three models were defined for each range, i.e., {M1a,M1b,M1c}, {M2a,M2b,M2c}, {M3a,M3b,M3c}, and {M4a,M4b,M4c} corresponded to ranges 1, 2, 3, and 4, respectively.

Table 6.1: Structural details of the investigated models.

Model ID	f_a range [Hz]	f_a [Hz]	b [mm]	t [mm]	H [m]	m [t]
M1a	~1.0	1.02	70	3.0	4.50	0.10
M1b		1.03	60	3.0	2.50	0.35
M1c		1.13	50	2.5	3.00	0.08
M2a	~1.5	1.48	70	3.0	3.50	0.10
M2b		1.52	60	3.0	2.50	0.16
M2c		1.52	60	2.5	3.00	0.08
M3a	~3.0	2.97	70	3.0	2.20	0.10
M3b		3.04	60	3.0	2.50	0.04
M3c		3.06	90	3.0	3.00	0.08
M4a	> ~3.0	5.86	70	3.0	1.40	0.10
M4b		7.34	80	4.0	1.50	0.10
M4c		9.02	70	3.0	1.05	0.10

6.2.5 Numerical modeling and analysis

The case study models were implemented in OpenSees [32] considering a lumped plasticity approach. In particular, each model consists in a series of an elastic vertical cantilever element and an inelastic moment-rotation spring, defined over three nodes (Figure 6.5a). In particular, (a) the spring was defined between a fixed node (node 1) and a (free) node (node 100) having the same coordinates of node 1 and (b) the vertical element was assigned between node 100 and a (free) node (node 2) having elevation coordinate equal to H and other coordinates equal to the ones of nodes 1 and 100.

The elastic and spring elements were modeled by an *elasticBeamColumn* element and a *zerolength* element, respectively. The moment-rotation backbone and hysteretic/deterioration parameters of the spring element were determined according to Lignos and Krawinkler [33], who calibrated the Ibarra-Medina-Krawinkler (IMK) model [34,35] for steel SHS columns, considering more than 120 literature tests on columns (including both cantilever columns and columns fixed at both ends). In particular, *uniaxialMaterial ModIMKPeakOriented* response was assigned to the *zerolength* element. The backbone is defined by yielding, capping and ultimate moment-rotation conditions, whereas cyclic deterioration is modeled according to an energy dissipation criterion, through the cumulative rotation capacity (Λ). Four deterioration modes can be implemented: strength, stiffness, post-capping stiffness, and reloading stiffness. Empirical formulations are provided by Lignos and Krawinkler (2010) for the estimation of pre-capping rotation (θ_p), i.e., the difference between the capping and the yielding rotation (Equation (6.1)), post-capping rotation (θ_{pc}), i.e., the difference between the ultimate rotation and the capping one (Equation (6.2)), and cumulative rotation capacity (Λ), i.e., the ratio between the reference hysteretic energy dissipation capacity (typical of the system) and the pre-capping rotation (Equation (6.3)). In particular, N is the applied axial load, N_y is the yield axial load, F_y is the expected yield strength (in MPa), and c is a coefficient for units conversion, which is equal to one if F_y is expressed in MPa. The denominator of the fourth factor, i.e., 380, aims at a normalizing the factor since it represents the nominal yield strength of steel typically used for tubular columns in Japan.

$$\theta_p = 0.614 \left(\frac{b}{t}\right)^{-1.05} \left(\frac{N}{N_y}\right)^{1.18} \left(\frac{c \cdot F_y}{380}\right)^{-0.11} \tag{6.1}$$

$$\theta_{pc} = 13.82 \left(\frac{b}{t}\right)^{-1.22} \left(\frac{N}{N_y}\right)^{3.04} \left(\frac{c \cdot F_y}{380}\right)^{-0.15} \tag{6.2}$$

$$\Lambda = 3012 \left(\frac{b}{t}\right)^{-2.49} \left(\frac{N}{N_y}\right)^{3.51} \left(\frac{c \cdot F_y}{380}\right)^{-0.20} \tag{6.3}$$

The provided equations are applicable within parameter ranges provided in Equations (6.4); the case study models are compatible with the abovementioned applicability conditions.

$$20 \le \frac{b}{t} \le 60 \tag{6.4.1}$$

$$0 \le \frac{N}{N_y} \le 0.5 \tag{6.4.2}$$

$$276\ MPa \le F_y \le 500\ MPa \tag{6.4.3}$$

Yielding moment (M_y) and yielding rotation (θ_y) were evaluated considering the elastic properties of the cross-sections, according to available handbooks. A strength reduction stabilization was taken into account by assuming a residual strength threshold (M_r), as a fraction of M_y, i.e., $M_r = k\, M_y$, with $k = 0.25$ (experimentally derived [33]). The global backbone curves (in-series members) related to the investigated models are depicted in Figure 6.5b considering shear-displacement response. Only the positive branch is illustrated in Figure 6.5b (the response is symmetric). It is worth noticing that backbone curves related to M1b, M2b, and M3b are overlapped since the models only differ in terms of mass (and other mechanical parameters are the same).

The member backbone response is associated with the in-series response of the elastic and spring elements (Figure 6.5c). In order to avoid convergence issues, the spring was modeled as elastic-plastic. The elastic and spring elastic stiffness were set by enforcing the following conditions: (a) spring stiffness equal to n times the elastic element and (b) in-series member stiffness corresponding to the backbone derived from the abovementioned formulation; n was assumed to be equal to ten according to the relevant literature [34,36]. Figure 6.5c depicts an example of backbone curves, expressed as shear-displacement response, associated with single series elements (elastic cantilever and elastic-plastic spring) and in-series member.

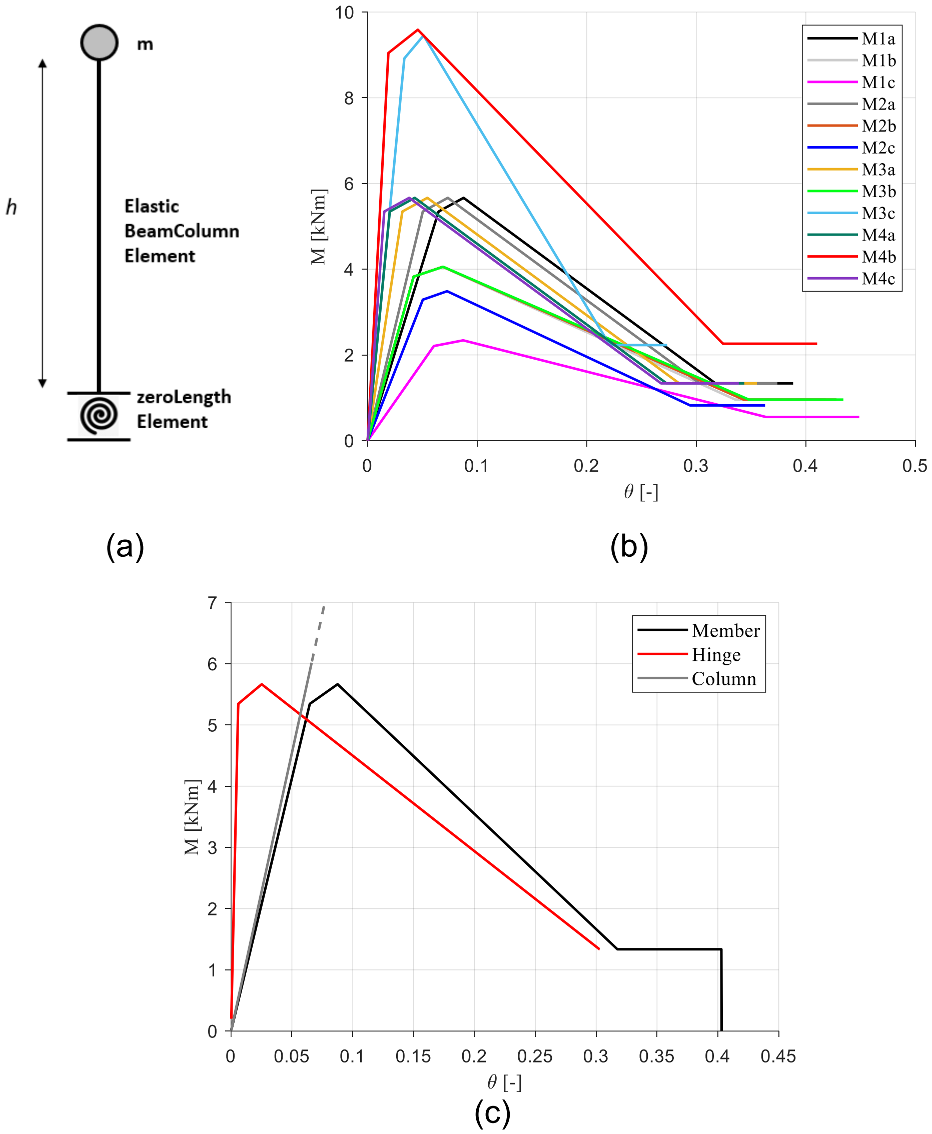

Figure 6.5: Depiction of the numerical models: (a) schematic of the implemented in-series system, (b) moment-rotation backbone curves related to investigated models, and (c) example of backbone response of elastic/spring elements and in-series member.

Second order geometric nonlinearities, namely *P-δ* effects, were implemented in the analyses. Rayleigh damping was assumed in the model (mass and initial tangent stiffness-proportional), considering a damping ratio equal to 5% [36]. The damping was only assigned to the elastic element in order to ease the analysis convergence (please, see [37,38]).

IDAs were carried out by scaling PFA from 0.05 g to component failure, through increments of 0.05 g. Structural resurrection [39] was not accounted for.

6.2.6 Engineering demand parameter (EDP) and damage states (DSs)

The damage of the systems was assessed considering the horizontal displacement of the concentrated mass Δ as an EDP. Five DSs were defined according to Figure 6.6, i.e., DS1, DS2, DS3, DS4, and DS5 achieved when Δ exceeds or equals the related displacement capacity thresholds Δ_{DS1}, Δ_{DS2}, Δ_{DS3}, Δ_{DS4}, and Δ_{DS5}. In particular, Δ_{DS1} is halved yielding displacement, Δ_{DS2} is yielding displacement, Δ_{DS3} is capping displacement, Δ_{DS4} is displacement associated with strength drop of 20% from the capping condition, and Δ_{DS5} is smallest displacement associated with residual strength (or onset of perfectly-plastic response). Table 6.2 reports the displacement capacities associated with the investigated models. These capacities are associated with global member response estimated through nonlinear static analyses (pushover curves) including P-δ effects. Considering the response of the spring instead of the global member for the damage assessment would not correctly account for the elastic contribution to the deformations since the spring is provided with a conventional aliquot of the global elastic stiffness.

Considering the modeled NEs (and not the hypothetical hosting facility), DS1 is representative of full functioning/operativity, DS2 is associated with damage limitation, DS3 is correlated with life safety, and DS4 is related to collapse/failure. Obviously, the performance levels to be guaranteed, the relevant limit states, and the associated seismic demand depend on the reference regulation and case study facility, and it is worth specifying that the present chapter aims at performing damage assessment rather than safety assessment.

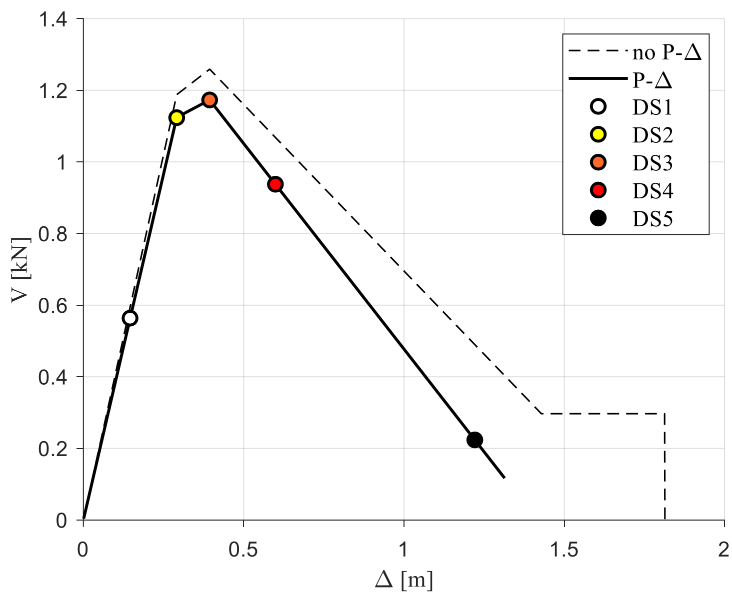

Figure 6.6: Schematic definition of damage states (DSs).

Table 6.2: Displacement capacities associated with investigated DSs, considering the global member response and including *P-δ* effects.

Model ID	Δ_{DS1} [m]	Δ_{DS2} [m]	Δ_{DS3} [m]	Δ_{DS4} [m]	Δ_{DS5} [m]
M1a	0.146	0.291	0.394	0.599	1.22
M1b	0.0524	0.105	0.171	0.257	0.515
M1c	0.0906	0.181	0.262	0.407	0.847
M2a	0.0881	0.176	0.256	0.427	0.945
M2b	0.0524	0.105	0.172	0.297	0.674
M2c	0.0755	0.151	0.218	0.357	0.778
M3a	0.0348	0.0696	0.1198	0.237	0.591
M3b	0.0524	0.105	0.172	0.338	0.841
M3c	0.0502	0.100	0.153	0.278	0.659
M4a	0.0141	0.0282	0.0601	0.138	0.376
M4b	0.0142	0.0283	0.0687	0.172	0.486
M4c	0.00793	0.0159	0.0398	0.100	0.281

6.2.7 Damage and reliability assessment

Damage assessment was carried out through estimation of fragility curves, associated with the response of the investigated models, according to [40], i.e., using an IM-based lognormal model (Porter *method A*). PFA was considered as an IM, and Δ was used as an EDP. The fragility was computed considering DS1 to DS5 defined in section 6.2.6. The fragility median value and logarithmic standard deviation are defined x_m and σ, respectively. The only record-to-record uncertainty was considered in this section.

The reliability of the investigated protocols was assessed by implementing the methodology developed in [13]. In particular, the reliability index β was computed according to second-level first-order reliability method (FORM) [41]. In particular, capacity (R) and demand (S) measures corresponded to capacities associated with FM (*actual capacities*) and protocol (*nominal capacities*), respectively, and capacity to demand margin (Z) corresponded to protocol overestimation of the capacity in relation to FM capacity (or equivalently, nominal overcapacity in relation to actual capacity). Accordingly, β accounts for the reliability of the protocol, considering FM capacities as a reference, and p_f, which is defined by $\Phi(-\beta)$, where Φ is the cumulative standard normal distribution, represents the failure probability of the protocol, i.e., the probability that the capacity assessed considering the protocol exceeds the capacity associated with FM. The probabilistic distributions of R and S were assessed considering the estimated fragility parameters. As a matter of fact, fragility parameters represent probabilistic distribution of capacities. β and p_f were computed as defined in [13,41] for all DSs, models, and protocols.

6.2.8 Estimation of reliability-targeted safety factors

In earthquake engineering, the concept of risk- and reliability-targeted design and assessment was widely applied to structures and infrastructures in the last few decades. However, no studies or applications, to the author' knowledge, extended these approaches to nonstructural elements, even though these latter are often associated with critical seismic risk. A major step towards a reliability-targeted design and assessment of nonstructural elements was carried out in this section. Safety factors are developed in the chapter for performing safety assessment of nonstructural element according to first-level reliability methods (semi-probabilistic approach). This allows the implementation of more reliable assessment procedures among practitioners and professionals. In particular, the chapter develops safety factors (k) to be applied to the capacities estimated according to the protocols, explicitly calibrated to achieve given levels of reliability associated with the use of the investigated protocol. Even though these factors are to be applied to capacities, the also account for the uncertainty associated with seismic demand, as it will be cleared in the following. Equation (6.5) was used to assess k considering a given target reliability index (failure probability), defined $\bar{\beta}$ ($\overline{p_f}$), where $x_{m,R}$ and σ_R ($x_{m,S}$ and σ_S) define the lognormal distribution parameters associated with FM (protocol) capacity (i.e., fragility parameters).

$$k = \exp\left(\bar{\beta}\sqrt{\sigma_S^2 + \sigma_R^2}\right)\left(\frac{x_{m,S}}{x_{m,R}}\right) \tag{6.5}$$

Equation (6.5) was derived by giving k explicitly from Equation (6.6), which expresses $\bar{\beta}$ as the β value associated with a set of protocol capacities having median and logarithmic standard deviation equal to $x_{m,S}/k$ and σ_S, respectively.

$$\bar{\beta} = \frac{ln\left(\frac{x_{m,R}}{\frac{x_{m,S}}{k}}\right)}{\sqrt{\sigma_S^2 + \sigma_R^2}} \tag{6.6}$$

As a matter of fact, if all members of protocol capacity set (S) are divided by *k* (in order to use the safety factor), the median of the lognormal distribution related to the resulting capacity set ($\bar{S}$) is equal to the median value of S set divided by k ($\overline{x_{m,S}} = x_{m,S}/k$), whereas the logarithmic standard deviation of $\bar{S}$ set is equal to the logarithmic standard deviation of the unmodified protocol capacity set ($\overline{\sigma_S} = \sigma_S$). Accordingly, Equation (5) allows identifying the value of k that determines the achievement of a target value of β ($\bar{\beta}$) for the related case study application (DS, model properties, and protocol). Therefore, *k* represents the reliability-targeted safety factors to be applied to capacity estimations related to the investigated protocols (S) to estimate the reliability-targeted protocol capacities ($\bar{S}$). Figure 6.7 depicts k as a function of $x_{m,S}/x_{m,R}$ and $\sigma_S^2 + \sigma_R^2$ or σ_S (for multiple values of σ_R), assuming $\bar{\beta}$ equal to 0.5, 1.0, and 2, which correspond to $\overline{p_f}$ approximately equal to 31%, 16%, and 7%, respectively.

Since *k* values were calibrated considering uncertainty associated with both capacity and demand measures, the reduction of the nominal capacity due to the application of the estimated safety factor also accounts for the increase of the seismic demand associated with a reasonable uncertainty assessment. In other words, the uncertainty associated with the seismic demand is included within the safety factor to be applied to the capacity. Analogously, it could be reasonably assumed that an aliquot of the safety factor is associated with the contribution of the demand uncertainty.

$\bar{\beta}$ equal to one represents a first tentative threshold for defining a relatively safe and not critically conservative target threshold [13]. It is worth specifying that the defined methodology is generally applicable, and different $\bar{\beta}$ ($\overline{p_f}$) can be selected according to the desired level of safety and significance of the element/facility. For each protocol, *k* values were assessed as a function of DSs and models. Finally, minimum values of *k* associated with $\beta \geq \bar{\beta}$ were assessed, and applicative correlation charts were developed for expeditious and practical estimations.

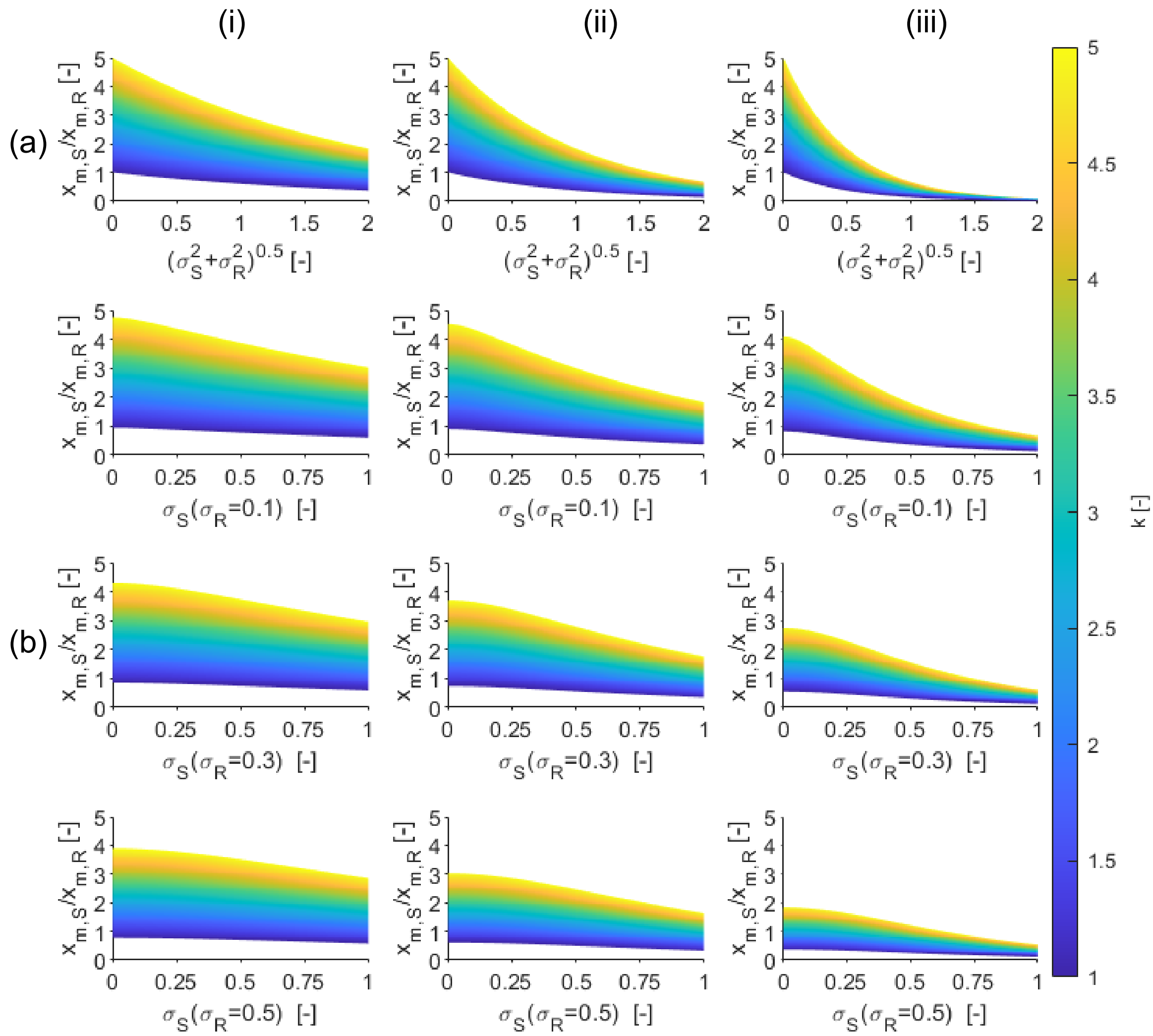

Figure 6.7: Safety factor (k) expressed as a function of $x_{m,S}/x_{m,R}$ and (a) $\sigma_S^2+\sigma_R^2$ and (b) σ_S (considering σ_R equal to 0.1, 0.3, and 0.5), assuming $\overline{\beta}$ equal to (i) 0.5, (ii) 1.0, and (iii) 2, corresponding to $\overline{p_f}$ approximately equal to 31%, 16%, and 7%.

6.3 Results and remarks

6.3.1 IDA curves

Figure 6.8 and Figure 6.9 show median and 84th percentile IDA curves, respectively, using PFA as an IM and Δ/Δ_{DS5} as an EDP, corresponding to single models and grouped frequency range models. The IDAs are estimated for each model and for each model range. The statistical curves were obtained by fixing PFA and estimating the statistical Δ/Δ_{DS5} values over the set of IDA curves. The 84th percentile curves represent a more conservative reference, i.e., considering a higher input severity. The comparison between the median and 84th percentile response allows identifying the dispersion of the single input IDAs within the different loading history sets, even though in a qualitative manner. However, the data dispersion associated with the seismic response of the investigated models is addressed in a more quantitative and explicit manner in the framework of the fragility and reliability assessment. Therefore, in this section, no comments are reported regarding the data dispersion in this section for the sake of redundancy.

The results are discussed in terms of the influence of loading history set and model features on the seismic response, also expressed as input/response IDAs severity, where higher severity is associated with larger EDP for given PFA or, equivalently, lower PFA for given EDP [42]. In particular, protocol input IDA responses are discussed considering FM ones as a reference, explicitly referring to the investigated model features (especially frequency ranges).

Severity patterns associated with the different loading histories can be observed. IEEE 693 (FEMA 461) inputs are the most severe for ranges 1 and 2 (3 and 4) models considering both median and 84th percentile response, even though in this latter case, even though 84th percentile IEEE 693 responses are quite similar to FEMA 461 for some models (e.g., M1c and range 3 models). Over the investigated protocols, AC156 is overall the least severe, as it was also found with regard to rigid block dynamics [20,42]. Considering 84th percentile (median) curves, AC156 is always (often) less severe than FM and other protocol responses (in particular, median AC156 curves are less severe than FM ones for ranges 1 and 2, over relatively larger Δ/Δ_{DS5} values (e.g., Δ/Δ_{DS5} > ~ 0.4 – 0.5), and for ranges 3 and 4, overall and especially in the post-yielding response. For ranges 1 and 2, median curves related to Zito et al. inputs are quite similar to IEEE 693 ones, whereas they are less severe than both FEMA 461 and IEEE 693 over Δ/Δ_{DS5} > ~ $\Delta_{DS3}/\Delta_{DS5}$ curves, but overall they are more similar to or more severe than FM ones. Zito et al. 84th percentile curves are similar to FEMA 461 and IEEE 693 and FM curves over relatively smaller Δ/Δ_{DS5} values, e.g., Δ/Δ_{DS5} < ~ 0.2 – 0.4, whereas they are less severe for larger values. Considering median and 84th percentile responses, IEEE 693 and FEMA 461 fit very well FM response over ranges 1 to 3, whereas Zito et al. are more consistent with FM curves for range 4. Both median and 84th percentile IDAs related to AC156w/o are overall similar to Zito et al. It is recalled that compatibility of IDA curves, even considering statistical curves, does not necessarily imply a higher reliability, which is estimated in the following sections considering an explicit quantitative approach.

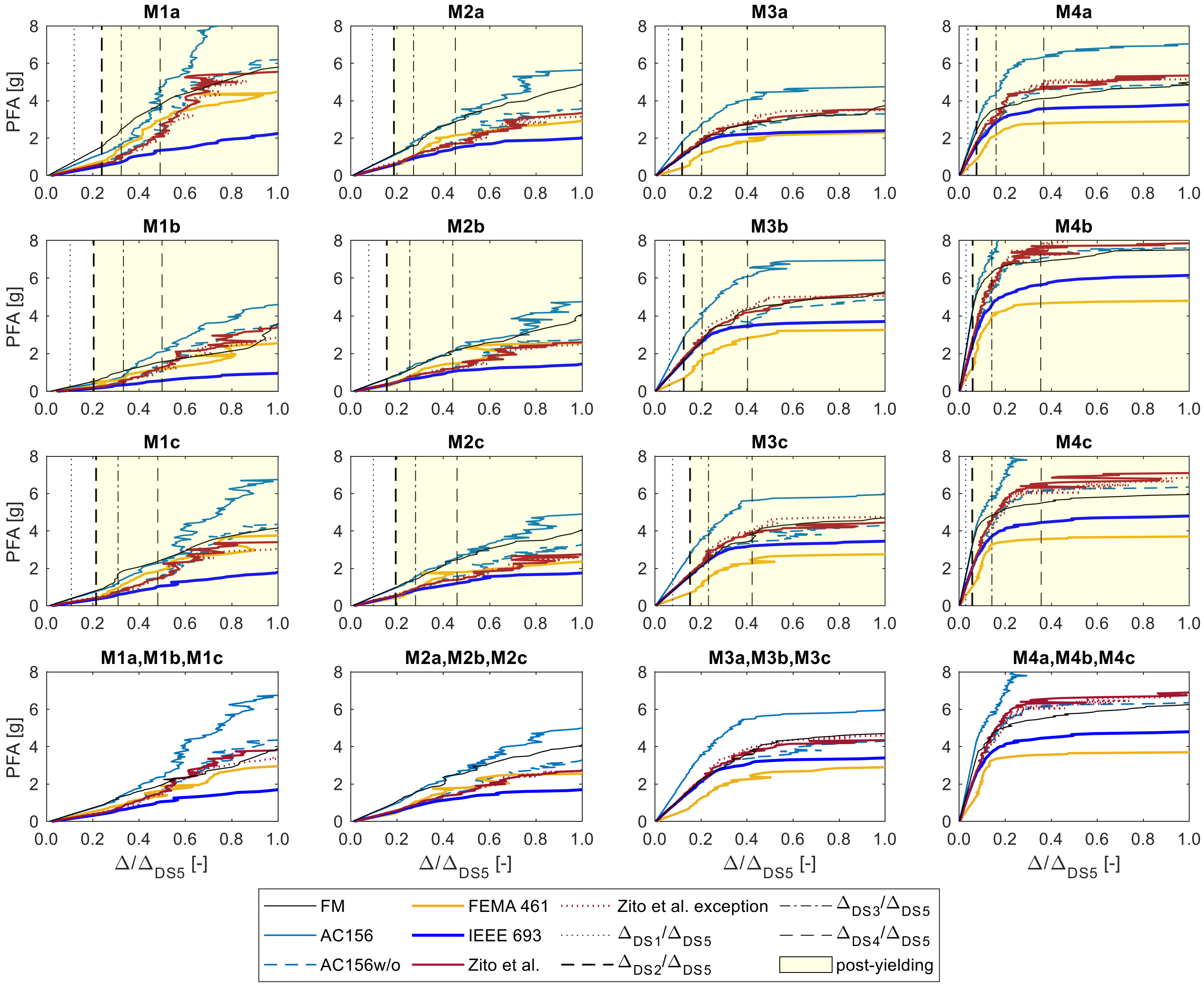

Figure 6.8: Median IDA curves (PFA as a function of Δ/Δ_{DS5}) associated with all loading history sets, corresponding to single models and grouped range models.

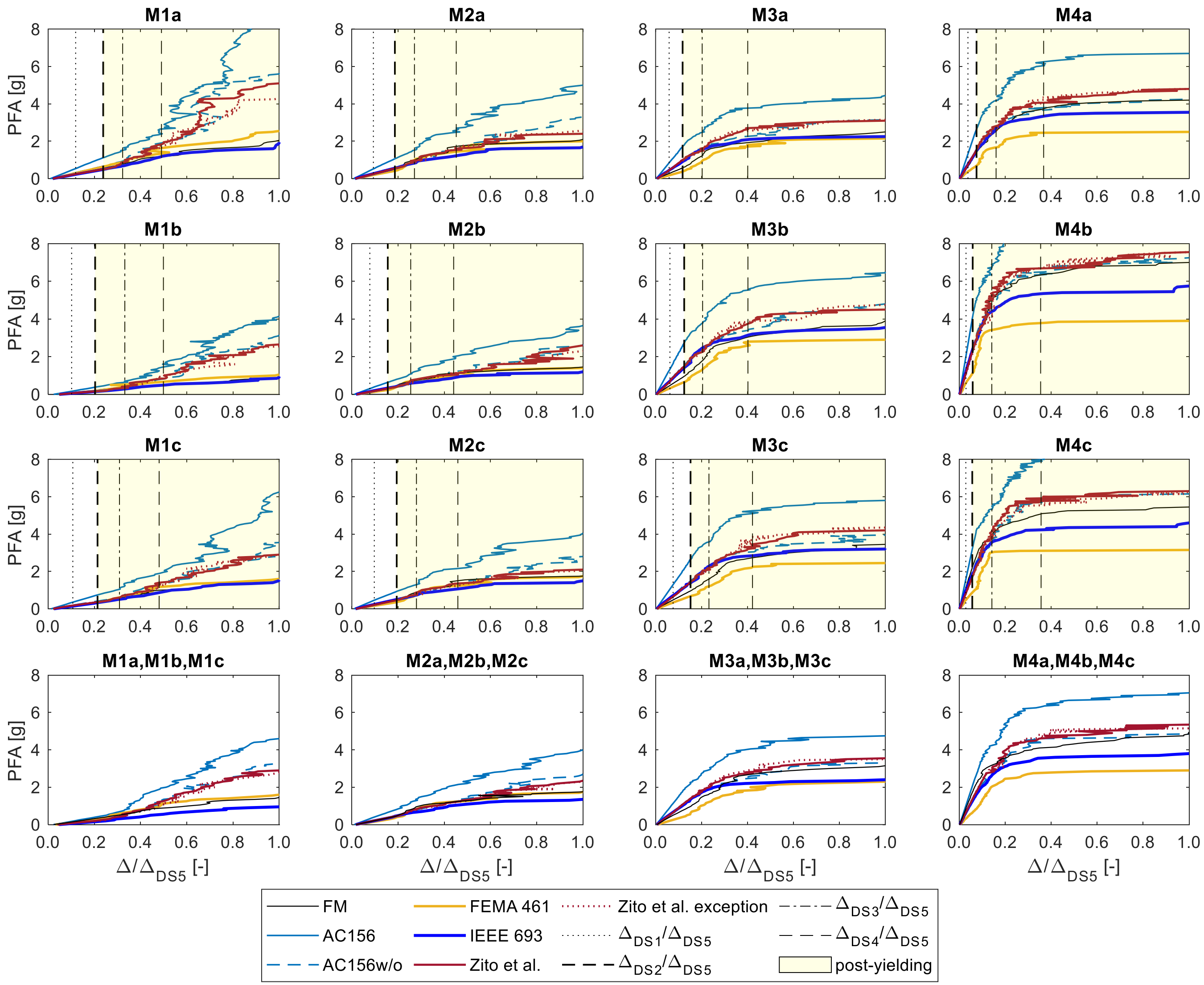

Figure 6.9: 84th percentile IDA curves (PFA as a function of Δ/Δ_{DS5}) associated with all loading history sets, corresponding to single models and grouped range models.

6.3.2 Fragility assessment

The study focuses on the influence of model frequency on the fragility parameters, which is more meaningful and revealing than fragility curves themselves. The fragility curves are presented for all models, loading histories, and DSs from Figure 6.10 to Figure 6.14. As a representative result. Moreover, the fragility parameters are reported for all models, loading histories, and DSs in Appendix B.

AC156 fragilities curves are lower than FEMA 461, IEEE 693, Zito et al., and AC156w/o for all models and DSs, and they are always lower than FM ones, except for models 1 and 2 relatively to DS1, DS2, and DS3. The fragility curves relating DS1 (Figure 6.10), DS2 (Figure 6.11), and DS3 (Figure 6.12) are quite similar among them for all models and loading histories. IEEE 693, Zito et al., and AC156w/o fragility curves are quite similar among them for all models, except for model M4b, where IEEE 693 fragility is slightly higher than Zito et al. and AC156w/o. In particular, IEEE 693, Zito et al., and AC156w/o fragilities are significantly higher than FM set ones, except for M3 models, where SFM fragilities are higher than the former fragilities. FEMA 461 fragilities are lower (higher) than IEEE 693, Zito et al., and AC156w/o for models M1 and M2 (M3 and M4), and they are always higher than FM ones.

Figure 6.13 shows the fragility curves assessed considering DS4. IEEE 693, Zito et al., and AC156w/o fragility curves are different among them for all models, except for M2 models. IEEE 693 fragility curves are higher than Zito et al. and AC156w/o for all models. In particular, Zito et al. and AC156w/o fragilities curves are higher (lower) than FM set ones for models M1 and M2 (M4), whereas for M3 models, Zito et al. and AC156w/o fragilities curves are quite similar to the FM sets. FEMA 461 fragilities are lower (higher) than IEEE 693, Zito et al., and AC156w/o for models M1 and M2 (M3 and M4), and they are always higher than FM ones. Finally, Figure 6.14 shows the fragility curves assessed considering DS5. IEEE 693, Zito et al., and AC156w/o fragility curves are different among them for all models. IEEE 693 fragility curves are higher than Zito et al. and AC156w/o for all models. In particular, Zito et al. and AC156w/o fragilities curves are higher (lower) than FM set ones for models M2 and M3 (M1 and M4, except M1c model). Moreover, Zito et al. and AC156w/o fragilities curves are quite similar to the FM sets for M3 models. FEMA 461 fragilities curves are lower (higher) than IEEE 693 for models M1 and M2 (M3 and M4), and they are always higher than FM ones. FEMA 461 fragilities are higher than Zito et al. and AC156w/o, except for M2 models where the median values of Zito et al. and FEMA 461 are quite similar to each other. Zito et al exception fragilities curves are quite similar to Zito et al. for all models and DSs. For this reason, in the analyses and results shown below the Zito et al exception protocol was neglected. Further comments on the fragility are reported in the following, regarding the evolution of the fragility parameters over the model frequencies.

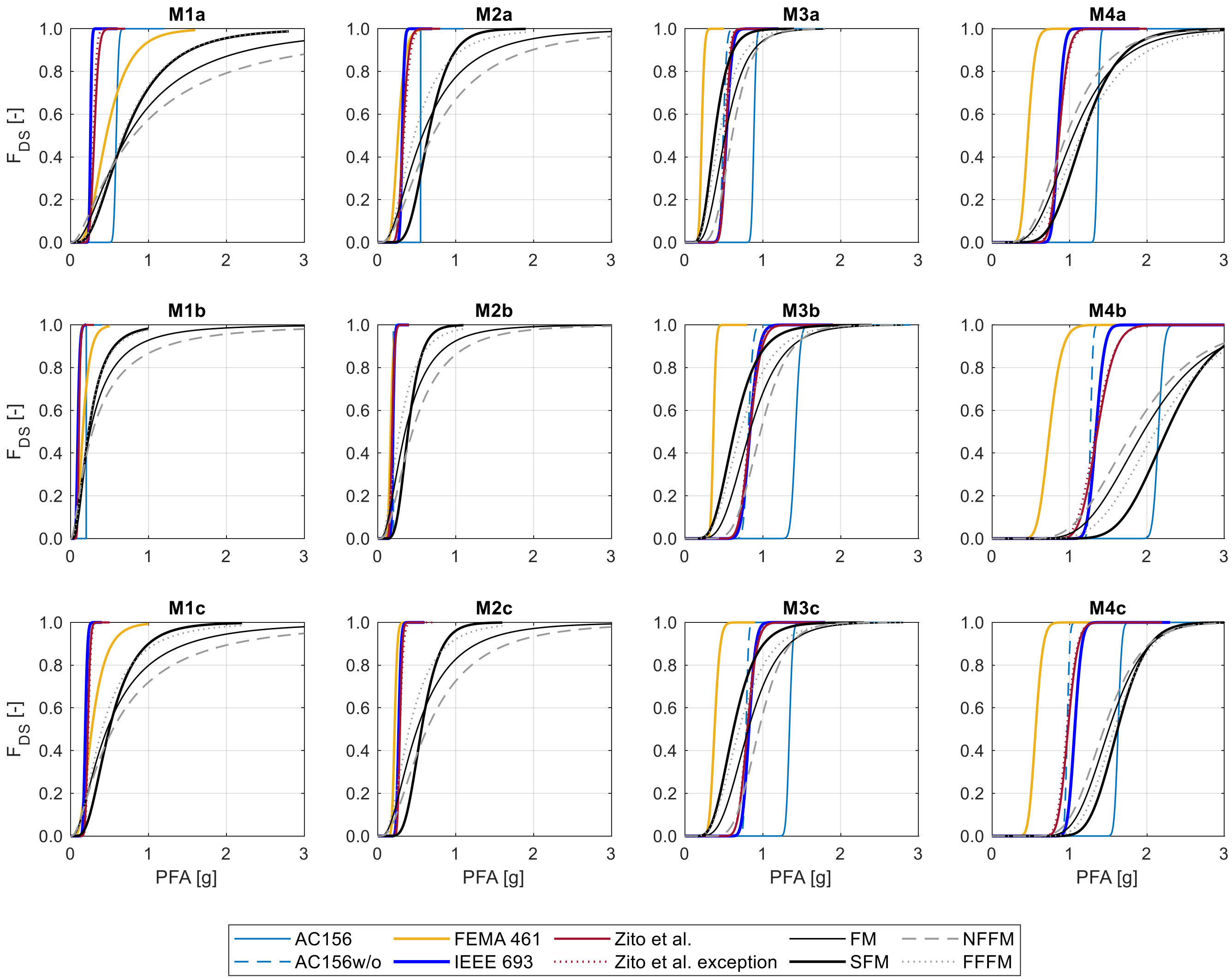

Figure 6.10: Fragility curves (FDS as a function of PFA) evaluated considering DS1, associated with all loading history sets, corresponding to single models and grouped range models.

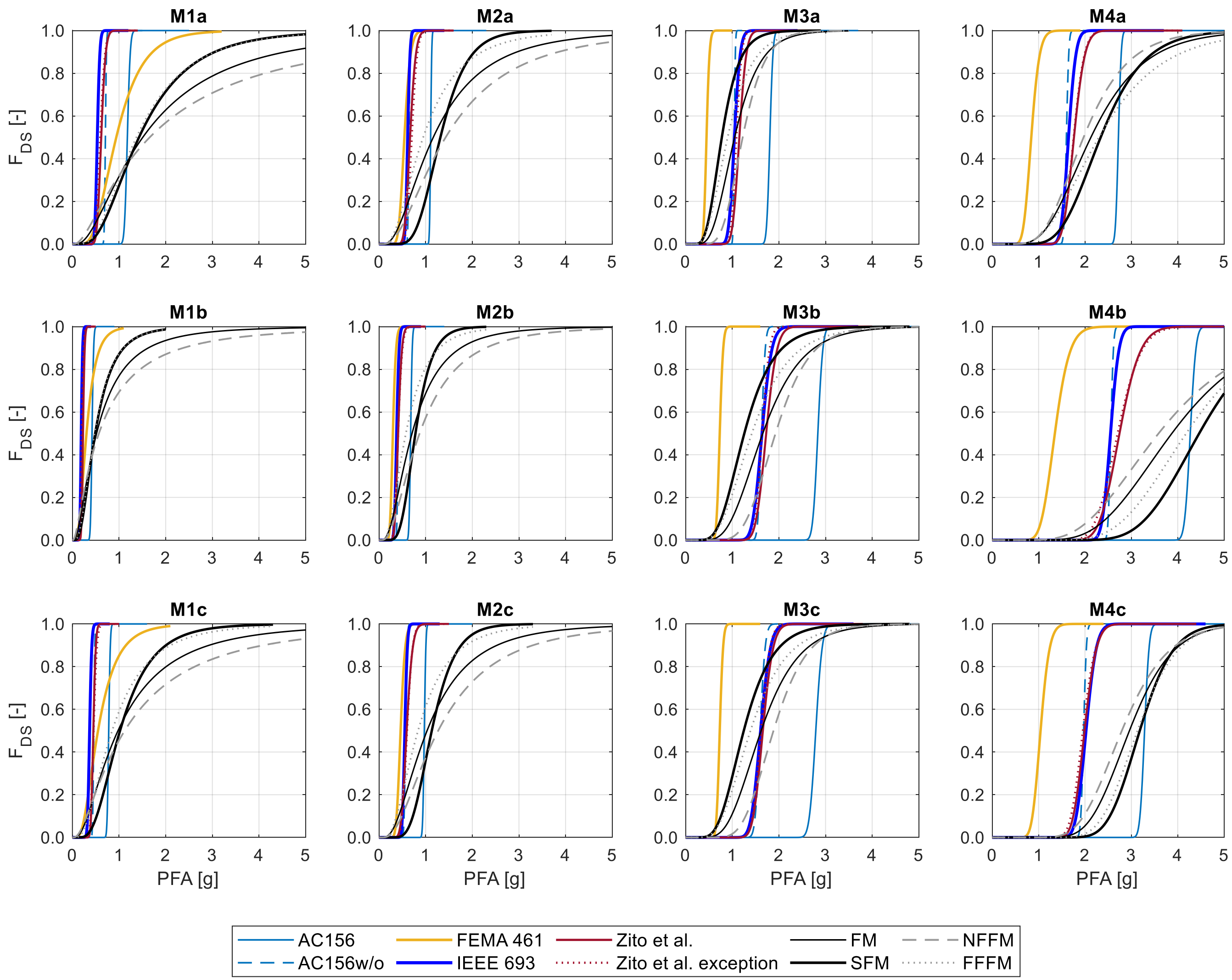

Figure 6.11: Fragility curves (FDS as a function of PFA) evaluated considering DS2, associated with all loading history sets, corresponding to single models and grouped range models.

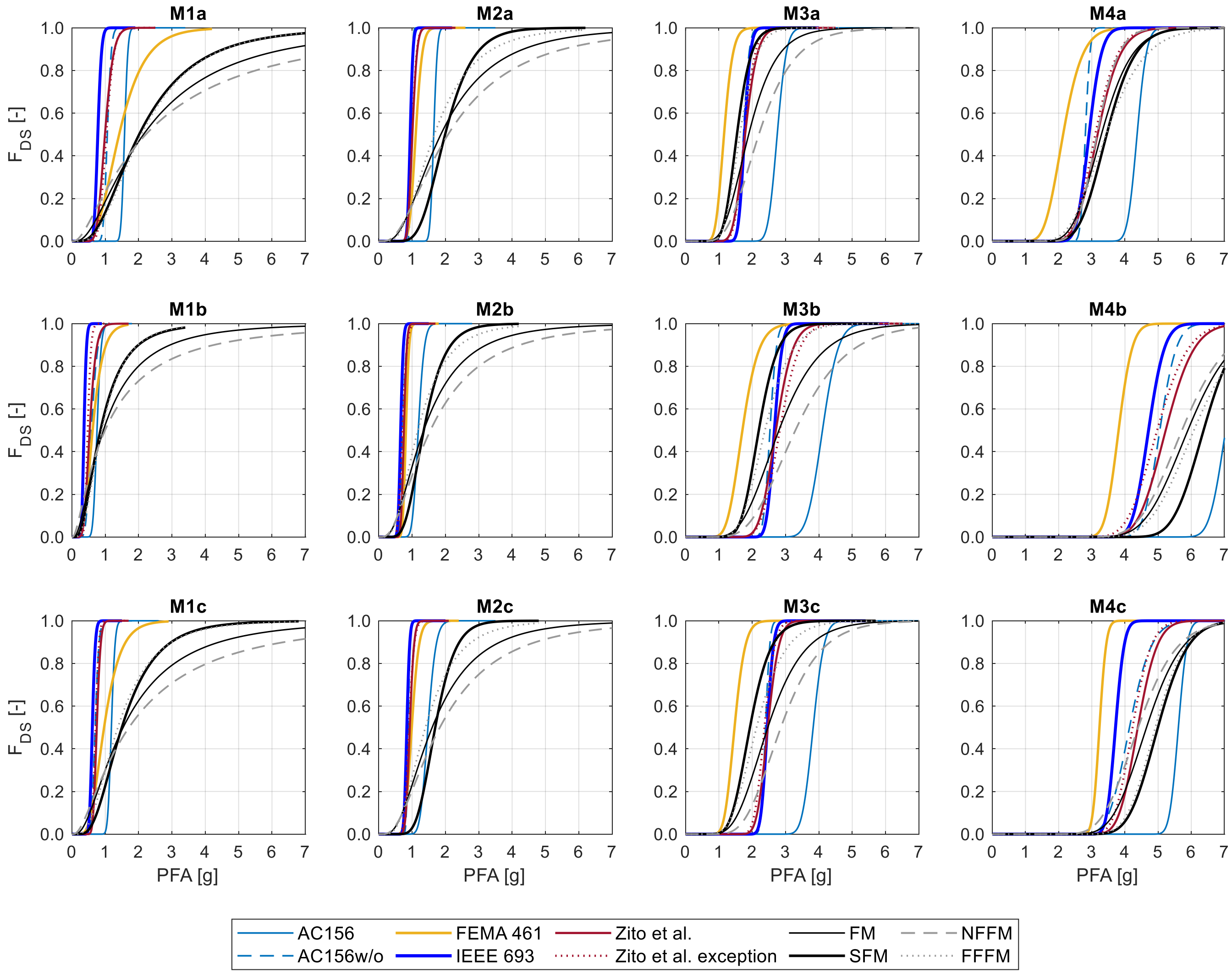

Figure 6.12: Fragility curves (FDS as a function of PFA) evaluated considering DS3, associated with all loading history sets, corresponding to single models and grouped range models.

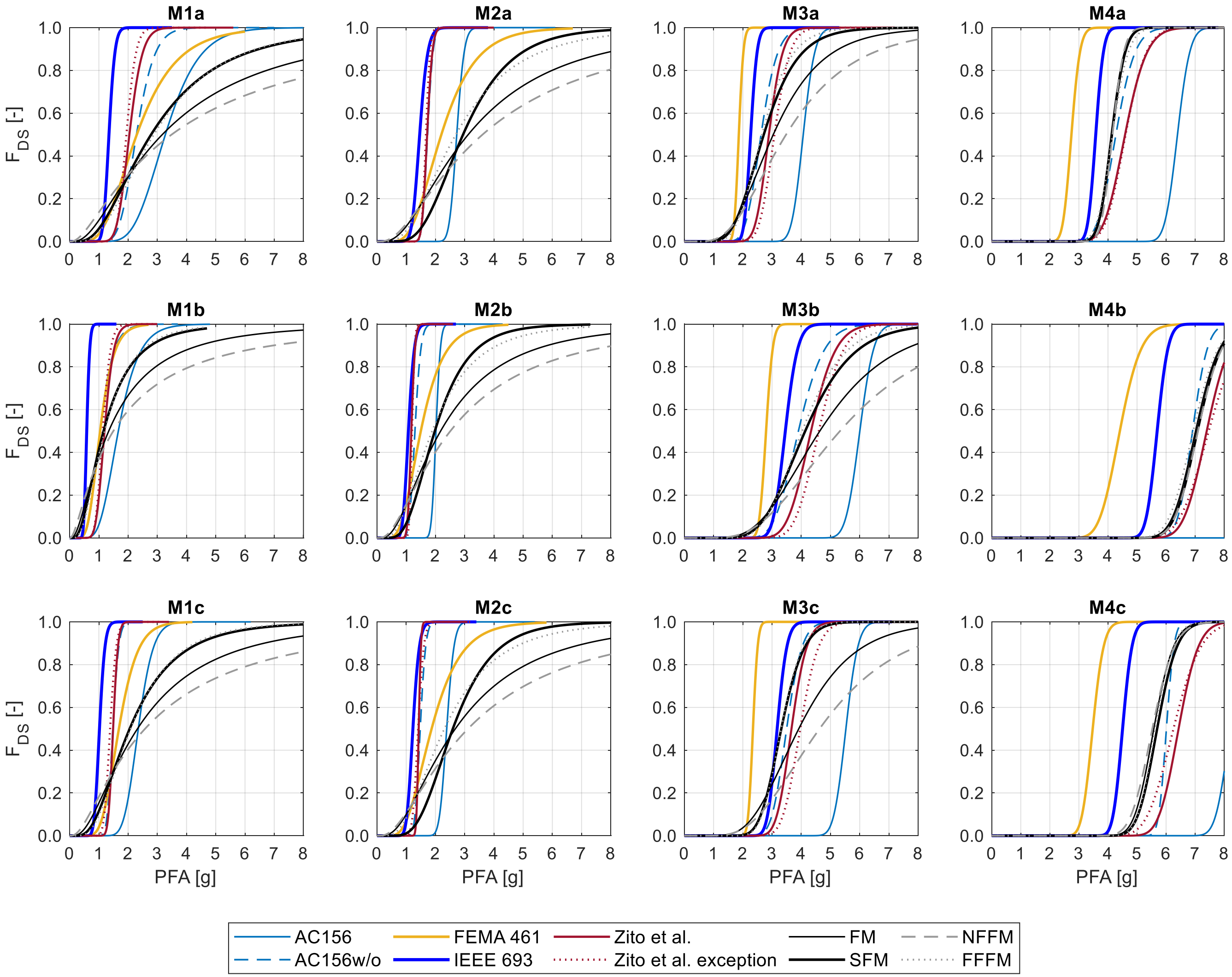

Figure 6.13: Fragility curves (FDS as a function of PFA) evaluated considering DS4, associated with all loading history sets, corresponding to single models and grouped range models.

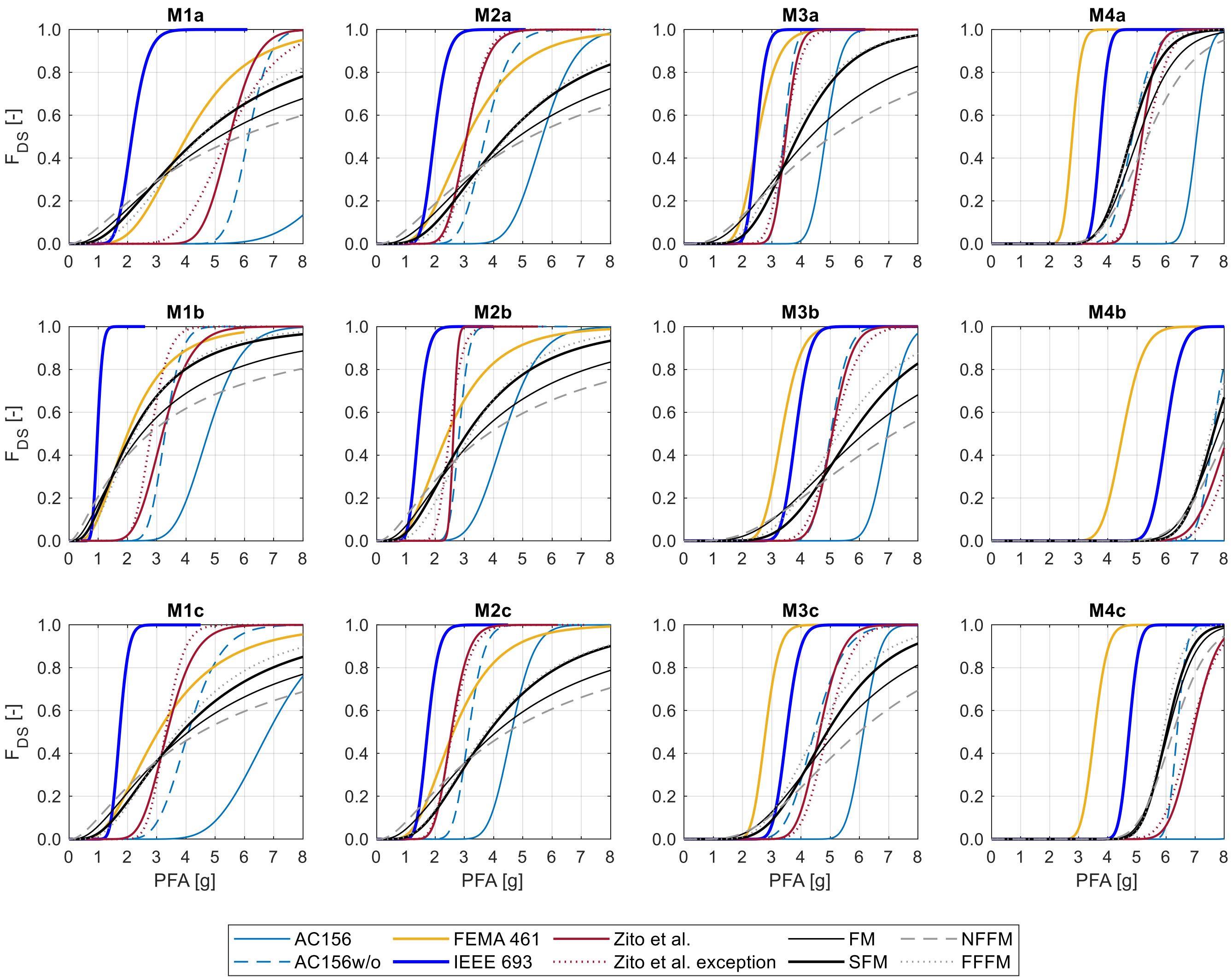

Figure 6.14: Fragility curves (FDS as a function of PFA) evaluated considering DS5, associated with all loading history sets, corresponding to single models and grouped range models.

Figure 6.15 and Figure 6.16 show the evolution of median x_M and logarithmic standard deviation σ over the model frequency f_a, respectively, considering FM sets. In particular, the single model results are reported as markers corresponding to relevant f_a, and fitting curves are also depicted. Fitting curves have a linear tendency and coefficient of determination R^2 ranges within 0.588-0.847 and 0.772-0.983; all fitting equations and R^2 are reported in Appendix B. For simplicity, the fitting curves were represented by linear equations. However, it can be observed that these equations exhibit a good quality of fit with relatively high coefficient of determination R^2. Further studies will assess whether higher-order or more complex correlations are better correlated with the results.

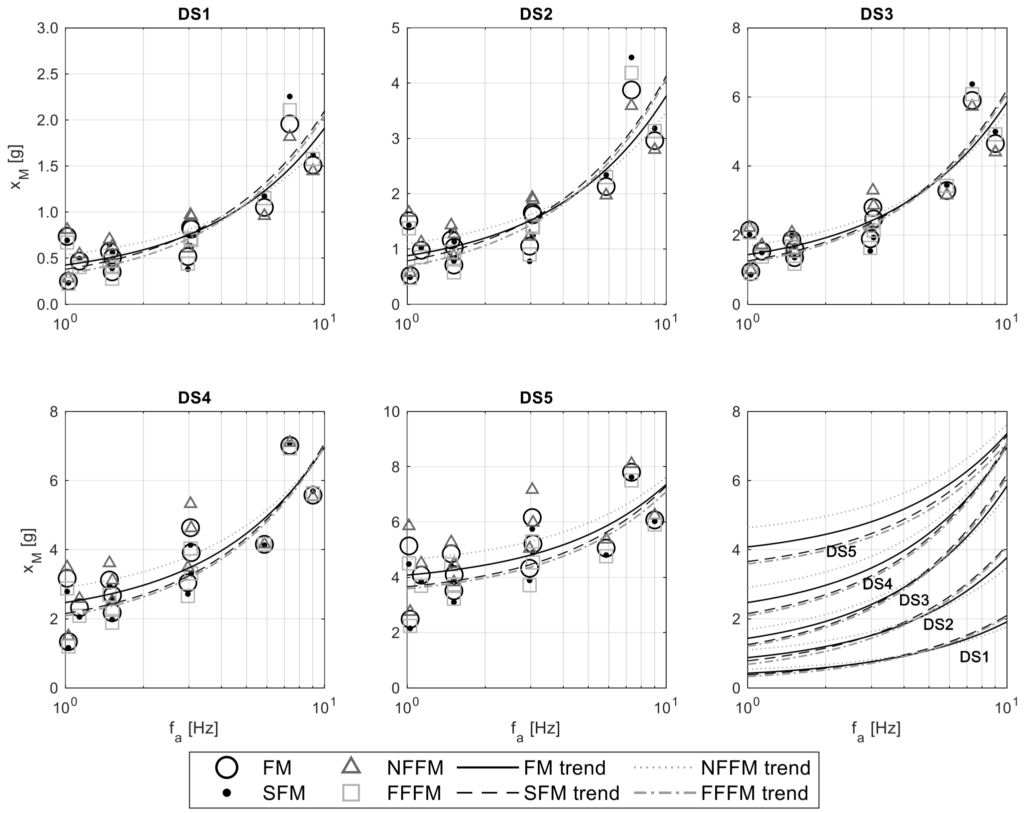

Figure 6.15: Fragility median x_M as a function of elastic frequency f_a associated with FM sets, evaluated for all DSs. The response associated with investigated models (depicted by markers) is fitted by linear trends; the equations and coefficient of determination (R^2) are reported in the Appendix B.

The different models belonging to same frequency range are associated with a non-negligible dispersion in terms of x_M, even within elastic response (i.e., considering DS1 and DS2). Nevertheless, clear and relatively robust x_M to f_a tendencies can be identified. As expected, the results corresponding to DS4 and DS5 are significantly less regular and dispersed than the ones associated with DS1 to DS3. This suggests that the elastic frequency might be correlated with seismic damage with a moderate efficiency even out of the elastic range, even though due consideration is needed. The influence of the FM set might be significant, depending on the frequency range and specific model. The tendency curves associated with the investigated DSs are clearly distinct among them and might considered to be references for expeditious but relatively reliable estimation of fragility medians, as a function of the elastic frequency of the element.

The logarithmic standard deviation σ is not particularly affected by the different DS; σ clearly decreases as fa increases (following a linear pattern, corresponding to the fitting curves). Within the same frequency ranges, the FM set has an influence on σ that is more significant than the different models.

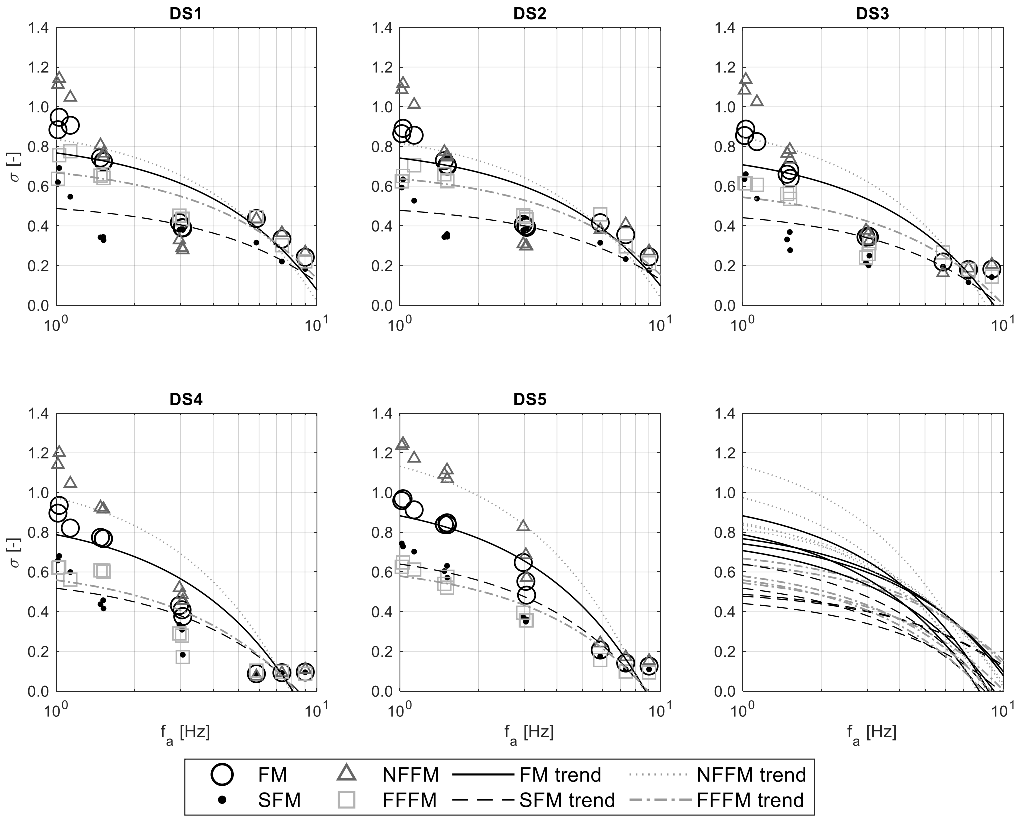

Figure 6.16: Fragility logarithmic standard deviation σ as a function of elastic frequency fa associated with FM sets, evaluated for all DSs. The response associated with investigated models (depicted by markers) is fitted by XXX; the equations and coefficient of determination (R^2) are reported in the Appendix B.

Figure 6.17 and Figure 6.18 depict the evolution of median x_M and logarithmic standard deviation σ over the model frequency f_a, respectively, for all protocols (single model results) and FM sets (fitting curves).

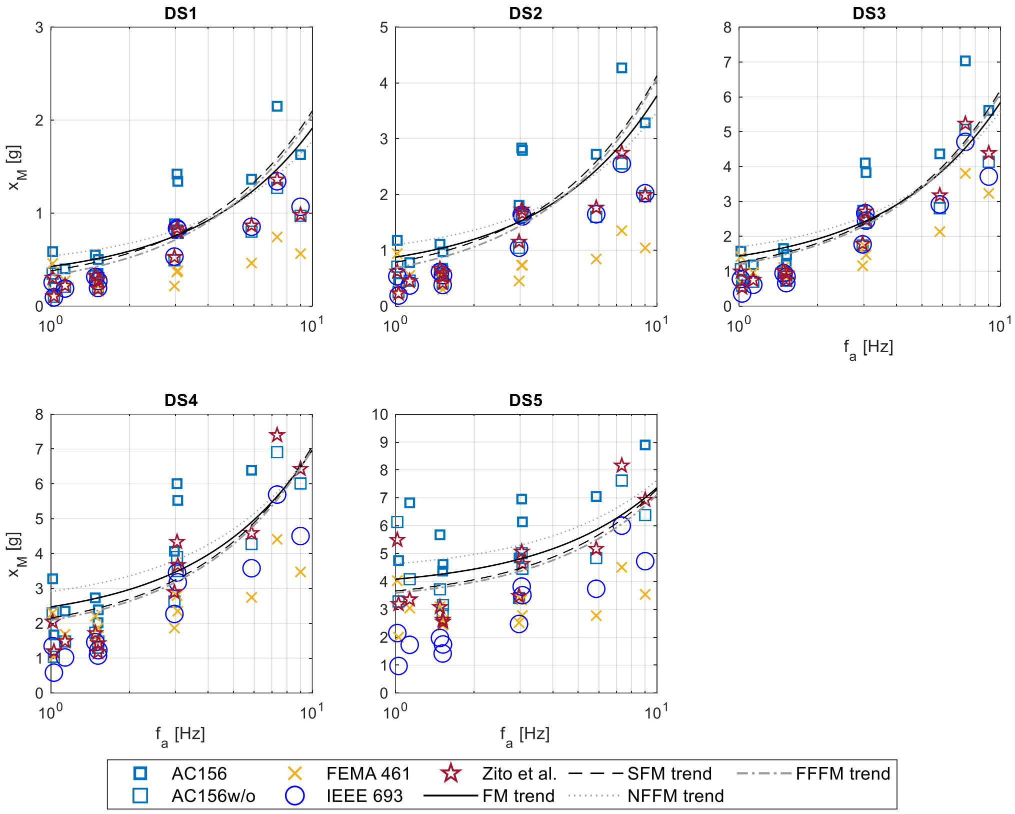

Figure 6.17: Fragility median x_M as a function of elastic frequency fa associated with all protocols (single model markers) and FM sets (fitting curves), evaluated for all DSs.

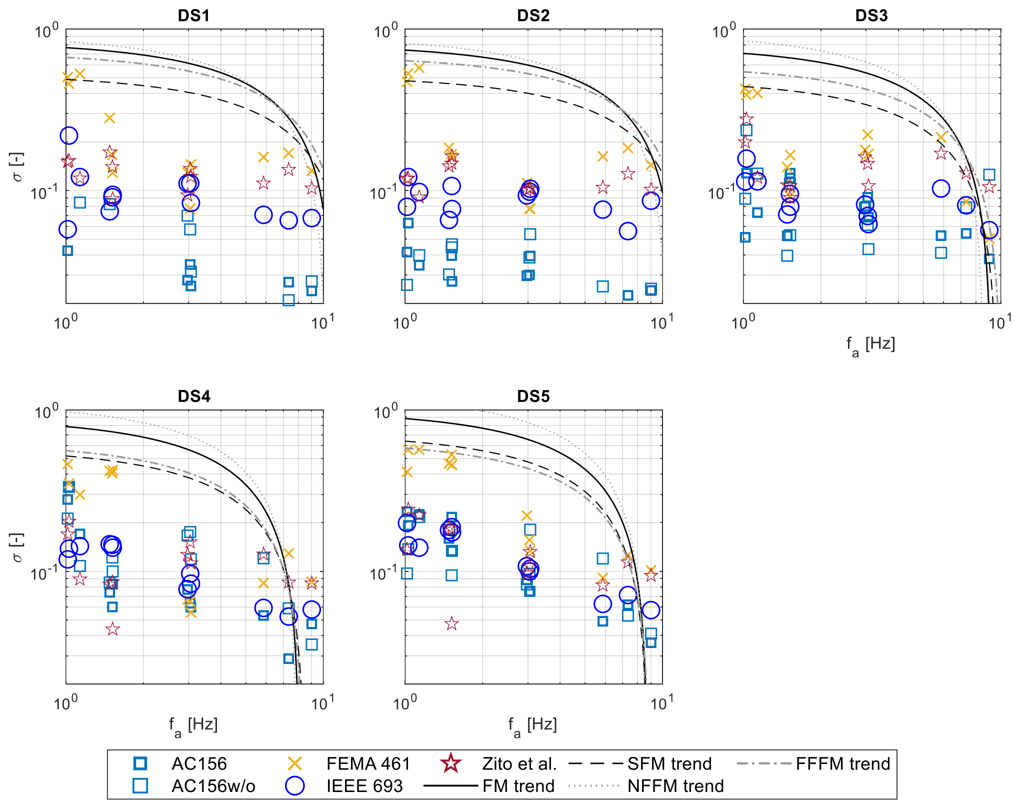

Figure 6.18: Fragility standard deviation σ as a function of elastic frequency fa associated with all protocols (single model markers) and FM sets (fitting curves), evaluated for all DSs.

6.3.3 Reliability indexes

The reliability index *β* and the failure probability of the protocol p_f, which is defined by *Φ(-β)*, were computed as defined in [13,41] for all DSs, models, and protocols (see section 6.2.8). In particular, from Figure 6.19 to Figure 6.22 are shown the failure probability of the protocol p_f for all DSs, models, and protocols, considering all FM sets capacities as a reference. From Figure 6.23 to Figure 6.26 are illustrated the reliability index *β* for all DSs, models, and protocols, considering all FM sets capacities as a reference. The reliability indexes related to Zito et al. exception are not shown since they are quite similar to Zito et al. results, confirming that the exception does not affect the reliability of the protocol itself.

The failure probability of AC156 is higher than all other protocols for all models and DSs, considering all FM sets capacities as a reference. In particular, the failure probability is less (higher) than or equal to 50% for M1 and M2 (M3 and M4) models, and DS1, DS2 and DS3 (DS4 and DS5), considering all FM sets capacities as a reference, expect FFFM set, where for M2 model exceeds 50%.

The failure probability of IEEE 693, Zito et al., and AC156w/o is quite similar among them for all models, and DS1, DS2 and DS3, considering all FM sets capacities as a reference. Especially, the failure probability is less than or equal to 20-30%, expect for M3 models, where almost always exceeds 50%. The failure probability trend of FEMA 461 is almost always decreasing as the elastic frequency of the models increases, while for all other protocols there is a more or less constant trend.

6.3.4 Calibration of safety factors

The safety factors *k* were computed as defined in section 6.2.8 for all DSs, models, and protocols. In particular, Figure 6.27 to Figure 6.30 show the safety factors *k* of the protocol for all DSs, models, and protocols, considering all FM sets capacities as a reference. k factors reflect the statistical distance between the reliability of the protocol and the reference value (i.e., equal to one), and k values larger (smaller) than the unity are associated with β values lower (lager) than the reference one. The safety factors related to Zito et al. exception are not provided since they are quite similar to Zito et al. ones; therefore, k values related to Zito et al. could be used also for Zito et al. exception cases.

Overall, *k* values are defined within a reasonable range, e.g., 1.0 – 2.5, except for DS5 (M1 and M2 models) and very few cases related to other DSs (mostly regarding AC156), where k also reaches extremely large values (e.g., larger than 3). There are cases in which k are lower than one, mostly for FEMA 461 and IEEE 693; in these cases, the protocols are clearly too conservative since assuming a safety factor lower than the unity is not a fully reasonable option.

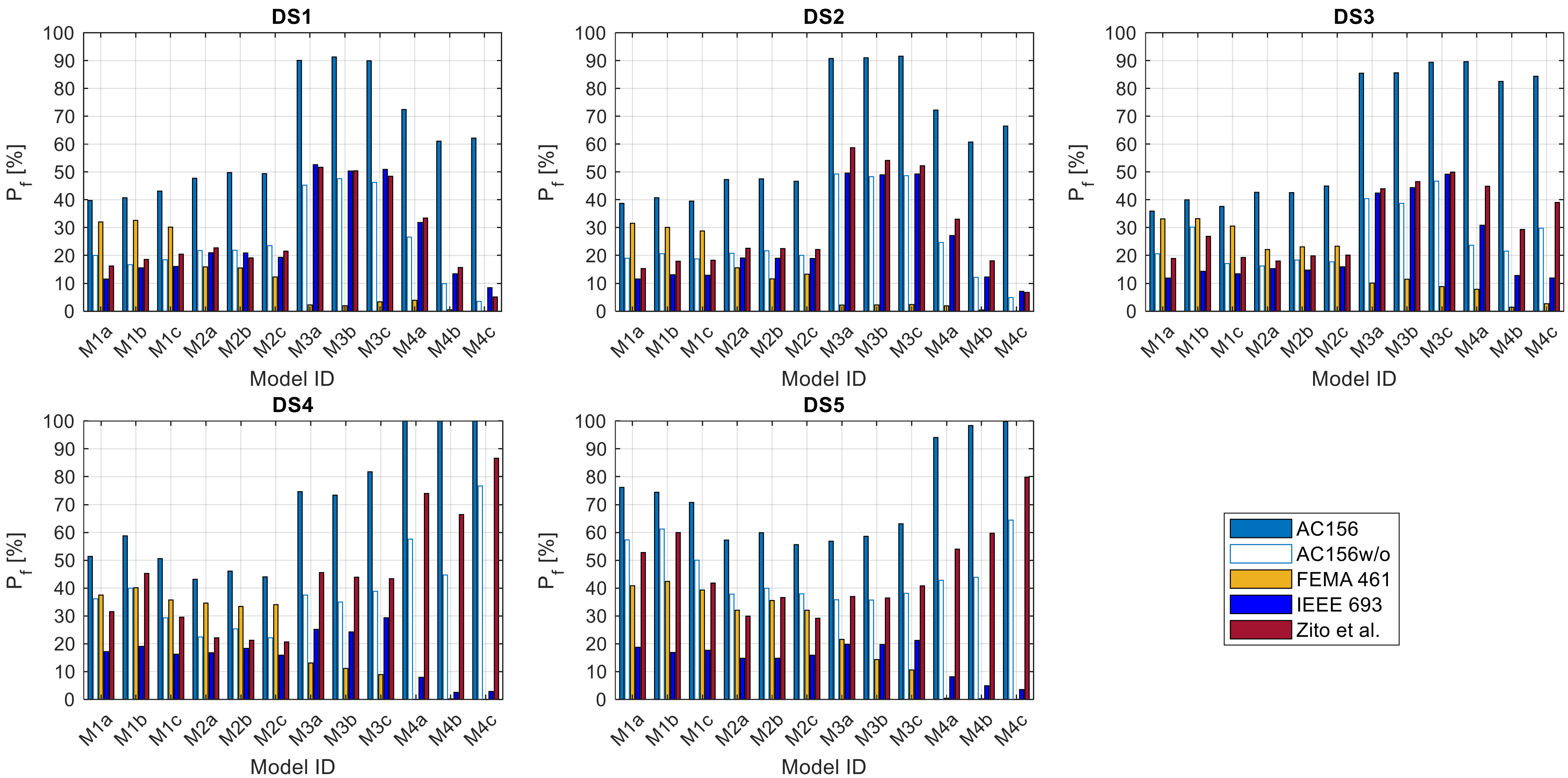

Figure 6.19: Failure probability (p_f) for all for all models and protocol input sets, evaluated for all DSs considering FM set.

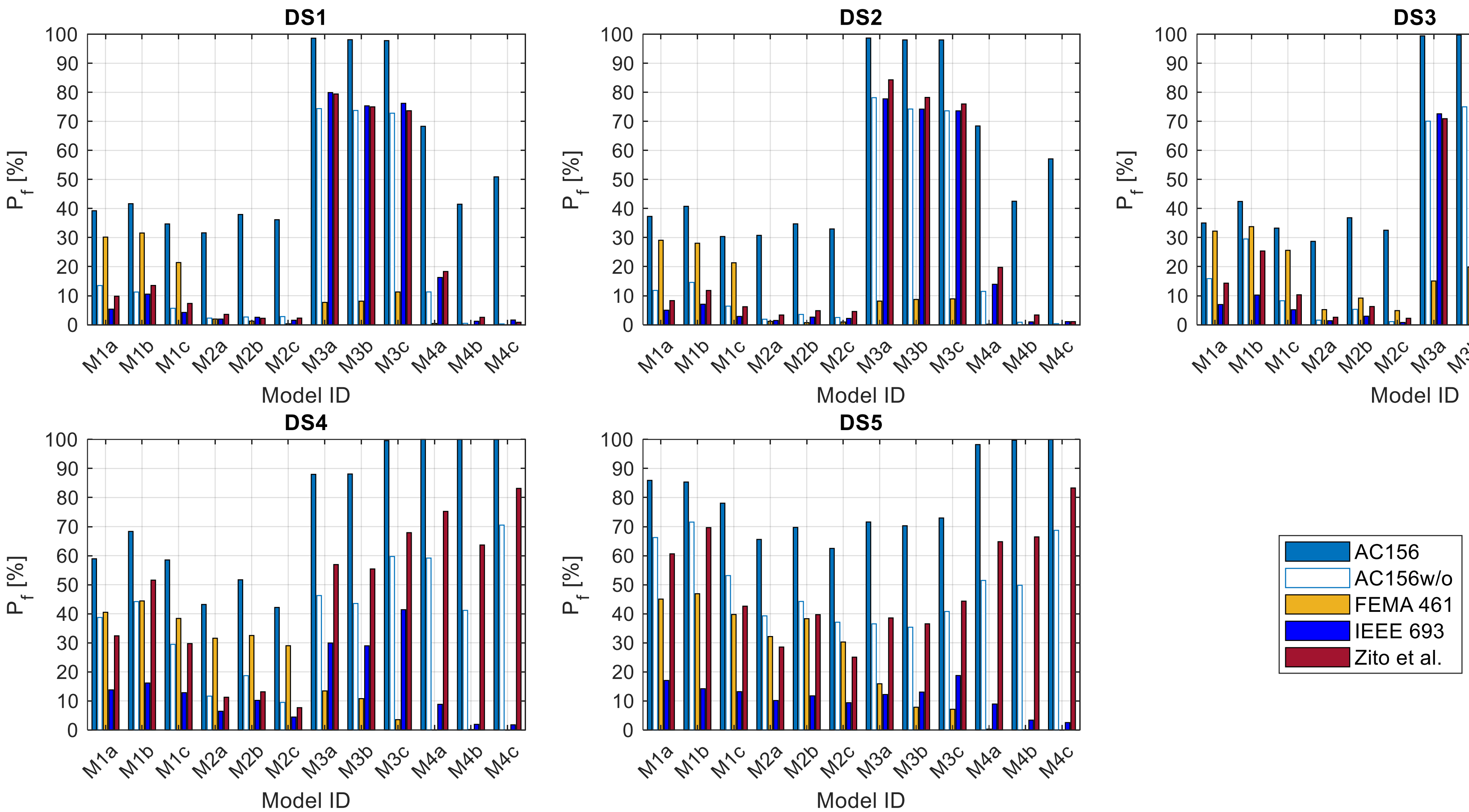

Figure 6.20: Failure probability (p_f) for all for all models and protocol input sets, evaluated for all DSs considering SFM set.

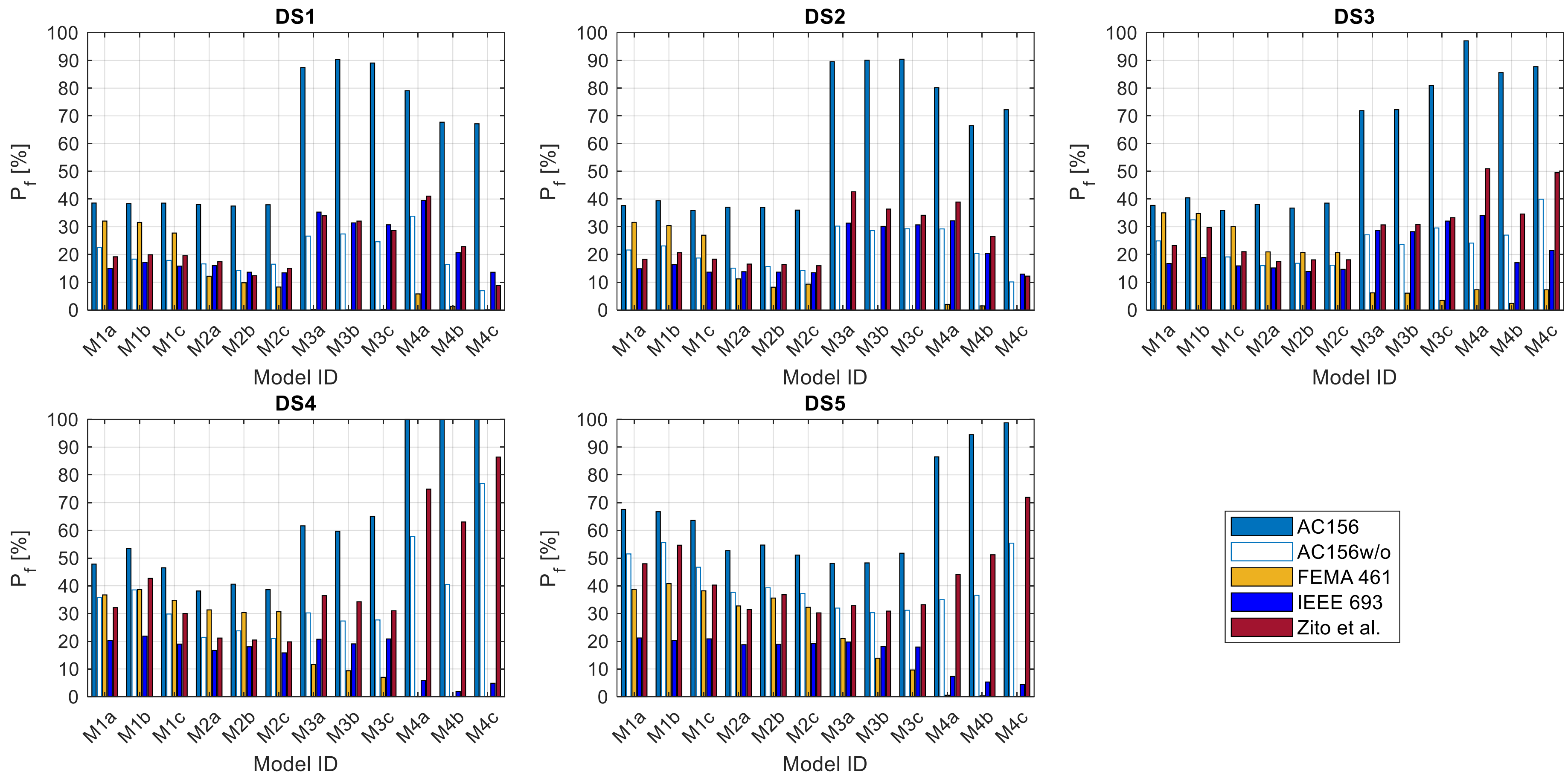

Figure 6.21: Failure probability (p_f) for all for all models and protocol input sets, evaluated for all DSs considering NFFM set.

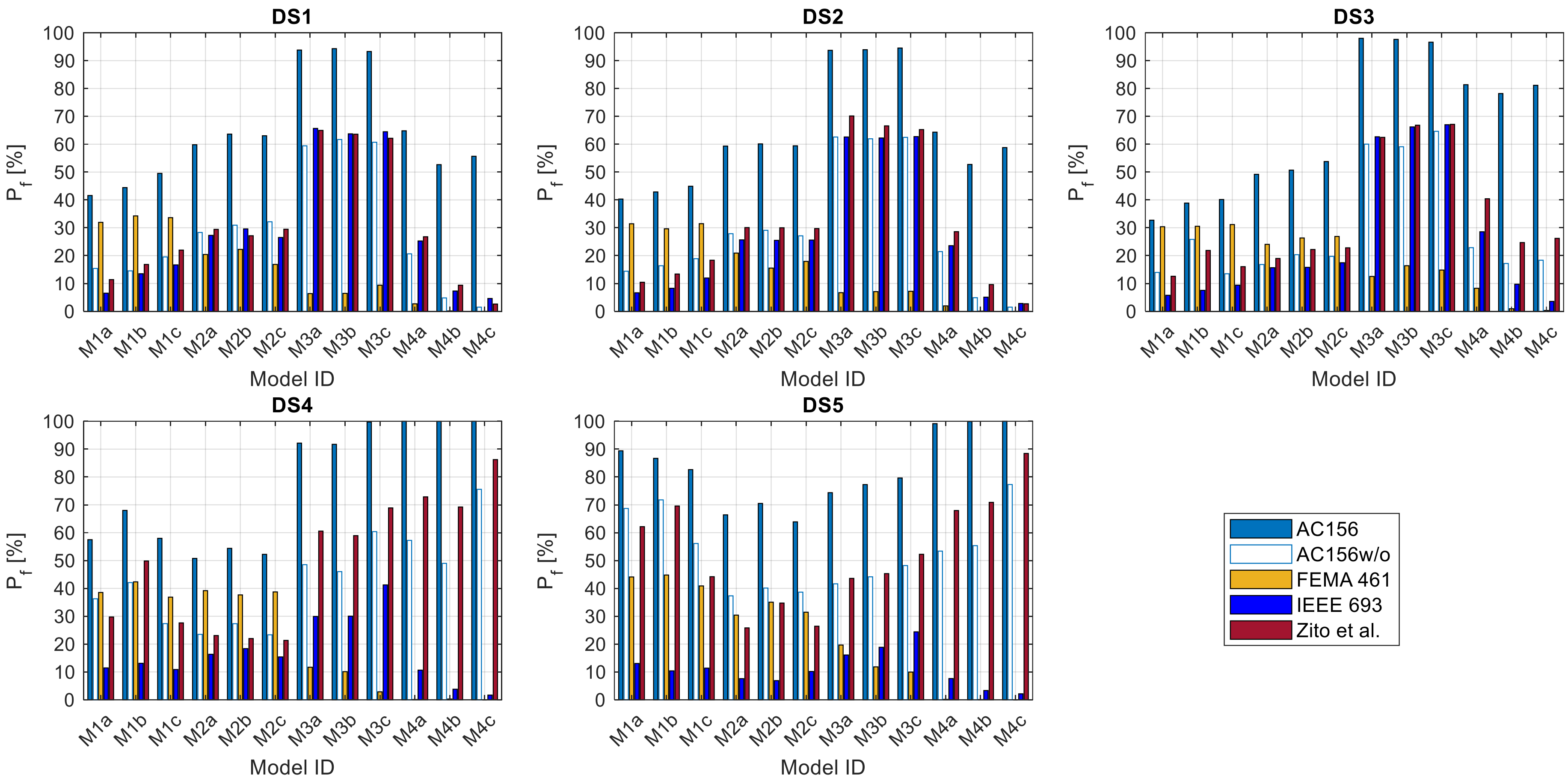

Figure 6.22: Failure probability (p_f) for all for all models and protocol input sets, evaluated for all DSs considering FFFM set.

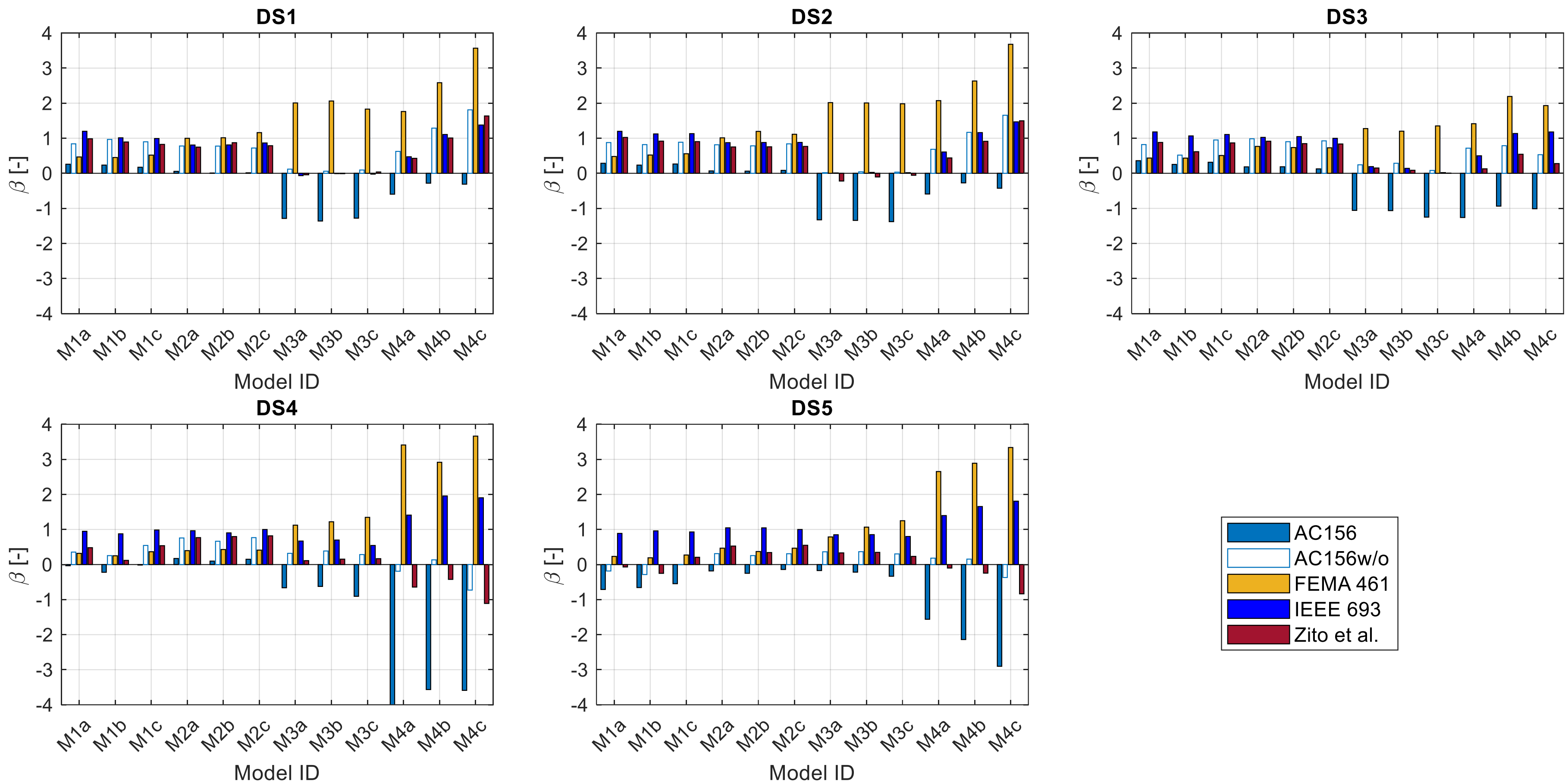

Figure 6.23: Reliability index (β) for all for all models and protocol input sets, evaluated for all DSs considering FM set.

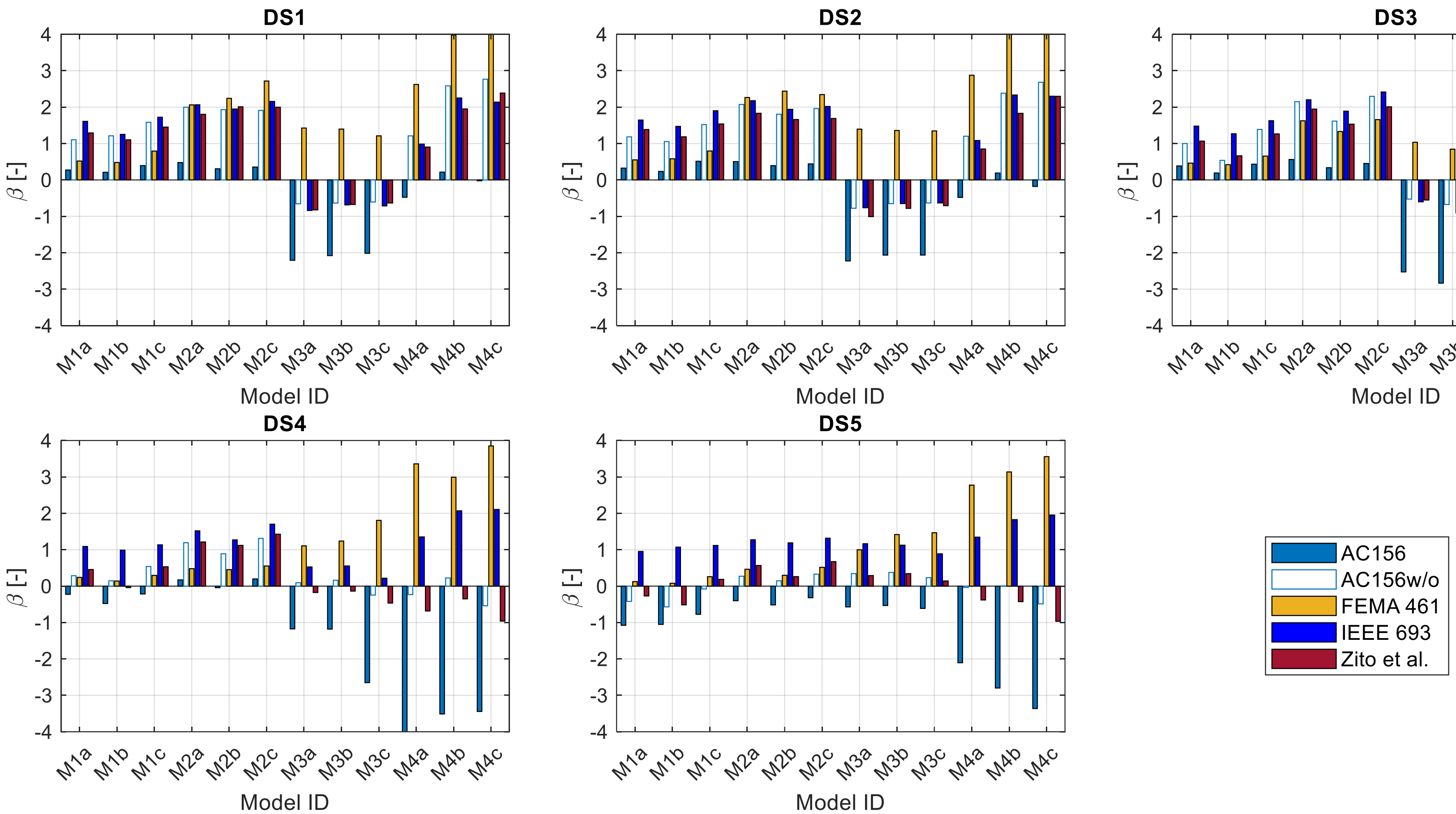

Figure 6.24: Reliability index (β) for all for all models and protocol input sets, evaluated for all DSs considering SFM set.

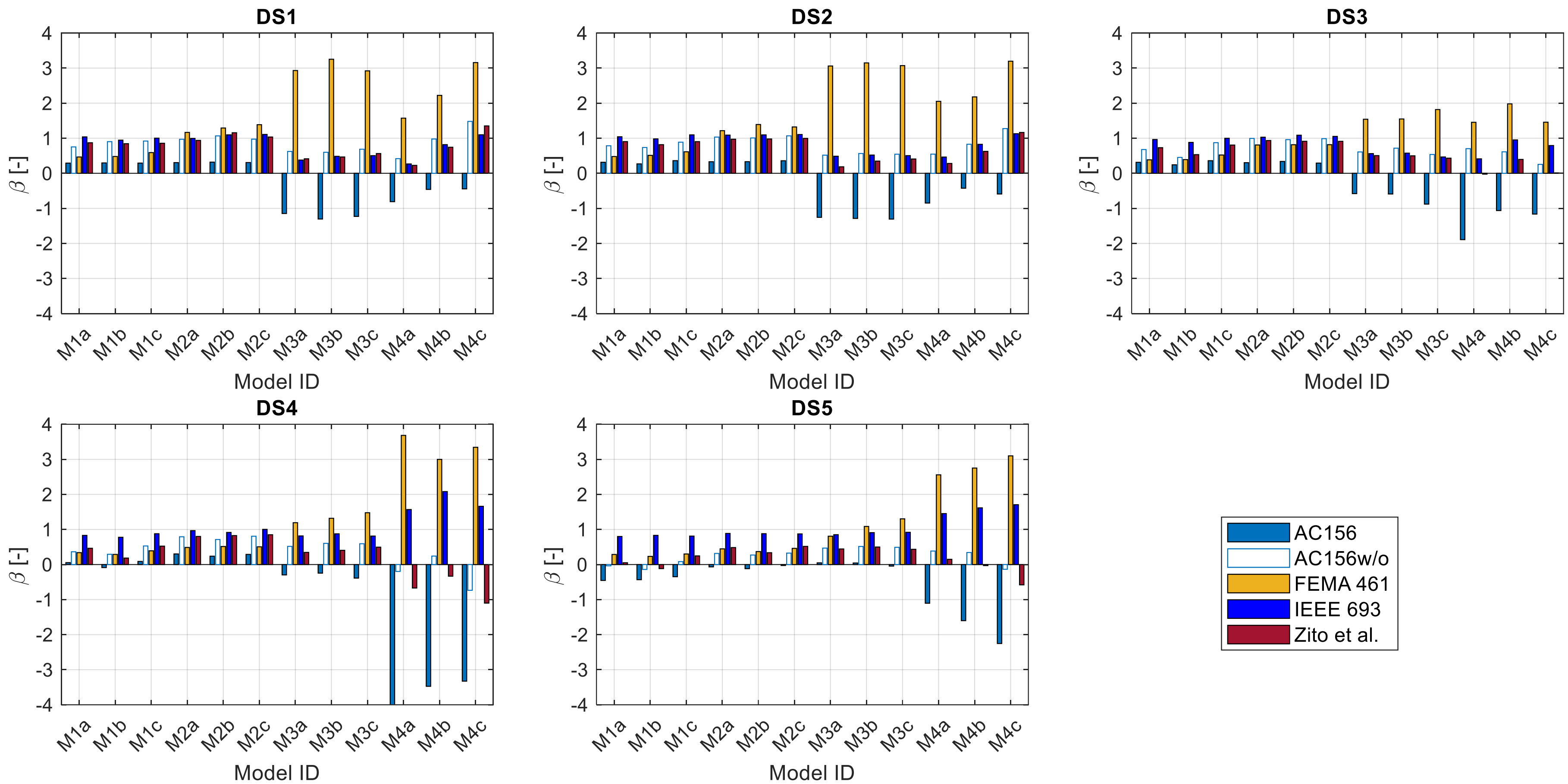

Figure 6.25: Reliability index (β) for all for all models and protocol input sets, evaluated for all DSs considering NFFM set.

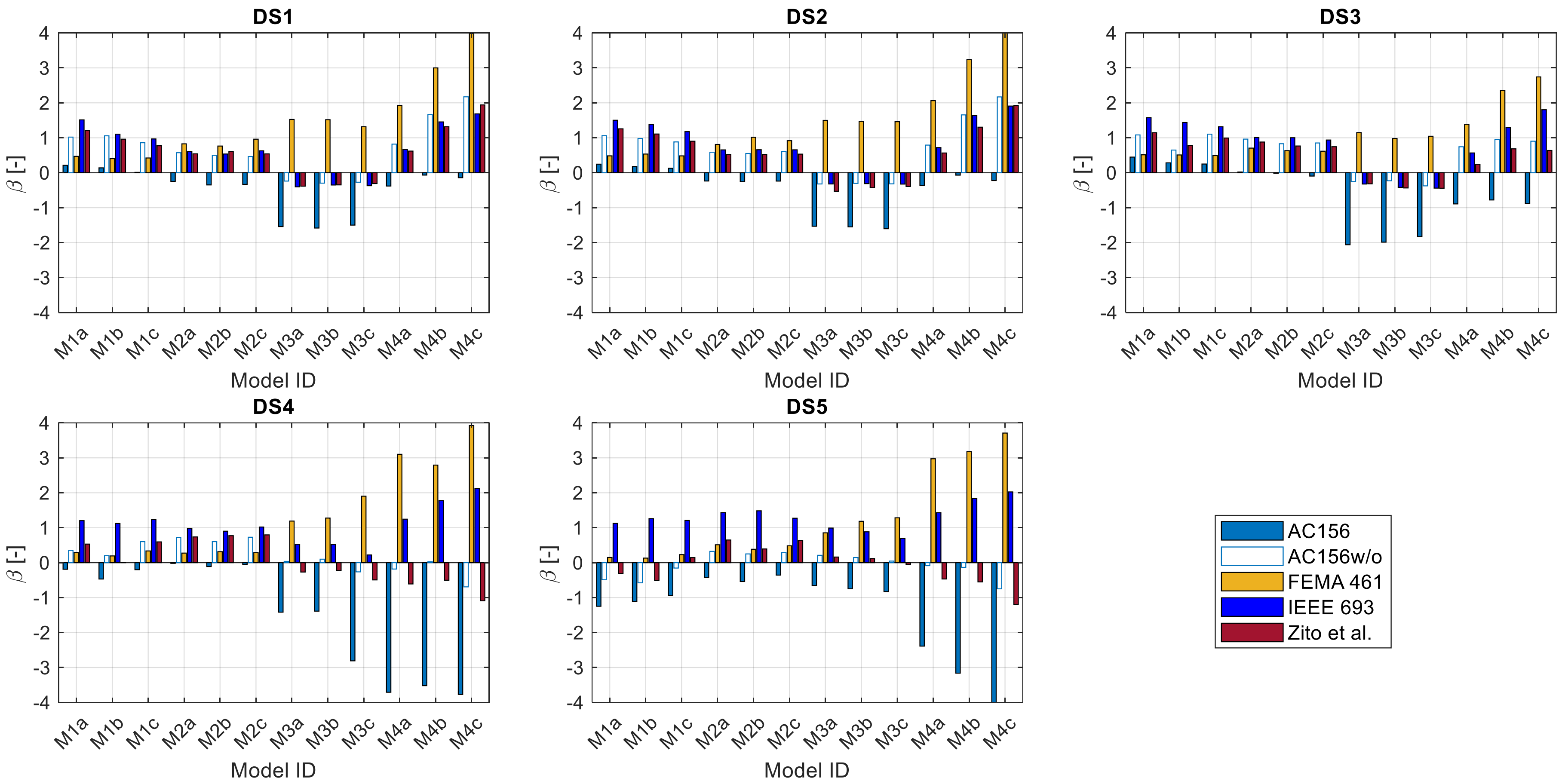

Figure 6.26: Reliability index (β) for all for all models and protocol input sets, evaluated for all DSs considering FFFM set.

As expectable, AC156 is associated with the largest *k* values as it is the least reliable; this was extensively discussed in section 6.3.3. Considering DS1 to DS3, assuming a value of *k* equal to 2-2.5 should be overall safe (considering all FM set), even though this might be slightly unsafe (conservative) in few cases, e.g., under FFFM and SFM sets, considering DS1 and DS2, for models M3 (overall for models M4). Considering DS4 and DS5, especially for DS5, AC156 might be extremely critical in terms of *k*, which reaches values larger than 3 (for DS4) and 5 (for DS5), with particular regard to models M1. It should be mentioned that the response associated with all FM set represents a reasonable reference for defining efficient and consistent *k* values. In particular, all FM set includes a wide variety of records that is representative of potential scenarios, which are not excessively severe (SFM set) or peculiar (NFSM); please, see section 6.2.3 for further details regarding the record sets and for comments regarding their representativity. Obviously, for elements that are to be installed in areas that are more likely to be represented by peculiar FM sets, e.g., NFSM, the reader is referred to the related evidence for determining applicable *k* values. In the following, general comments regarding the possible selection of *k* values are reported, with regard to overall comments, and the reader is referred to the specific results for more accurate estimations of *k* values.

Considering DS1 to DS3, assuming *k* values equal to about 1-1.5 might be safe for FEMA 461 (considering all FM set), even though it might be excessively conservative slightly unsafe) in some cases, e.g., overall, for models M3 and M4 (M1); therefore, the assumption of *k* might be correlated with the frequency of the element, and, for example, k might decrease as the frequency increases. For DS4 and DS5, especially for DS5, larger *k* values, e.g., equal to about 2-2.5, might be safe for models M1, and lower *k* might be used as the frequency increases, up to values comparable with DS1 to DS3.

As it was already found regarding FEMA 461, a *k* value equal to about 1-1.5 might be overall safe for IEEE 693, even though it might be excessively more conservative than FEMA 461 in most cases but models M1. However, a *k* value lower than the unity, as it was previously mentioned, might not be a reasonable assumption. Therefore, use of IEEE 693 and FEMA 461 might be aimed at assessing and qualifying the seismic performance of elements that are required to be extremely performing; actually, IEEE 693 is intended for extremely peculiar and critical elements, and this is compatible with the reported evidence. Accordingly, for these protocols, *k* could be defined considering a larger target β.

The case of Zito et al. and AC156w/o is more compatible with generic elements, since the reliability was found to be consistent with the assumed target value (please, see section 6.3.3) and the associated k values are more consistent with typical safety factors reported in the literature [13]. In particular, considering DS1 to DS3 and all FM sets, k values related to AC156w/o are quite similar to Zito et al. With particular reference to all FM set, which is the more representative set in general cases, a value equal to 1.5 might be considered, not being excessively conservative, differently from FEMA 461 and IEEE 693. For DS4 and only regarding models M1, a value equal to 2 should be adequately safe (considering all FM set), whereas a larger value, e.g., equal to about 3-3.5 might be more consistent for DS5 and models M1. Regarding DS4 and DS5 and models M2 to M4, a *k* value equal to 2 can be considered to be adequate for both protocols. For further information regarding other FM sets, the reader is referred to the reported evidence.

6.4 Novel perspectives and concluding remarks

According to the results, AC156 protocol might be relatively unreliable, whereas FEMA 461 protocol might overall be reliable or excessively conservative in some cases. It should be noted that the analyses did not account for reduction capacities by means of safety factors/coefficients; therefore, after the reduction of the nominal capacities derived according to the protocols, the reliability of FEMA 461 estimations might significantly increase, potentially resulting in relatively antieconomic capacities (relatively too reduced). Therefore, seismic assessment and qualification by means of the AC156 protocol might be associated with overestimated capacities, which might be highly unsafe, especially given that AC156 is the generally most authoritative reference for seismic qualification and certification of NEs. Conversely, capacities estimations obtained according to FEMA 461 might be excessively antieconomic.

The provided reliability indexes can be considered as a quantitative reference for classifying the investigated protocols. In particular, IEEE 693 and FEMA 461 might be aimed at assessing and qualifying particularly critical elements, which are required to fully functional under rare earthquakes, or that should be generally associated with higher reliability targets. Protocol AC156 seems to not be adequate to provide reliable capacity estimations. The modified version of AC156, i.e., AC156w/o, and the protocol developed by Zito et al. (including Zito et al. exception application) are more adequate for assessment and qualification of generic nonstructural elements. In particular, they are associated with relatively optimum reliability.

The provided methodology for determining reliability-targeted safety factor represents a useful means towards a more reliable and robust assessment and qualification of nonstructural elements by means of shake table testing and reference protocols. In particular, quantitative recommendations are provided in the study to enforce the wanted level of reliability, and first tentative coefficients are explicitly proposed.

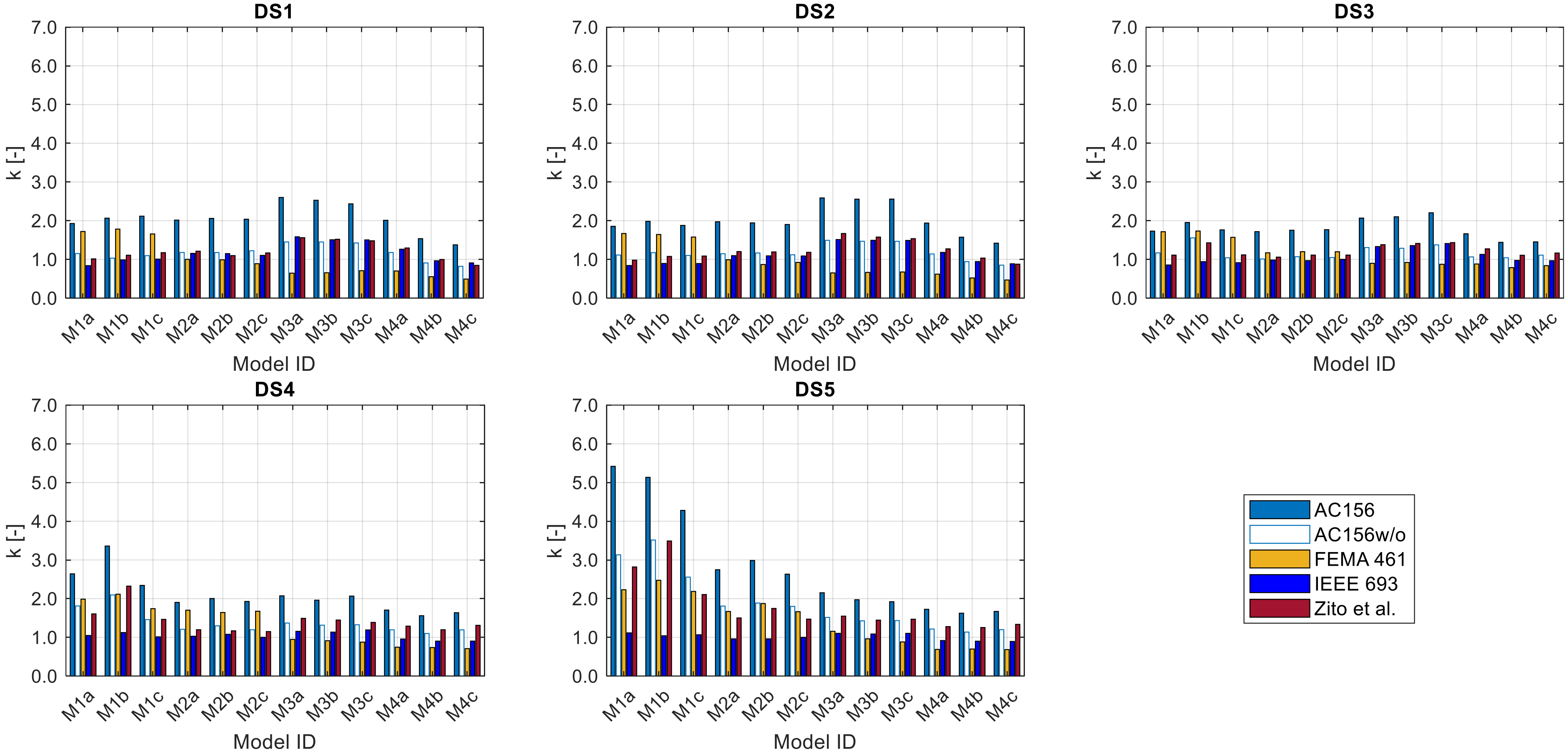

Figure 6.27: Safety factors (k) for all models and protocol input sets, evaluated for all DSs considering FM set and setting target reliability index ($\bar{\beta}$) equal to 1.

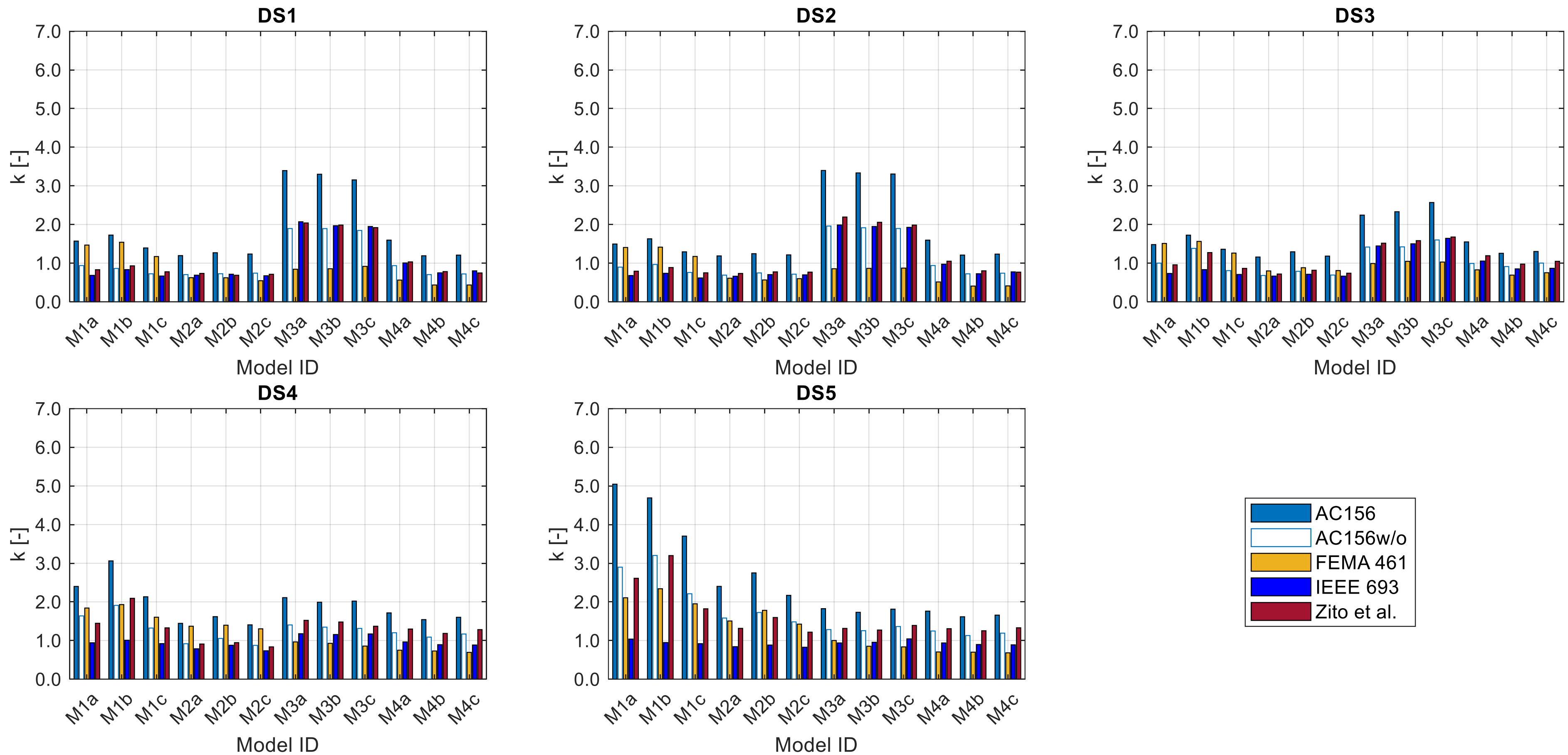

Figure 6.28: Safety factors (k) for all models and protocol input sets, evaluated for all DSs considering SFM set and setting target reliability index ($\bar{\beta}$) equal to 1.

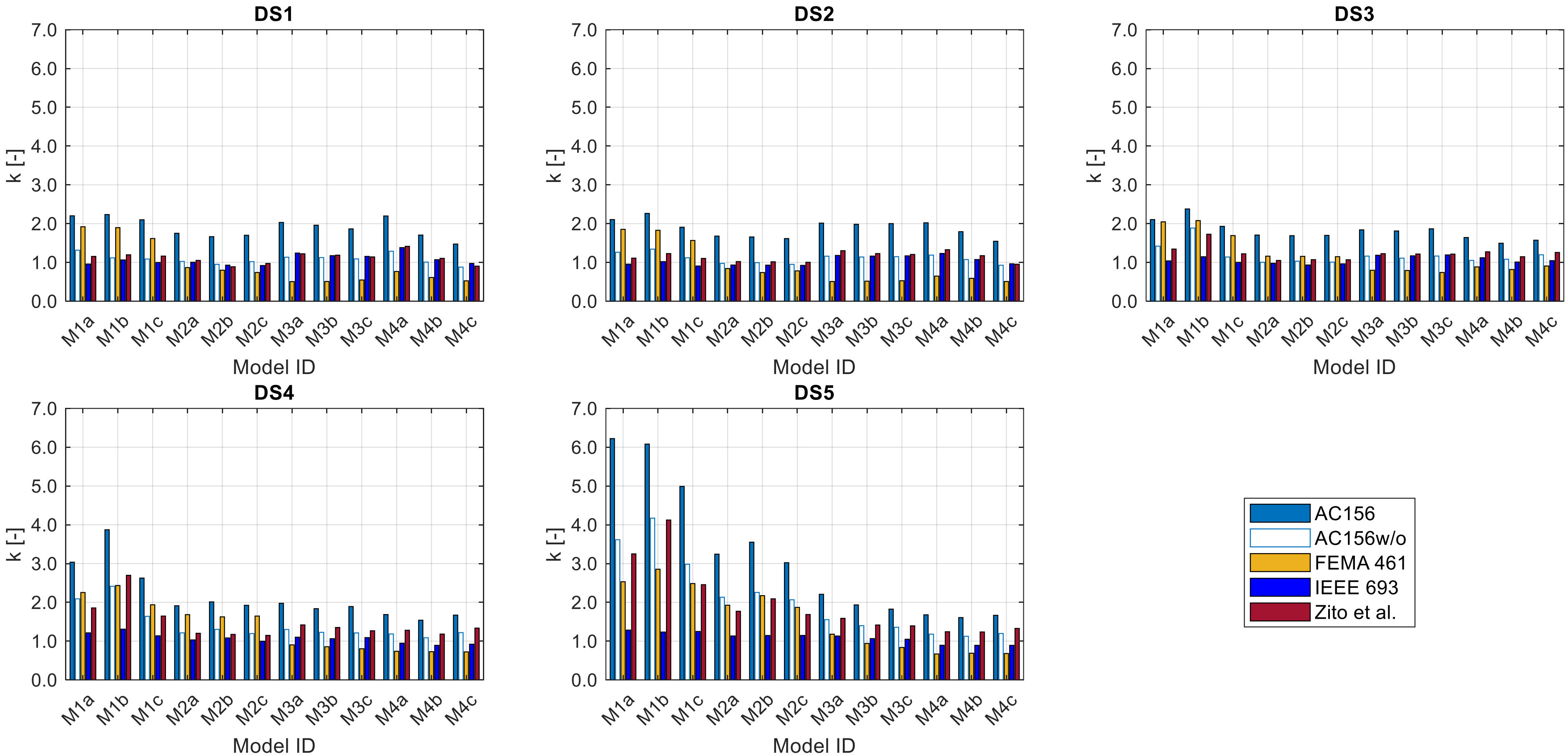

Figure 6.29: Safety factors (k) for all models and protocol input sets, evaluated for all DSs considering NFFM set and setting target reliability index ($\bar{\beta}$) equal to 1.

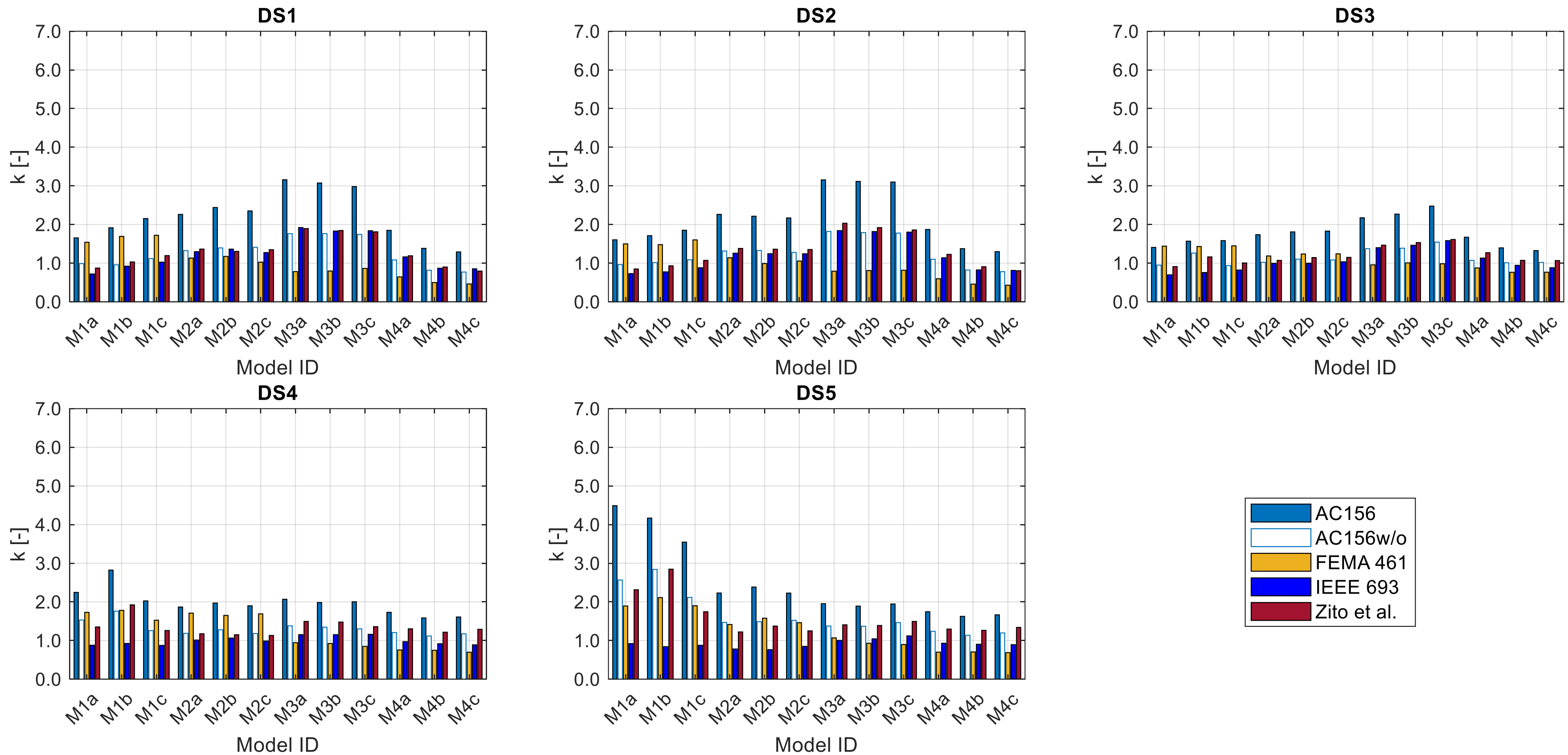

Figure 6.30: Safety factors (k) for all models and protocol input sets, evaluated for all DSs considering FFFM set and setting target reliability index ($\bar{\beta}$) equal to 1.

The reader is referred to the reported evidence to select safety factors that are consistent with peculiar conditions, i.e., specific frequency range, DS of interest, and type of ground motion. Further studies should define operative abaci or correlation tables based on the reported results, even varying the target reliability according to the wanted level of safety and reliability.

As a final comment, it is worth stressing that the reported evidence is related to preliminary findings and further studies should be carried out to generalize and extend the specific findings reported in this thesis. Further NE case studies should be considered, as well as alternative shake table protocols should also be investigated.

6.5 References

[1] Achour, N., Miyajima, M., Kitaura, M., Price, A. Earthquake-Induced Structural and Nonstructural Damage in Hospitals. Earthq. Spectra 27, 617–634, 2011. https://doi.org/10.1193/1.3604815

[2] De Angelis, A., Pecce, M. Seismic nonstructural vulnerability assessment in school buildings. Nat. Hazards 79, 1333–1358, 2015. https://doi.org/10.1007/s11069-015-1907-3

[3] Perrone, D., Calvi, P.M., Nascimbene, R., Fischer, E.C., Magliulo, G. Seismic performance of non-structural elements during the 2016 Central Italy earthquake. Bull. Earthq. Eng. 17, 5655–5677, 2019. https://doi.org/10.1007/s10518-018-0361-5

[4] Cosenza, E., Di Sarno, L., Maddaloni, G., Magliulo, G., Petrone, C., Prota, A. Shake table tests for the seismic fragility evaluation of hospital rooms Earthq. Eng. Struct. Dyn. 44, 23–40, 2015. https://doi.org/10.1002/eqe.2456

[5] Soroushian, S., Zaghi, A.E., Maragakis, E. “Manos”, Echevarria, A. Seismic Fragility Study of Displacement Demand on Fire Sprinkler Piping Systems. J. Earthq. Eng. 18, 1129–1150, 2014. https://doi.org/10.1080/13632469.2014.917059

[6] Di Sarno, L., Magliulo, G., D’Angela, D., Cosenza, E. Experimental assessment of the seismic performance of hospital cabinets using shake table testing. Earthq. Eng. Struct. Dyn. 48, 103–123, 2019. https://doi.org/10.1002/eqe.3127

[7] American Society of Civil Engineers. Minimum Design Loads and Associated Criteria for Buildings and Other Structures. 7th ed. American Society of Civil Engineers, Reston, VA. 2017 https://doi.org/10.1061/9780784414248

[8] Federal Emergency Management Agency (FEMA). Interim protocols for determining seismic performance characteristics of structural and nonstructural components through laboratory testing. Report No. FEMA 461, 2007. Washington D.C., USA.

[9] International Code Council Evaluation Service (ICC-ES). AC156 Acceptance Criteria for the Seismic Qualification of Nonstructural Components. Brea, California, USA: 2012.

[10] Institute of Electrical and Electronics Engineers. 693-2006 IEEE Recommended practice for seismic design for substations. New York: Institute of Electrical and Electronics Engineers; 2006.
[11] Telcordia Technologies (2006). NEBS Requirements: Physical Protection. Telcordia Technologies Generic Requirements, GR-63-CORE. Piscataway, NJ 08854-41821.866.672.6997 (USA).
[12] Burningham, C., Mosqueda, G., Saavedra, R.R. Comparison of seismic fragility of free standing equipment using current testing protocols and recorded building floor motions. in: Proceedings, Earthquake Engineering Symposium for Young Researchers, 2007. Seattle, WA.
[13] D'Angela, D., Magliulo, G., Cosenza, E. Towards a reliable seismic assessment of rocking components. Eng. Struct. 230, 111673, 2021. https://doi.org/10.1016/j.engstruct.2020.111673
[14] Zito, M., D'Angela, D.,Maddaloni, G., & Magliulo, G. (2022). A shake table protocol for seismic assessment and qualification of acceleration-sensitive nonstructural elements. Computer-Aided Civil and Infrastructure Engineering, 1–28.https://doi.org/10.1111/mice.12951
[15] Akkar, S., Bommer, J.J. Prediction of elastic displacement response spectra in Europe and the Middle East. Earthq. Eng. Struct. Dyn. 36, 1275–1301, 2007. https://doi.org/10.1002/eqe.679
[16] Merino, R.J., Perrone, D., Filiatrault, A. Consistent floor response spectra for performance-based seismic design of nonstructural elements. Earthq. Eng. Struct. Dyn. 49, 261–284, 2020. https://doi.org/10.1002/eqe.3236
[17] International Code Council. 2018 IBC code and commentary. 2018.
[18] Perrone D, Brunesi E, Decarro F, Peloso S, Filiatrault A. Seismic Assessment and Qualification of Non-structural Elements in Europe: a Critical Review. 4th International Workshop on the Seismic Performance of Non-Structural Elements (SPONSE), Pavia, Italy: 2019. https://doi.org/10.7414/4sponse.ID.10.
[19] Petrone C, Magliulo G, Manfredi G. Floor response spectra in RC frame structures designed according to Eurocode 8. Bull Earthquake Eng 2016;14:747–67. https://doi.org/10.1007/s10518-015-9846-7
[20] D'Angela D, Magliulo G, Cosenza E. Seismic damage assessment of unanchored nonstructural components taking into account the building response. Structural Safety 2021;93:102126. https://doi.org/10.1016/j.strusafe.2021.102126
[21] Wilcoski J, Gambill J, Smith S. CERL equipment fragility and protection procedure (CEFAPP). USACERL Technical Rep. No. 97/58. Champaign, IL: 1997.

[22] Takhirov SM, Fujisaki E, Power B, Vancouver A, Riley WM, Low B. PEER Report No. 2017/10. Development of Time Histories for IEEE693 Testing and Analysis (Including Seismically Isolated Equipment). Berkeley (CA): Pacific Earthquake Engineering Research Center, University of California; 2017.
[23] Ministero delle Infrastrutture e dei Trasporti. Circolare 21 gennaio 2019, n. 7 C.S.LL.PP. Istruzioni per l'applicazione dell'«Aggiornamento delle "Norme tecniche per le costruzioni"» di cui al decreto ministeriale 17 gennaio 2018. 2019.
[24] Ministero delle Infrastrutture e dei Trasporti. D.M. del 17/01/2018 – "Aggiornamento delle Norme tecniche per le Costruzioni 2018" NTC 2018 (in Italian) 2018.
[25] Petrone C, Magliulo G, Manfredi G. Seismic demand on light acceleration-sensitive nonstructural components in European reinforced concrete buildings. Earthquake Engineering & Structural Dynamics 2015;44:1203–17. https://doi.org/10.1002/eqe.2508
[26] Chichino B, Peloso S, Bolognini D, Moroni C, Perrone D, Brunesi E. Towards Seismic Design of Nonstructural Elements: Italian Code-Compliant Acceleration Floor Response Spectra. Advances in Civil Engineering 2021;2021:1–18. https://doi.org/10.1155/2021/4762110
[27] Di Domenico M, Ricci P, Verderame GM. Floor spectra for bare and infilled reinforced concrete frames designed according to Eurocodes. Earthquake Engng Struct Dyn 2021:eqe.3523. https://doi.org/10.1002/eqe.3523
[28] Magliulo G, Pentangelo V, Maddaloni G, Capozzi V, Petrone C, Lopez P, et al. Shake table tests for seismic assessment of suspended continuous ceilings. Bulletin of Earthquake Engineering 2012;10:1819–32. https://doi.org/10.1007/s10518-012-9383-6
[29] Di Sarno L, Magliulo G, D'Angela D, Cosenza E. Experimental assessment of the seismic performance of hospital cabinets using shake table testing. Earthquake Engineering & Structural Dynamics 2019;48:103–23. https://doi.org/10.1002/eqe.3127
[30] Petrone C, Magliulo G, Manfredi G. Shake table tests on standard and innovative temporary partition walls. Earthquake Engineering & Structural Dynamics 2017;46:1599–624. https://doi.org/10.1002/eqe.2872
[31] British Standards Institution, European Committee for Standardization. Eurocode 8, design of structures for earthquake resistance. London: British Standards Institution; 2005.
[32] McKenna F, Fenves GL, Scott MH. OpenSees: Open System for Earthquake Engineering Simulation. Pacific Earthquake Engineering Research Center. University of

California,Berkeley, CA. Available at: http://opensees.berkeley.edu 2000.
[33] Lignos, D.G., Krawinkler, H. A steel database for component deterioration of tubular hollow square steel columns under varying axial load for collapse assessment of steel structures under earthquakes. in: Proceedings of the 7th International Conference on Urban Earthquake Engineering (7CUEE) & 5th International Conference on Earthquake Engineering (5ICEE) 2010. Tokyo, Japan.
[34] Ibarra LF, Krawinkler H. Global collapse of frame structures under seismic excitations. Stanford CA: The John A. Blume Earthquake Engineering Center. Department of Civil and Environmental engineering. Stanford University; 2005.
[35] Ibarra LF, Medina RA, Krawinkler H. Hysteretic models that incorporate strength and stiffness deterioration. Earthquake Engng Struct Dyn 2005;34:1489–511. https://doi.org/10.1002/eqe.495
[36] Ricci P, Manfredi V, Noto F, et al (2018) Modeling and Seismic Response Analysis of Italian Code-Conforming Reinforced Concrete Buildings. J Earthq Eng 22:105–139. https://doi.org/10.1080/13632469.2018.1527733
[37] Charney FA. Unintended Consequences of Modeling Damping in Structures. J Struct Eng 2008;134:581–92. https://doi.org/10.1061/(ASCE)0733-9445(2008)134:4(581)
[38] D’Angela D, Magliulo G, Cosenza E. Characterization of local and global capacity criteria for collapse assessment of code-conforming RC buildings. Bull Earthquake Eng 2021. https://doi.org/10.1007/s10518-021-01115-y
[39] Vamvatsikos D, Cornell CA. Incremental dynamic analysis. Earthquake Engineering & Structural Dynamics 2002;31:491–514. https://doi.org/10.1002/eqe.141
[40] Porter K, Kennedy R, Bachman R. Creating Fragility Functions for Performance-Based Earthquake Engineering. Earthquake Spectra 2007;23:471–89. https://doi.org/10.1193/1.2720892
[41] Schultz MT, Gouldby BP, Simm D, Wibowo JL. Beyond the Factor of Safety: Developing Fragility Curves to Characterize System Reliability. US Army Corps of Engineeris. Engineer Research and Development Center.; 2010.
[42] D’Angela A, Magliulo G, Cosenza E. Incremental Dynamic Analysis of Rigid Blocks Subjected to Ground and Floor Motions and Shake Table Protocol Inputs. Bulletin of the New Zealand Society for Earthquake Engineering 2022;55. https://www.bulletin.nzsee.org.nz/index.php/bnzsee

Chapter 7

7 Conclusions and future developments

Non-structural elements (NEs) of a building consist of building elements/equipment and contents that are not part of the structural resisting system. The past earthquakes stress that NEs are typically associated with major seismic risk. The potential consequences of seismic damage to NEs are typically classified in terms of critical functioning disruption, economic losses, and casualties. In particular, seismic risk can be more critical for NEs installed/housed within critical and strategic buildings (i.e., hospitals, fire stations and base transceiver stations), whose operations are essential for post-seismic and emergency management. For this reason, the current European and international codes and standards were recently update referring to Performance-Based Earthquake Engineering (PBEE) approach for design and assessment of NEs. The evaluation of NEs can be carried out via different methods. Recent studies and codes emphasize that the shake table testing represents the most reliable method for seismic assessment and qualification of NEs, especially for critical/complex NEs. However, several protocols and testing inputs were defined in literature and codes but none of them has been assessed in terms of seismic scenario representativity and reliability.

The main objectives of this dissertation were (a) to evaluate the seismic behavior of some NEs through the shake table tests; (b) to outline novel perspectives for developing more reliable shake table protocols and seismic input; and (c) to assess and analyze the reliability of existing shake table protocols for seismic qualification of acceleration-sensitive systems and to estimate of reliability-targeted capacity safety factors.

After a brief introduction, the latest literature studies and regulations/codes regarding seismic damage and classification of NEs are reviewed, providing novel evaluation remarks. Quasi-static, single-floor dynamic (shake table), and multi-floor dynamic testing procedures were considered, including multiple protocols, when available. The relevant parameters and features that are essential for carrying out experimental assessment and qualification procedures were defined for a wide range of NEs, also providing general rules for identifying the relevant NEs in terms of response/damage sensitivity. Furthermore, the appropriate testing method is also recommended, whereas the technical information and evaluation remarks provided regarding the available protocols might be useful for selecting the most appropriate testing protocols. The technical recommendations provided in the chapter lay the groundwork for a more robust and standardized testing and qualification framework.

In the light of the review and technical recommendations provided, the ICC-ES AC156 protocol was chosen to perform the shake table tests of two critical/complex NEs: i) an innovative cleanroom used in the pharmaceutical and healthcare industries and ii) a typical museum display case containing a representative art object of the exhibition equipment of the National Archaeological Museum of Naples (MANN), Italy. The tests were carried out according to AC156 protocol, as the novel protocol was developed and refined at a later step in the shake table tests of the two systems. The main dynamic properties of both NEs were estimated, with particular regard to transfer functions, vibration modes, fundamental frequencies, and damping ratios. The seismic response was characterized in terms of time histories, peak values, and component amplification ratios, considering accelerograms/displacements recorded over several of both NEs locations/components; both peak values and amplification ratios were correlated with testing intensity. Technical and constructive requirements and innovative technologic solutions are supplied for the enhancement of the seismic performance of cleanrooms. In particular, innovation components and connection arrangements are technically illustrated and discussed, and their efficiency is experimentally proven. Regarding the critical response of the tested display case and vase, the study sheds light on the critical behavior of the tested specimens, stressing the need for further studies toward a more comprehensive assessment of freestanding museum objects and artifacts.

A novel protocol is developed for seismic assessment and qualification purposes through shake table testing. The most significant and contributing parts of the developed protocol consist in the definition of novel required response spectra and the generation of input signals for seismic performance evaluation tests. This definition follows the extension of a recently developed seismic demand formulation (Italian building code), which is compliant with consistent evaluations and proven reliability. In particular, this formulation is implemented considering an innovative approach, which accounts for a wide variability of building periods. The results of the preliminary validation stress the reliability of the developed protocol, also with regard to seismic and building scenarios considered to develop the seismic demand associated with RRS. Moreover, this evidence proves the generality and wide applicability of the developed protocol.

Finally, the study evaluated the reliability of existing shake table protocols for seismic qualification of acceleration-sensitive systems, also estimating reliability-targeted capacity safety factors. In particular, existing reference shake table protocols defined by regulations/codes were assessed in terms of seismic damage potential/severity considering inelastic single degree of freedom (SDOF) systems and assuming the reliability index as an evaluation parameter. The provided reliability indexes can be considered as a quantitative reference for classifying the investigated protocols. Quantitative recommendations are provided in the study to enforce the wanted level of reliability, and first tentative coefficients are explicitly proposed. In particular, the results showed that FEMA 461 and IEEE 693 protocols might be clearly excessively conservative, AC156 is likely to be the least reliable protocol, whereas in contrast the Zito et al. and AC156w/o protocol have intermediate reliability compared to all other protocols and might be considered to be the optimum options.

The study offers several potential ideas for future research studies in the field. In particular, the third chapter highlights the need for further studies investigating the operation of cleanrooms and other critical (building) systems integrating electric/electronic/ventilation facilities under seismic actions. Analytical and numerical methods should be developed to estimate the dynamic properties and the seismic performance of cleanroom and similar systems.

The fourth chapter stresses the need for further experimental and numerical studies investigating the seismic performance of valuable freestanding systems and objects, also considering a performance-based engineering approach. Moreover, fragility and vulnerability curves should also be assessed to provide useful tools for expeditious assessment.

The methodology defined in the fifth chapter for defining the required response spectrum and input signals for shake table tests could be used to develop other test protocols consistent with different seismic demand formulations or peculiar conditions (e.g., near field earthquakes). Moreover, the validation could be extended to other seismic parameters or against other FM sets, for example with regard to other structural systems (i.e., moment resisting or braced steel frames).

Finally, the sixth chapter studies could lead to the definition operative abaci or correlation tables based on the reported results, even varying the target reliability according to the wanted level of safety and reliability. Moreover, other studies might predict correlation of reliability index and safety factors may be correlated with other parameters (i.e., inelastic frequency) of the case study models. Other types of models (i.e., multi-degree-freedom systems) may be considered and analyzed. Finally, structural systems different from reinforced concrete buildings (e.g., moment resisting or braced steel frames) could be considered as a reference to extend the scope of the developed protocol.

Appendix

Appendix A

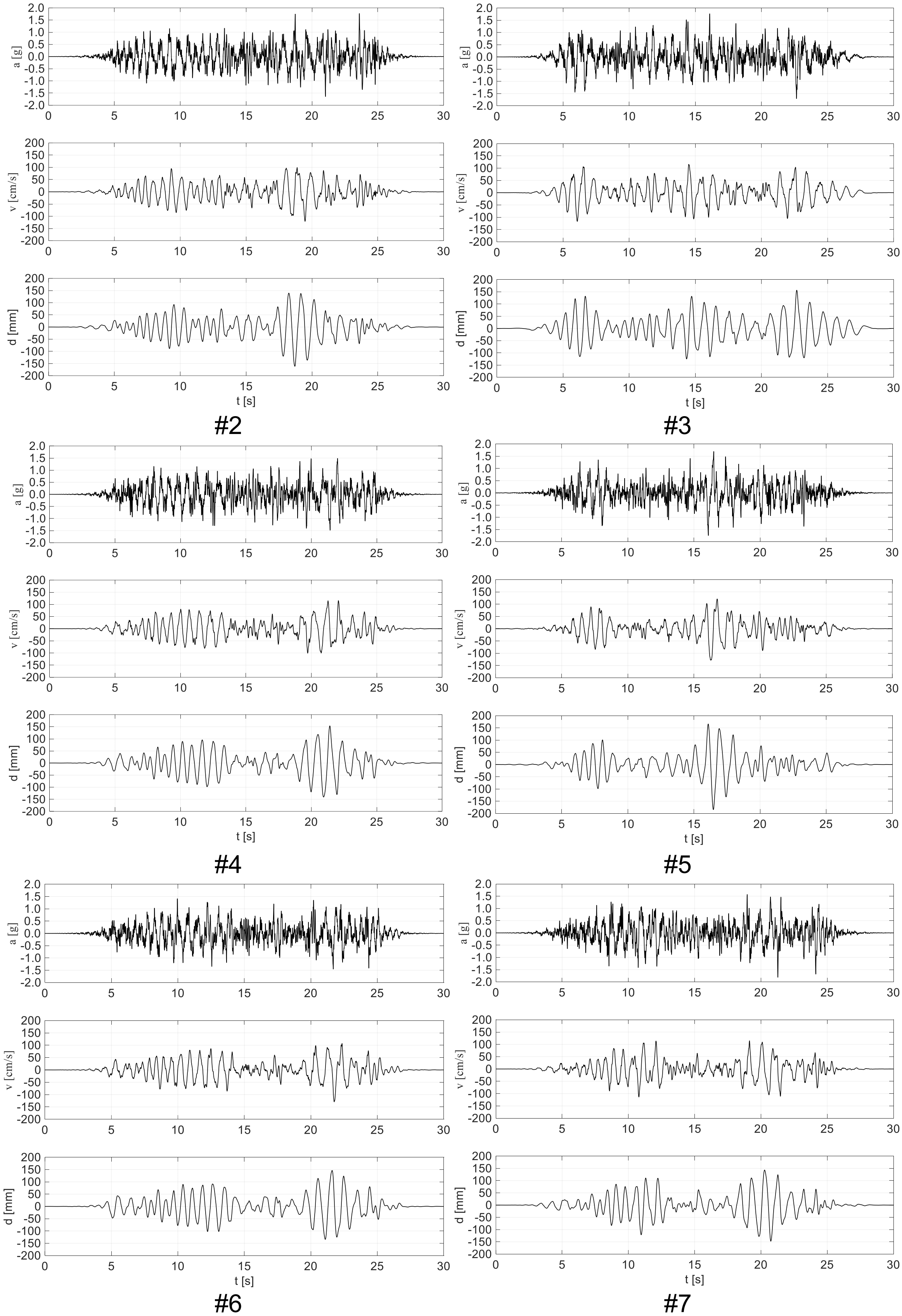

Figure A.1: Acceleration, velocity, and displacement time histories related to NPS #2 to #7. NPSs are related to RRS having PGA equal to 0.40 g and assuming z/h equal to one.

Appendix B

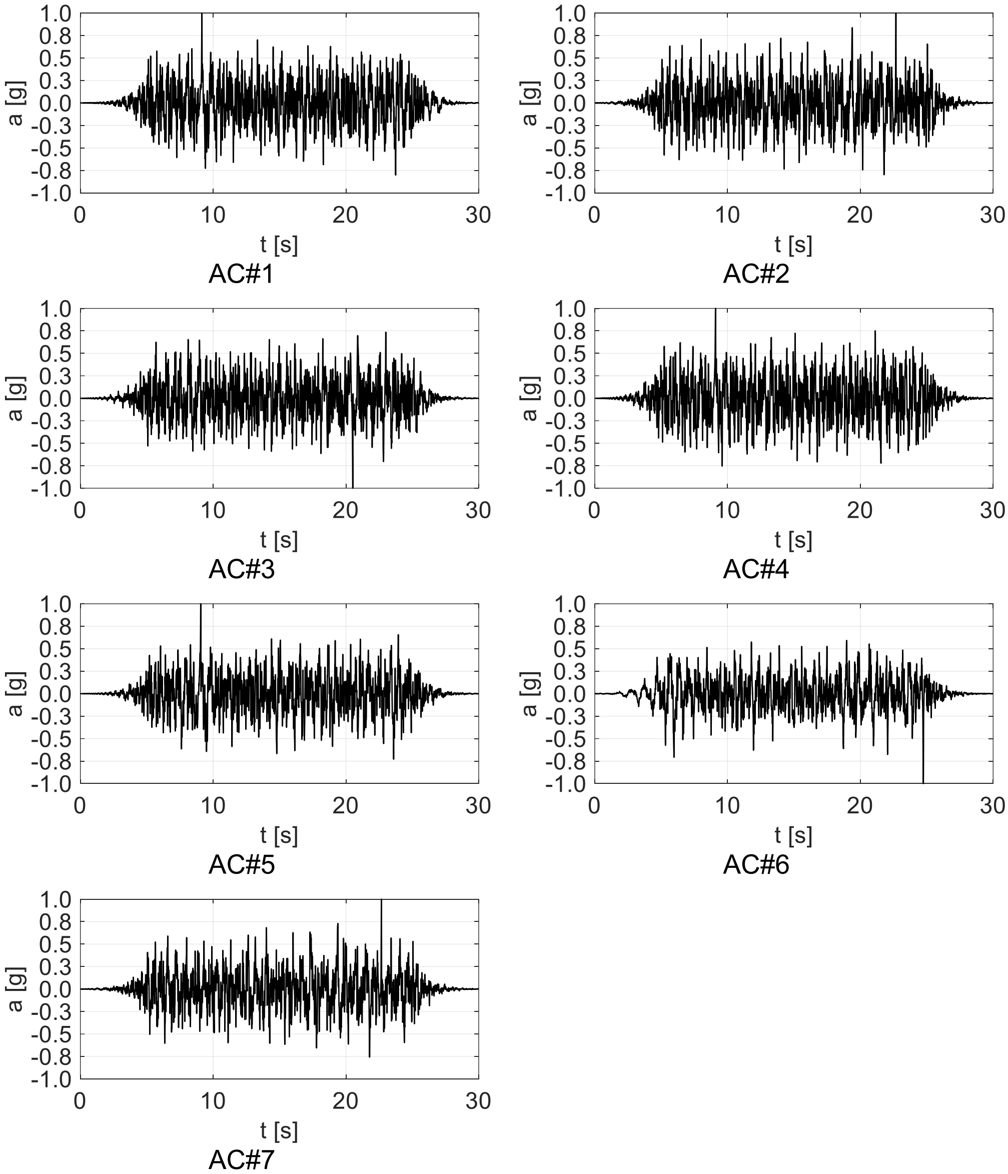

Figure B.1: Acceleration time histories related to AC156 #1 to #7 assuming PFA equal to 1.0 g.

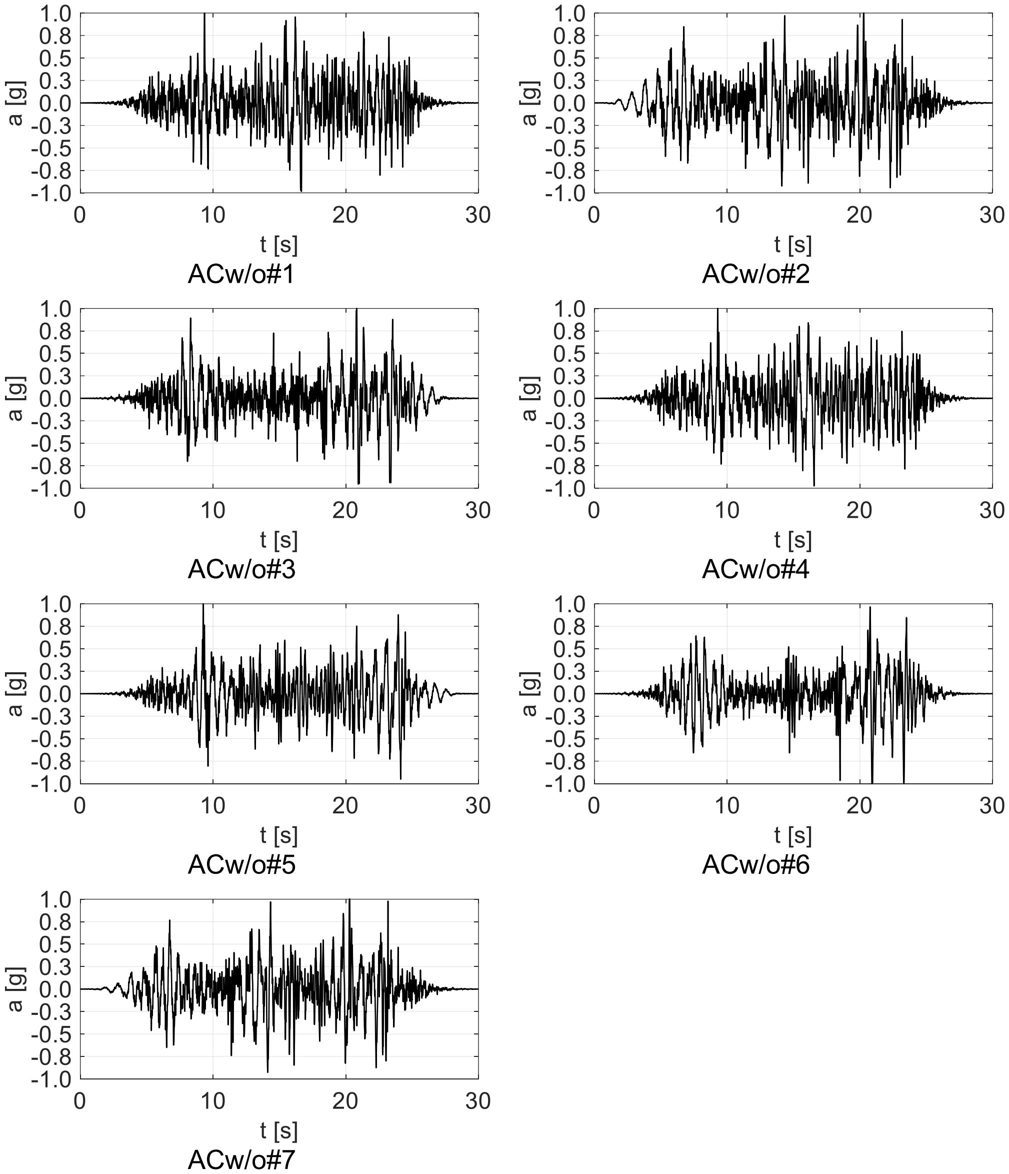

Figure B.2: Acceleration time histories related to AC156w/o #1 to #7 assuming PFA equal to 1.0 g.

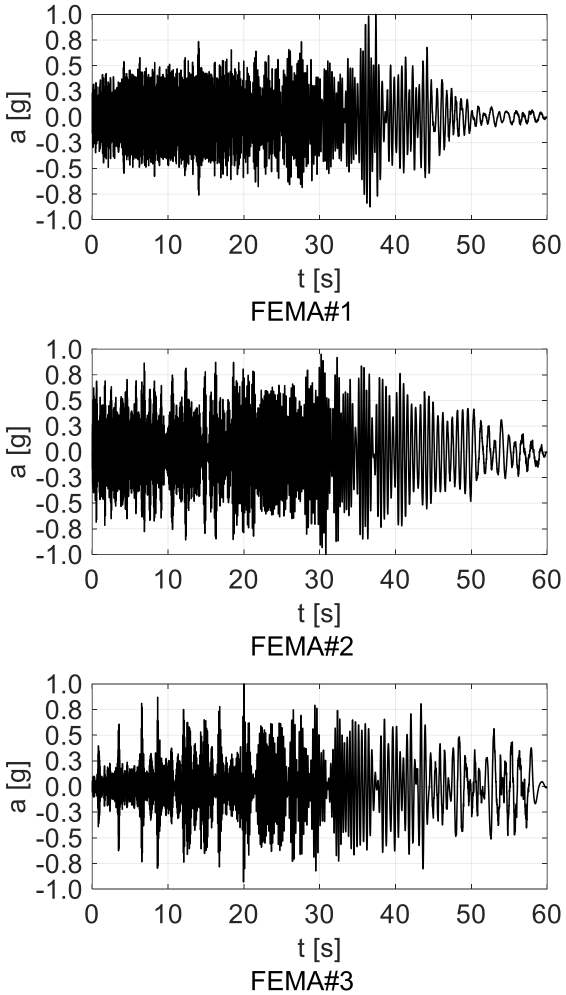

Figure B.3: Acceleration time histories related to FEMA 461 #1 to #3 assuming PFA equal to 1.0 g.

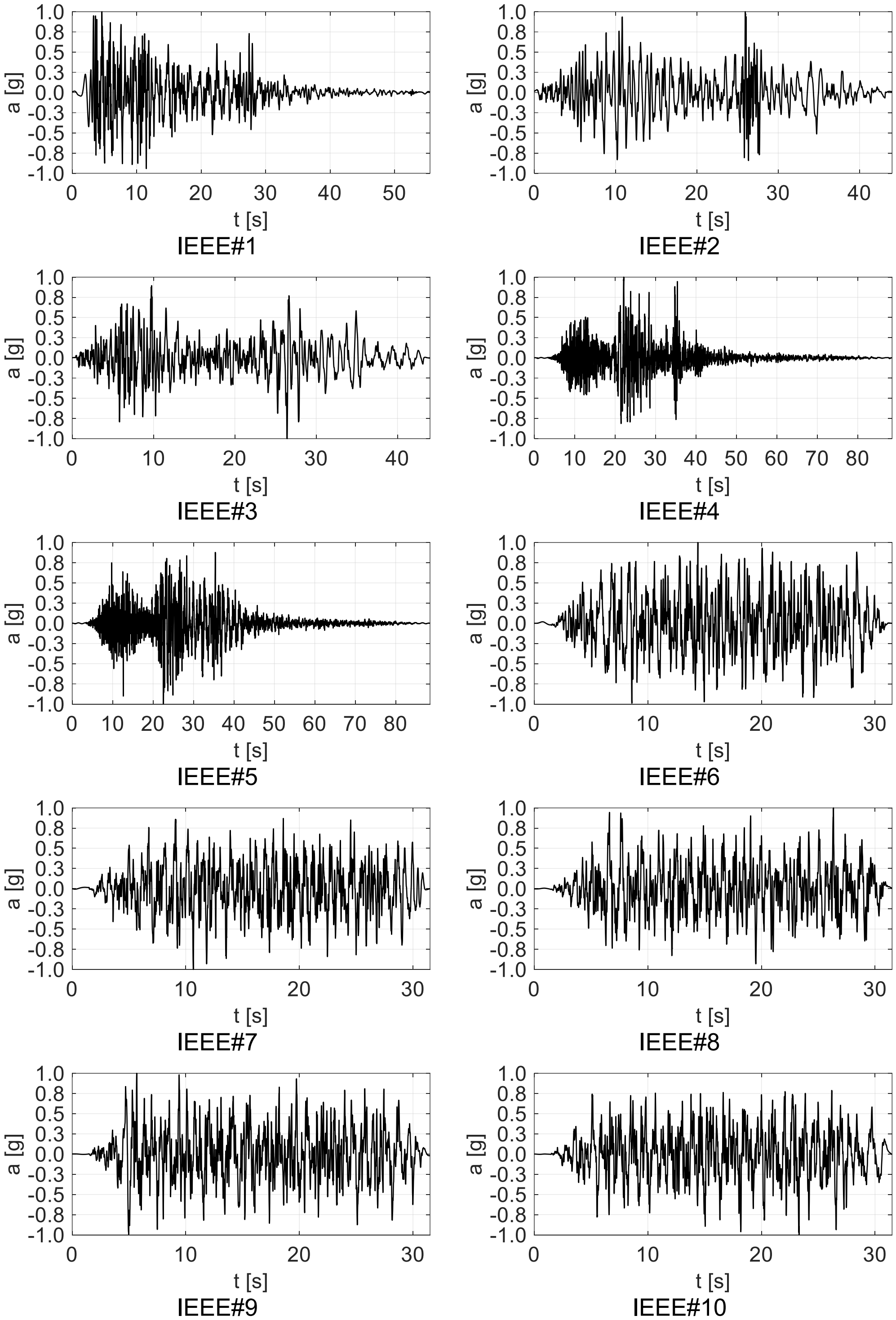

Figure B.4: Acceleration time histories related to IEEE 693 #1 to #10 assuming PFA equal to 1.0 g.

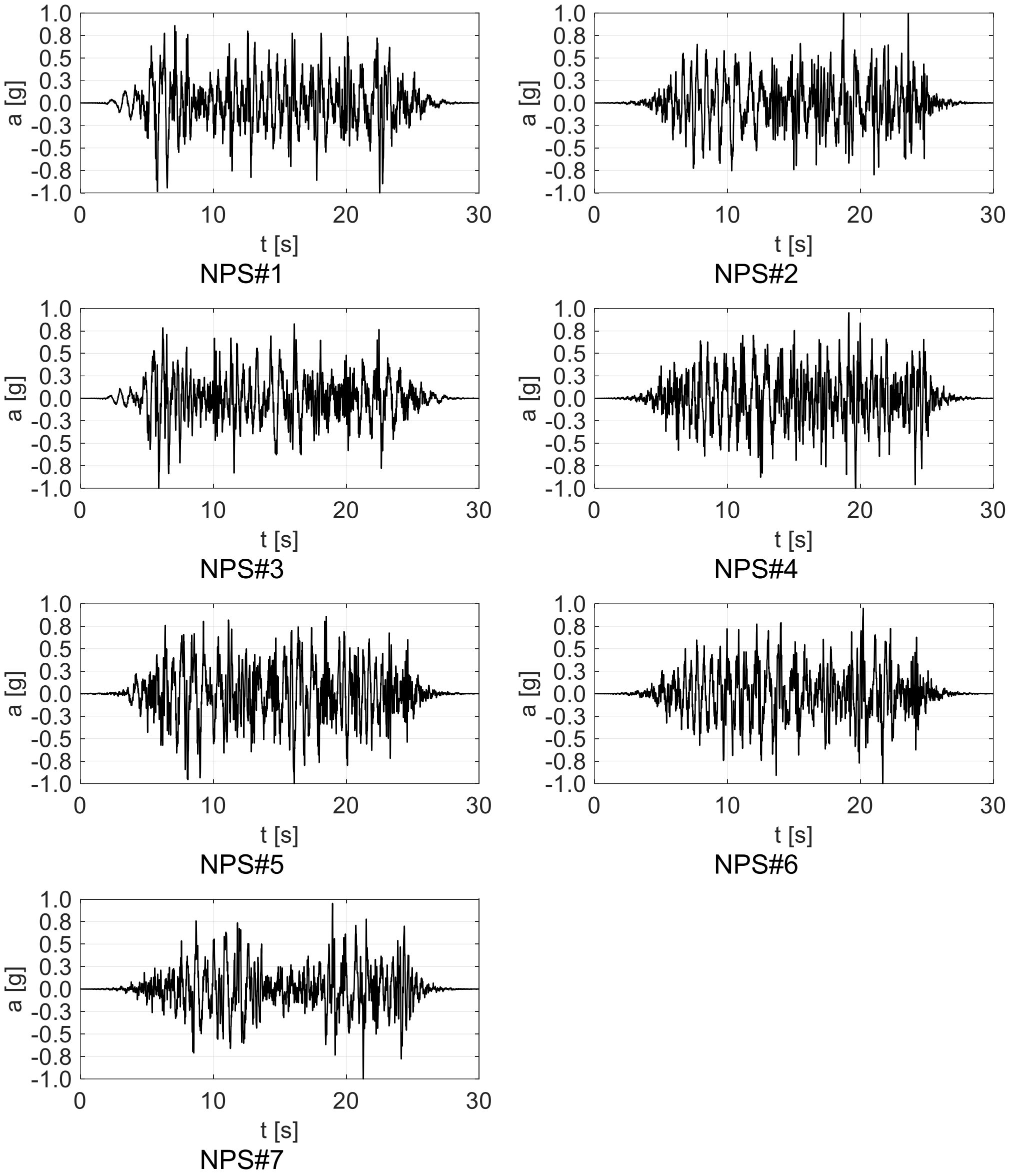

Figure B.5: Acceleration time histories related to Zito et al #1 to #7 assuming PFA equal to 1.0 g.

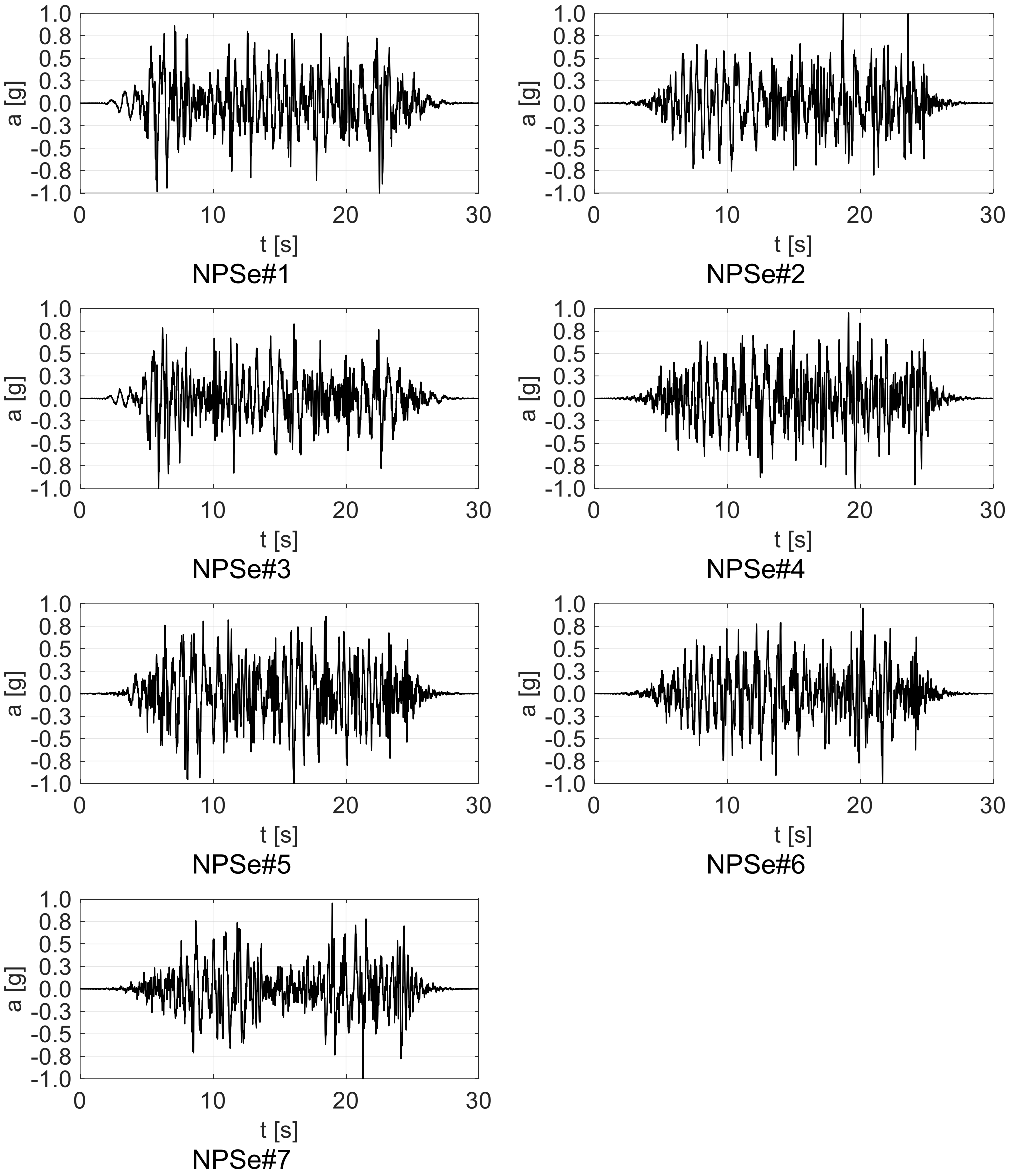

Figure B.6: Acceleration time histories related to Zito et al exception #1 to #7 assuming PFA equal to 1.0 g.

Table B-1: Fragility median (x_m) and logarithmic standard deviation (σ) considering DS1 for all models.

Model ID	f_a	x_m (σ)								
	[Hz]	FM	SFM	NFFM	FFFM	AC156	AC156w/o	FEMA 461	IEEE 693	Zito et al.
M1a	1.02	0.736 (0.884)	0.694 (0.62)	0.809 (1.11)	0.670 (0.637)	0.585 (0.0425)	0.350 (0.00)	0.458 (0.504)	0.255 (0.0577)	0.304 (0.151)
M1b	1.03	0.250 (0.947)	0.231 (0.692)	0.280 (1.14)	0.222 (0.756)	0.200 (2.4e-16)	0.100 (0.00)	0.155 (0.459)	0.0933 (0.219)	0.106 (0.153)
M1c	1.13	0.468 (0.907)	0.496 (0.547)	0.543 (1.05)	0.404 (0.776)	0.400 (0.00)	0.206 (0.0843)	0.271 (0.529)	0.189 (0.121)	0.22 (0.119)
M2a	1.48	0.574 (0.742)	0.648 (0.342)	0.703 (0.806)	0.468 (0.653)	0.550 (1.2e-16)	0.320 (0.0824)	0.260 (0.282)	0.314 (0.0745)	0.324 (0.173)
M2b	1.52	0.351 (0.726)	0.389 (0.344)	0.444 (0.748)	0.278 (0.661)	0.350 (0.00)	0.200 (2.4e-16)	0.165 (0.166)	0.194 (0.091)	0.184 (0.14)
M2c	1.52	0.505 (0.723)	0.562 (0.328)	0.632 (0.766)	0.404 (0.641)	0.500 (0.00)	0.300 (0.00)	0.215 (0.129)	0.269 (0.0942)	0.285 (0.089)
M3a	2.97	0.517 (0.417)	0.382 (0.380)	0.607 (0.329)	0.441 (0.452)	0.885 (0.0279)	0.492 (0.0700)	0.215 (0.129)	0.532 (0.111)	0.527 (0.0938)
M3b	3.04	0.833 (0.391)	0.634 (0.386)	0.971 (0.290)	0.714 (0.433)	1.42 (0.0349)	0.813 (0.0575)	0.366 (0.0771)	0.835 (0.111)	0.836 (0.137)
M3c	3.06	0.815 (0.390)	0.623 (0.380)	0.952 (0.278)	0.697 (0.436)	1.34 (0.0257)	0.785 (0.0315)	0.381 (0.145)	0.822 (0.0839)	0.802 (0.122)
M4a	5.86	1.05 (0.437)	1.17 (0.316)	0.959 (0.435)	1.15 (0.445)	1.36 (0.0177)	0.800 (0.00)	0.463 (0.161)	0.853 (0.0708)	0.867 (0.111)
M4b	7.34	1.96 (0.334)	2.25 (0.221)	1.82 (0.365)	2.11 (0.303)	2.15 (0.0271)	1.27 (0.021)	0.743 (0.171)	1.34 (0.0654)	1.36 (0.135)
M4c	9.02	1.51 (0.242)	1.62 (0.183)	1.45 (0.267)	1.58 (0.222)	1.63 (0.0239)	0.971 (0.0274)	0.563 (0.133)	1.07 (0.0676)	0.981 (0.103)

Table B-2: Fragility median (x_m) and logarithmic standard deviation (σ) considering DS2 for all models.

Model ID	f_a	x_m (σ)								
	[Hz]	FM	SFM	NFFM	FFFM	AC156	AC156w/o	FEMA 461	IEEE 693	Zito et al.
M1a	1.02	1.51 (0.864)	1.43 (0.593)	1.66 (1.09)	1.37 (0.624)	1.18 (0.0416)	0.707 (0.0261)	0.941 (0.472)	0.534 (0.0794)	0.618 (0.118)
M1b	1.03	0.519 (0.891)	0.488 (0.635)	0.568 (1.12)	0.473 (0.651)	0.421 (0.063)	0.250 (0.00)	0.302 (0.531)	0.189 (0.121)	0.227 (0.119)
M1c	1.13	0.977 (0.857)	1.02 (0.527)	1.12 (1.01)	0.852 (0.705)	0.778 (0.0345)	0.457 (0.0398)	0.549 (0.576)	0.368 (0.0981)	0.448 (0.0912)
M2a	1.48	1.16 (0.729)	1.32 (0.344)	1.43 (0.773)	0.947 (0.66)	1.11 (0.0168)	0.643 (0.0303)	0.544 (0.184)	0.614 (0.0658)	0.666 (0.142)
M2b	1.52	0.709 (0.707)	0.781 (0.359)	0.871 (0.754)	0.577 (0.631)	0.678 (0.0396)	0.407 (0.0445)	0.297 (0.168)	0.378 (0.107)	0.410 (0.148)
M2c	1.52	1.03 (0.701)	1.13 (0.346)	1.27 (0.746)	0.837 (0.625)	0.971 (0.0274)	0.571 (0.0465)	0.463 (0.161)	0.554 (0.0769)	0.593 (0.164)
M3a	2.97	1.05 (0.407)	0.777 (0.378)	1.22 (0.309)	0.902 (0.453)	1.81 (0.0297)	1.04 (0.0184)	0.448 (0.112)	1.05 (0.0935)	1.15 (0.101)
M3b	3.04	1.66 (0.399)	1.26 (0.392)	1.93 (0.298)	1.42 (0.445)	2.83 (0.0300)	1.63 (0.0385)	0.732 (0.0771)	1.64 (0.0986)	1.73 (0.103)
M3c	3.06	1.62 (0.393)	1.25 (0.388)	1.88 (0.298)	1.39 (0.433)	2.79 (0.0394)	1.60 (0.0537)	0.732 (0.0771)	1.61 (0.103)	1.66 (0.104)
M4a	5.86	2.13 (0.416)	2.34 (0.315)	1.97 (0.380)	2.30 (0.458)	2.72 (0.0179)	1.60 (0.0255)	0.843 (0.163)	1.65 (0.0763)	1.76 (0.105)
M4b	7.34	3.87 (0.356)	4.46 (0.233)	3.59 (0.409)	4.18 (0.297)	4.27 (0.0225)	2.56 (0.0176)	1.35 (0.184)	2.55 (0.0561)	2.75 (0.127)
M4c	9.02	2.96 (0.244)	3.18 (0.177)	2.79 (0.273)	3.13 (0.212)	3.28 (0.0241)	1.97 (0.0247)	1.04 (0.144)	2.02 (0.0865)	1.99 (0.102)

Table B-3: Fragility median (x_m) and logarithmic standard deviation (σ) considering DS3 for all models.

Model ID	f_a	x_m (σ)								
	[Hz]	FM	SFM	NFFM	FFFM	AC156	AC156w/o	FEMA 461	IEEE 693	Zito et al.
M1a	1.02	2.15 (0.855)	2.01 (0.636)	2.22 (1.08)	2.08 (0.616)	1.58 (0.0514)	1.06 (0.0891)	1.42 (0.427)	0.775 (0.114)	0.990 (0.200)
M1b	1.03	0.944 (0.888)	0.855 (0.661)	0.992 (1.14)	0.898 (0.614)	0.752 (0.128)	0.586 (0.236)	0.620 (0.391)	0.361 (0.158)	0.532 (0.277)
M1c	1.13	1.54 (0.824)	1.50 (0.538)	1.71 (1.02)	1.38 (0.607)	1.18 (0.0731)	0.695 (0.127)	0.964 (0.401)	0.611 (0.114)	0.745 (0.121)
M2a	1.48	1.86 (0.66)	1.99 (0.332)	2.08 (0.765)	1.67 (0.561)	1.65 (0.0526)	0.971 (0.0395)	1.11 (0.140)	0.943 (0.0712)	1.01 (0.108)
M2b	1.52	1.35 (0.68)	1.35 (0.369)	1.55 (0.784)	1.17 (0.57)	1.19 (0.120)	0.725 (0.110)	0.814 (0.0924)	0.657 (0.0954)	0.755 (0.0904)
M2c	1.52	1.60 (0.639)	1.69 (0.278)	1.83 (0.735)	1.40 (0.536)	1.48 (0.128)	0.885 (0.0530)	0.991 (0.166)	0.843 (0.0796)	0.931 (0.107)
M3a	2.97	1.89 (0.344)	1.54 (0.215)	2.20 (0.378)	1.63 (0.241)	2.75 (0.0799)	1.74 (0.0779)	1.15 (0.179)	1.77 (0.0819)	1.79 (0.161)
M3b	3.04	2.80 (0.348)	2.20 (0.201)	3.29 (0.362)	2.38 (0.259)	4.11 (0.0909)	2.53 (0.0613)	1.71 (0.222)	2.66 (0.0696)	2.71 (0.147)
M3c	3.06	2.47 (0.345)	1.93 (0.25)	2.86 (0.325)	2.13 (0.313)	3.83 (0.0685)	2.4 (0.0434)	1.47 (0.169)	2.45 (0.0621)	2.47 (0.107)
M4a	5.86	3.29 (0.218)	3.45 (0.195)	3.16 (0.163)	3.43 (0.266)	4.37 (0.0526)	2.81 (0.0412)	2.13 (0.214)	2.92 (0.103)	3.17 (0.170)
M4b	7.34	5.90 (0.18)	6.37 (0.116)	5.72 (0.187)	6.08 (0.179)	7.03 (0.0543)	5.05 (0.0786)	3.81 (0.0854)	4.71 (0.0811)	5.23 (0.129)
M4c	9.02	4.65 (0.182)	4.99 (0.142)	4.40 (0.206)	4.92 (0.145)	5.61 (0.0378)	4.14 (0.125)	3.23 (0.0504)	3.71 (0.0569)	4.39 (0.105)

Table B-4: Fragility median (x_m) and logarithmic standard deviation (σ) considering DS4 for all models.

Model ID	f_a	x_m (σ)								
	[Hz]	FM	SFM	NFFM	FFFM	AC156	AC156w/o	FEMA 461	IEEE 693	Zito et al.
M1a	1.02	3.17 (0.896)	2.79 (0.658)	3.49 (1.14)	2.88 (0.621)	3.28 (0.279)	2.29 (0.212)	2.30 (0.461)	1.35 (0.119)	2.05 (0.170)
M1b	1.03	1.34 (0.935)	1.16 (0.68)	1.50 (1.20)	1.20 (0.624)	1.67 (0.332)	1.04 (0.333)	1.04 (0.350)	0.585 (0.138)	1.19 (0.204)
M1c	1.13	2.32 (0.821)	2.05 (0.599)	2.58 (1.05)	2.09 (0.562)	2.35 (0.170)	1.48 (0.108)	1.69 (0.298)	1.02 (0.143)	1.49 (0.0894)
M2a	1.48	3.12 (0.774)	2.95 (0.438)	3.61 (0.925)	2.70 (0.608)	2.73 (0.0742)	1.73 (0.0853)	2.20 (0.419)	1.46 (0.147)	1.72 (0.0831)
M2b	1.52	2.18 (0.768)	1.98 (0.458)	2.51 (0.916)	1.89 (0.608)	2.02 (0.0602)	1.30 (0.122)	1.50 (0.405)	1.07 (0.146)	1.17 (0.0857)
M2c	1.52	2.68 (0.768)	2.59 (0.416)	3.11 (0.917)	2.31 (0.602)	2.39 (0.0832)	1.48 (0.0999)	1.87 (0.422)	1.23 (0.140)	1.43 (0.0438)
M3a	2.97	3.04 (0.431)	2.72 (0.335)	3.48 (0.519)	2.66 (0.290)	4.07 (0.0772)	2.62 (0.167)	1.86 (0.0671)	2.27 (0.0775)	2.89 (0.127)
M3b	3.04	4.64 (0.409)	4.14 (0.309)	5.33 (0.484)	4.03 (0.280)	6.00 (0.0635)	3.90 (0.175)	2.8 (0.0653)	3.46 (0.0969)	4.33 (0.152)
M3c	3.06	3.91 (0.376)	3.32 (0.183)	4.63 (0.456)	3.31 (0.172)	5.53 (0.0598)	3.50 (0.119)	2.35 (0.0556)	3.17 (0.0838)	3.67 (0.112)
M4a	5.86	4.15 (0.0874)	4.13 (0.0875)	4.16 (0.0745)	4.15 (0.103)	6.39 (0.0533)	4.27 (0.120)	2.74 (0.0846)	3.58 (0.0594)	4.59 (0.128)
M4b	7.34	7.01 (0.0928)	7.08 (0.0915)	7.10 (0.092)	6.93 (0.0977)	9.92 (0.0288)	6.91 (0.059)	4.41 (0.129)	5.69 (0.0525)	7.40 (0.0855)
M4c	9.02	5.58 (0.0964)	5.69 (0.0949)	5.53 (0.109)	5.63 (0.0877)	8.20 (0.0473)	6.01 (0.0352)	3.47 (0.0861)	4.50 (0.0580)	6.43 (0.0844)

Table B-5: Fragility median (x_m) and logarithmic standard deviation (σ) considering DS5 for all models.

Model ID	f_a	x_m (σ)								
	[Hz]	FM	SFM	NFFM	FFFM	AC156	AC156w/o	FEMA 461	IEEE 693	Zito et al.
M1a	1.02	5.14 (0.959)	4.48 (0.744)	5.85 (1.23)	4.50 (0.626)	10.4 (0.234)	6.13 (0.097)	4.03 (0.413)	2.15 (0.199)	5.49 (0.137)
M1b	1.03	2.48 (0.969)	2.15 (0.728)	2.75 (1.25)	2.24 (0.648)	4.75 (0.192)	3.28 (0.137)	2.00 (0.565)	0.971 (0.145)	3.19 (0.242)
M1c	1.13	4.08 (0.913)	3.85 (0.703)	4.51 (1.17)	3.69 (0.612)	6.82 (0.225)	4.08 (0.217)	3.05 (0.567)	1.73 (0.140)	3.36 (0.223)
M2a	1.48	4.85 (0.839)	4.41 (0.604)	5.27 (1.09)	4.47 (0.540)	5.67 (0.160)	3.72 (0.180)	3.10 (0.465)	1.98 (0.180)	3.08 (0.187)
M2b	1.52	3.51 (0.848)	3.10 (0.631)	3.83 (1.11)	3.23 (0.521)	4.37 (0.217)	2.82 (0.0945)	2.43 (0.527)	1.42 (0.188)	2.63 (0.0473)
M2c	1.52	4.10 (0.838)	3.83 (0.572)	4.48 (1.07)	3.74 (0.576)	4.62 (0.134)	3.15 (0.134)	2.62 (0.456)	1.74 (0.174)	2.56 (0.182)
M3a	2.97	4.33 (0.648)	3.89 (0.372)	5.04 (0.827)	3.71 (0.395)	4.84 (0.0885)	3.41 (0.0829)	2.52 (0.222)	2.48 (0.108)	3.48 (0.0976)
M3b	3.04	6.16 (0.553)	5.75 (0.350)	7.17 (0.686)	5.30 (0.357)	6.95 (0.0749)	5.02 (0.0967)	3.34 (0.156)	3.82 (0.0999)	5.07 (0.108)
M3c	3.06	5.21 (0.483)	4.90 (0.361)	5.98 (0.572)	4.54 (0.356)	6.13 (0.0753)	4.46 (0.181)	2.78 (0.134)	3.51 (0.104)	4.64 (0.132)
M4a	5.86	5.06 (0.207)	4.80 (0.175)	5.37 (0.241)	4.76 (0.157)	7.05 (0.0491)	4.84 (0.120)	2.78 (0.091)	3.74 (0.0628)	5.17 (0.082)
M4b	7.34	7.80 (0.141)	7.62 (0.110)	8.10 (0.172)	7.51 (0.0988)	10.9 (0.0621)	7.62 (0.0532)	4.51 (0.126)	6.00 (0.0713)	8.15 (0.114)
M4c	9.02	6.08 (0.126)	6.03 (0.110)	6.25 (0.153)	5.91 (0.0940)	8.90 (0.0362)	6.38 (0.0411)	3.54 (0.101)	4.73 (0.0575)	6.93 (0.0942)

Table B-6: Fitting equation coefficients and coefficients of determination R^2 of the fitting curves of Fragility median x_M as a function of elastic frequency ($x_m = m \cdot f_a + q$), associated with FM sets, evaluated considering DS1.

Fm sets	m	q	R^2
	$[g \cdot s]$	$[g]$	[-]
FM	0.165	0.260	0.802
SFM	0.191	0.188	0.766
NFFM	0.137	0.401	0.743
FFFM	0.192	0.137	0.824

Table B-7: Fitting equation coefficients and coefficients of determination R^2 of the fitting curves of Fragility median x_M as a function of elastic frequency ($x_m = m \cdot f_a + q$), associated with FM sets, evaluated considering DS2.

Fm sets	m	q	R^2
	$[g \cdot s]$	$[g]$	[-]
FM	0.322	0.555	0.795
SFM	0.372	0.411	0.757
NFFM	0.264	0.833	0.731
FFFM	0.377	0.308	0.820

Table B-8: Fitting equation coefficients and coefficients of determination R^2 of the fitting curves of Fragility median x_M as a function of elastic frequency ($x_m = m \cdot f_a + q$), associated with FM sets, evaluated considering DS3.

Fm sets	m	q	R^2
	$[g \cdot s]$	$[g]$	[-]
FM	0.490	0.945	0.825
SFM	0.550	0.704	0.809
NFFM	0.433	1.26	0.772
FFFM	0.545	0.659	0.847

Table B-9: Fitting equation coefficients and coefficients of determination R^2 of the fitting curves of Fragility median x_M as a function of elastic frequency ($x_m = m \cdot f_a + q$), associated with FM sets, evaluated considering DS4.

Fm sets	m	q	R^2
	$[g \cdot s]$	$[g]$	[-]
FM	0.500	1.97	0.778
SFM	0.548	1.60	0.802
NFFM	0.449	2.46	0.682
FFFM	0.546	1.54	0.828

Table B-10: Fitting equation coefficients and coefficients of determination R^2 of the fitting curves of Fragility median x_M as a function of elastic frequency ($x_m = m \cdot f_a + q$), associated with FM sets, evaluated considering DS5.

Fm sets	m	q	R^2
	$[g \cdot s]$	$[g]$	[-]
FM	0.364	3.71	0.714
SFM	0.405	3.25	0.758
NFFM	0.333	4.30	0.588
FFFM	0.391	3.20	0.788

Table B-11: Fitting equation coefficients and coefficients of determination R^2 of the fitting curves of logarithmic standard deviation σ as a function of elastic frequency ($\sigma = m \cdot f_a + q$), associated with FM sets, evaluated considering DS1.

Fm sets	m	q	R^2
	$[s]$	[-]	[-]
FM	-0.0768	0.844	0.924
SFM	-0.0412	0.529	0.959
NFFM	-0.0908	0.927	0.772
FFFM	-0.0593	0.727	0.979

Table B-12: Fitting equation coefficients and coefficients of determination R^2 of the fitting curves of logarithmic standard deviation σ as a function of elastic frequency ($\sigma = m \cdot f_a + q$), associated with FM sets, evaluated considering DS2.

Fm sets	m	q	R^2
	$[s]$	[-]	[-]
FM	-0.0716	0.813	0.931
SFM	-0.0390	0.517	0.966
NFFM	-0.0865	0.902	0.780
FFFM	-0.0539	0.691	0.983

Table B-13: Fitting equation coefficients and coefficients of determination R^2 of the fitting curves of logarithmic standard deviation σ as a function of elastic frequency ($\sigma = m \cdot f_a + q$), associated with FM sets, evaluated considering DS3.

Fm sets	m	q	R^2
	$[s]$	[-]	[-]
FM	-0.0863	0.794	0.931
SFM	-0.0506	0.492	0.956
NFFM	-0.111	0.957	0.798
FFFM	-0.0602	0.604	0.978

Table B-14: Fitting equation coefficients and coefficients of determination R^2 of the fitting curves of logarithmic standard deviation σ as a function of elastic frequency ($\sigma = \boldsymbol{m} \cdot \boldsymbol{f_a} + \boldsymbol{q}$), associated with FM sets, evaluated considering DS4.

Fm sets	m	q	R^2
	$[s]$	[-]	[-]
FM	-0.111	0.899	0.933
SFM	-0.0692	0.587	0.955
NFFM	-0.141	1.11	0.817
FFFM	-0.0761	0.635	0.971

Table B-15: Fitting equation coefficients and coefficients of determination R^2 of the fitting curves of logarithmic standard deviation σ as a function of elastic frequency ($\sigma = \boldsymbol{m} \cdot \boldsymbol{f_a} + \boldsymbol{q}$), associated with FM sets, evaluated considering DS5.

Fm sets	m	q	R^2
	$[s]$	[-]	[-]
FM	-0.114	0.997	0.939
SFM	-0.0822	0.722	0.959
NFFM	-0.149	1.28	0.826
FFFM	-0.0730	0.652	0.974

Author’s publications

[1] Magliulo G., Zito M, Manfredi G. Development of seismic resistant glass partitions. *XVIII ANIDIS Conference on Seismic Engineering in Italy.* Ascoli Piceno, Italy - september 2019.

[2] Magliulo G., Zito M., Manfredi G., Seismic response of innovative glass partitions, *17th World Conference on Earthquake Engineering (WCEE)* Sendai, Japan - september 2020.

[3] Prota A., Zito M.; D’Angela D., Toscano G., Ceraldi C., Fiorillo A., Magliulo G. Preliminary Results of Shake Table Tests of a Typical Museum Display Case Containing an Art Object. *Advances in Civil Engineering* 2022, 2022, 1–18, doi:10.1155/2022/3975958.

[4] Zito, M., D’Angela, D., Maddaloni, G., & Magliulo, G. (2022). A shake table protocol for seismic assessment and qualification of acceleration-sensitive nonstructural elements. *Computer-Aided Civil and Infrastructure Engineering*, 1–28. https://doi.org/10.1111/mice.12951

[5] Prota A., Zito M.; D’Angela D., Toscano G., Ceraldi C., Fiorillo A., Magliulo G. Dynamic properties and seismic response of a museum display case with an art object. *17th World Conference on Seismic Isolation, Energy Dissipation and Active Vibration Control of Structures (XVII ASSISI Conference 2022).* Torino, Italy 11-15 september 2022.

[6] Zito M., D’Angela D., Maddaloni G., Magliulo G. Required response spectra and acceleration loading histories for seismic assessment of acceleration-sensitive nonstructural elements according to the Italian building code. *17th World Conference on Seismic Isolation, Energy Dissipation and Active Vibration Control of Structures (XVII ASSISI Conference 2022)*. Torino, Italy 11-15 september 2022.

[7] Zito, M., Nascimbene R., Dubini P., D’Angela D., Magliulo G. Experimental Seismic Assessment of Nonstructural Elements: Testing Protocols and Novel Perspectives. *Buildings* 2022, 12, 1871. https://doi.org/10.3390/buildings12111871

[8] Zito M., D’Angela D., Magliulo G. Dynamic properties and seismic performance of an innovative cleanroom. *5th International Workshop on the Seismic Performance of Non-Structural Elements (SPONSE) 2022*. Stanford, California 5-7 December 2022.

[9] Zito M., D’Angela D., Maddaloni G., Magliulo G. Development of a code-compliant seismic input for shake table testing of acceleration-sensitive nonstructural elements. *5th International Workshop on the Seismic Performance of Non-Structural*

Elements (SPONSE) 2022. Stanford, California 5-7 December 2022.

[10] D'Angela D., Zito M., Di Salvatore C., Toscano G., Magliulo G. Seismic Assessment of Acceleration-Sensitive Nonstructural Elements: Reliability of Existing Shake Table Protocols and Novel Perspectives. *5th International Workshop on the Seismic Performance of Non-Structural Elements (SPONSE) 2022.* Stanford, California 5-7 December 2022.

[11] Zito, M., D'Angela D., and Magliulo G. Shake table testing of an innovative cleanroom with walkable ceiling system under operation conditions. *Earthq Eng Struct Dyn*. 2023. (under review).